

Geosynthetic Soil Reinforcement Testing Procedures

S. C. Jonathan Cheng, editor



STP 1190

STP 1190

Geosynthetic Soil Reinforcement Testing Procedures

S. C. Jonathan Cheng, editor

ASTM Publication Code Number (PCN)
04-011900-38



ASTM
1916 Race Street
Philadelphia, PA 19103

Library of Congress Cataloging-in-Publication Data

Geosynthetic soil reinforcement testing procedures / S.C. Jonathan Cheng, editor.

(STP ; 1190)

Includes bibliographical references and index.

ISBN 0-8031-1885-6

1. Soil stabilization--Testing. 2. Geosynthetics--Testing.

I. Cheng, S. C. Jonathan (Shi-Chieh Jonathan) II. Series: ASTM special technical publication ; 1190.

TA710.5.G44 1993

624.1'51363--dc20

93-8893

CIP

Copyright © 1993 AMERICAN SOCIETY FOR TESTING AND MATERIALS, Philadelphia, PA. All rights reserved. This material may not be reproduced or copied, in whole or in part, in any printed, mechanical, electronic, film, or other distribution and storage media, without the written consent of the publisher.

Photocopy Rights

Authorization to photocopy items for internal or personal use, or the internal or personal use of specific clients, is granted by the AMERICAN SOCIETY FOR TESTING AND MATERIALS for users registered with the Copyright Clearance Center (CCC) Transactional Reporting Service, provided that the base fee of \$2.50 per copy, plus \$0.50 per page is paid directly to CCC, 27 Congress St., Salem, MA 01970; (508) 744-3350. For those organizations that have been granted a photocopy license by CCC, a separate system of payment has been arranged. The fee code for users of the Transactional Reporting Service is 0-8031-1885-6/93 \$2.50 + .50.

Peer Review Policy

Each paper published in this volume was evaluated by three peer reviewers. The authors addressed all of the reviewers' comments to the satisfaction of both the technical editor(s) and the ASTM Committee on Publications.

To make technical information available as quickly as possible, the peer-reviewed papers in this publication were printed "camera-ready," as submitted by the authors.

The quality of the papers in this publication reflects not only the obvious efforts of the authors and the technical editor(s), but also the work of these peer reviewers. The ASTM Committee on Publications acknowledges with appreciation their dedication and contribution to time and effort on behalf of ASTM.

Printed in Fredericksburg, VA
August 1993

Foreword

This publication, *Geosynthetic Soil Reinforcement Testing Procedures*, contains papers presented at the symposium of the same name, held in San Antonio, TX on 19 Jan. 1993. The symposium was sponsored by ASTM Committee D-35 on Geosynthetics. S. C. Jonathan Cheng of Drexel University in Philadelphia, PA, presided as symposium chairman and is the editor of the resulting publication.

Contents

Overview—S. C. JONATHAN CHENG	vii
A New Device for Evaluating Load-Transfer in Geosynthetic Reinforced Soils— A. J. WHITTLE, D. G. LARSON, J. T. GERMAINE, AND M. ABRAMENTO	1
Intrinsic Confined and Unconfined Load-Deformation Properties of Geotextiles— J. P. BALLEGEER AND J. T. H. WU	16
Laboratory Testing of Modular Masonry Concrete Block-Geogrid Facing Connections—R. J. BATHURST AND M.R. SIMAC	32
Unconfined and Confined Wide Width Tension Testing of Geosynthetics— R. F. WILSON-FAHMY, R. M. KOERNER, AND J. A. FLECK	49
Index and Performance Tests for Geocells in Different Applications—A. CANCELLI, P. RIMOLDI, AND F. MONTANELLI	64
Pull-Out Testing of Geogrids in Cohesive Soils—K. A. FARRAG AND P. GRIFFIN	76
The Influence of Test Parameters and Procedures on the Tensile Modulus of Still Geogrids—D. N. AUSTIN, K. J. WU, AND D. F. WHITE	90
High Strength Polyester Geotextile Testing and Material Property Evaluation— J. N. PAULSON	111
Laboratory Investigations on the Shear Strength of Geogrid Reinforced Soils— D. CAZZUFFI, L. PICARELLI, A. RICCIUTI, AND P. RIMOLDI	119
Evaluation of Shear Strength and Dilatancy Behavior of Reinforced Soil from Direct Shear Tests—G. E. BAUER AND Y. ZHAO	138
Material Parameters Used in Design of Geosynthetic Reinforced Soil Structures— R. R. BERG AND J. G. COLLIN	152
Geosynthetic Installation Damage under Two Different Backfill Conditions— G. R. KOERNER, R. M. KOERNER, AND V. ELIAS	163
Comparison of Short-Term and Long-Term Pullout Testing of Geogrid Reinforcements—J. G. COLLIN AND R. R. BERG	184
Pullout Resistance and Load-Slip Response of Mechanically Damaged Geogrids— A. G. RAZAQPUR, G. E. BAUER, A. O. A. HALIM, AND Y. ZHAO	195

Chemical Stability of Polyester Fibers and Geotextiles Without and Under Stress—A. N. NETRAVALI, R. KRSTIC, J. L. CROUSE, AND L. E. RICHMOND	207
Testing for Biological Deterioration of Geosynthetics in Soil Reinforcement and Stabilization—D. G. BRIGHT	218
A Review of the Degradation of Geosynthetic Reinforcing Materials and Various Polymer Stabilization Methods—Y. G. HSUAN, R. M. KOERNER, AND A. E. LORD, JR.	228
Author Index	245
Subject Index	247

Overview

This ASTM symposium provides a forum for presentation of state-of-the-art technologies and new developments in geosynthetic soil reinforcement testing. The topics addressed include mechanical and durability properties with respect to the reinforcement function of geosynthetics, analysis of reinforcement testing results, and evaluation of testing results in relation to design. This symposium was also a result of an ASTM Committee D-35 seminar held in June 1991, concerning the same topic of geosynthetic soil reinforcement testing.

Since the use of geosynthetics in reinforcement applications is rapidly increasing, there is a need to institute a rational technical base for an understanding of the performance of geosynthetics in reinforcement applications. The corner stone of this technical base is the timely development of standardizing test methods, that is the charter of Committee D-35 on Geosynthetics. Although much progress has been witnessed as more testing methods are made available through ASTM processes, there is a significant lag between the state-of-the-art and present standardized test methods. This symposium attempts to provide a bridge between this time gap.

The organization of this Special Technical Publication (STP) is as follows:

- (1) Papers associated with either new testing equipment/procedures, or testing procedures for new reinforcement applications are included. These papers provide direction in the development of standard testing methods (papers 1 through 5).
- (2) Papers evaluating procedures of testing methods that are standardized or widely used are also included. The discussions are focused on those factors that influence test results (papers 6 through 10).
- (3) The next section of papers are concerned with the analysis of testing results in relation to design. In terms of standard practice, this is an area of need within ASTM (papers 11 through 14).
- (4) Finally, papers associated with the durability issue of geosynthetic reinforcement applications conclude this STP (papers 15 through 17).

All of the papers in this STP went through a rigorous review process. I would like to extend my most sincere appreciation to the authors for their enthusiastic participation and to the reviewers for their professional critiques. My work as editor of this publication has been very rewarding, but the credit must go to the authors and reviewers. In addition, I would like to thank the administrative support group from ASTM, especially Mrs. Dorothy Savini, Ms. Rita Hippensteel, and Mrs. Therese Pravitz.

This symposium is a step towards fully understanding the technical performance of geosynthetics. It is my most sincere hope that it will catalyze further research work and technical advancement.

Shi-Chieh Cheng

Drexel University, Philadelphia, PA; symposium
chairman and editor.

Andrew J. Whittle¹, Douglas G. Larson¹, John T. Germaine¹ and Mauricio Abramento¹

A NEW DEVICE FOR EVALUATING LOAD-TRANSFER IN GEOSYNTHETIC REINFORCED SOILS

REFERENCE: Whittle, A.J., Larson, D.G., Germaine, J.T. and Abramento, M. "A NEW DEVICE FOR EVALUATING LOAD-TRANSFER IN GEOSYNTHETIC REINFORCED SOILS," Geosynthetic Soil Reinforcement Testing Procedures, ASTM STP 1190, S.C. Jonathan Cheng, Ed., American Society for Testing and Materials, Philadelphia, 1993.

ABSTRACT: Although geosynthetics are often used in soil reinforcement applications, there are currently no methods for estimating reliably the stresses within the reinforcements at working load levels. This paper summarizes the design of a new laboratory device, referred to as the Automated Plane Strain Reinforcement (APSR) cell, which measures the maximum tensile stress that develops at the center of a single planar inclusion due to shearing of the surrounding soil. The cell can accommodate a wide range of reinforcing materials and can be equipped with additional instrumentation to measure the distribution of strains and/or stresses with inclusions of half-lengths up to 450mm. Test data, obtained for an instrumented steel sheet inclusion embedded in Ticino sand, demonstrate the capabilities of the APSR cell for measuring load-transfer at working load levels. Simple closed form solutions based on shear lag analysis describe accurately the tensile stresses measured in the elastic steel sheet inclusion. The new device provides the capability to compare load-transfer characteristics for different classes of geosynthetic reinforcing materials.

KEYWORDS: New plane strain test, planar reinforcement, tensile stress measurement, shear lag analysis, sand-steel data.

INTRODUCTION

High strength polymer grids and strips, woven and non-woven fabrics are widely used to reinforce soil masses in the construction of retaining walls, embankments, foundations and pavements. The performance of these composite soil structures depends, in large part, on the interaction between the soil matrix and the inclusions which determines the magnitude of loads carried by the reinforcement. The mechanisms of interaction are particularly complex for reinforcements with non-planar

¹Assistant Professor, Research Assistant, Principal Research Associate and Research Assistant, respectively, Massachusetts Institute of Technology, Cambridge, MA 02139.

2 GEOSYNTHETIC SOIL REINFORCEMENT TESTING PROCEDURES

surfaces, such as grids and for geosynthetic materials which exhibit non-linear and/or time dependent behavior. Existing analyses of soil-reinforcement interaction focus mainly on ultimate limit conditions using homogenization or limit equilibrium methods.

Homogenization methods [1] typically assume that the soil mass is reinforced with uniform, closely spaced inclusions and can be analyzed (at the macroscopic level) as an homogeneous, anisotropic composite material. Failure of composite reinforced soils has been investigated experimentally from measurements of boundary tractions and displacements in a variety of laboratory shear tests [2, 3]. These data show that the reinforcements produce an apparent cohesive strength component that is directly proportional to the density and strength of the inclusions. However, measurements in laboratory tests cannot be scaled reliably to field situations which are generally characterized by a relatively small number of reinforcing layers.

Current design methods for reinforced soil masses are generally based on limit equilibrium analyses [4] which postulate different mechanisms of failure and require input parameters to characterize the bond resistance between the soil and reinforcement in two modes: 1) direct shearing along the soil-reinforcement interface, and 2) tensile anchorage within the stable soil mass. These parameters are usually obtained from laboratory direct shear box (interface) and pullout tests, respectively. The measurements suffer from a number of well known practical limitations associated with poorly controlled test boundary conditions and are especially difficult to interpret for relatively extensible reinforcements (including many geosynthetics) and for inclusions with non-planar surfaces.

More comprehensive studies of soil-reinforcement interaction are necessary to understand the stress distribution within a reinforced soil mass at working load conditions. In principle, comprehensive stress analyses can be achieved using non-linear finite element (or boundary element) methods which model explicitly the constitutive properties of the soil, reinforcement and interfaces. Although these analyses offer great flexibility for simulating complex problem geometries, construction histories, etc., it is difficult to interpret the underlying mechanisms of soil-reinforcement interaction from complex numerical analyses. In contrast, this paper describes the development of a simple analytical framework for predicting and interpreting tensile stresses in a planar inclusion due to shearing of the surrounding soil. The analysis considers plane strain compression shearing of the soil mass with the inclusion oriented parallel to the minor, external principal stress. These studies provide the basis for the design of a new laboratory apparatus, referred to as the APSR cell, which is capable of measuring directly the tensile stresses within the reinforcement and imposes well defined boundary conditions on the soil specimen. Measurements in the APSR cell provide a method for comparing load-transfer characteristics for different types of geosynthetic reinforcements.

TENSILE STRESSES IN A PLANAR REINFORCEMENT

Figure 1 shows the idealized geometry for a composite plane strain element of reinforced soil which comprises a planar inclusion of thickness, f , and length, L , embedded in a soil matrix of overall height, $m+f$ (corresponding to the typical inclusion spacing). The orientation of the inclusion is parallel to the minor, external, principal stress acting on the soil matrix, σ_3 . The soil is sheared in a

plane strain compression mode by increasing the major principal stress, σ_1 , at the boundary of the element (with σ_3 constant). For these loading conditions, the inclusion reduces the lateral tensile strains which would otherwise develop in the soil and hence, represents the optimal orientation for a planar tensile reinforcement. Abramanto and Whittle [5] have adapted techniques of 'shear lag' analyses, widely used in the mechanics of composites [6, 7, 8], in order to derive approximate analytical expressions for the tensile stresses in the reinforcement, σ_{xx}^f . Initially these analyses have assumed the following:

1. The soil matrix and reinforcement behave as linear, isotropic and elastic materials (with properties G_m, ν_m and E_f, ν_f , respectively, Fig. 1). It should be noted that deformation properties of the soil (and also some non-woven geosynthetic materials) are dependent on the confining stress level.
2. The soil matrix and reinforcing inclusion are linked through a frictional interface, described by an angle of interface friction, δ .
3. There is no axial stress acting at the ends of the reinforcement, (i.e. $\sigma_{xx}^f=0$ at $x=\pm L/2$) as the inclusion is thin and is not physically bonded to the soil matrix.

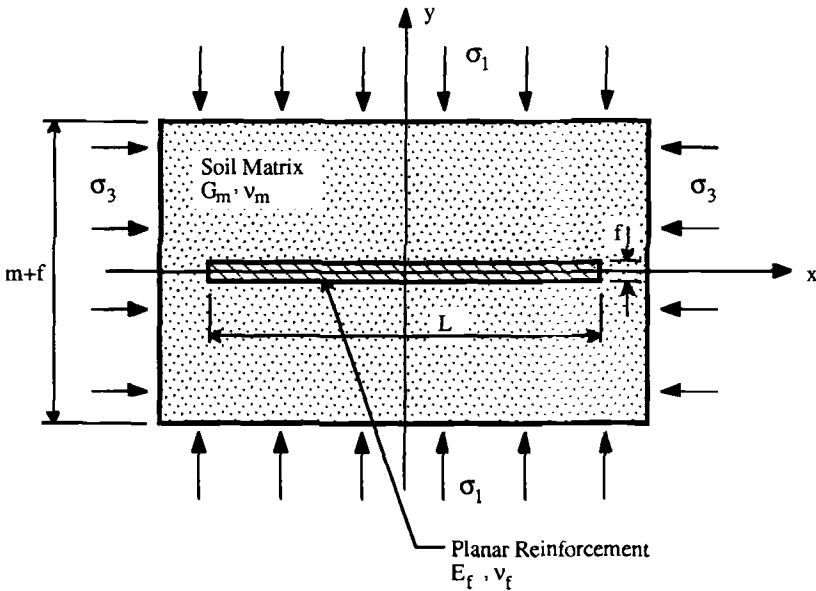


FIG. 1 Geometry of the reinforced soil element

For the case where there is no slippage at the soil-reinforcement interface, the tensile stress in the reinforcement can be written as a linear function of the external principal stresses σ_1 and σ_3 :

$$\sigma_{xx}^f = \frac{K_2}{K_1} \sigma \left[1 - \frac{\cosh \sqrt{K_1} x}{\cosh \sqrt{K_1} \frac{L}{2}} \right] \quad (1)$$

where,

4 GEOSYNTHETIC SOIL REINFORCEMENT TESTING PROCEDURES

$$K_2 \sigma = K_2^1 \sigma_1 + K_2^3 \sigma_3 \quad (2)$$

and the coefficients K_1 , K_2 can be written in terms of the elastic properties of the soil and reinforcement material, and the geometry (Fig. 1):

$$K_1 = \frac{6}{m f} \frac{\left[(1 - \nu_m) a + 2 \frac{G_m}{E_f} (1 + \nu_f) (1 - \nu_f) \right]}{\left[1 + \frac{1}{4} \nu_m - \frac{3}{2} \frac{G_m}{E_f} (1 + \nu_f) \nu_f \right]} \quad (2a)$$

$$K_2^1 = \frac{6}{m f} \frac{\left[\nu_m - 2 \frac{G_m}{E_f} (1 + \nu_f) \nu_f \right]}{\left[1 + \frac{1}{4} \nu_m - \frac{3}{2} \frac{G_m}{E_f} (1 + \nu_f) \nu_f \right]} \quad (2b)$$

$$K_2^3 = - \frac{6}{m f} \frac{(1 - \nu_m) (1 + a)}{\left[1 + \frac{1}{4} \nu_m - \frac{3}{2} \frac{G_m}{E_f} (1 + \nu_f) \nu_f \right]} \quad (2c)$$

where $a=f/m$.

The accuracy of these expressions has been established through comparisons with numerical results from finite element analyses [5].

It is clear from equation 1 that the maximum tensile stress occurs at the center of the inclusion (i.e., σ_{max}^f occurs at $x=0$) and that the maximum stress in a long reinforcement (i.e., typical of the field situation) is given by:

$$\sigma_{\infty}^f = (\sigma_{xx}^f)_{L=\infty} = \frac{K_2 \sigma}{K_1} \quad (3)$$

This result shows that the maximum tensile stress in a long inclusion is controlled by three factors: 1) the shear stress mobilized in the soil matrix, σ_1/σ_3 ; 2) the relative stiffness of the inclusion

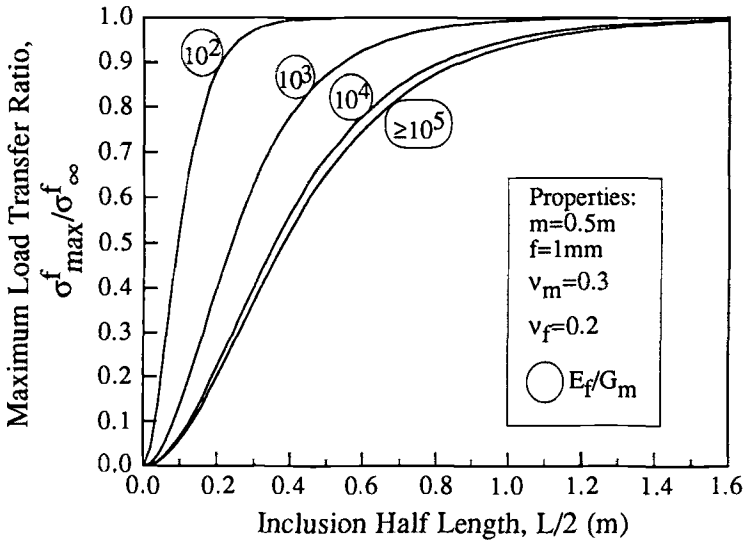


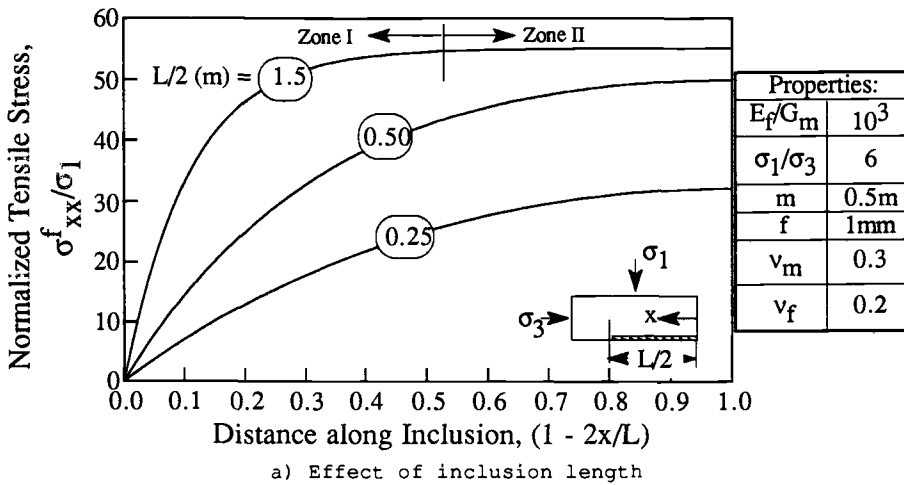
FIG. 2 Effect of inclusion length and stiffness on maximum load transfer ratio

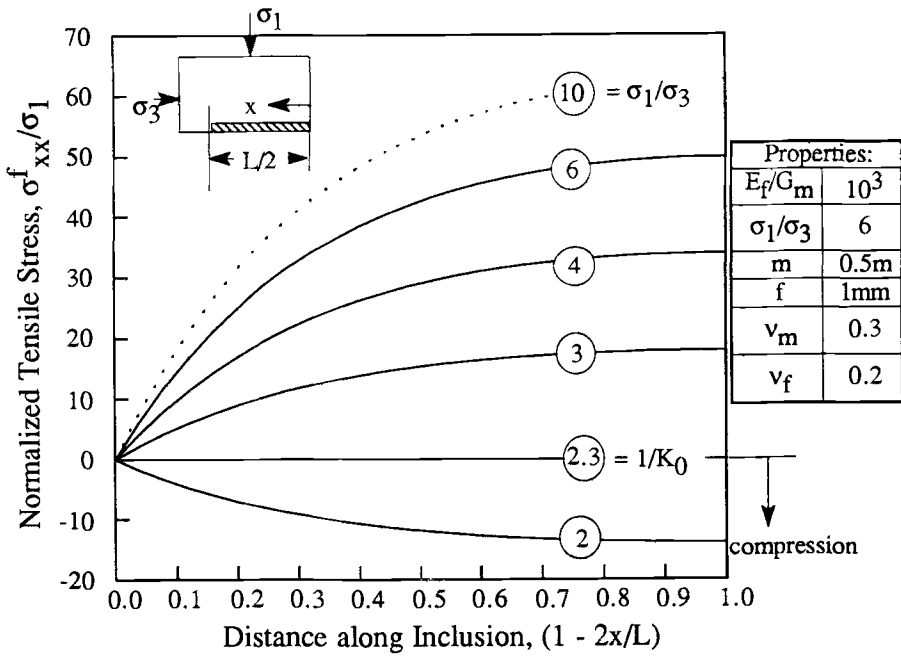
and soil, E_f/G_m ; and 3) the volume ratio of the reinforcement, $a=f/m$.

Figure 2 summarizes the 'maximum load transfer ratio', $\sigma_{max}^f/\sigma_{\infty}^f$ as a function of the inclusion half-length, $L/2$, and the stiffness ratio, E_f/G_m , for an inclusion with typical thickness, $f=1\text{mm}$, and spacing, $m=0.5\text{m}$. The results show that the 'pick-up length' necessary to achieve maximum load transfer (i.e., $\sigma_{max}^f \Rightarrow \sigma_{\infty}^f$) increases significantly with the stiffness ratio. For a relatively inextensible reinforcement such as steel ($E_f/G_m=10^4$, Fig. 2), the maximum load transfer occurs for inclusions with half-lengths $L/2 \geq 1.5\text{m}$; while more extensible materials ($E_f/G_m=10^2$, Fig. 2) achieve similar conditions for $L/2 \approx 0.4\text{m}$. These results have important implications on the measurements of load transfer in small scale laboratory tests and in the application of these data for predicting field performance.

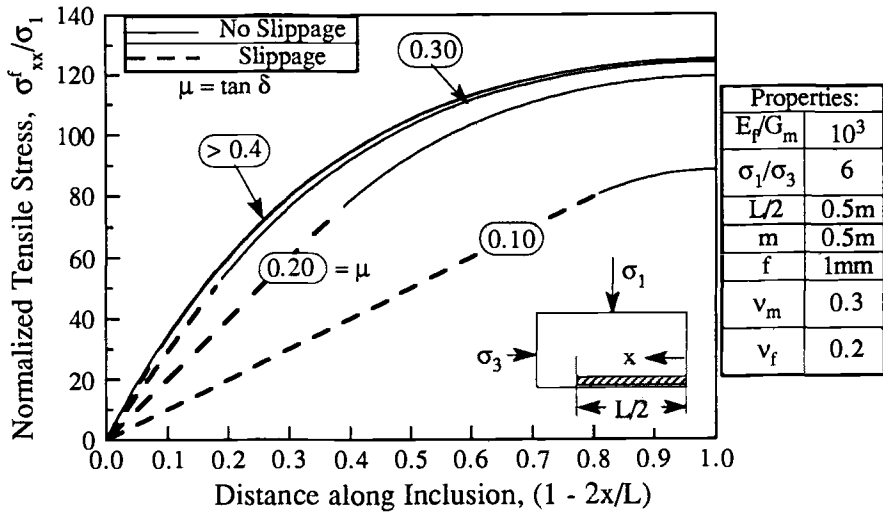
Figure 3 illustrates the distribution of the tensile stress, σ_{xx}^f , normalized by the major principal stress, σ_1 , for typical material properties, spacing and thickness of the reinforcement (Fig. 3). The results for inclusions with half-lengths, $L/2=0.25, 0.5$ and 1.5m , at an external stress ratio, $\sigma_1/\sigma_3=6$ (Fig. 3a), show that there are two distinct regions which characterize the soil-reinforcement interaction: I) the zone close to the tip of the inclusion, in which the tensile stress accumulates due to shear stresses acting along the soil-reinforcement interface and II) the zone of constant axial inclusion stress (i.e., $\sigma_{xx}^f \Rightarrow \sigma_{\infty}^f$). These two regions are fully developed for 'long' inclusions (e.g., $L/2=1.5\text{m}$; Fig.3a). For 'short' inclusions ($L/2=0.25, 0.5\text{m}$; Fig.3), the maximum load transfer is not achieved, and the shear lag parameter, K_1 (Eqn. 2a) controls the distribution of tensile stresses in zone I.

Figure 3b shows the load transfer for a short inclusion with half-length, $L/2=0.5\text{m}$, as a function of the applied stress ratio, σ_1/σ_3 in the soil matrix. For a soil matrix with linear, isotropic properties, the ratio $\sigma_1/\sigma_3 = (1-\nu_m)/\nu_m = 1/K_0$ (i.e., for $\nu_m=0.3$, $1/K_0= 2.3$; Fig.





b) Load transfer due to shearing of the soil



c) Effects of interface friction

FIG. 3 Distribution of tensile stresses in a planar reinforcement

3b) corresponds to one-dimensional deformation of the unreinforced soil matrix (i.e., $\epsilon_{xx} = 0$). Tensile stresses only develop in the reinforcement when $\sigma_1/\sigma_3 > 1/K_0$. There are two important limitations on the interpretation of results in Figure 3b:

1. For drained shearing of dry, cohesionless soils (e.g. good quality granular fills), the shear strength is most commonly described by a Mohr-Coulomb failure criterion with friction angle $\sin \phi = (\sigma_1 - \sigma_3)/(\sigma_1 + \sigma_3)$. Ladd et al. [2] report $35^\circ \leq \phi_{ps} \leq 57^\circ$ ($3.7 \leq \sigma_1/\sigma_3 \leq 11.7$) for typical sands sheared in plane strain compression. Thus, local failure will initiate in the matrix (at locations close to the tip of the inclusion) when the stress ratio mobilizes the frictional strength of the soil.
2. The linear, isotropic model of soil behavior does not describe accurately the volumetric response of cohesionless soils in drained shearing at high stress ratios. Extensive observations show that sands dilate when the mobilized friction exceeds a threshold value, $\phi_{cv} = 35^\circ$ to 45° ($\sigma_1/\sigma_3 = 3.7$ to 5.8) [10, 11]. The practical implication of this behavior is that the proposed analysis will tend to underestimate both the lateral strains in the soil matrix and the tensile stresses in the reinforcement (especially for $\sigma_1/\sigma_3 > 6$).

The preceding results assume that there is no slip between the soil matrix and the planar reinforcement. The results in Figure 3c show the effects of the interface friction angle, δ , on the load transfer for an inclusion of half-length, $L/2=0.5m$, at a stress ratio, $\sigma_1/\sigma_3=6$. For the selected material properties and geometry, interface slippage has very little influence on tensile stresses in the reinforcement for $\delta \geq 17^\circ$ ($\mu = \tan \delta \geq 0.3$). However, there are significant reductions in load transfer when the friction ratio is artificially low ($\mu=0.1$, $\delta=7^\circ$). Further studies [5] also show that, for practical values of interface friction, $\delta=10^\circ-30^\circ$, interface slippage has little effect on the expected load transfer for a wide range of constituent material properties and inclusion geometries.

THE APSR CELL

The analysis summarized in the previous section provides a framework for predicting and interpreting the load transfer for the unit element geometry shown in Figure 1. The framework also provides the basis for the design of a new laboratory device, referred to as the Automated Plane Strain Reinforcement (APSR) cell, for measuring the maximum tensile stress transferred to a planar reinforcement due to plane strain shearing of the surrounding soil [11]. The boundary conditions along the plane of symmetry, $x=0$, in the unit element (Fig. 1) are well defined by 1) zero lateral displacement in both the soil and reinforcement (i.e., $u_x=0$), 2) no shear tractions acting along the plane (i.e., $\sigma_{xy}=0$). These conditions are simulated in the design of the APSR cell (Fig. 4) which corresponds to one-half of the unit element containing an inclusion of length, $L/2$. The rear wall of the cell is rigid and lubricated to minimize friction along the centerplane of the unit element. The key design feature of the APSR cell is that the inclusion is clamped externally to a load cell which measures the force in the reinforcement at a location equivalent to the centerline of an inclusion with length, L . In order to maintain the symmetry along the rear wall, a hydraulic piston controls the position of the reinforcement such that there is no displacement of the inclusion at the reference entry point, marked X in Figure 4.

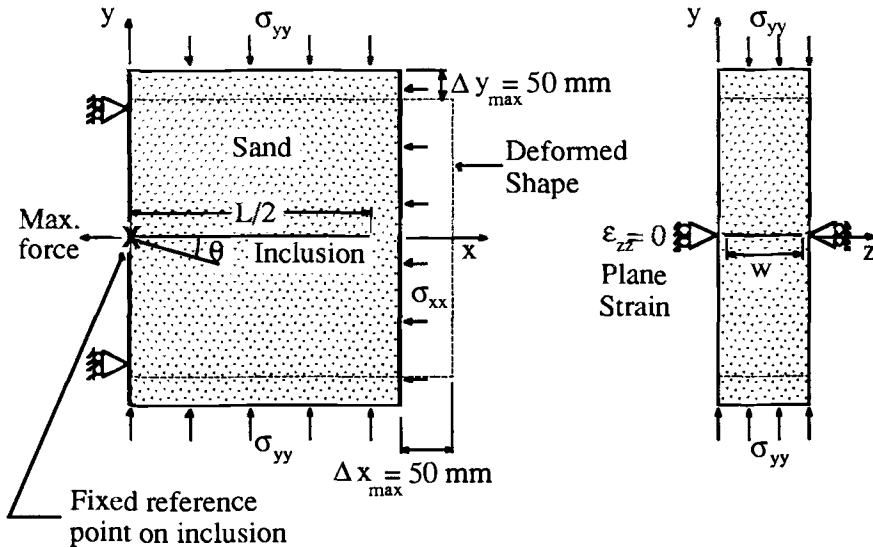


FIG. 4 Schematic diagram of the APSR cell

Figure 5 shows the actual cross-section through the APSR cell. It contains a soil specimen of overall dimensions 570mm high by 450mm wide by 150mm deep (plane strain direction), which is enclosed by a thin rubber membrane. The reinforcing inclusion, with half-length up to $L/2=450\text{mm}$, passes through a slot in the rear wall of the cell and is supported by jacking against an external support arch. The entry slot can be custom designed for inclusions up to 10mm thick. The cell applies air pressure to the outside of the specimen to control the confining stress ($\sigma_3 \leq 50\text{kPa}$), while the major principal stress is imposed through two loading platforms via waterbags which provide uniform boundary tractions. The device can impose relatively large axial strains (up to 10%), which are necessary for investigating load transfer using extensible reinforcements [12], while the specimen is free to deform laterally into the air void at the front of the cell. The plane strain walls of the APSR cell have a unique active control system which ensures that the lateral strains, $\epsilon_{zz} \leq 0.01\%$ throughout the test.

The following paragraphs summarize the principal design features of the APSR cell [11]:

1. The length of the reinforcing inclusion is an important factor in selecting the dimensions for the APSR cell. Shear lag analyses show that maximum load transfer, corresponding to prototype field conditions can be achieved for inclusions with half-lengths, $L/2=1.0$ to 2.0m (cf. Fig. 2). These dimensions cannot readily be achieved in a laboratory test. Instead, the dimensions of the APSR cell have been selected to handle commercially available reinforcing materials including typical geogrids.

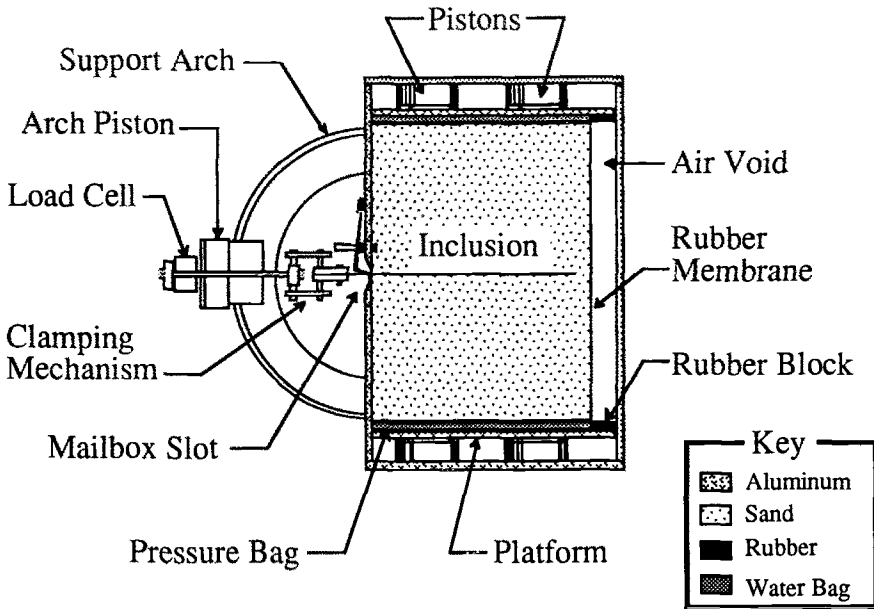


FIG. 5 Section through the APSR cell

Measurements of load transfer obtained for inclusions of different lengths then provide the basis for evaluating tensile stresses at prototype scale.

2. The magnitudes of the applied boundary tractions determine the structural (strong box) design of the APSR cell. The device can apply a major principal stress, $\sigma_1 \leq 500\text{kPa}$ (Fig. 4) through two water bags mounted on moveable rigid platforms. Uniform lateral confinement, $\sigma_3 \leq 50\text{kPa}$ is provided by air pressure acting on the rubber membrane which encloses the soil specimen. All contact surfaces are lubricated with a 50-50 mixture of high vacuum silicon grease and a release agent in order to minimize friction in the system.
3. The cell can impose axial strains of up to 10% on the specimen which are sufficient to cause failure of unreinforced sand specimens and to develop maximum load transfer even for relatively extensible geosynthetic reinforcements. Plane strain conditions are achieved through an active system using a pressurized water diaphragm within the side walls. This novel design reduces significantly the size of the walls that would otherwise be required, and enables remote measurement of the displacements within the specimen using radiography. Radiographic measurements provide a method for establishing the uniformity of strains in the unreinforced soil specimen and can also monitor the mechanisms of soil-reinforcement interaction.
4. The APSR cell is fully automated and includes eight independent, closed, feedback control loops for the displacements of the drive pistons, lateral diaphragm walls, arch support jack and confining air pressure. These are controlled by a single microcomputer and three custom-built, analog feedback circuits. Automation provides great flexibility in test procedures and enables soil specimens to be sheared under conditions of stress or displacement control. These

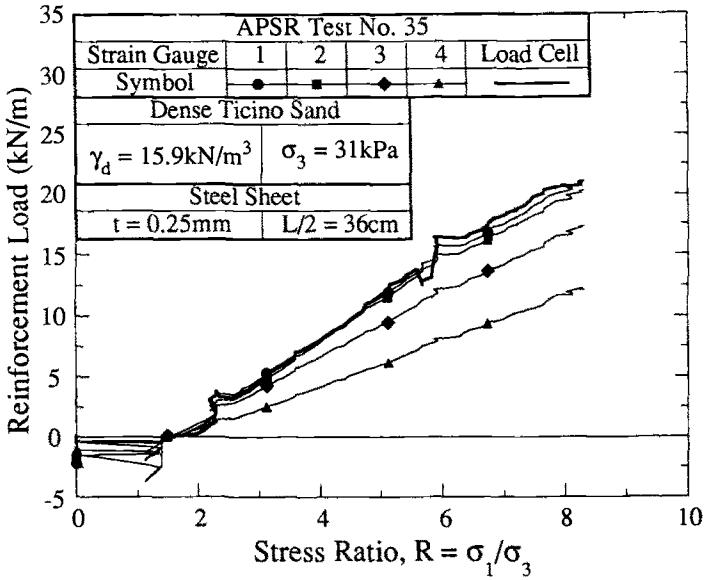
capabilities are particularly useful in measuring load transfer for geosynthetic reinforcements which exhibit significant time dependent properties. Instrumentation for the control of boundary tractions and displacements includes: a) a proximity sensor to monitor the reference position, X (Fig. 4); b) pressure transducers, which measure the hydraulic pressure in the water bags and the confining air pressure; c) displacement transducers, which monitor and control the movement of the platforms and side walls; and d) additional displacement transducers which measure directly the axial and lateral deformations of the specimen.

5. Sand specimens are prepared by raining particles through an assembly of sieves (dry pluviation) in order to achieve specimens of specified target densities which are homogeneous and exhibit repeatable engineering properties. The raining apparatus for the APSR cell comprises a sand hopper with a perforated base mounted on a 1.4m high chimney which contains a series of wire mesh screens. The depositional process also introduces a structure or fabric such that the mechanical properties of the sand are cross-anisotropic. The APSR cell is designed such that the specimen can be deposited along either the z or y axes (Fig. 4). Sand specimens deposited in the z direction initially exhibit isotropic properties for plane strain shearing in the x - y plane, while those formed in the y -direction have cross-anisotropic properties. This important design feature decouples the effects of soil anisotropy in the measurements of load transfer using the APSR cell.
6. The external load cell measures the maximum tensile force in the reinforcement at the reference location X (Fig. 4). Additional instrumentation can be designed to measure local strains and/or stresses at locations along the inclusion for different types of reinforcing material. Deformations within the soil specimen are computed from radiographic measurements of the displacements of tungsten-steel markers embedded in the soil [13].

Larson [11] describes the extensive program of proof tests which have been performed to evaluate the design and performance of the APSR cell. The tests are all performed using dry Ticino sand as the reference soil. The physical and engineering properties of Ticino sand are typical of many natural sands and are well documented in the literature [14]. The sand is deposited along the z -axis of the APSR cell (Fig. 4) with initial relative densities, $D_r=30$ and 75% (loose and dense specimens, respectively). The proof tests have: a) established that the silicon grease lubrication is successful in minimizing wall friction in the APSR cell; and b) refined test procedures such that measurements of stress-strain behavior (for the unreinforced sand) and load transfer for elastic inclusions are repeatable and consistent. The stress-strain-strength properties of the unreinforced Ticino sand, measured in the APSR cell, are in good agreement with results from other plane strain devices reported in the literature [2].

MEASUREMENTS OF LOAD TRANSFER FOR A STEEL SHEET INCLUSION

A comprehensive reference program of load transfer measurements have been obtained in the APSR cell using dense and loose Ticino sand reinforced with two-ply, elastic steel sheet inclusions [11]. All of the tests were performed at a confining stress $\sigma_3=31\text{kPa}$ and include local measurements of the strain distribution within the reinforcement from a series of uniformly spaced, bonded resistance strain gauges which are sandwiched between the two thin steel sheets (each 0.13mm thick).



a) Load cell and strain gauge measurements

b) Load distribution

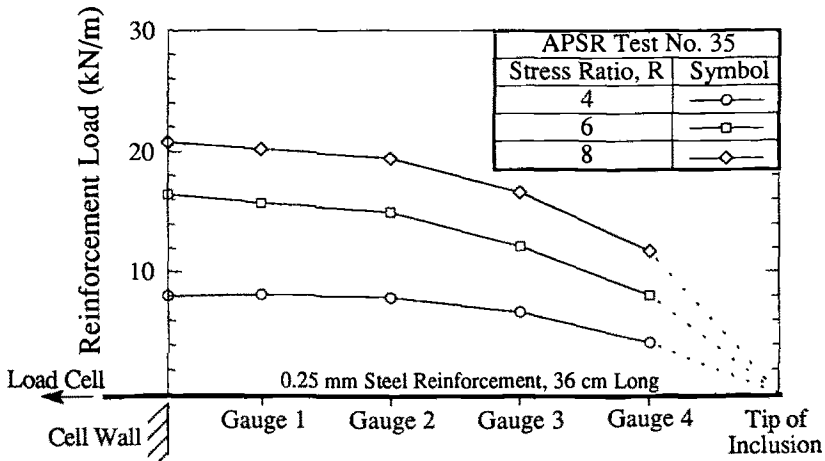


FIG 6. Typical measurements of stresses in a steel sheet inclusion

Uniaxial tension tests were conducted on each of the inclusions to check the performance and calibration of the strain gauges.

Figure 6 shows typical measurements of the reinforcement loads for an inclusion of half-length $L/2=0.36\text{m}$ in dense Ticino sand. The figure reports the reinforcement stresses, measured at the centerline and at

four locations along the inclusion, as functions of the external stress ratio in the soil, $R = \sigma_1 / \sigma_3$. The results show the following:

1. At all locations along the inclusion, the tensile stress is a linear function of the stress ratio, R (for $R \leq 8$, corresponding to a mobilized friction angle, $\phi_{mob} = 51^\circ$).
2. The tensile force accumulates monotonically with distance from the tip of the inclusion and reaches a maximum value at the center of the inclusion.
3. There is minimal development of tensile stresses in the reinforcement for stress ratios, $R \leq 1.4$.

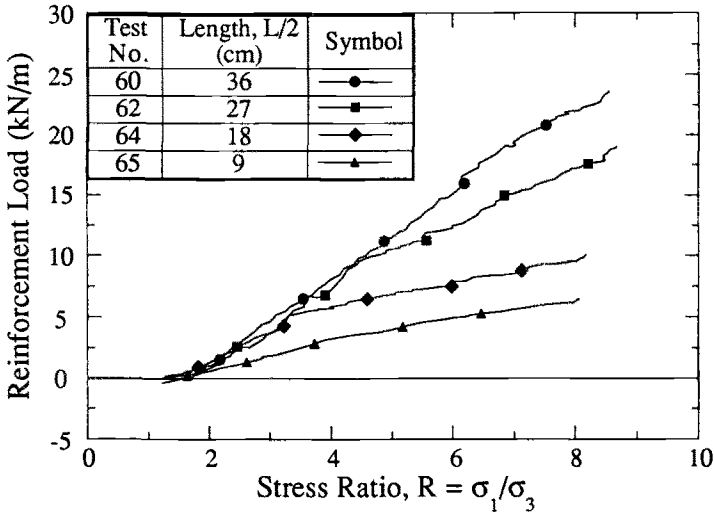


FIG. 7 Effect of inclusion length on maximum tensile force

The steel sheets are relatively inextensible reinforcements ($E_f/G_m = 3.5 \times 10^4$ for dense Ticino sand at $\sigma_3 = 31 \text{ kPa}$) and hence, the shear lag analyses show that maximum load transfer can only be achieved for inclusions with half-length $L/2 \geq 1.5 \text{ m}$. Figure 7 shows APSR measurements of the maximum tensile forces obtained by the external load cell for inclusions which range in length from $L/2 = 9 \text{ cm}$ to 36 cm . These results confirm that the inclusion length has a very significant effect on the tensile stresses transferred to the reinforcement. Although there is some non-linearity in the data (notably in test no. 64, $L/2 = 18 \text{ cm}$), the accumulation of tensile force is approximately a linear function of the applied stress ratio for $R \leq 8$ (i.e., for loading up to peak shear resistance of the soil).

INTERPRETATION OF APSR DATA

Shear lag analyses provide a simple framework for interpreting measurements in the APSR cell at working stress levels. The analytical predictions use elastic material properties determined from plane strain shear tests on the unreinforced sand in the APSR cell, and in-isolation, uniaxial tension tests on the steel sheet inclusion. Figure 8 compares the predicted and measured tensile force distributions for an inclusion

of half-length $L/2=36\text{cm}$ in deposits of both dense and loose Ticino sand at two specified stress ratios. For the dense sand ($\gamma_d=15.9\text{kN/m}^3$; Fig. 8a), the predictions are in very good agreement with the data measured by the external load cell and strain gauges at stress ratios $R=3, 6$ (with a maximum deviation of approximately 15%). Measurements in the loose sand ($\gamma_d=14.3\text{kN/m}^3$; Fig. 8b) show tensile forces which are typically $20\pm 5\%$ smaller than those obtained at the higher density. The shear lag analysis is also in good agreement with these data.

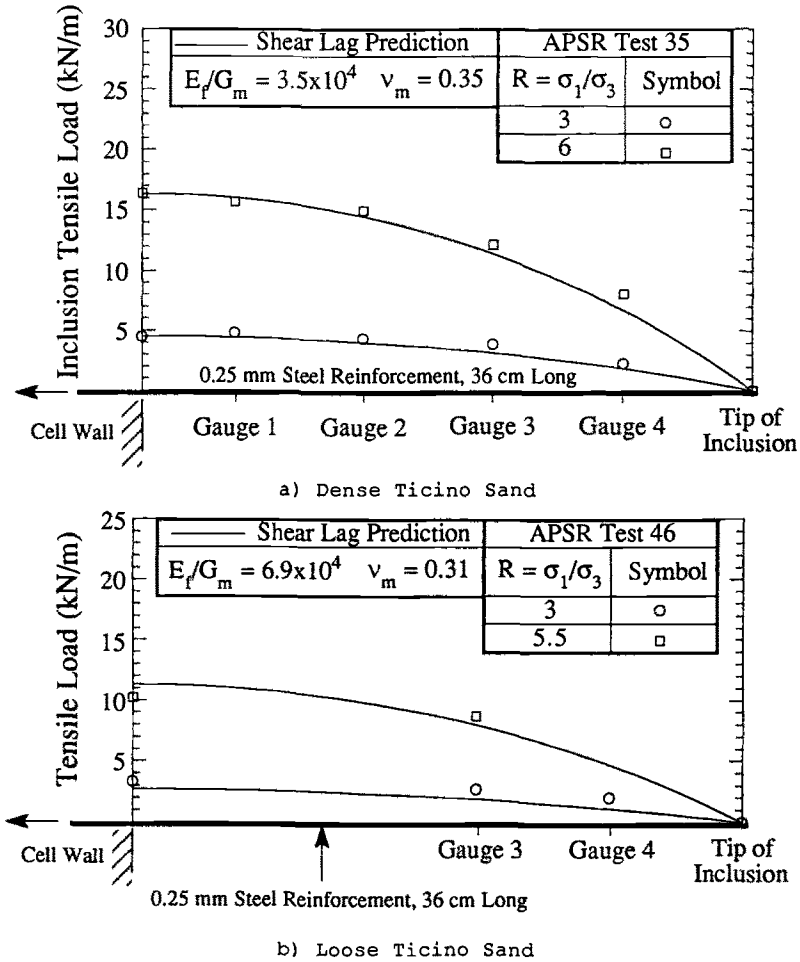


FIG. 8 Comparison of load transfer for a steel sheet inclusion measured in the APSR cell with shear lag predictions

Figure 9 summarizes measurements and predictions of the maximum tensile force at a stress ratio, $R=6$, which show the load transfer as a function of the inclusion length. These results confirm that there is good agreement between the APSR cell data and the shear lag analyses for

an elastic steel sheet inclusion. Load transfer for long reinforcements can be extrapolated using the shear lag framework in conjunction with APSR measurements for a number of short inclusions of different lengths.

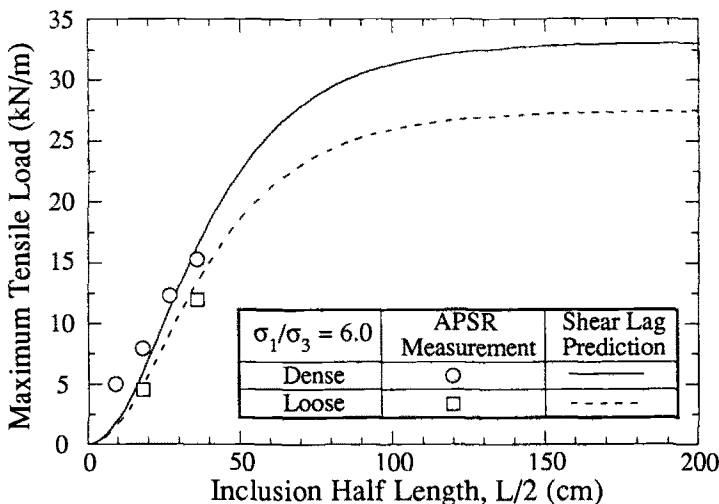


FIG. 9 Evaluation of maximum load transfer

CONCLUSIONS

The Automated Plane Strain Reinforcement cell is a new laboratory device which provides accurate measurements of the load-transfer for a planar reinforcing inclusion as the surrounding soil matrix is deformed in a plane strain compression mode of shearing. The APSR cell applies well controlled uniform boundary tractions and measures directly the major tensile force at the center of the planar inclusion. Simple analytical solutions, based on shear lag analysis, provide a framework for predicting and interpreting measurements in the APSR cell. The paper summarizes the mechanics of soil-reinforcement interaction, using shear lag analyses, and demonstrates how these studies have been applied in the design of the APSR cell. Measurements of tensile stress distributions are reported for elastic steel sheet reinforcements in dry Ticino sand. These data illustrate the importance of the inclusion length on the load-transfer and are in good agreement with shear lag predictions. The APSR cell offers a new experimental capability for evaluating the performance of geosynthetic reinforcing materials at working load levels.

ACKNOWLEDGEMENT

This work was supported by the US Army Research Office through the MIT Program for Advanced Construction Technology.

REFERENCES

- [1] De Buhan, P., Mangiavacchi, R., Nova, R., Pellegrini, G. & Salençon, J. "Yield Design of Reinforced Earth Walls by a Homogenization Method," Géotechnique, Vol. 39, No. 2, 1989, pp. 189-203.
- [2] Schlosser, F. and Long, N.T., Proceedings of the 5th European Conference on Soil Mechanics and Foundation Engineering, Madrid, 1972.
- [3] Fukushima, S., Mochizuki, Y., and Kagawa, K., Proceedings of the International Symposium on Theory and Practice of Earth Reinforcement, Fukuoka, 1988.
- [4] Jewell, R.A. Proceedings of the International Conference on Geotextiles, Geomembranes & Related Products, The Hague, 1990.
- [5] Abramento, M. and Whittle, A.J. "Shear lag analysis of a planar soil reinforcement in plane strain compression", to appear ASCE Journal of Engineering Mechanics, 1992.
- [6] Cox, H.A. "The elasticity and strength of paper and other fibrous materials," British Journal of Applied Physics, Vol. 3, 1952, pp. 72-79.
- [7] Kuhn, P. Stresses in aircraft and shell structures. McGraw-Hill, New York, 1956.
- [8] Budiansky, B., Hutchinson, J.W., and Evans, A.G. "Matrix fracture in fiber-reinforced ceramics," Journal of the Mechanics and Physics of Solids, Vol. 34, No. 2, 1986, pp. 167-189.
- [9] Ladd, C.C., Foott, R., Ishihara, K., Schlosser, F. and Poulos, H.G. Proceedings 9th International Conference on Soil Mechanics and Foundation Engineering, Tokyo, 1977.
- [10] Bolton, M.D. "The strength and dilatancy of sands," Géotechnique, Vol. 36, No. 1, 1986, pp. 65-79.
- [11] Larson, D.G. "A laboratory investigation of load-transfer in reinforced soil," PhD Thesis, MIT, Cambridge, MA., 1992.
- [12] Palmeira, E.M., and Milligan, G.W.E. "Large scale direct shear tests of reinforced soils," Soils and Foundations, Vol. 9, No. 1, 1989, pp. 18-30.
- [13] Arthur, J.R.F. "Industrial radiography in soil mechanics," British Journal of Non-Destructive Testing, Vol. 29, No. 1, 1977, pp. 9-13.
- [14] Baldi, G. et al., Proceedings of the 11th International Conference on Soil Mechanics and Foundation Engineering, AGI Jubilee Volume, 1985.

John P. Ballegeer,¹ and Jonathan T. H. Wu²

INTRINSIC CONFINED AND UNCONFINED LOAD-DEFORMATION PROPERTIES OF GEOTEXTILES

REFERENCE: Ballegeer, J. P. and Wu, J. T. H., "Intrinsic Confined and Unconfined Load-Deformation Properties of Geotextiles," Geosynthetic Soil Reinforcement Testing Procedures, ASTM STP 1190, S. C. Jonathan Cheng, Ed., American Society for Testing and Materials, Philadelphia, 1993.

ABSTRACT: This paper presents intrinsic load-deformation properties of different geotextiles under confined and unconfined conditions. The confined load-deformation properties were determined by a test method (the intrinsic confined test) proposed by Wu (1991) for design and specification of geotextile-reinforced soil structures. The intrinsic confined test has three distinct characteristics: (1) it is an "element" test, thus the load-deformation properties determined from the test are the intrinsic properties of the geotextile; (2) the test measures the confined stiffness and strength of geotextiles without inducing soil-geotextile interface adhesion, thereby simulates the predominant operational condition in geotextile-reinforced soil structures; and (3) the stiffness and strength obtained from the test are conservative values if soil-geotextile interface slippage does occur. A detailed procedure for the intrinsic test method is described. The described method uses only a thin rubber membrane, without soil, for confinement. Four nonwoven geotextiles and one woven geotextile were tested. Discussions of the test results are presented.

KEYWORDS: geotextiles, stress-strain curves, test procedures, confinement, design, soil-geotextile interaction

The load-deformation properties of geotextiles, including their stiffness (modulus) and ultimate strength, employed in the analysis and design of geotextile reinforced soil structures have commonly been obtained from unconfined tests such as the grab tensile test or the strip tensile test (ASTM D-1682), or the wide grip tensile test (ASTM 61-2101). These tests are performed with the geotextile in isolation, where the geotextile is exposed to atmospheric conditions during the test. However, the actual operating conditions for most geotextile applications involve soil confinement pressures.

It has been demonstrated that confinement pressures have a significant influence on the load-deformation characteristics of some

¹GEI Consultants, Inc., Englewood CO 80111;

²Department of Civil Engineering, University of Colorado at Denver, Denver, CO 80217

geotextiles. Several test methods have been developed to determine the load-deformation properties of these geotextiles under a confined condition [1, 2, 3, 4, 5, 6].

The second author presented a critique of the existing confined test methods, including their drawbacks and applicability to the design and analysis of geotextile-reinforced soil structures [7]. He pointed out that nearly all the confined test methods suffered from three serious problems: (1) They are not "element" tests and the measured properties are dependent on the imposed geometric and boundary conditions; (2) Most tests hold the confining soil stationary while the geotextile deforms, simulating a unrealistic condition in which soil-geotextile slippage "must" occur in order for the geotextile to deform; and (3) The measured load-extension properties are on the "unsafe side" in design computations.

A new test (referred to as the intrinsic confined test) for determining the confined load-deformation properties of geotextiles for design and specification of reinforced soil structures has been proposed by the second author [7, 8, 9]. The intrinsic confined test is superior to other confined tests and has the following four distinct characteristics:

- (1) It is an element test (as opposed to a model test), in which the entire geotextile specimen is subjected to uniform straining, thus the measured properties are not significantly affected by the geometric/boundary conditions of the test.
- (2) It measures the stiffness and strength of a geotextile under confined conditions simulating the predominant operational state in geotextile-reinforced soil structures, i.e., the geotextile deforms "with" the confining material.
- (3) The stiffness and strength obtained from the test are conservative values if slippage at the interface does occur in a reinforced structure.
- (4) The measured properties are independent of the confining material type, and are most appropriate for design specifications of pressure-sensitive geotextiles.

Initially, the intrinsic confined tests were performed with a geotextile specimen confined inside a thin soil layer and encased in a rubber membrane. The entire assembly was then subjected to tensile stress. The test method allowed the soil to deform with the geotextile in a compatible manner. The second author indicated that similar conditions of confinement and strain compatibility can be achieved using only a thin rubber membrane without soil as the confining material [7]. This technique simplifies the test method and eliminates the need for corrections required for the tensile resistance of the confining soil. Figure 1 shows the load-deformation relationships of a spun-bonded polypropylene nonwoven geotextile under three different conditions: confined in soil, confined in rubber membrane, and unconfined [8]. The tests in Figure 1 were performed at a constant, 2% per minute, strain rate with specimens having a width-to-length ratio equal to 8. Toyoura sand (a uniform fine sand) was used as the confining soil and a constant confining pressure of 78.5 kN/m² was applied during the confined tests. It is seen that application of the confining pressure using either a rubber membrane or soil as the confining material yields nearly the same results. Test results presented in this paper are from intrinsic confined tests performed using only the thin rubber membrane as the confining material.

18 GEOSYNTHETIC SOIL REINFORCEMENT TESTING PROCEDURES

In this study, four nonwoven geotextiles and one woven geotextile were tested under both confined and unconfined conditions using the intrinsic confined test method. This paper describes in detail the procedure for the load-deformation test and presents the test results and a discussion of the test results.

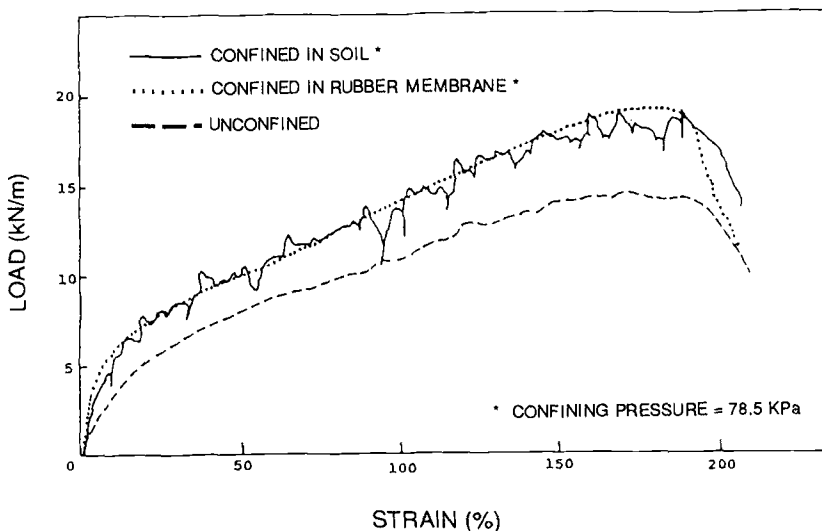


FIG. 1--Load-deformation relationships for a nonwoven geotextile under different confinement conditions [8].

EXPERIMENTAL TESTS

Test Materials--Five geotextiles of different structures and polymer types were selected for testing. Each geotextile was tested under membrane confined and unconfined (in-air) conditions. One geotextile was of woven structure. The other four were nonwoven geotextiles, among which two were needle-punched and two were heat-bonded. Selected index properties of these geotextiles, as provided by the manufacturers, are shown in Table 1.

Specimen Dimensions--Load-deformation testing using geotextile specimens of small aspect ratio (the ratio of width to gage length) may result in significant lateral retraction (i.e., "necking" due to Poisson effect), especially when the strains are large [2,3]. To simulate plane strain conditions typical of field installation of geotextiles, specimens with a high aspect ratio should be used. The aspect ratio required to achieve a near-plane-strain condition is known to differ for different geotextiles; however, an aspect ratio of four(4) is generally considered adequate for most geotextiles.

In this study, an aspect ratio of six(6) was chosen for all specimens tested. Each geotextile specimen was cut into a rectangular

TABLE 1--Geotextile properties

Geotextile Properties	Geotextile A	Geotextile B	Geotextile C	Geotextile D	Geotextile E
Structure	NW,NP	NW,NP	NW,HB	NW,HB	W
Polymer Type	PES	PES	PP	PP	PP
Thickness,mm (ASTM D 1777-64)	2.4	3.2	0.30	0.38	0.51
Mass Per Unit Area,g/m ² (ASTM D 3776-84)	241	339	98	136	136
Grab Tensile/Elongation,kN/% (ASTM D 4632-86)	0.934/60	1.357/60	0.534/60	0.578/50	0.890/15
Wide Width Strength/Elongation Machine Direction, kN/m/% (ASTM D 4595-86)	17.1/65	26.8/74	NA	NA	24.5/12

W = Woven
 NW = Nonwoven
 NP = Needle-punched
 HB = Heat-bonded
 PES = Polyester
 PP = Polypropylene
 NA = Data not available

20 GEOSYNTHETIC SOIL REINFORCEMENT TESTING PROCEDURES

shape approximately 150 mm by 75 mm. After application of the epoxy reinforcement, the "deformable" area of the geotextile specimen (i.e., not reinforced by the epoxy) is approximately 150 mm by 25 mm resulting in an aspect ratio of six(6).

Preparation of Test Specimen--Test specimens were prepared by a procedure involving the following steps:

- Step 1: The geotextile was cut to the desired length and width. The "length" direction was aligned with the direction of testing.
- Step 2: The geotextile specimen was reinforced along two edges with a stiff epoxy (see Figure 2). The stiff epoxy was applied to prevent slippage or tearing of the geotextile within the clamping mechanism which could result in significant error in the load-extension measurements. The epoxy acted as a reinforcement in the clamping mechanism and also as a frame to hold the rubber membrane to be used as confinement. A thick epoxy reinforcement was formed around the geotextile specimen using a mold constructed from high density polyethylene (HDPE). The mold was formed by two sheets of HDPE with the desired shape of the reinforcement or frame cut out of the sheets (see Figure 3). The geotextile specimen was placed between the two sheets of HDPE and the sheets were clamped together onto a flat surface. The cut out shapes were filled with epoxy and the specimen was left overnight to allow the epoxy to completely cure. The epoxy completely enclosed and saturated the edges of the geotextile leaving the internal structure of the fabric fixed. A 25 mm strip of HDPE between the cut out shapes defined the "deformable" area of the geotextile and served to mask that area from the epoxy.
- Step 3: After the epoxy reached full strength, the edges were filed smooth.
- Step 4: Small diameter holes were drilled through the epoxy to match the holes on the clamping mechanism.

Test Apparatus--The test apparatus comprises two brackets and a pair of metal clamps with a series of bolt holes (see Figure 4). The brackets are securely attached to the top and bottom platens of a tensile loading machine.

The brackets are constructed of steel and reinforced with additional steel bars to prevent yielding in the brackets while testing the higher strength geotextiles. The brackets are fastened to the test machine by a threaded connection at the top of the bracket and at the bottom by a larger bracket that fits over the testing machine platen. The brackets are shaped such that the clamps can be quickly and easily installed or removed from the test machine.

The clamps were designed to hold any range of geotextile specimen sizes with widths up to 300 mm. The bolt holes in the clamps are evenly spaced at 25 mm centers to provide a uniform clamping pressure along the entire width of the geotextile specimen. The bolts are recessed into the clamp to allow the clamps to sit symmetrically in the brackets and in line with the axis of the testing machine.

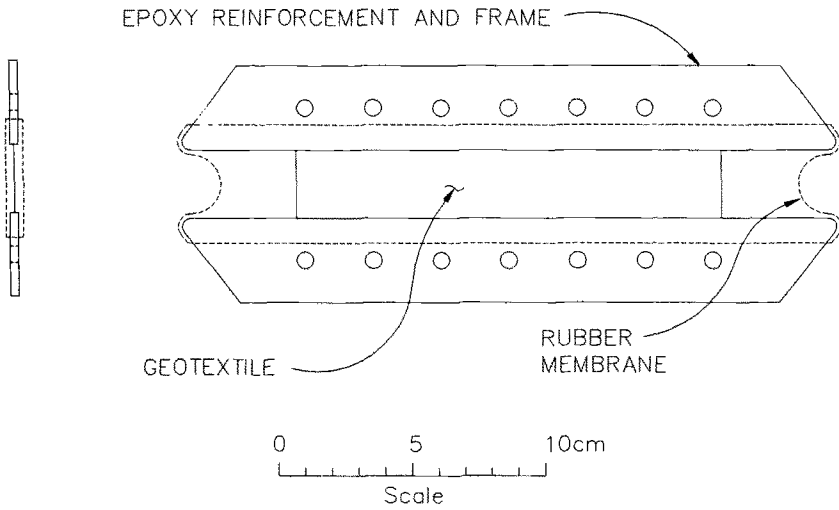


FIG. 2--Schematic of epoxy reinforced geotextile specimen with confining rubber membrane.

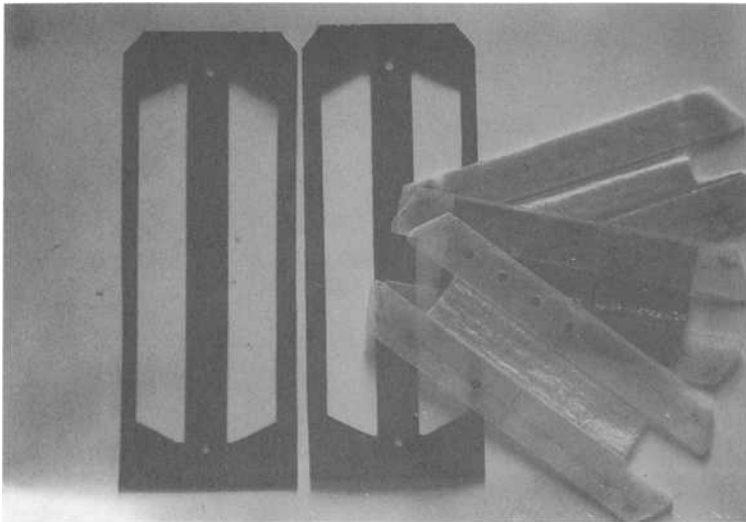


FIG. 3--Epoxy mold and reinforced specimens.

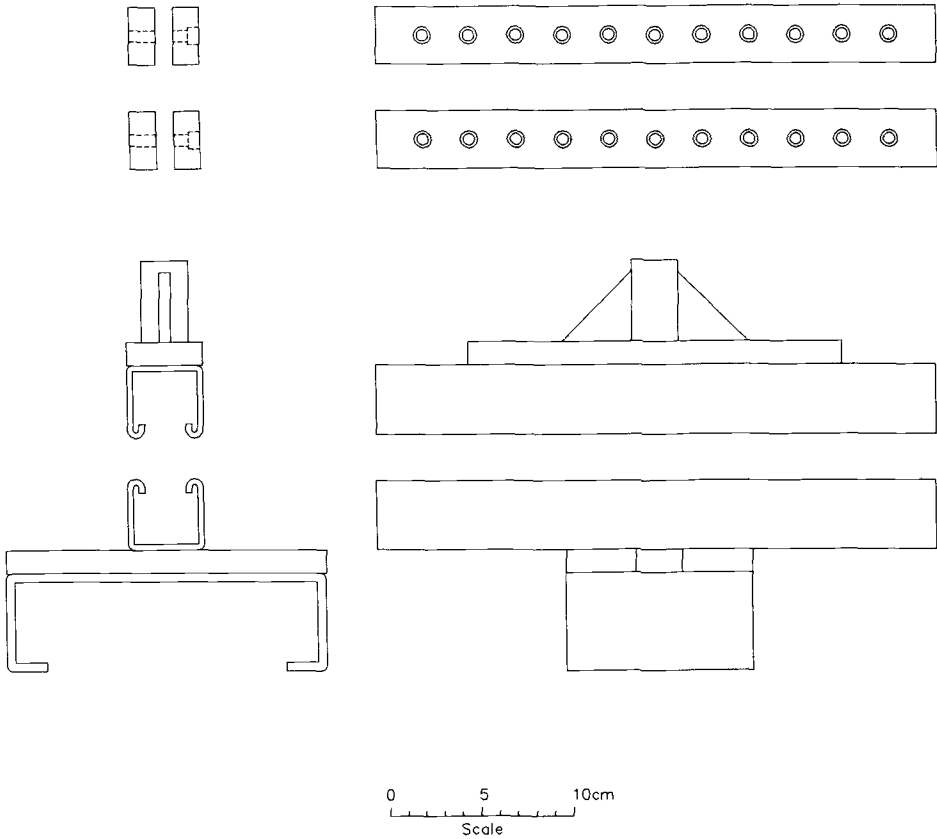


FIG. 4--Schematic of testing apparatus clamps (above) and brackets (below).

Test Procedure--The procedure for the intrinsic confined test method can be described by the following steps:

- Step 1: A rubber membrane is stretched over the epoxy frame enclosing the entire unreinforced area of the geotextile. The specimen is bolted (through the holes in the epoxy) inside a pair of metal clamps creating a seal at the top and bottom of the geotextile along its entire width. The rubber membrane is equipped with a length of nylon tubing for application of vacuum pressures (see Figure 5). The tubing is glued to the membrane at a flange on the end of the tubing. The flange is created by touching the end of the tubing to a heated hot plate and then quickly

touching the melted end to a smooth surface. The membrane can be used repeatedly, but care must be taken not to damage the membrane while inserting and tightening the bolts on the clamps.

- Step 2: The entire assembly of membrane-geotextile-membrane in top and bottom clamps is placed in a tensile testing machine by sliding the clamping mechanism into brackets which are securely attached to the testing machine (Figure 6).
- Step 3: A vacuum pump is connected to the nylon tubing and a vacuum is applied to the membrane-geotextile-membrane assembly.
- Step 4: The geotextile specimen is stressed at a constant rate of strain until failure occurs. Throughout the test, the geotextile specimen is subjected to a uniform confining pressure by maintaining a constant vacuum inside the rubber membrane.

For the unconfined tests, the procedure is identical to that of the confined test except that the geotextile specimen is not subjected to pressure confinement, i.e., Steps 1 and 3 are omitted.

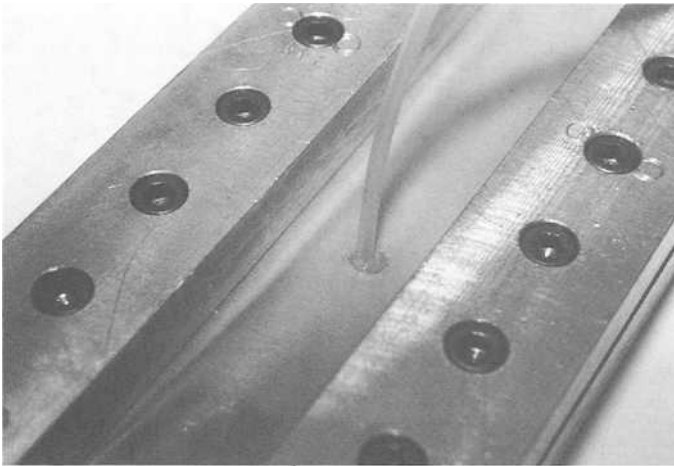


FIG. 5--Rubber membrane with attached vacuum tubing enclosing a geotextile specimen and bolted in clamps.

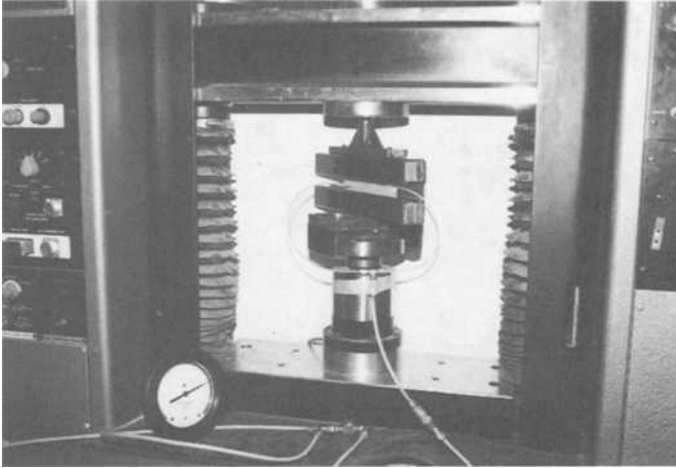


FIG. 6--Geotextile, membrane, and clamps assembled and installed in the testing machine with vacuum applied.

Test Conditions--Each test was performed at a constant rate of extension of two(2) percent per minute. A constant confining pressure of 80 kN/m² was maintained on the specimen by applying a vacuum to the rubber membrane enclosing the geotextile specimen. All the specimens were tested in their roll (machine) direction. Room temperatures and humidity were recorded for each test to determine if major fluctuations had occurred.

TEST RESULTS AND DISCUSSIONS

Load-deformation properties measured by the intrinsic confined test method are highly reproducible, confirming results indicated by Wu in an earlier paper published in the ASTM Geotechnical Testing Journal [7]. The load-deformation relationships for six tests performed on Geotextile A are shown in Figure 7. Three tests each were performed in both confined and unconfined conditions.

Figure 8 shows the variations in confined load-deformation properties for the five geotextiles tested. The curves representing the load-deformation relationships form three distinct groups of geotextiles. Each group is comprised of geotextiles with the same manufacturing process and similar internal structures. Variations

within a group are explained by differences in the geotextile thickness and mass per unit area.

Figures 9A through 9E show the load-deformation relationships for the five geotextiles tested. Each figure contains two curves typical of the tested geotextile under confined and unconfined conditions.

The needle-punched nonwoven geotextiles in Figures 9A and 9B experience a substantial increase in stiffness under confined conditions at low strains. At strains above 5 to 10 percent the curves become somewhat parallel indicating that confinement does not effect the (tangent) stiffness of these geotextiles at large strains.

For heat-bonded nonwoven geotextiles (see Figures 9C and 9D), there is little or no change in the stiffness due to confining pressures at strains smaller than 10 percent. However, at larger strains the confined samples display slightly higher stiffness and strength.

For the woven geotextile shown in Figure 9E. The confinement effect is seen to be very small.

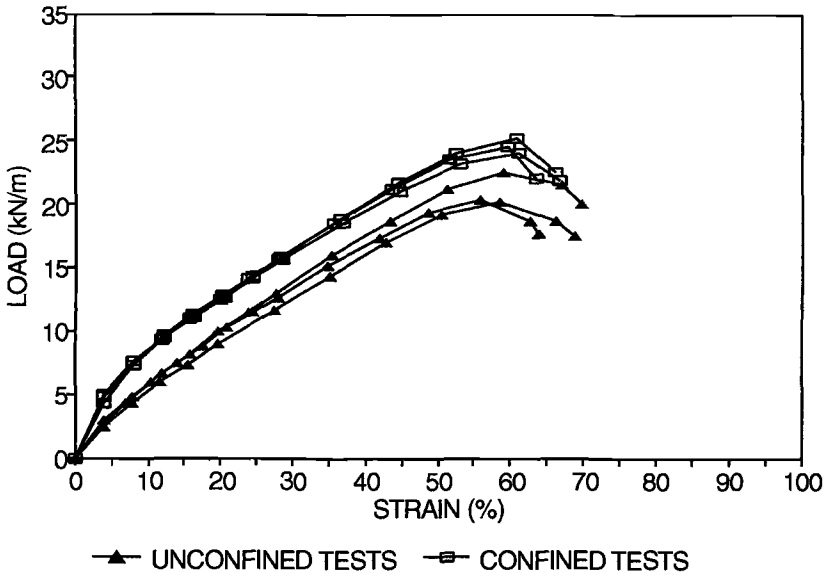


FIG. 7--Load-deformation relationships for six specimens of Geotextile A.

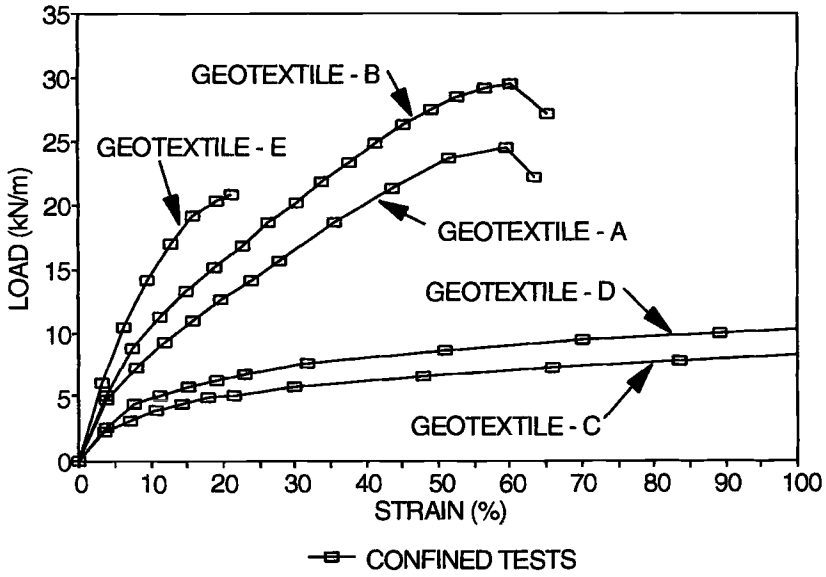


FIG. 8--Typical load-deformation properties for five different geotextiles under confined conditions.

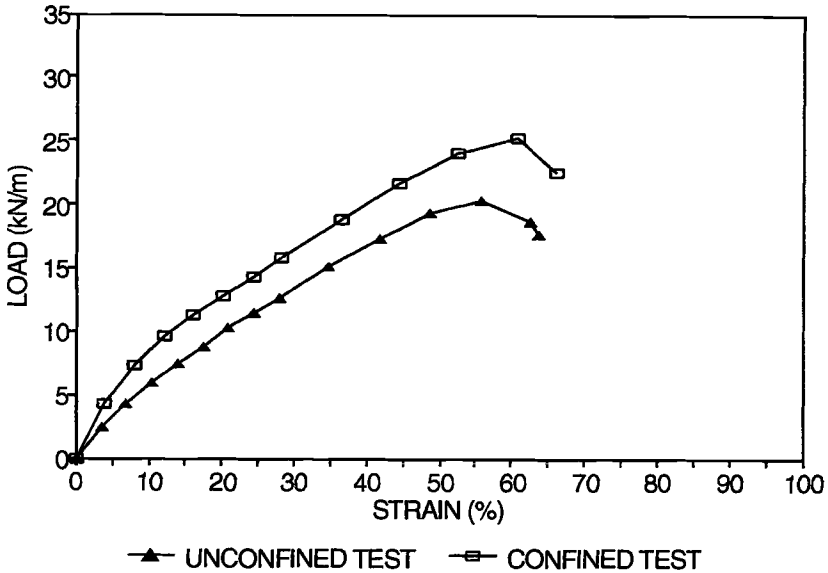


FIG. 9A--Load-deformation properties for Geotextile A, a nonwoven, needle-punched polyester.

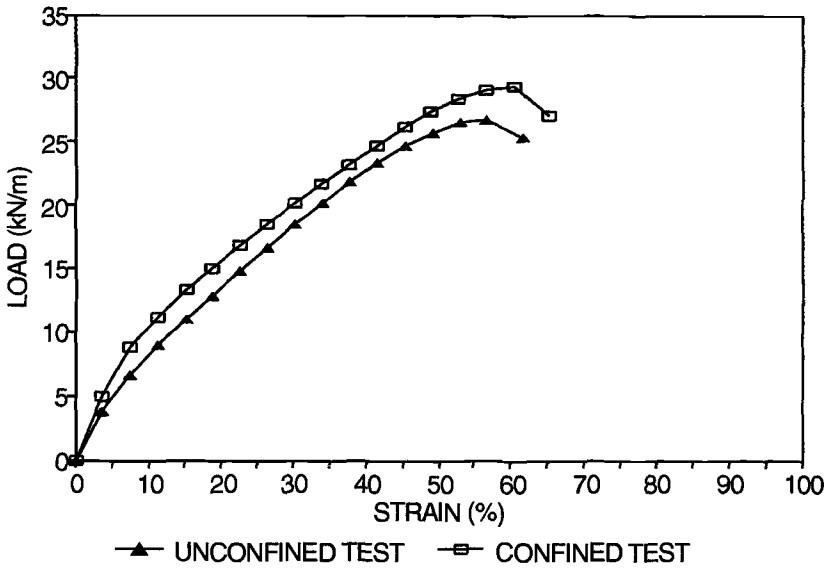


FIG. 9B--Load-deformation properties for Geotextile B, a nonwoven, needle-punched polyester.

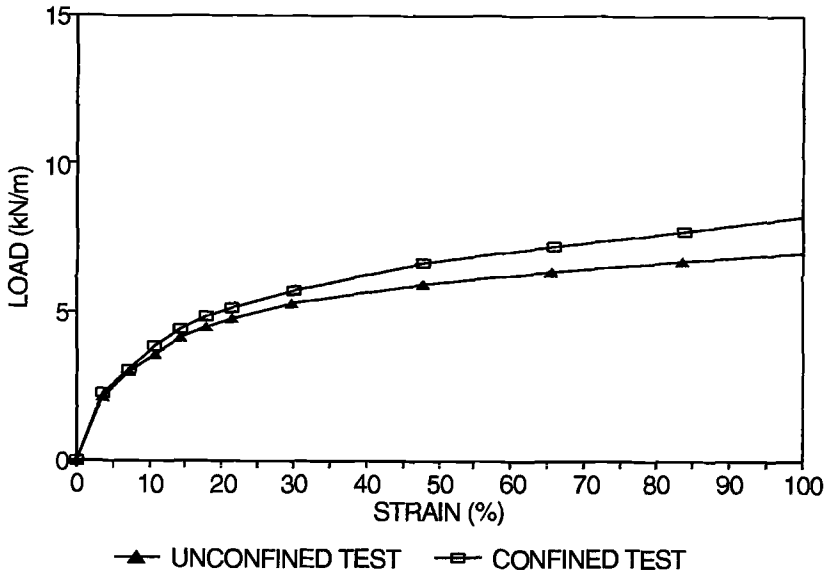


FIG. 9C--Load-deformation properties for Geotextile C, a nonwoven, heat-bonded polypropylene.

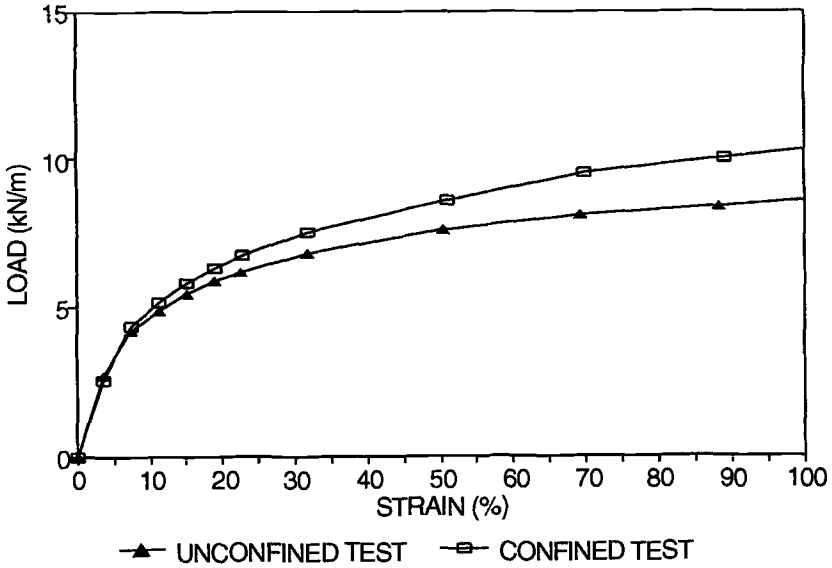


FIG. 9D--Load-deformation properties for Geotextile D, a nonwoven, heat-bonded polypropylene.

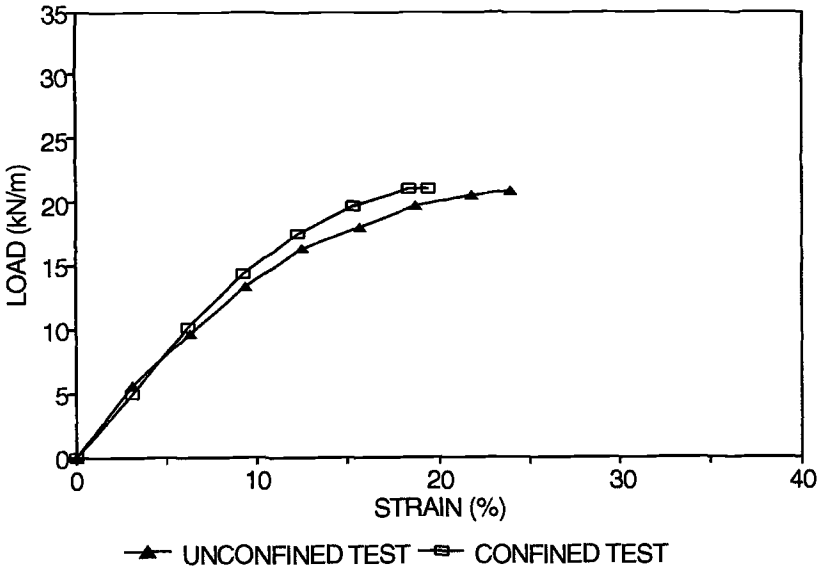


FIG. 9E--Load-deformation properties for Geotextile E, a woven, polypropylene.

Table 2 shows average values for the secant modulus at 5 percent strain and the strength (at failure) for the five geotextiles. The changes in the load-deformation properties due to confinement ranged from almost nil for geotextiles D and E to a 67 percent increase in stiffness for geotextile A.

The nonwoven, needle-punched, polyester geotextiles, A and B (Table 2), displayed the most significant changes resulting from confinement. The confining pressures caused a 67 percent increase in the stiffness and a 17 percent increase in the strength of Geotextile A. The loose internal structure of the needle-punched geotextile explains the dramatic results. Geotextile B displayed a 33 percent increase in stiffness and a 10 percent increase in strength due to confinement. Geotextile B is of the same structure and polymer type as Geotextile A, but Geotextile B is thicker and has more mass per unit area (Table 1).

In contrast, the load-deformation properties of the woven, polypropylene geotextile, geotextile E, displayed little change as a result of confinement. The small decrease in stiffness observed for the confined condition is more the result of variations in the data than changes due to confinement. The strength values for the high strength woven geotextile are masked by failure occurring in the clamping mechanism. At strains greater than 15 percent individual fibers began to pull out of the epoxy reinforcement masking the true load-deformation properties of the geotextile (Table 2).

The nonwoven, heat-bonded, polypropylene geotextiles, C and D, showed little or no change in stiffness, but displayed a slight increase in strength due to confinement (Table 2). Confinement of Geotextile C resulted in a 6 percent increase in the stiffness and over 16 percent increase in the strength. Under confined conditions, Geotextile D showed no increase in stiffness and more than 14 percent increase in strength. This response to confining pressures at small strains may be explained by the internal structure of the geotextiles. The internal structure of the heat-bonded geotextile is essentially confined by the manufacturing process and additional confining pressure produces little change in the already confined geotextile. However, at larger strains the structure of the geotextile has become loosened and the affects of confining pressures are more pronounced. Also, similar to Geotextiles A and B, Geotextiles C and D have the same polymer type and internal structure, but Geotextile D is thicker, has more mass per unit area, and shows less response to confinement pressures (Table 1).

For the design of geotextile-reinforced soil structures with pressure-sensitive geotextiles, one must ascertain the affects of confinement on the geotextile. The load-deformation properties of geotextiles, as affected by pressure confinement, may vary widely for different geotextiles. It is to be noted that the magnitude of the changes due to confining pressures, as revealed by the results of this study, are drastically less than previously suggested [e.g., 1, 3, 4]. Test results obtained by confined test methods other than the intrinsic confined test do not allow the soil to strain compatibly with the geotextile and induce a shear resistance at the soil-geotextile interface, thus greatly exaggerating the stiffness and strength of the geotextile under typical operational conditions.

TABLE 2--Mean values of stiffness and strength for five geotextiles, intrinsic confined and unconfined tests

Geotextile	Stiffness (Sec. Mod. @ 5%) (kN/m)	Strength (Load at failure) (kN/m)
Nonwoven Needle-punched		
Geotextile A (Unconfined)	66	21.1
(Confined)	110	24.6
Geotextile B (Unconfined)	97	26.8
(Confined)	129	29.5
Nonwoven Heat-bonded		
Geotextile C (Unconfined)	48	6.97
(Confined)	51	8.57+
Geotextile D (Unconfined)	65	9.17
(Confined)	65	10.97+
Woven		
Geotextile E (Unconfined)	167	21.0
(Confined)	164	21.1

CONCLUSIONS

The intrinsic confined test provides an efficient and effective means of measuring the intrinsic load-deformation properties of geotextiles under the predominant operational conditions in geotextile-reinforced soil structures. The tests are highly reproducible and the measured properties are superior to other confined tests for purposes of design and specifications.

Test results using the intrinsic confined test method indicate that pressure confinement results in geotextile stiffness increases from nil to 67 percent and geotextile strength increases from 7 to about 30 percent. The strength values for woven, polypropelene geotextiles using the intrinsic confined test method are limited to the bonding strength of the epoxy reinforcement along the edges of the geotextile. Test results obtained by confined test methods other than the intrinsic confined test method include a shear resistance at the soil-geotextile interface, thus greatly exaggerating the stiffness and strength of the geotextile under typical operational conditions.

REFERENCES

- [1] McGown, A., Andrawes, K. Z., and Kabir, M. H., "Load-Extension Testing of Geotextiles Confined In-Soil," Proceedings of the Second International Conference on Geotextiles, Las Vegas, U.S.A., 1982, pp. 793-798.
- [2] Christopher, B. R., Holtz, R. D., and Bell, W. D., "New Tests for Determining the In-Soil Stress-Strain Properties of Geotextiles," Proceedings of the Third International Conference on Geotextiles, Vienna, Austria, 1986, pp. 683-688.
- [3] Siel, B. D., Wu, J. T. H., and Chou, N. S., "In-Soil Stress-Strain Behavior of Geotextile," Proceedings of Geosynthetics '87, New Orleans, U.S.A., 1987, pp. 260-265.
- [4] El-Fermaoui, A. and Nowatzki, E., "Effect of Confining Pressure on Performance of Geotextiles in Soils," Proceedings of the Second International Conference on Geotextiles, Las Vegas, U.S.A., 1982, pp. 799-804.
- [5] Leshchinsky, D. and Field, D. A., "In-Soil Load Elongation, Tensile Strength and Interface Friction of Nonwoven Geotextiles," Proceedings of Geosynthetics '87, New Orleans, U.S.A., 1987, pp. 238-249.
- [6] Kokkalis, A. and Papacharisis, N., "A Simple Laboratory Method to Estimate the In-Soil Behavior of Geotextiles," Geotextiles and Geomembranes, Vol. 8, 1989, pp. 147-157.
- [7] Wu, J. T. H., "Measuring Inherent Load-Extension Properties of Geotextiles for Design of Reinforced Structures," Geotechnical Testing Journal, GTJODJ, Vol. 14, No. 2, June 1991, pp. 157-165.
- [8] Ling, H.I., Wu, J. T. H., and Tatsuoka, F., "Short-Term Strength and Deformation Characteristics of Geotextiles Under Typical Operational Conditions," Geotextiles and Geomembranes, 1992, pp. 185-219.
- [9] Wu, J. T. H. and Arabian, V., "New Tests for Determining In-Soil Stress-Strain Properties of Geotextiles," Geotechnical Engineering Report, CU-Denver, 1988.

Richard J. Bathurst¹ and Michael R. Simac²

Laboratory Testing of Modular Masonry Concrete Block-Geogrid Facing Connections

REFERENCE: Bathurst, R. J., "Laboratory Testing of Modular Masonry Concrete Block-Geogrid Facing Connections," Geosynthetic Soil Reinforcement Testing Procedures, ASTM STP 1190, S. C. Jonathan Cheng, Ed., American Society for Testing and Materials, Philadelphia, 1993.

ABSTRACT: This paper describes a laboratory apparatus and test procedure that was developed by the authors to quantify the mechanical behavior of the connection between mortarless modular concrete block units and geogrid reinforcement materials. The paper illustrates that the tests should be carried out with 1-m wide samples of geogrid reinforcement in order to account for the influence of block joints and surface geometry irregularities that occur along the length of typical geogrid-reinforced concrete block walls. This paper gives recommendations for a 20 mm/min rate of loading. The interpretation of connection strength and efficiency for modular block-geogrid reinforcement connection systems is related to conventional index strengths that are routinely reported in the literature based on the ASTM D 4595 method of test.

KEYWORDS: geosynthetic testing, masonry concrete, geogrid modular block, geosynthetic reinforcement, connections

The use of modular masonry concrete block facing systems in geosynthetic-reinforced soil retaining wall structures has gained great popularity in recent years. The majority of these structures have been built using polymeric geogrid materials as the geosynthetic reinforcement. The reinforcement layers are placed between the masonry units to form an essentially frictional connection (for example, [1-3]).

Conventional design and analysis methods such as those recommended in guide-lines published by AASHTO [4, 5], the Federal Highways Administration [6] and the National Concrete Masonry

¹Professor, Civil Engineering Department, Royal Military College of Canada, Kingston, Ontario K7K 5L0.

²Principal, Earth Improvement Technologies, 100 Mayflower Court, Cramerton, NC 28032.

Association (NCMA) [7],[8] recognize that the internal stability of the reinforced soil wall structure may be controlled by the mechanical performance of the modular unit-geosynthetic reinforcement connection. However, the load-deformation properties of the connection can only be quantified by full-scale laboratory connection testing. The tensile load-deformation properties are influenced by: a) geometry and type of geosynthetic-facing unit interface (i.e. continuous keys, lips, dowels or pins), b) quality of the concrete, c) whether the facing units are hollow or solid, d) whether the hollow core is left empty or infilled with a granular soil, e) tolerances on block dimensions, f) quality of construction and, g) thickness, structure and polymer type of the geosynthetic amongst other factors.

At the Royal Military College (RMC) of Canada a large-scale apparatus has been constructed that allows connections up to 1m in width to be tested under simulated wall heights as great as 10m. The test apparatus allows geotextile and geogrid reinforcement materials to be used. However, this Paper is restricted to the experience gained from the testing of geogrid reinforcement products since they are currently the most common geosynthetic reinforcement used in modular concrete wall systems in North America. Approximately a dozen different types of modular blocks in combination with several different rigid and flexible geogrids have been tested over a period of two years using the equipment and procedures described in this Paper. In addition, full scale wire basket and polymeric geocell facing connections have also been evaluated for actual field structures.

At the time of this investigation there was only one specification for the testing of modular concrete-geosynthetic connections (Test Method GS-8) published by the Geotechnical Research Institute (GRI) [9]. The test method described in this Paper together with test results shows that there are some potential shortcomings in the current GRI standard [9] with respect to: rate of loading; interpretation of test results; definition of connection efficiency; and the influence of narrow modular block-geogrid fascia systems on measured connection strengths. Recently, the method of test reported in this Paper has been adopted by the NCMA as the protocol for concrete block-geosynthetic facing connection testing [7].

EXPERIMENTAL METHOD

Test Apparatus

The test apparatus that has been developed for connection testing is illustrated on **Fig.1**. The test apparatus allows tensile loads to be applied to the geogrid while it is confined between two dry stacked masonry concrete unit layers. The concrete units are laterally restrained and surcharged vertically. The wall sections are constructed using the technique that is anticipated in the field. Variable connection depths with respect to the crest of a wall are simulated by applying a surcharge load using the vertically-oriented hydraulic jack shown in the figure. The pullout force is applied at a constant rate of displacement using a computer-controlled hydraulic actuator. The hydraulic actuator has a capacity that is at least equal to the rated tensile strength of the reinforcement based on the ASTM Test Method for Tensile Properties of Geotextiles by the Wide-Width Strip Method (D 4595) [10]. The present configuration comprises a MTS actuator rated at 50 kN capacity and it has proven adequate for most reinforcement materials tested by the authors to date.

Test Procedure

A bottom row of modular block units is placed so that the interface elevation is coincident with the horizontal axis of the hydraulic actuator. Next, a strip of geogrid reinforcement 1000mm wide is attached to a rigid thick-walled 200mm diameter roller clamp and the reinforcement extended to the front of the interface between fascia units. The construction technique that is to be used in the field is adopted in the preparation of the simulated wall sections. For example, some block systems are constructed with dowels or clips to maintain wall alignment and in some systems the units are infilled with a compacted granular infill [7]. Similarly, the geogrid sample is trimmed to sufficient length to cover the entire toe to heel width of the bottom course of fascia units to conform to recommended construction practice in the field. For facing unit systems that include vertical dowels, the dowels can be used to anchor the geogrid reinforcement during laying out.

Two wire-line extensometers are connected to a bar clamp (two 15mm wide aluminium strips) that is in turn lightly clamped onto the geogrid reinforcement to measure reinforcement displacements immediately at the back of the facing units. The extensometers are mounted approximately 350mm apart and equidistant from the center of loading in order to measure the average reinforce-

LEGEND

- | | | |
|--------------------------|------------------------------|---|
| 1 masonry concrete block | 6 lateral restraining system | 11 spacers |
| 2 geogrid | 7 guide rail | 12 platform |
| 3 loading platen | 8 extensometer clamp | 13 wire-line extensometer |
| 4 gum rubber mat | 9 surcharge actuator | 14 computer-controlled hydraulic actuator |
| 5 roller clamp | 10 loading frame | 15 load cell |

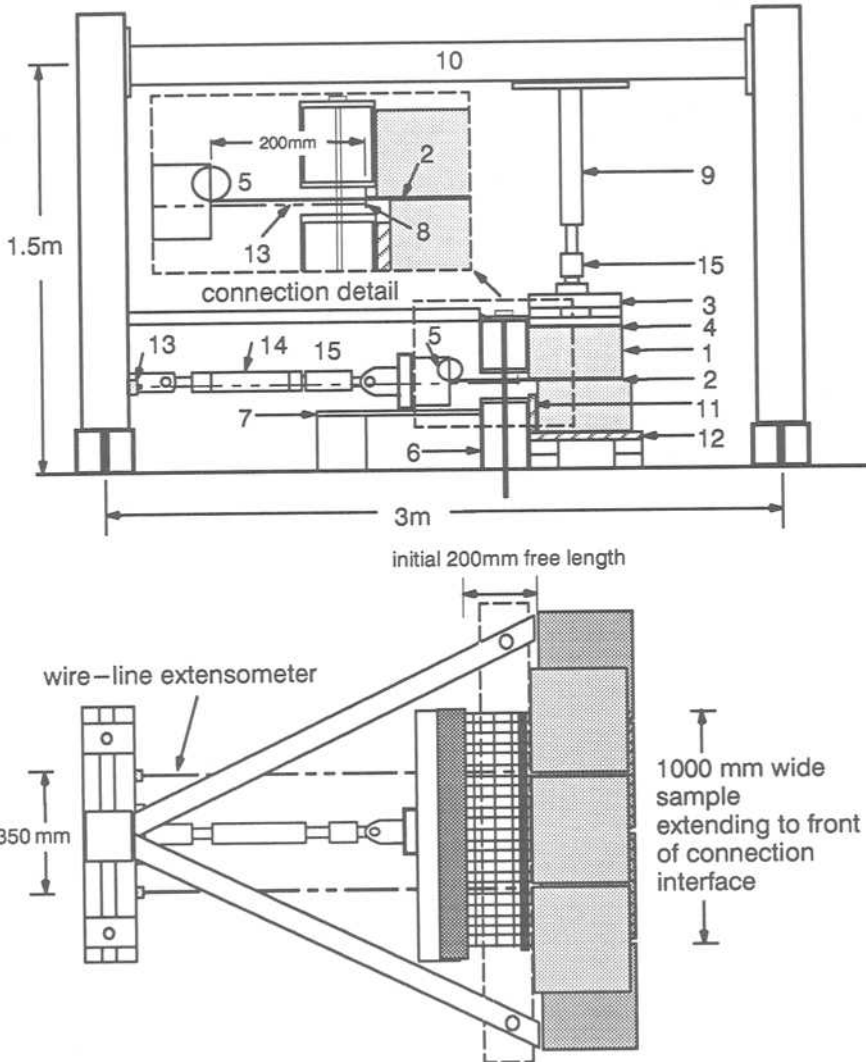


FIG. 1-- Schematic of pullout test apparatus showing typical masonry concrete block units and geogrid reinforcement

ment displacement during the test. The free length of reinforcement between the roller clamp and extensometer bar clamp is 200mm.

A single layer of concrete units is placed over the connection interface. A heavy rigid steel box and plate section is used to transfer the vertical surcharge load to the top row of modular blocks. To ensure an even distribution of load to each concrete block unit a stiff gum rubber mat is placed between the loading platen and masonry units. The vertical actuator is charged using a hand-operated hydraulic pump and has a capacity sufficient to simulate wall heights up to 10m above the elevation of the connection. An electronic load cell is attached to the vertical actuator piston to control applied surcharge loads. The loading platen arrangement was found to give a more uniform distribution of interface vertical pressure than a system using a pyramid-shaped stack of concrete blocks. Small variations in the dimensions of concrete blocks that are typical of dry cast units will result in uneven load distribution when the units are stacked in a pyramid shape over the connection.

The tensile load in the reinforcement is measured by a load cell located between the roller clamp and actuator piston. The MTS actuator comes equipped with an internal LVDT that can be used to measure displacements at the roller clamp. The load and displacements measured by the internal LVDT and wire-line extensometers are recorded continuously during the test using a micro-computer/data acquisition system operating under MS-DOS. Custom software developed by the first author is used to control the actuator in constant rate of displacement mode (i.e. 20mm/min) and to give a real-time screen output of the test results.

Prior to the start of loading the actuator position is adjusted to ensure that the any slackness in the free length of reinforcement is removed. Each test is continued until there is a sustained loss in connection capacity. Failure may be due to: a) pullout of the reinforcement through the interface, b) rupture of the reinforcement, c) failure of the concrete units or, d) any combination of these mechanisms. Following each test, the concrete units are removed and the reinforcement examined to confirm failure modes. A virgin sample of reinforcement is used for each test and damaged concrete units are replaced.

Interpretation of Test Results

The typical variable in a test series is the magnitude of surcharge load (normal stress) applied to the connection interface. The surcharge pressures used in a series of connection

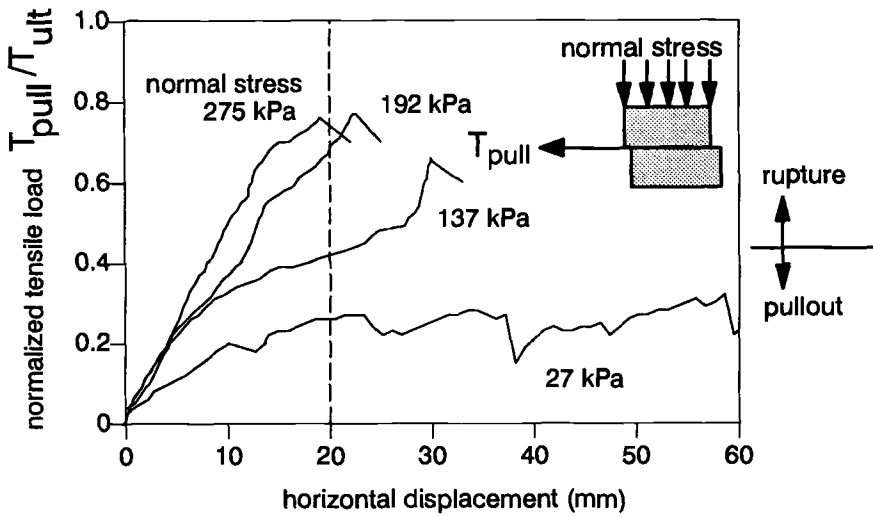
tests are selected to cover the range of equivalent connection elevations in the proposed wall design. The connection load in kN/m of sample is plotted against average reinforcement displacement (mm) recorded by the wire-line extensometers. A typical set of normalized load-displacement curves is illustrated on **Fig. 2**. (All connection tensile load values in this Paper have been normalized with respect to the ultimate tensile strength T_{ult} (ASTM D 4595) to prevent identification of the geogrid products that have been used for illustration purposes). If insufficient slack was removed from any sample prior to the start of loading it may be necessary to shift the data curve so that the origin of the curves represents reinforcement load take up. A pre-load of 0.25 kN/m is often sufficient to take the slack out of the connection. The maximum connection load and the tensile load recorded after 20mm of deformation are identified on each curve. The results from a series of tests are presented as connection strength (T_{conn}) versus normal stress envelopes that capture the trend in the data. It is often more useful for design purposes to present the results on a plot of normalized connection strength (T_{conn}/T_{ult}) versus equivalent depth of connection below the wall crest (**Fig. 3**). As before, normalization is carried out with respect to the ultimate tensile strength (T_{ult}) of the reinforcement (ASTM D 4595). The experience of the authors has been that, regardless of the choice of axes, the trend in the data is best represented by a linear or bi-linear curve with each segment of the curve established using a standard first-order linear regression. The magnitude of the ratio T_{conn}/T_{ult} provides the designer with a practical relative measure of the efficiency of the connection system that can be used to trace the efficiency of the connection with wall elevation and to compare the efficiency of different connection systems. Ideally, the best connection detail would be one that achieves the index strength (ASTM D 4595). However, a large amount of test data collected by the authors shows that this is seldom the case, particularly at low surcharge pressures (e.g. **Fig. 3**).

DISCUSSION

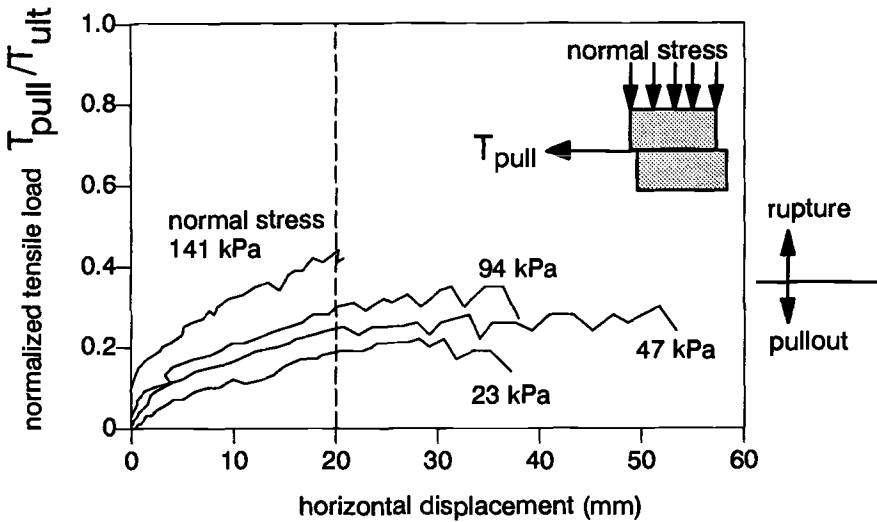
Development of the Method of Test

A number of important considerations were addressed during the development of the test apparatus, procedures and interpretation of results described above.

Reinforcement Sample Width-- The 1m wide sample adopted in our test procedure has proven necessary to ensure that the rein-



a) Strong uniaxial polyethylene geogrid in combination with solid masonry concrete units (2m long) constructed with continuous concrete key



b) Weak uniaxial woven polyester geogrid in combination with hollow masonry concrete units (300mm long) infilled with crushed stone

FIG. 2— Typical normalized load–displacement curves

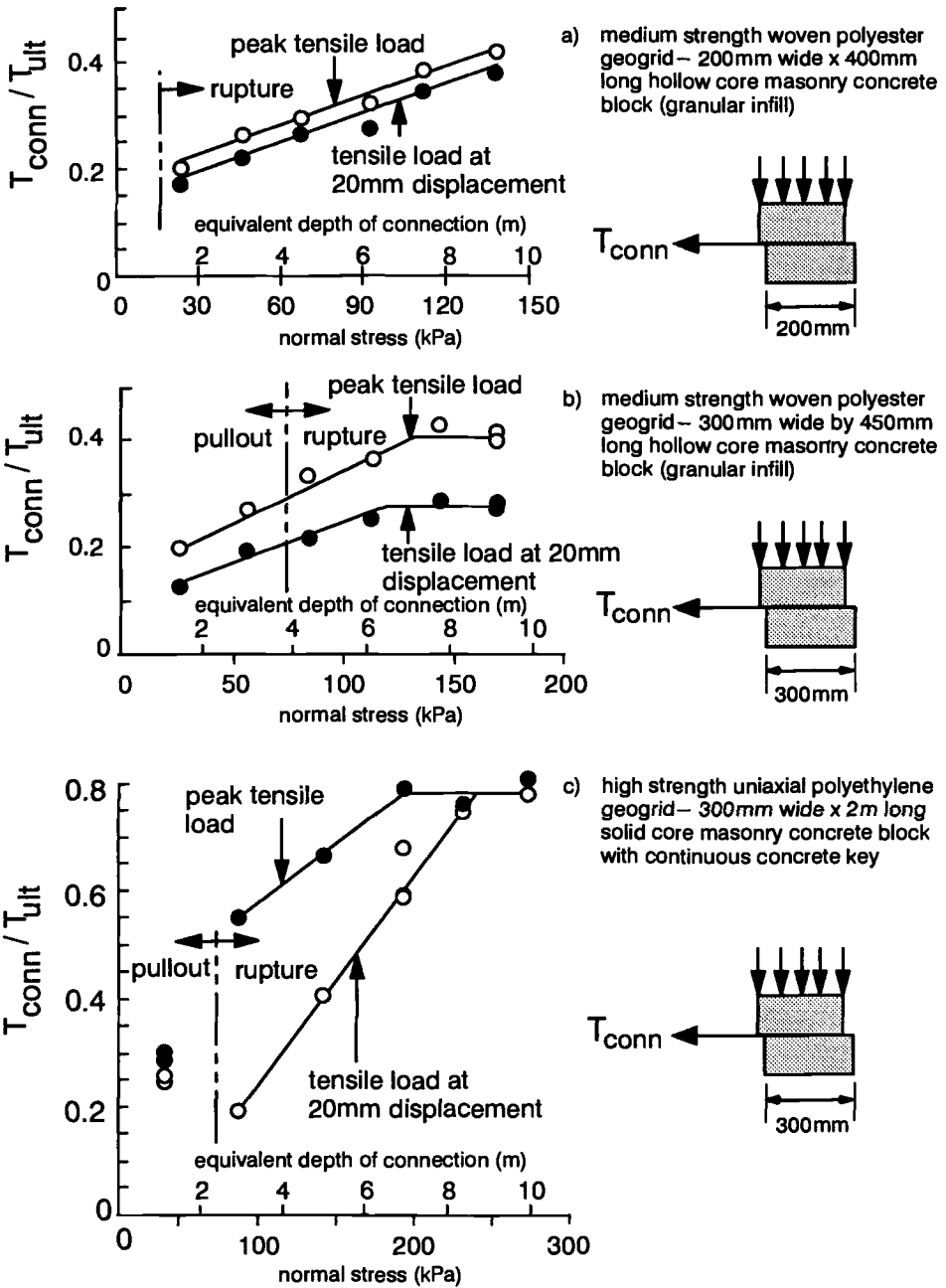


FIG. 3— Example normalized connection strength curves

forcement covers a reasonable number of vertical joints between block units. The majority of block units available in the market at the time of writing are 200 to 450mm in length (i.e. measured perpendicular to the direction of pull). The irregularities in the interface surface geometry that are introduced by the joints, edges, corners and small variations in dimensions between units have a major influence on the magnitude of tensile capacity available at the connection. The influence of sample width on nominal identical test configurations is illustrated on **Fig. 4** for typical dry cast masonry concrete units in combination with three different woven polyester geogrids. The figure illustrates that tensile capacities based on either a displacement criterion of 20mm or peak load using a single stack of blocks may be 200% greater than for the identical system constructed with 1m wide courses (i.e. 5 blocks and 4 running joints). The current GRI method of test [9] recommends a sample width of 200mm or the dimension of the facing element perpendicular to the direction of pull, whichever is less. Our results show that this standard would greatly over-estimate facing connection strengths for the example connections described here.

Free Length of Reinforcement and Rate of Loading-- The 200mm free length of reinforcement was chosen as a compromise between the need to allow for a uniform pull across the connection and the need to minimize the required stroke of the actuator. The rate of loading was selected to match the 10% axial strain/min rate recommended in the ASTM D 4595 method of test. Consequently, the connection capacity based on either a peak capacity or displacement criterion can be compared fairly against index values that are used routinely as a reference strength in current methods of analysis for geosynthetic reinforced-soil wall systems (e.g. [4],[5],[6]). Essentially, the connection test method that has been developed at RMC can be thought of as the standard in-isolation tensile test performed with one set of poor clamps (i.e. the block-geosynthetic connection). Similarity between index and connection tests also extends to temperature and humidity since the ambient conditions in the RMC laboratory are within the values recommended in ASTM D 4595.

The influence of rate of loading was investigated during the development of the test apparatus. The results of these tests are summarized on **Fig. 5**. The 10% loading rate is equivalent to that recommended in ASTM D 4595 and is taken with respect to the initial 200mm free length of reinforcement. The tests were carried out with 300mm wide x 2m long solid concrete units constructed with a continuous concrete key. This unit was selected in order to eliminate the influence of masonry unit joints on connection performance. The reference strengths (T_{ult}) were

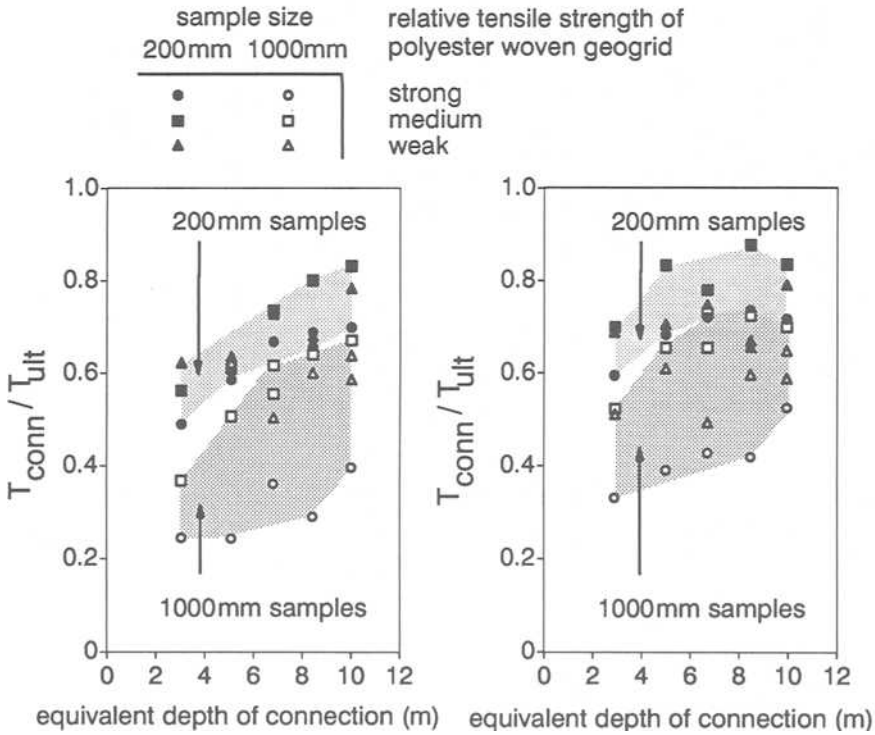
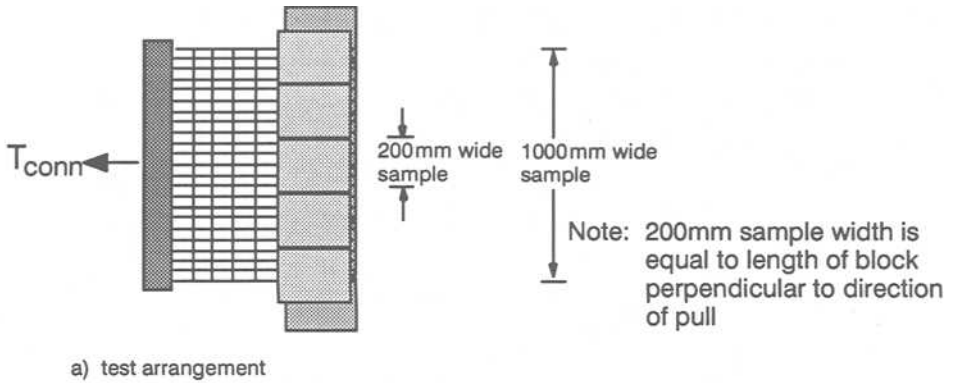


FIG. 4-- Influence of sample size on connection strength

- (1) 300mm wide x 2m long solid concrete block with continuous concrete key
- (2) normal stress = 190kPa (7m connection depth)
- (3) 1000mm wide sample ±10% scatter band

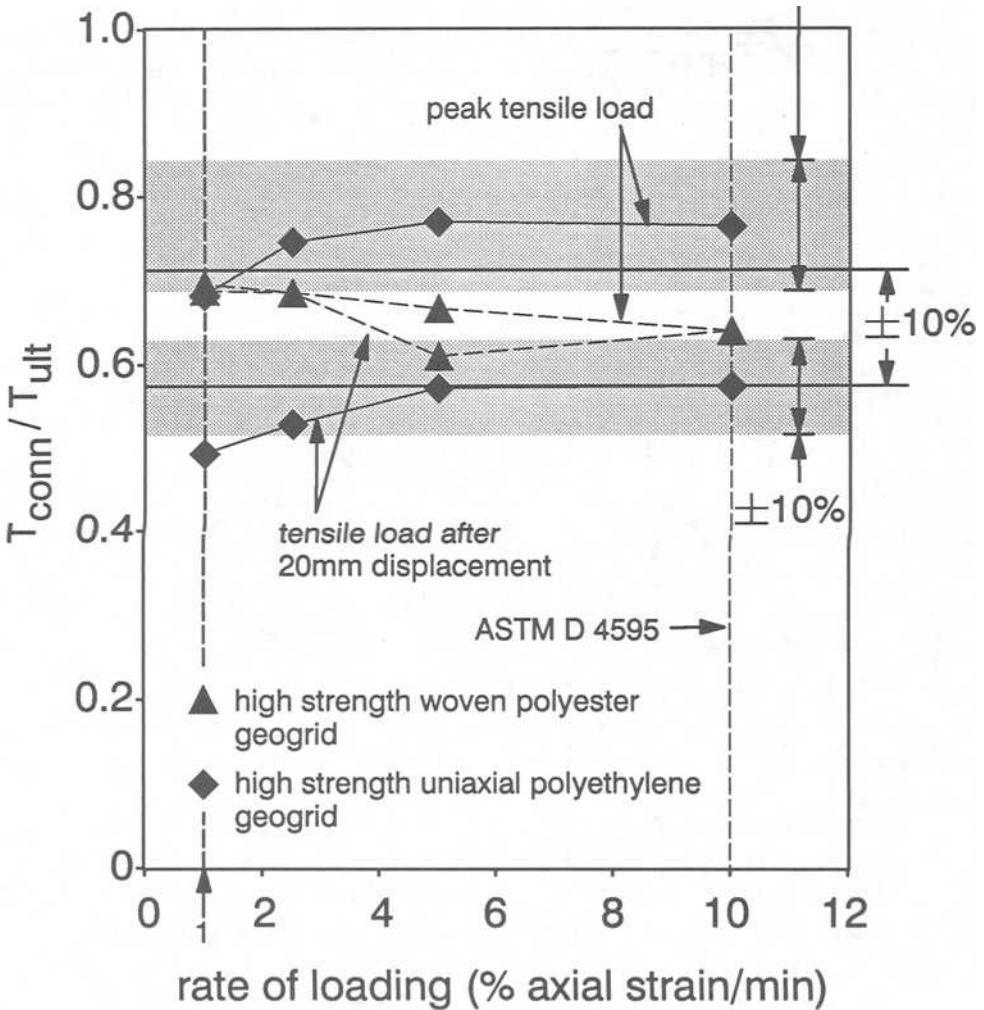


FIG. 5 -- Influence of rate of loading on connection strength

established from independent laboratory tests carried out at RMC on representative samples of the geogrid materials using the ASTM D 4595 method of test. Within experimental error (see section on test repeatability) the values for connection strength for the polyester grid connections are sensibly constant over the practical range of displacement rates investigated. For the polyethylene grid samples the connection strengths were observed to fall outside of the 10% scatter band for samples tested at 1% strain/min. Based on these limited results and the practical benefit of relating the connection test results to a widely accepted index strength test protocol, the authors recommend that the tests be carried out at the equivalent strain rate of 10% recommended in ASTM D 4595. The current recommendation of 1mm/min in the GRI Test Method GS-8 [2] is equivalent to an axial strain rate of 0.2% strain/min which is significantly slower than the reference in-isolation test (ASTM D 4595). As the trend in the data for the polyethylene grid samples in **Fig. 5** suggests, the calculation of connection efficiency based on tests carried out at strain rates that differ by a factor of 50 may be misleading.

Displacement Criterion-- The 20mm displacement (serviceability) criterion for the interpretation of connection capacity was chosen to be compliant with recommendations currently found in AASHTO guidelines [4], [5] related to pullout of geosynthetic reinforcement from within soil. Conventional practice is to apply this pullout criterion to the geosynthetic-facing connection performance to ensure that design connection capacity is not developed at the expense of unacceptable wall movement. As experience with modular block-geosynthetic reinforced soil wall structures increases, other displacement criteria may apply. A displacement criterion is currently not included in the GRI Test Method GS-8 [2].

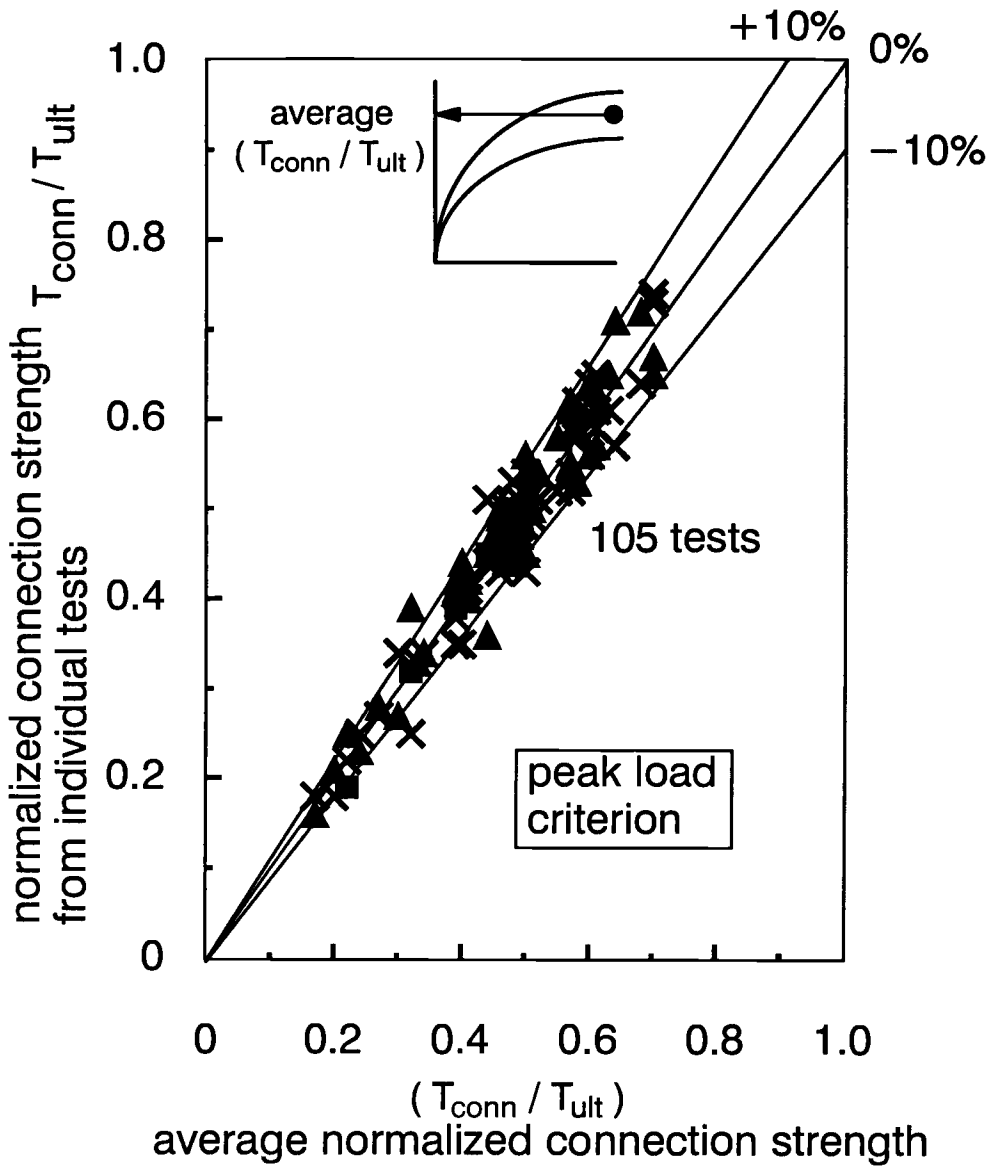
Test Repeatability-- Variability in test results can be anticipated for nominal identical connection tests as a result of small variations in test setup, variations in the dimensions of masonry concrete units and laying out of the reinforcement. In addition, the connection capacity is sensitive to the quality of infill placement and compaction in the case of hollow core units. To investigate variability in test results the connection strengths from all repeat tests catalogued by the authors to date have been summarized on **Fig. 6a, 6b**. The data shows that the method of test using our test equipment and procedures results in calculated strengths that are typically within $\pm 10\%$ of the average of nominal identical tests. Based on this data the test method appears to give an acceptable degree of test repeatability. Recently, the essential features of the test procedure described in this Paper have been adopted by the NCMA. In the NCMA

method of test, a minimum of three repeat tests are required in a test series in order to establish anticipated variation in test results [7].

Magnitude of Surcharging-- The results of more than 500 pullout connection tests carried out by the authors using a large number of masonry concrete unit types and geogrid reinforcement products has shown that the tests must be carried out over the full range of equivalent connection elevations anticipated for the wall in the field. The data in **Fig. 3b, 3c** illustrate that the trend in connection capacity for some block-geogrid combinations carried out with a maximum surcharge equivalent to a 6m deep connection may greatly over-estimate the connection strength at greater depths below the crest of the wall if the data is simply extrapolated. A possible explanation for the bi-linear trend in the data is that the geogrid reinforcement suffers mechanical damage when placed between concrete block units, particularly after large surcharge pressures have been applied. Mechanical damage to the geogrid occurs as a result of (typically) rough concrete surfaces, irregularities in unit dimensions, joints between the blocks, and sharp edges. These conditions lead to pinching and crushing of the reinforcement during construction and result in uneven load transfer within the connection. The initial mechanical damage increases at higher confining pressures and prevents the further increase in connection capacity with depth that might otherwise be anticipated for an essentially frictional connection.

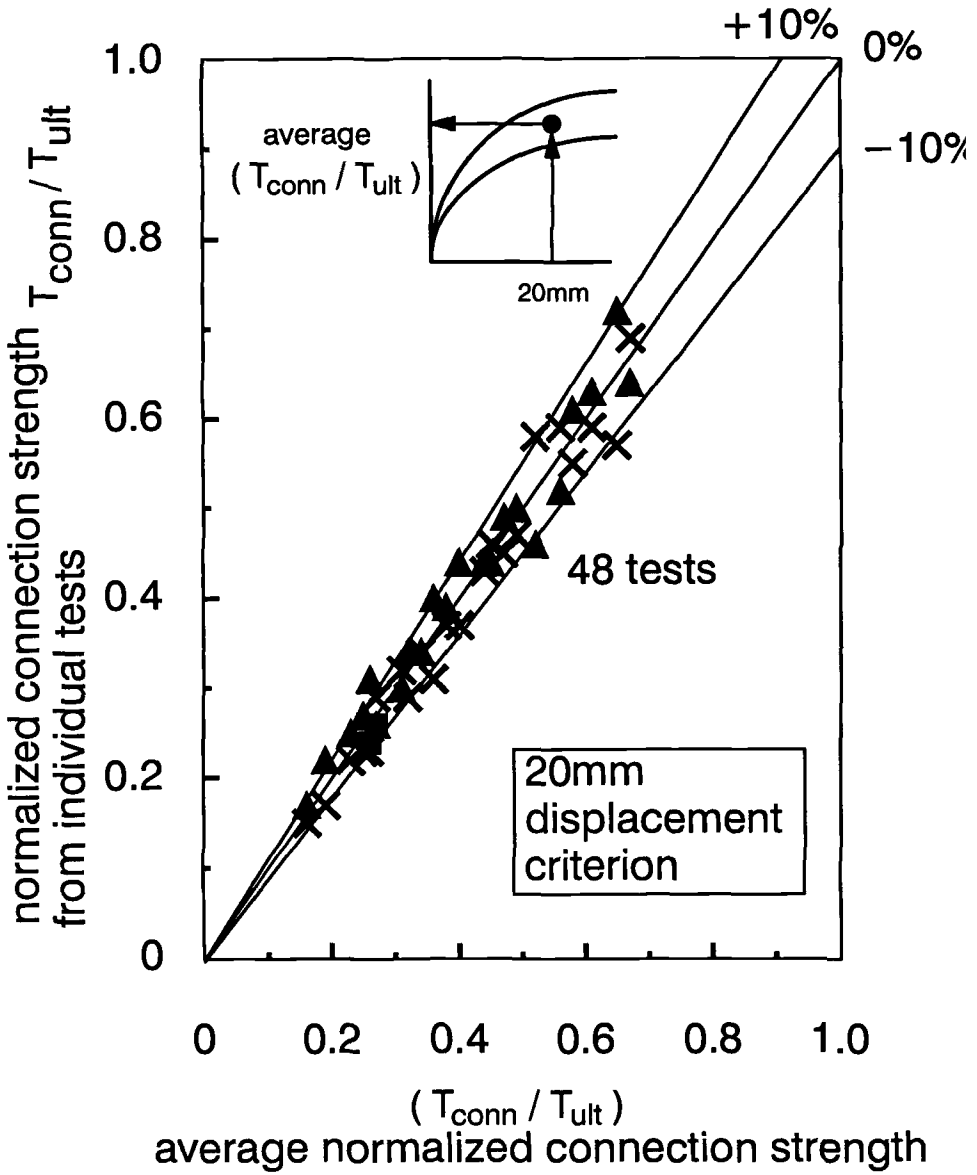
CONCLUDING REMARKS

This Paper outlines details of a test procedure that has been developed by the authors to evaluate the mechanical performance of the connection between geogrid reinforcement layers and mortarless modular concrete masonry block units. The essential features of the test method have been recently adopted by the NCMA. The Paper illustrates that test dimensions can have an important influence on connection strength results. In particular, under-size wall models may significantly over-estimate tensile connection capacities for nominal identical models built with greater width. The Paper emphasises the need to standardize the rate of loading to match recommendations found in the ASTM D 4595 method of test. If the recommendations in this Paper are applied then a rational interpretation of the efficiency of connections with respect to the conventional reference tensile strength (ASTM D 4595) of a reinforcement material is possible.



a) peak load criterion

FIG. 6-- Variability in connection strengths from nominal identical tests



b) 20mm displacement criterion

FIG. 6 (cont'd) --- Variability in connection strengths from nominal identical tests

The data in **Fig. 3** illustrates that the trend and magnitude of connection capacities with surcharge level is sensitive to a large number of parameters many of which have been listed at the beginning of the Paper. Clearly, it is not possible to predict in advance the relationship between mechanical strength and deformation of the connection with depth below the crest of the wall without full-scale testing.

The results of our investigation have shown that the test procedure to establish connection strengths based on either a peak load criterion or displacement criterion is repeatable within $\pm 10\%$ for block units taken from the same batch and geogrid samples trimmed from the same product roll. However, it is important to note that nominal identical modular masonry concrete unit products can vary from plant to plant. For example, the amount of coarse aggregate or segregation can have an influence on connection strength. Dimensional variations can be expected to increase as dry cast molds wear with repeated use. The need to perform site and product specific connection testing for geosynthetic-reinforced soil walls cannot be over-emphasized.

A detailed interpretation of test results with respect to long-term design life of the connection in the field is beyond the scope of this Paper. However, it is reasonable to expect that the quality of construction in a carefully controlled laboratory environment is greater than what may be anticipated in the field. Uncertainties in wall geometry, properties of soils and block units, and external loading are also present as are chemical durability concerns in some aggressive chemical, biological or elevated temperature environments. As a result, a partial factor of safety should be applied to the peak connection strength envelope determined from our test procedure when selecting long-term design connection strength values. Current recommended partial factors for connection strength design can be found in the recently published NCMA design manual for modular concrete block retaining wall systems [7], [8].

ACKNOWLEDGEMENTS

The authors would like to acknowledge the contribution of Peter Clarabut (Research Assistant) who carried out the tests reported in this Paper. Financial support for this study was provided by the Department of National Defence (Canada) in the form a research grant awarded to the first author.

REFERENCES

- [1] Simac, M.R., Christopher, B.R. and Bonczkiewicz, C., "Instrumented Field Performance of a 6m Geogrid Soil Wall", Proceedings of the 4'th Int. Conf. on Geotextiles, Geomembranes and Related Products, The Hague, May-June 1990, Vol 1, pp 53-59.
- [2] Simac, M.R., Bathurst, R.J. and Goodrum, R., "Design and Analysis of Three Reinforced Soil Retaining Walls", Geosynthetics'91, Atlanta, Georgia, 1991, pp 781-798.
- [3] Bathurst, R.J., Crowe, R.E. and Simac, M.R., "Recent Innovations in Modular-Facing Retaining Wall Structures Using Geosynthetics", 1991 CSCE Annual Conference, Vancouver, May 1991, pp 142-151,.
- [4] "Standard Specifications for Highway Bridges, 14'th Edition with Interim Specifications - Bridges -1991", American Association of State Highway and Transportation Officials, Washington, DC, 1991.
- [5] "Design Guide-lines for Use of Extensible Reinforcements (Geosynthetic) for Mechanically Stabilized Earth Walls in Permanent Applications", Task Force 27 Report, In Situ Soil Improvement Techniques, American Association of State Highway and Transportation Officials, Washington, DC, August 1990.
- [6] Christopher, B.R., Gill, S.A., Giroud, J-P., Juran, I., Schlosser F., Mitchell, J.K. and Dunnicliff, J., "Reinforced Soil Structures: Volume I. Design and Construction Guide-lines", Report No. FHWA-RD-89-043, Washington, DC, November 1989.
- [7] "Design Manual for Segmental Retaining Walls (Modular Concrete Block Retaining Wall Systems)", 1st Edition, National Concrete Masonry Association, Herndon, VA, 1993, pp. 336
- [8] Bathurst, R.J., Simac, M.R., and Berg, R.R., "Review of the NCMA Segmental Retaining Wall Design Manual for Geosynthetic-Reinforced Structures", Transportation Research Record, Washington, D.C. (in press)
- [9] Standard Test Method for Determining the Tensile Strength of Mechanically Anchored Geosynthetics, GRI Test Method GS-8, Geosynthetic Research Institute, Philadelphia, PA
- [10] Standard Test Method for Tensile Properties of Geotextiles by the Wide-Width Strip Method, ASTM Designation: D 4595-86, ASTM, Philadelphia, PA

Ragui F. Wilson-Fahmy¹, Robert M. Koerner² and James A. Fleck³

**UNCONFINED AND CONFINED WIDE WIDTH TENSION TESTING OF
GEOSYNTHETICS**

REFERENCE: Wilson-Fahmy, R.F., Koerner, R.M., and Fleck, J.A., "Unconfined and Confined Wide Width Tension Testing of Geosynthetics," Geosynthetic Soil Reinforcement Testing Procedures, ASTM STP 1190, S.C. Jonathan Cheng, Ed., American Society for Testing and Materials, Philadelphia, 1993.

ABSTRACT: The thrust of this paper stems from the classical confined wide width testing work of McGown, Andrawes and their co-workers in 1981 and 1982 on geotextiles and extends it into the following geosynthetics which are currently used in various waste containment applications:

- Woven and nonwoven geotextiles
- Geomembranes
- Geosynthetic clay liners
- Geonets

Confining (normal) pressures up to 138 kPa are utilized to note the effects and, in particular, the variation from the standard unconfined behavior. A range of commercially available materials is used in each of the above categories. The test device used is based on the design principles set by McGown, Andrawes and their co-workers with some modifications being made to simplify the testing technique. The test results substantiate the successful performance of the apparatus. With the exception of nonwoven geotextiles and in particular needle-punched nonwoven geotextiles, the influence of normal stress is shown to be insignificant. This is considered to be the major finding in this study. Confinement does, however, enhance greatly the load-extension modulus of needle-punched geotextiles while it has little effect on their tensile strength.

KEYWORDS: geotextiles, geomembranes, geosynthetic clay liners, geonets, geosynthetics, wide width tension test, confinement

¹Research Professor, Geosynthetic Research Institute, Drexel University, Philadelphia PA 19104.

²H.L. Bowman Professor of Civil Engineering and Director, Geosynthetic Research Institute, Drexel University, Philadelphia PA 19104.

³Research Specialist, Geosynthetic Research Institute, Drexel University, Philadelphia PA 19104

The load transfer between geosynthetics in multiliner waste containment systems, e.g. landfills, is a function of their stress-strain behavior and the frictional behavior of their interfaces. The accurate evaluation of these properties is, therefore, a critical element in design. A comprehensive theoretical and experimental study is being carried out at the Geosynthetic Research Institute to investigate the load transfer mechanism under realistic loading conditions. As part of this research, this paper is concerned with the evaluation of representative stress-strain behavior of the various geosynthetics involved in multiliner systems.

Since the plane strain condition is a realistic simulation of the actual situation in the field, it is logical to determine the load-extension properties of the geosynthetics involved using wide width tests. Current test standards use samples having a length of 100 mm and a width of 200 mm to simulate as practically as possible the plane strain loading condition (e.g., ASTM Standards D4595: "Standard Test Method for Tensile Properties of Geotextiles by the Wide-Width Strip Method" and D4885: "Standard Test Method for Determining Performance Strength of Geomembranes by the Wide Strip Tensile Method"). However, because the stress-strain behavior of some geosynthetics is likely to be affected by confinement, it further seems appropriate to use confined wide width test data in design. It is to this end that this paper is concerned. The main objectives are to investigate the reliability of a test device developed for confined wide width testing and to assess the need for conducting confined wide width tests on the various types of geosynthetic materials used in landfill construction.

APPARATUS

The confined, wide-width test apparatus is similar, in principle, to that developed by McGown et al [1] and adapted for creep testing by McGown et al [2]. However, in the experimental set-up developed by McGown et al [1 and 2], the box is mounted in the vertical direction as opposed to the test device used herein where loading is applied horizontally to the test specimen. This modification greatly simplifies the test setup and procedure.

Figure 1 shows the components of the test device which basically consists of a box housing two pressure bellows for the application of the normal stress to the tested specimen. In the figure, sand is used as the confining medium. The box has inner dimensions of 381 x 203 x 76 mm in length, width and height respectively and is constructed of 13 mm thick aluminum plates. It is made of two halves which can be firmly attached to each other while leaving a 13 mm gap on both ends of the box to accommodate the clamps holding the tested specimen. The box is linked top and bottom to an air pressure system which consists of a compressor and a pressure regulator. Each of the two clamps holding the tested specimen is made of two 3.2 mm thick steel plates attached to each other using countersunk screws. Sand is placed between the two clamps above and below the geosynthetic test specimen. Two relatively stiff rubber sheets separate the pressure bellows from the sand. The sheets are covered on the sand side with a system of latex membranes lubricated at

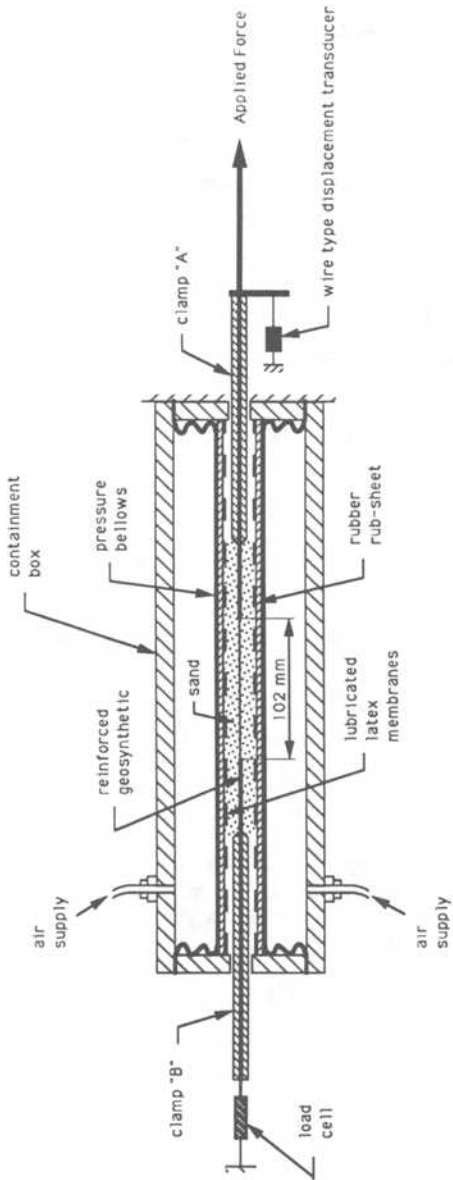


Fig. 1 Cross-Section of Horizontally Deployed Containment Box in a Confined Wide Width Test

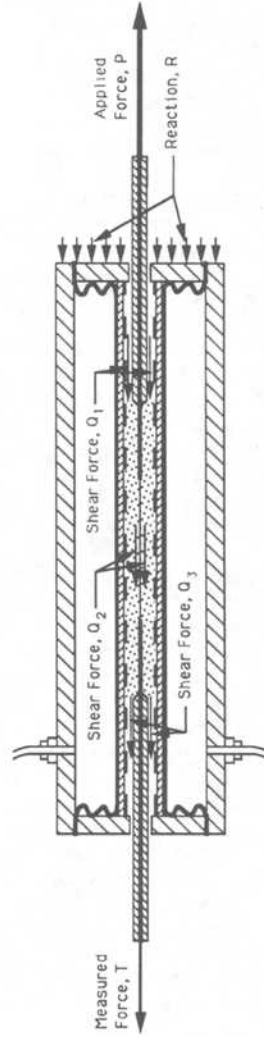


Fig. 2 Load Transfer in Confining Box

52 GEOSYNTHETIC SOIL REINFORCEMENT TESTING PROCEDURES

their interface with the rubber using generous layers of silicone grease in order to reduce as much as possible friction mobilized by sand movement during sand deformation.

Loading is applied via a screw jack connected to a motor allowing for a wide variation of strain rates. The jack is attached to the clamp marked "A" in Figure 1 while the clamp marked "B" is connected to a load cell fixed to the loading frame. The box is prevented from movement during the application of the tensile load with the aid of a reaction bar. Strain is measured using a wire type constant force displacement transducer mounted on the loading frame and connected to clamp "A". Separate readout units are connected to the load cell and the strain transducer which directly provide the tensile load in pounds and the clamp displacement in inches. An X-Y plotter attached to the two readout units can provide plotted load-extension curves for the tested specimen.

TEST SPECIMEN PREPARATION

The geosynthetic test specimen is first cut to a length and width equal to 600 and 202 mm respectively. The specimen is then reinforced with the exception of the central 102 mm as indicated in Figure 1. This leaves an intact portion conforming with the specimen size specified by ASTM test methods D4595 and D4885 for geotextiles and geomembranes respectively. This specimen size was used for all the tested geosynthetics which included geotextiles, geomembranes, geosynthetic clay liners and geonets.

Polyester resin was used for reinforcement of geotextiles, geosynthetic clay liners and geonets beyond the edges of the central intact portion of the test specimens. With geotextiles and geosynthetic clay liners, an inverted channel of height equal to 102 mm was placed over the middle portion of the specimen with added weights to prevent infiltration of the resin into the unreinforced part (test section) of the geosynthetic. Of all methods used in applying the resin, this method was found to be the easiest and most efficient. On the other hand, moulding clay was used as a barrier to the resin in reinforcing the geonet specimens due to their large apertures.

HDPE geomembranes were reinforced by joining HDPE geomembrane sheets on both sides of the area to be strengthened. A hot air seaming device was used for this purpose. With PVC geomembranes, reinforcement was achieved by sticking sheets of HDPE on both sides of the geomembranes using a strong quick setting adhesive. Examination of the various geosynthetics after testing indicated the successful performance of the various reinforcement techniques.

TESTING PROCEDURE

Preparation for testing of the positioned test specimen can be summarized in the following steps (see Figure 1):

- Mount the bottom half of the box on the loading frame. Place the stiff pre-lubricated rubber sheet on top of the pressure bellows with

- the lubricated surface facing upward.
- Spread the sand evenly over the area to be covered by the geosynthetic material. Angles made of stiff paper are placed at the boundaries to ensure that the sand does not extend beyond the marked locations of the edges of the clamps.
 - Place the clamps and the contained test specimen assembly in position and connect the clamps to the loading and measuring devices. Apply a small tension force to remove any slack in the specimen.
 - Place sand over the specimen between the clamp edges.
 - Place the top lubricated rubber sheet in position on top of the sand and clamps with the lubricated surface facing downward.
 - Place the top half of the box in position and fix the two halves together.
 - Apply the required confining pressure to the bellows while ensuring that the box is in firm contact with the reaction bar.
 - Apply the tension force to the test specimen at the required strain rate and continuously monitor load and strain.

LOAD TRANSFER

Figure 2 illustrates the tension and friction forces acting during the tension test. Force Q_1 is assumed to occur due to friction between clamp "A" and the lubricated rubber sheets in addition to friction developing between the attached reinforced part of the geosynthetic and the sand. Force Q_2 is due to friction that may develop between the geosynthetic test specimen and the sand. The third frictional force, Q_3 , results from friction developing at clamp "B" and the attached reinforced geosynthetic. If the box is assumed to be stationary, all these frictional forces will be transmitted to the box support represented by the reaction force "R" in Figure 2. Thus, the force measured by the load cell will be equal to the tension force transmitted to the leading edge of the geosynthetic test specimen minus the friction forces Q_2 and Q_3 . It is, however, logical to assume that the relative displacement between clamp "B" and the box is negligible and hence friction between them can be neglected. Note, also, that both the box and clamp "B" tend to move in the same direction which again reduces their relative displacement.

From the above discussion, it can be seen that the major source of error in measuring the tension force is the frictional force, Q_2 , which constitutes the difference between the tensile load at the leading and trailing ends of the geosynthetic test specimen. Therefore, minimizing this frictional force is essential for the evaluation of the effect of confinement. Note that its magnitude will be governed by the low interface friction between the sand and the lubricated rubber sheets.

Finally, it can be clearly seen that the mobilization of friction in the box can only reduce the actual effect of confinement. Thus, the test should be regarded as a lower bound evaluation of the effect of confinement. However, as will be shown later, test results indicate that the effect of friction is minimal.

TEST RESULTS

Various geosynthetics commonly used in waste containment systems were tested in confined and unconfined wide width tests. The confining pressure varied between 0 and 138 kPa. The tested geosynthetics included geotextiles, geomembranes, geosynthetic clay liners and geonets. In all cases, the testing rate was 10.2 mm/min which is the loading rate specified by ASTM D4595 test method for geotextiles. It may be noted that a slower rate of 1 mm/min is required as per ASTM test method D4885 for geomembranes. However, the test method allows for other rates which adequately simulate actual field conditions.

Geotextiles

Four geotextiles of different types were tested in-isolation and under confinement in their machine direction. The geotextiles which will be referred to as geotextiles "A", "B", "C" and "D" are described in Table 1 below.

Table 1 - Geotextiles Tested

Geotextile	Manufacturing Process	Material	Mass/unit area, g/m ²
A	Woven and calendered monofilament	Polypropylene	190
B	Nonwoven heat bonded	Polypropylene	200
C	Nonwoven needle-punched	Polypropylene	270
D	Nonwoven needle-punched	Polyester	550

Owing to its manufacturing process, geotextile "A" has fibers in the machine direction which are slightly crimped. However, the load-extension behavior of the geotextile for various confining pressures shows practically no effect of confinement, see Figure 3. The fact that the 138 kPa test behavior gave the lowest response is not felt to be statistically valid, particularly in light of test results to be seen later.

The load-extension curves for the heat bonded nonwoven geotextile "B" are given in Figure 4 for different confining pressures. The variations between the curves up to strains in excess of about 10% appear to be the same with no trends established from the different confining pressures. In general, however, an increase in load at any particular strain is apparent at strains greater than 15%, the effect becoming greater at higher confining pressures. This can be explained, at least partly, by the fact that the behavior of heat bonded geotextiles changes at high loads after the fiber crossover bonds start to deteriorate [3]. In the unconfined case, a bond rupture would

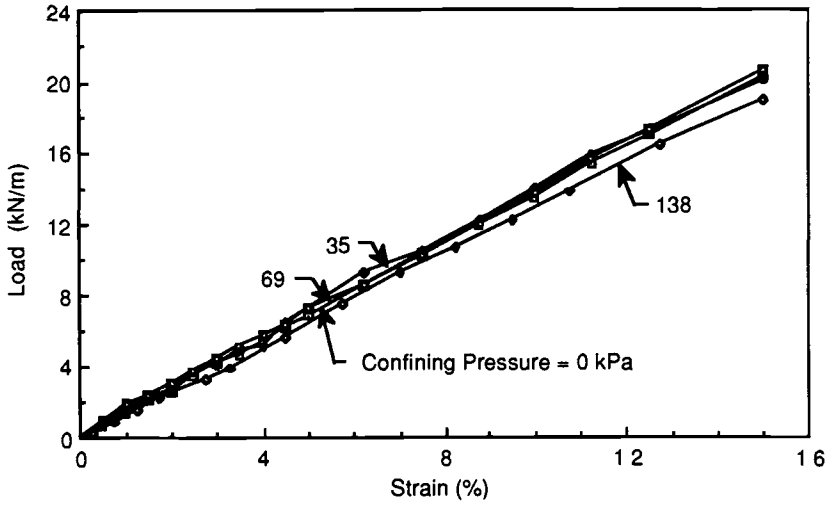


Fig. 3 Load-Extension Behavior of Geotextile "A"

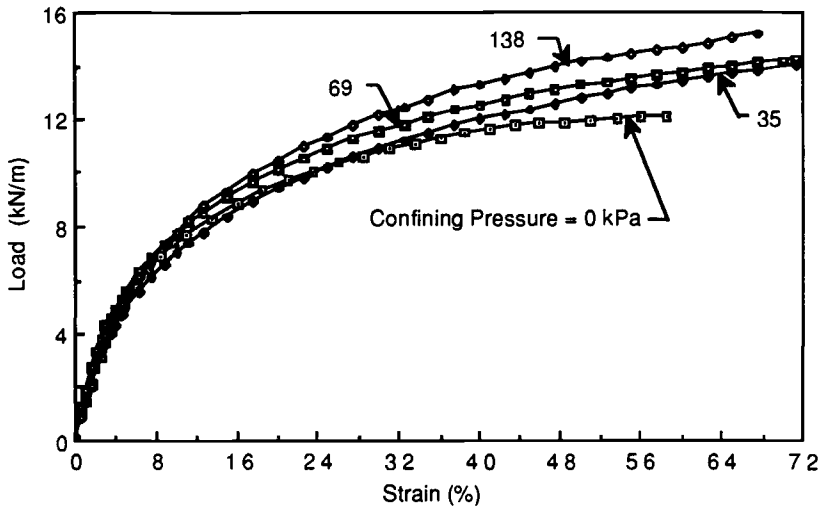


Fig. 4 Load-Extension Behavior of Geotextile "B"

introduce a considerable amount of fiber curl and hence a sudden drop in fiber stress [3]. Compression would be expected to inhibit the effect of bond deterioration by providing frictional resistance at the crossover points of magnitude dependent on the applied normal stress. As a result, the loss in fiber stress is expected to occur in a gradual manner and to be less than that in the case of no confinement. Thus, the effect of confinement would be to enhance the overall strength of the geotextile. According to Figure 4, the improvement in strength ranges between 14 and 28% due to confinement. It should be recognized, however, that these results correspond to one type of heat bonded geotextile and should not be generalized to other types. Indeed, a variation from the measured behavior was reported by McGown et al [1] who recorded an increase in modulus of about 75% in a heat bonded geotextile composed of 67% polypropylene and 33% polyethylene and involving heterofil bonding.

The results for the two different types of needle-punched nonwoven geotextiles "C" and "D" are given in Figures 5 and 6 respectively. The effect of confinement on modulus is shown to be dramatic in both cases. However, little effect on ultimate strength can be detected. Table 2 below gives the secant modulus at 5% strain at different confining pressures for both geotextiles.

Table 2 - Secant Modulus at Various Confining Pressures for NeedlePunched Nonwoven Geotextiles

Geotextile	Normal stress, kPa	Secant modulus at 5% strain, kN/m
C	0	14
	35	25
	69	27
	138	33
D	0	44
	35	140
	69	193
	138	210

The above values indicate that the ratio between the modulus under confinement and that with no confinement ranges between 1.8 to 4.8. Variations in this ratio depend on confining pressure and geotextile tested. This substantial improvement can be attributed to the increase in inter-fiber friction as a result of confinement. It is well known that slippage at the crossover points and straightening of the fibers in needle-punched geotextiles are highly responsible for their low initial modulus in an unconfined state [4]. Increased friction due to compression would be expected to greatly limit such slippage and inhibit

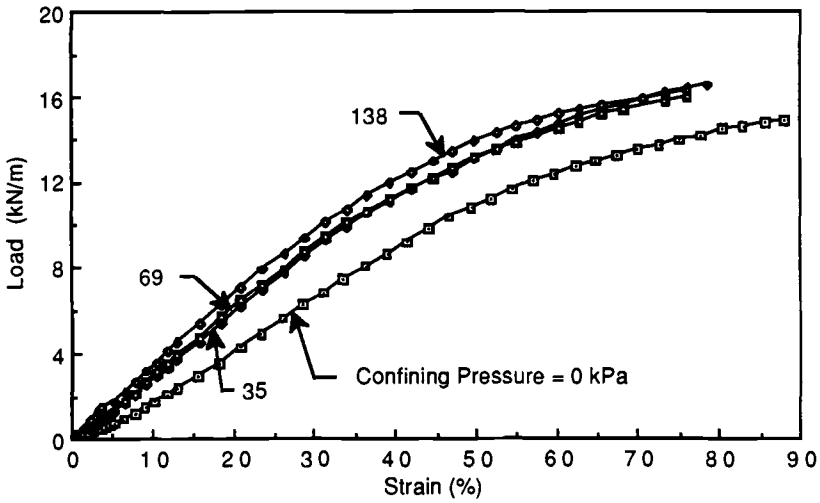


Fig. 5 Load-Extension Behavior of Geotextile "C"

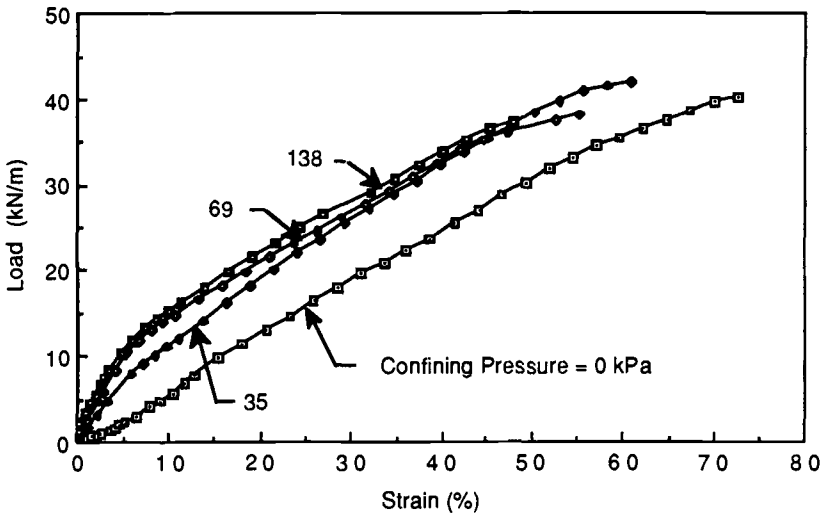


Fig. 6 Load-Extension Behavior of Geotextile "D"

the free motion of the fibers in adapting to the tensile stress.

Compression via normal stress is expected to have two opposing effects on ultimate strength. First, a reduction in strength is possible due to the fact that fiber reorientation under confinement is less than in isolation. Therefore, fibers will reach their ultimate strengths earlier in the confined case in comparison with the unconfined case where fibers have more freedom to align in the load direction. Note that specimens subjected to confining pressure fail at a lower strain compared to specimens tested under no confinement, see Figures 5 and 6. As a result, the overall strength of the geotextile could be lower under compression. On the other hand, the loss of contribution of a ruptured fiber will be greater for unconfined geotextiles compared to those under confinement since in the latter case greater friction between the fibers is expected to maintain a greater resistance by the ruptured fiber. This would lead to a more progressive failure mechanism and an increase in strength. These two opposing effects may explain the relatively small influence of confinement on the strength of the tested needle-punched geotextiles. Note that both reduction and increase in strength can be depicted in Figures 5 and 6 as a result of confinement.

Geomembranes

HDPE (1.5 mm thick) and PVC (0.5 mm thick) geomembranes were tested both confined and unconfined. The test results are shown in Figures 7 and 8 where it can be seen that there is practically no effect of confinement on both materials especially at strains up to about 10%. The lower resistance provided by the geomembranes at high loads possibly reflects some edge stress concentration enhanced by friction along the geomembrane. At maximum load, the difference between the highest and lowest loads does not exceed 8% for HDPE and 12% for PVC.

Geosynthetic Clay Liners

Two geosynthetic clay liners (GCL) were tested in their as-received dry state. The first referred to as GCL "A" consisted of bentonite clay sandwiched between a needle punched geotextile on one side and a composite geotextile on the other side. The composite geotextile is a woven slit film geotextile incorporated into a needle-punched geotextile. Geosynthetic clay liner "B" consisted of bentonite clay sandwiched between a woven slit film geotextile and a needle punched nonwoven geotextile. All geotextiles used in the manufacture of GCL's "A" and "B" were made from polypropylene.

Figure 9 shows the load-extension response of GCL "A". It can be seen that up to peak load, there is practically no effect of confinement. This is not surprising since most of the load is carried by the woven slit film geotextile which has a much higher modulus compared to the needle-punched geotextiles making up the remainder of the product. In fact, the peak load is always associated with the rupture of the woven geotextile. The same behavior is noticed in Figure 10 for GCL "B" where load up to peak is again carried by the woven slit film geotextile. After peak is reached in both types of GCL's evaluated, the stress drops off significantly and very erratic behavior is observed.

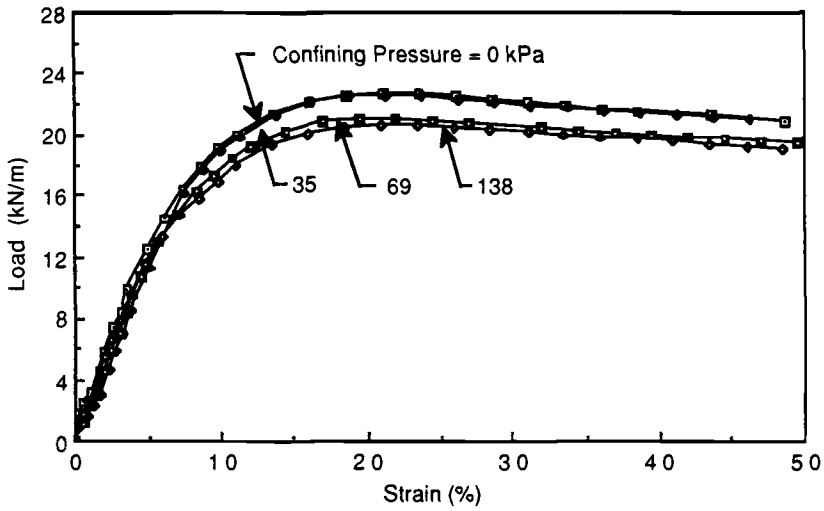


Fig. 7 Load-Extension Behavior of HDPE Geomembrane

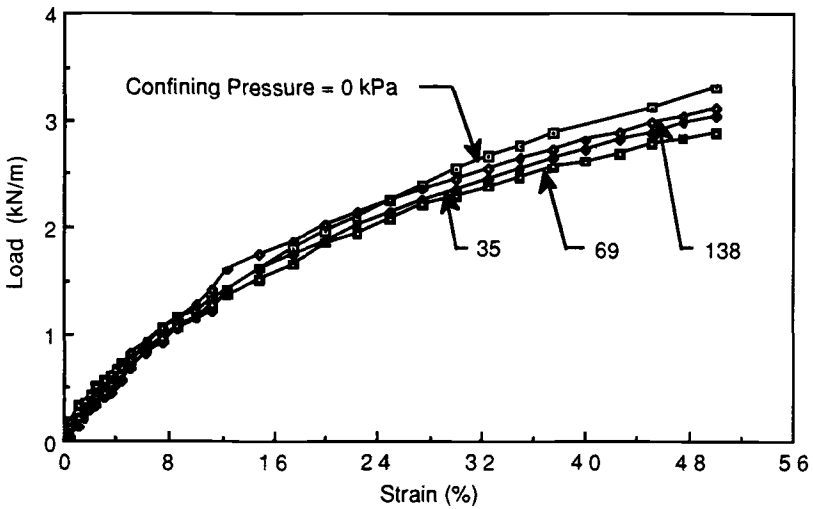


Fig. 8 Load-Extension Behavior of PVC Geomembrane

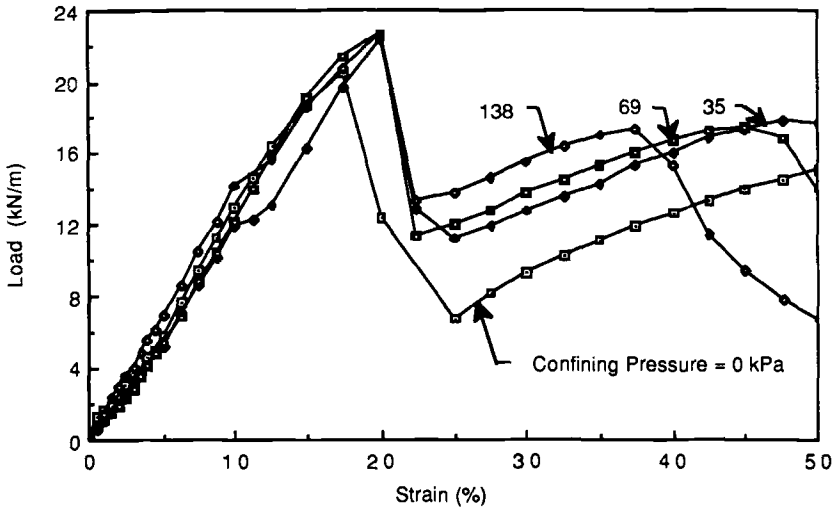


Fig. 9 Load-Extension Behavior of GCL "A"

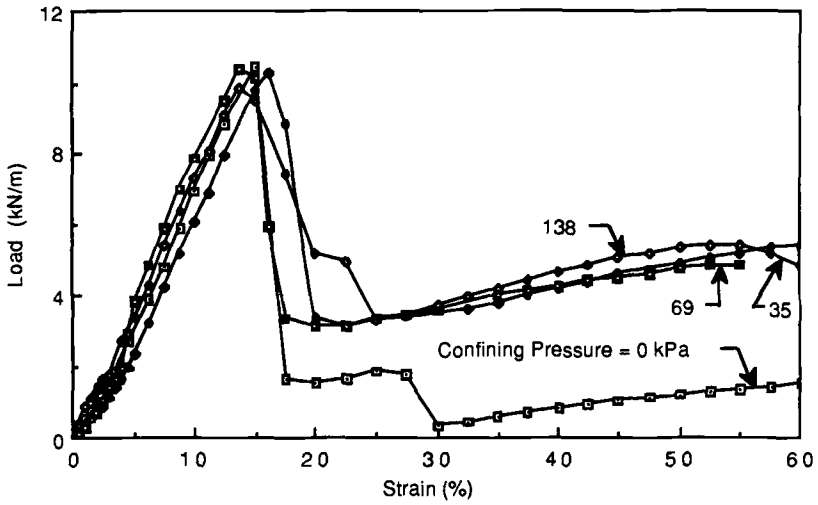


Fig. 10 Load-Extension Behavior of GCL "B"

This behavior is very complex in that the nonwoven needle-punched geotextiles, the needling process and the interaction of the clay particles are all involved in some way. For the purposes of reinforcement, however, it is academic since the modulus, peak strength and strain at peak are the focal points of any design process.

Geonets

A polyethylene geonet 5.6 mm thick was tested in a slightly different manner from other geosynthetics due to its large opening apertures. Heat bonded geotextiles of mass per unit area of 200 g/m² separated the geonet from the underlying and overlying sand. In order to reduce the effect of friction, the geotextiles were wrapped with very thin plastic sheets lubricated on both sides with silicone grease. It should be recognized that with this test arrangement, the intrusion of the geotextile into the geonet is likely to induce some additional resistance along the geonet by bearing against the geonet ribs. The amount of this resistance, however, cannot be quantified although it can be conjectured that the initial strain behavior may be only nominally affected and the phenomenon increasing as strain increases. Its effect, however, is to lead to stress concentrations at the leading edge of the geonet. The test results should, therefore, be viewed in terms of these limitations. Notwithstanding the above limitation, the load-extension curves of the tested geonet given in Figure 11 are useful in indicating that the modulus up to 5% strain is practically unchanged by confining pressure. The effect of stress concentration at the leading edge is evident in the curves where strength is shown to decrease with increasing normal stress.

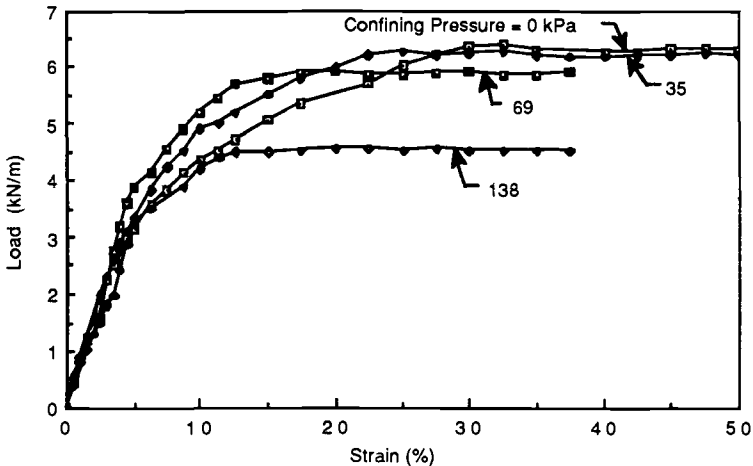


Fig. 11 Load-Extension Behavior of Geonet

CONCLUSIONS

Confined and unconfined wide width tests were conducted on a variety of geosynthetics used in waste containment applications. The tested materials included geotextiles, geomembranes, geosynthetic clay liners and geonets. An apparatus based on the design principles set by McGown, Andrawes and their co-workers [1 and 2] was used in the tests. The test results indicated the successful performance of the apparatus. Of all the tested geosynthetics, only heat bonded and needle-punched nonwoven geotextiles exhibited a positive effect of confinement. The confined modulus of needle-punched geotextiles was found to be as high as 1.8 to 4.8 times that under no confinement. However, the effect of confinement on ultimate strength was negligible. With the tested heat bonded geotextile, the effect of compression was mainly to improve ultimate strength. The increase in strength varied between 14 and 28%.

For the other geosynthetics evaluated;

- woven monofilament geotextiles
- HDPE and PVC geomembranes
- geosynthetic clay liners whose strength is governed by woven slit film geotextile carrier layers
- polyethylene geonets

the stress-strain characteristics are essentially the same when tested with and without confinement. This leads to the important conclusion that test results via ASTM D4595 and D4885 (both unconfined tests) are representation of geosynthetic behavior insofar as modulus, strength and failure strain are concerned. Thus, there is no compelling need to conduct the more difficult, tedious and time consuming laterally confined tension tests on any geosynthetics except for nonwoven geotextiles.

ACKNOWLEDGEMENTS

This study is part of the overall research and development efforts undertaken by the Geosynthetic Research Institute of Drexel University. Funding is by the 50 member organizations who form the consortium and to whom the authors express sincere appreciation.

REFERENCES :

- [1] McGown A., Andrawes, K.Z., Wilson-Fahmy, R.F. and Brady, K.C., "A New Method of Determining the Load-Extension Properties of Geotechnical Fabrics," Department of Environment, Department of Transport, U.K., Report SR 704, 1981, pp. 14.
- [2] McGown, A., Andrawes, K.Z. and Kabir, M.H., "Load-Extension Testing of Geotextiles Confined In-Soil," Proceedings of the Second International Conference on Geotextiles, Las Vegas, U.S.A., Vol. 3, 1982, pp. 793-798.

- [3] Hearle, J.W.S. and Stevenson, P.J., "Studies in Nonwoven Fabrics, Part 4: Prediction of Tensile Properties," Textile Research Journal, Vol. 34, No. 3, 1964, pp. 181-191.
- [4] Hearle, J.W.S., "A Theory of the Mechanics of Needled Fabrics," The Textile Trade Press, Manchester.

Andrea Cancelli,¹ Pietro Rimoldi,² and Filippo Montanelli³

INDEX AND PERFORMANCE TESTS FOR GEOCELLS IN DIFFERENT APPLICATIONS

REFERENCE: Cancelli, A., Rimoldi, P., and Montanelli, F., "Index and Performance Tests for Geocells in Different Applications," Geosynthetic Soil Reinforcement Testing Procedures, ASTM STP 1190, S.C. Jonathan Cheng, Ed., American Society for Testing and Materials, Philadelphia, 1993.

ABSTRACT: The use of geocells in base reinforcement of structural fill allows confinement of the soil from lateral spreading, therefore preventing shear failure and increasing the soil bearing capacity. Geocells are typically loaded by the live loads on the surface and the overall structure is tensioned while the underlying foundation soil settles. Geocells are regularly used for soil confinement on steep slopes to prevent severe erosion. The geocells are sometimes installed even over slippery geomembranes to contain and reinforce the cover soil. The geocells in these applications should withstand high tensile stresses both in the strands and the junctions without breaking and sliding down the slope. A need for more accurate and specific geocells testing is needed by the design engineers when designing such a critical applications. The testing procedures appropriate for geocells will be investigated, performed and analyzed in this paper. The description of the above tests and some preliminary results are presented and discussed. A final proposal for test standards concerning geocells will be presented for consideration by the existing geosynthetics testing committees.

KEYWORDS: geocells, index tests, performance tests, mechanical testing, hydraulic testing, damage during installation.

Lack of available land to accommodate expanding suburban areas constantly provides interesting challenges to country planners and local engineers. Limited money and scarcity of land are forcing engineers to become more innovative and to utilize new products. One type of material which is receiving particular attention from these professionals is erosion control geosynthetics.

Synthetic materials, specifically manufactured to prevent erosion, date back to ca. 1958 when a textile company produced a "geotextile" to

¹Professor, University of Milano, Dept. of Earth Sciences, Milano, Italy.

²Director, Geosynthetics Division, Tenax SpA, Vigano', Italy.

³Laboratory Manager, RDB Plastotecnica SpA, Vigano', Italy.

replace a granular filter behind a concrete revetment along a beach. Since then, geotextiles have gained much attention and other geosynthetic products have developed for erosion control [1, 2].

Some of these synthetic materials are currently being utilized in the prevention of slope erosion including geomats and geocells. Typically, geomats are used to intertwine with young seedlings, improve the frictional behaviour of the these two dissimilar materials and reinforce the root systems once vegetation is established. These erosion control products are typically used where proper vegetation cover is required to improve the durability of the slope face. Other times, steep slopes exist (or need to be constructed) in areas where vegetation may be difficult to establish, or the potential erosive forces could overcome the strength of the root system. In these cases, a geocell is typically used to ensure the surface soil is retained on the slope.

Geocells have received a draft definition by the International Erosion Control Association as a three-dimensional, polymeric, honeycomb-like structure of cells interconnected by manufactured joints used for containment of soil, rock, earth, or any other geotechnical engineering-related material (Figure 1). Geocells prevent mass sliding of the surface layer while vegetation is being established.

Some geocells are used where heavy runoff, or channel scouring is anticipated. The cell walls confine the soil and decrease the velocity of water passing across the surface. In these instances, geocells often replace expensive rip-rap or concrete slope protection. Geocells are also used in a wide range of load support applications, from single-layer road bases on soft soil and pipe beds to multi-layer retaining walls and protective barriers. In these cases geocells are used to increase the shear strength and stiffness of the infill soil, to reduce load deformations, to minimize settlements and to prevent penetration of fill into the subgrade.

On one hand, the large number of products available on the market allows designers to choose the product with the appropriate properties for each specific application; on the other hand, it allows users and contractors to buy products physically similar to the one specified, but sometimes exhibiting important differences concerning identification, mechanical and hydraulic properties (i.e. intrinsic properties).

New applications and new installation methods require careful measurements not only of intrinsic properties, but also of the possible damage during installation and of the durability characteristics of the different products. Designers also need performance tests in order to evaluate the ability of each product to exhibit suitable erosion-control characteristics in the various possible situation typical of each site. At this stage of development of the geocell market, there is therefore a need for the development of standard tests to measure all the main characteristics of these products.

Geocells are manufactured by either a single extrusion process from HDPE granules, either by glueing together strips of nonwoven geotextiles or either by bonding together strips of HDPE geomembranes.

Among the various geosynthetics for erosion control, the "honeycomb" geocells seem to be the most "technical" products; in fact these products exhibit a structural pattern, fundamental for improving the veneer stability of the coversoil (for example when laid on a smooth geomembrane in landfill capping applications). The same structural

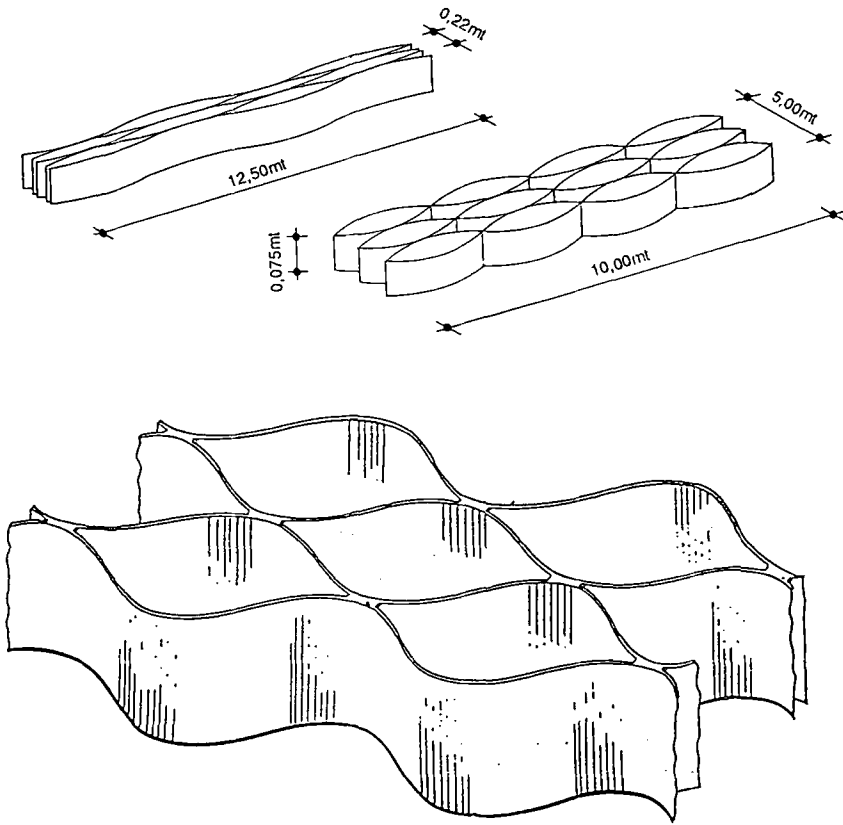


Fig. 1 - The honeycomb structure of the geocells.

functions are played when geocells are used for improving the bearing capacity of soft soils.

For these materials the mechanical properties are of crucial importance and must be fully and properly evaluated.

The presentation of the testing activity is divided in three main parts:

- identification testing;
- mechanical and hydraulic testing;
- damage during installation and durability testing.

IDENTIFICATION TESTING

First of all, panel sizes (length and width) shall be reported. ASTM D4873-88 (Guide for Identification, Storage and Handling of Geotextiles) should be followed. The standards for the sampling (ASTM D4354-89 Practice for Sampling of Geosynthetics for Testing) and the thickness of geosynthetics (ASTM D1777 Standard Method for Measuring Thickness of Textile Materials), can be applied to geocells but with a certain care. The thickness can be referred to the thickness of the single strips or to the total thickness of the products; usually both values shall be measured.

The overall geocell covered area can greatly change if the product is more or less expanded during the installation (Figure 1). If the geocell is expanded over the nominal width, than it will be shorter in the longitudinal direction. Thus the geocell covered area will change and with it it will change the mass per unit area. The mass per unit area shall be calculated by dividing the total weight of the geocell panels by the nominal covered surface indicated by the manufacturer.

MECHANICAL AND HYDRAULIC TESTING

Tensile strength

The tensile test is applicable, in principle, to every geosynthetic product. The test standards, however, must be adapted to the different classes of products.

The wide-width tensile test (ASTM D 4595 Test Method for Tensile Properties of Geotextiles by the Wide-Width Strip Method, and ISO or CEN draft standards) is applicable, in general to all the geosynthetics: it consists in pulling a sample (200 mm width and 100 mm distance between clamps) at a constant rate of extension. But the wide-width tensile test is not suitable for geocells, which are strip based products. Therefore the tensile test should be used is the narrow strip tensile test (ASTM D 1682 Standard Test Method for Breaking Load and Elongation of Textile Fabrics), eventually modified to take into account the width of the strips (corresponding to the height of the cells).

The specimens must be:

- a single strip cut between adjacent junctions;
- a double strip cut across a junction.

Figure 2 shows the schemes of these tests.

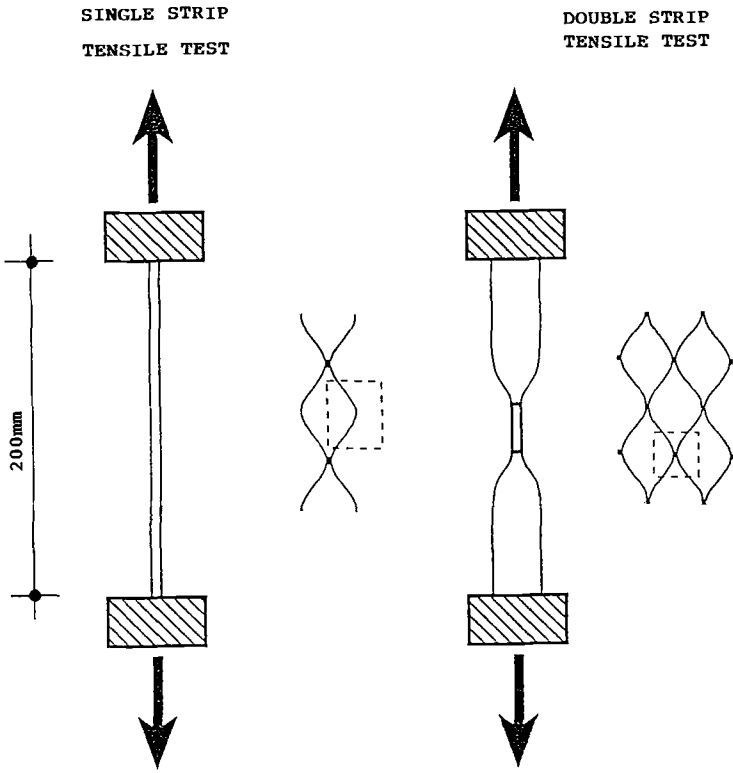


Fig. 2 - Schemes of the tensile tests for geocells.

Junction strength

The test for junction strength is particularly relevant for geocells. The junctions of these products, in fact, must support and transfer high loads, for example when the geocells are used to stabilize a topsoil layer on a long and steep slope. The geocell junctions can fail due to three main mechanisms: shear, which means that one strip is displaced relatively to the adjacent strip along the strips direction; peel, which means that one strip is displaced relatively to the adjacent one perpendicularly to the strips direction; split, which means that two of the four strips occurring in a junction are pulled relatively to the other two, perpendicularly to the junction. Three types of test are therefore needed: junction shear tensile test, junction peel tensile test and junction split tensile test. The schemes of the three tests are shown in Figure 3.

Junction shear and peel tests can be performed with standard clamps, while the junction split test requires special clamps to hold the four strips in the same pattern as they would be when the geocell panel is open. A suitable type of clamp is shown in the same Fig. 3.

These three tests have not been standardized yet. The Authors recommend to the various national and international geosynthetics testing committees to take these tests into consideration in the near future.

Opening size

To measure the geocells opening size, it should be suitable to open the structure according to manufacturer's recommendations and then to divide the total width and length by the number of cells to obtain the average dimensions of the cell itself in the two main directions.

Hydraulic testing: artificial rain simulator

The most significant hydraulic test is a typical "performance" test: the artificial rain simulator. This apparatus measures in the laboratory the ability of some products to resist the erosion induced by artificial rainwater and runoff. Various laboratory investigations dealing with this subject are available in literature (see for example Cancelli et al. [3]).

The results obtained from the test may represent a base for design of erosion-control applications, in order to establish precise guidelines, according to the different products and the different site conditions.

DAMAGE DURING INSTALLATION

Every type of geosynthetic is subject to a certain degree of damage during installation, due to the stresses applied by the soil and by the construction equipment machines. Damage during installation occurs mainly during the phases of soil filling and compaction and when the

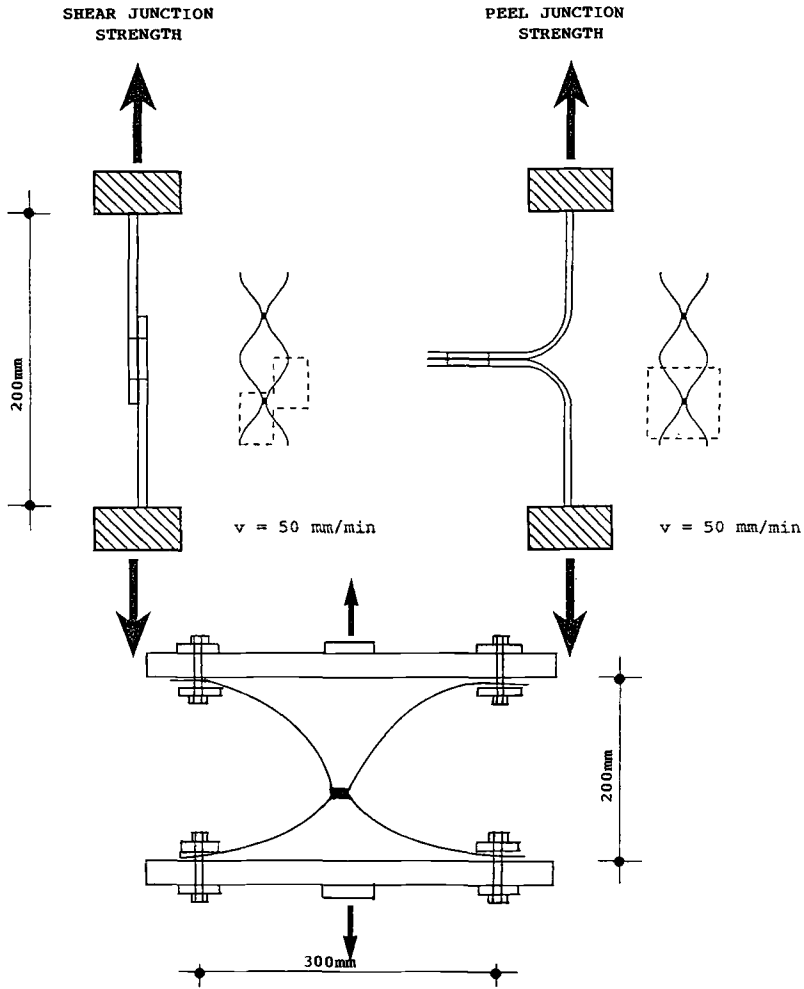


Fig. 3 - Schemes of the junction tests for geocells.

geosynthetic is fixed to the soil with staples or to adjacent panels with connections. The effects of both these mechanisms, which are quite important for geocells shall be evaluated with purposely designed performance tests.

The laboratory method for simulating the effect of soil compaction on geosynthetics is currently under development in Europe by the Working Group 3 of CEN (European Standards Committee) TC 189. This standard method, which should be checked through interlaboratories testing during 1992 and finally adopted in 1993, follows a simple scheme: the geosynthetic specimen is placed in a large testing box, in the middle of two layers of loose soil of standard type (sand or gravel) and characteristics (Figure 4).

In the case of a geocell, the specimen is overfilled with a standard soil and then a cyclic load is applied. The present proposal is to cycle 60 times the load at 1 Hz frequency, varying the applied pressure up to 200 kPa. After the damaging procedure, standard tests are run on the specimen and the average results are compared with the results of the same tests run on virgin specimens from the same strip or roll. Even if every type of test could be carried out after damaging the specimens, for practical purposes the evaluation shall be limited to tensile tests and junction tests, according to the methods described in the previous paragraph. The ratio between the two values defines the minimum Factor of Safety for Compaction Damages FSc:

$$F_{Sc} = F_i / F_d$$

where: F_d = average results of the tests on the damaged specimens;
 F_i = average results of the tests on virgin specimens.

The Factor of Safety FSc shall be applied to the mechanical characteristics (tensile strength, junction strength, etc.) every time they are used in design calculations.

CONNECTION AND STAPLES EFFICIENCY

Braids and U-shaped steel bars used to connect adjacent panels of geocells and to fix the panels to the ground, can damage or even break the junctions between cells, thus causing a very dangerous local instability which may cause a progressive global failure.

This failure mechanism is particularly important when the geocells are used to stabilize the cover soil in landfills capping applications. The junctions play a fundamental structural role since they have to bear and transfer all the component of the soil weight along the slope. In this case a wrong type of connection must be avoided, therefore a performance test to select the proper connections is needed. A typical test, suitable for simulating the stresses applied on the junctions by both connections and staples, is proposed by the Authors as follows: according to the scheme in Fig. 5, a tensile test is run using special clamps which allow to fix the strips of geocells having different cell diameter.

The specimen is cut with the junction in the middle, while the four half strips protruding from the junction are fixed to the clamps simulating the real open cell. Then the connection under consideration

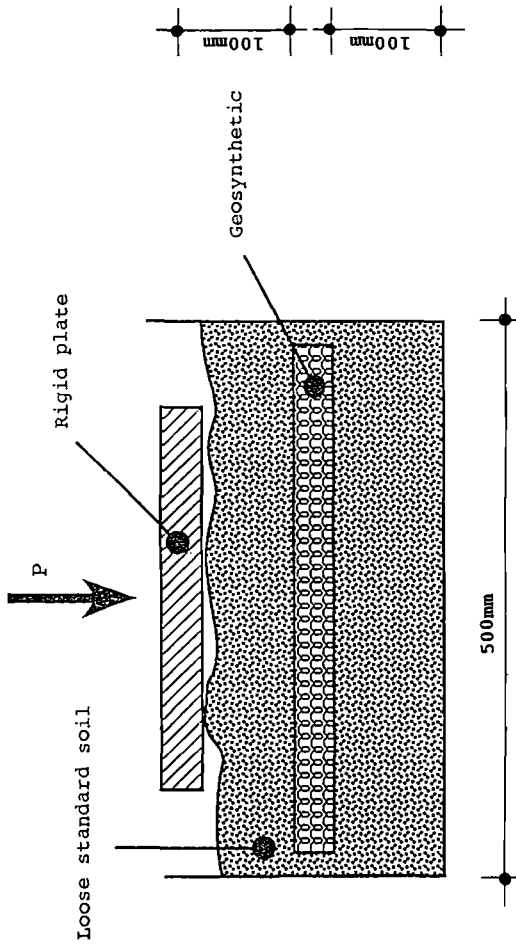


Fig. 4 - Scheme of the Damage During Compaction test for geocells.

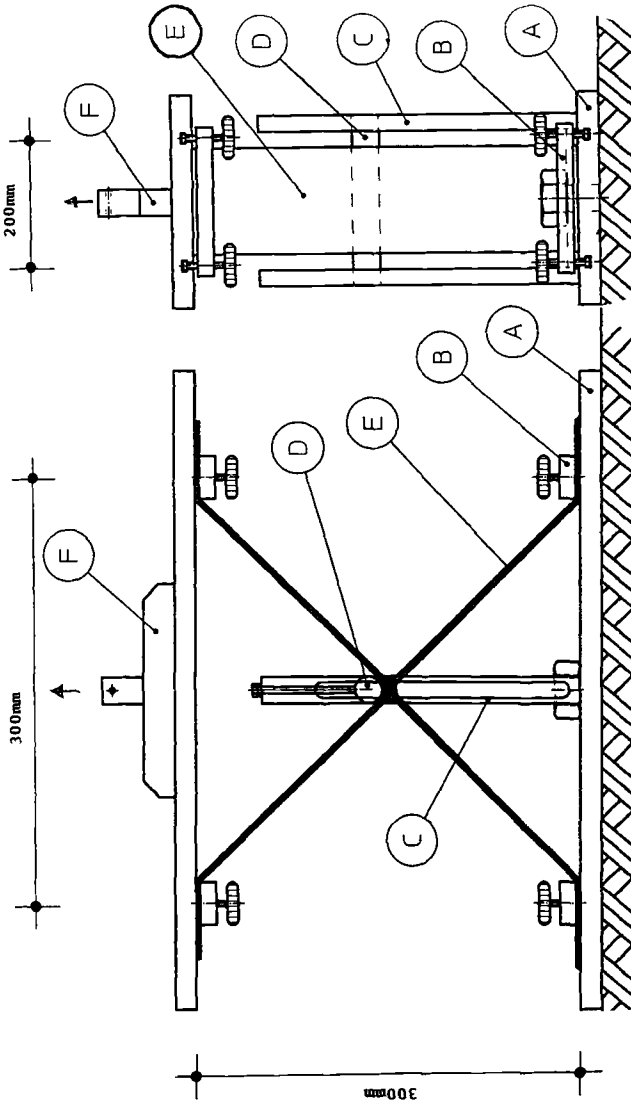


Fig. 5 - Scheme of the Staples/Connections Efficiency test for geocells: A) basement; B) sliding bars to clamp the geocell strips; C) staple sliding support; D) steel bar simulating the staple; E) geocell specimen; F) upper clamp.

is fixed to the junction or a steel bar is positioned at the top of the junction and fixed to the testing machine: a tensile test is then run at slow rate of extension (the Authors propose a testing rate of 5 mm/min) to simulate the effect of soil self weight and downward movement on the junction. Different types of connections and steel bars of different diameter are tested with this method, until a type of connection or staple is found which gives a junction strength in excess of the one measured with the index test described in the previous paragraph.

TEST RESULTS

A series of preliminary tests were carried at the Tenax Geosynthetics Testing Laboratory on two type of geocells: Tenax Tenweb 300, produced in Italy by Tenax SpA, and Geoweb, produced in USA by Presto Products. The results of the tests are summarized in Table 1.

Table 1 - Results of preliminary tests on different geocells.

Type of test	Unit	Tenweb 300	Geoweb
Panel length	m	10.0	2.45
Panel width	m	5.0	6.10
Average cells diameter	mm	300	200
Panel Thickness	mm	1.50	1.15
Cells height	mm	75	100
Unit weight of open panels	g/m ²	800	1570
Tensile strength, single strip	kN	1.2	2.85
Tensile strength, double strip	kN	2.6	6.0
Junction shear	kN	0.8	2.8
Junction peel	kN	0.35	1.35
Junction split	kN	1.1	2.7
Staples efficiency (Φ 10 mm)	kN	1.1	2.6

CONCLUSION AND PROPOSAL FOR STANDARDIZATION

Test Methods appropriate for geocells have been investigated performed and analyzed. At present, most of these tests have not been standardized yet, or the existing ones need to be modified to be adapted to the special characteristics of geocells.

The Authors feel that the following tests need an urgent consideration from the Geosynthetics Standard Committees:

- Junction shear tensile test;
- Junction peel tensile test;
- Junction split tensile test;
- Staples/connections efficiency;
- Damage during installation;
- Hydraulic and erosion testing.

All of the above tests have been fully described in this paper. The Authors hope that this contribution will speed up the standardization

process, which is needed by both producers and technical Authorities.

REFERENCES

- [1] Agnew, W., "Erosion Control Product Selection," Geotechnical Fabrics Report, No. 4, 1991.
- [2] Jagielski, K., "Erosion-Control Market Takes Hold.," Geotechnical Fabrics Report, No.3, 1991.
- [3] Cancelli, A., Monti, R., and Rimoldi, P., "Comparative Study of Geosynthetics for Erosion Control," Proc. IV Int. Conf. on Geotextiles, Geomembranes and Related Products, The Hague, The Netherlands, 1990.

Khalid A. Farrag¹, Paul Griffin²

PULL-OUT TESTING OF GEOGRIDS IN COHESIVE SOILS

REFERENCE: Farrag, K., and Griffin, P., "Pull-out Testing of Geogrids in Cohesive Soils," Geosynthetic Soil Reinforcement Testing Procedures, ASTM STP 1190, S.C. Jonathan Cheng, Ed., American Society for Testing and Materials, Philadelphia, 1993.

ABSTRACT:

The growing interest in utilizing on-site cohesive soils in reinforced-soil structures raises the need for development of testing procedures to evaluate their interaction properties (i.e. pull-out resistance and shear stress-strain characteristics). In determining the pull-out resistance of geosynthetics in clay, several factors can influence the measured properties. These factors are generally related to the testing equipment, the associated boundary effects, testing procedure, pull-out rate, geosynthetics characteristics, soil properties (e.g. soil density, grain size distribution and moisture content), compaction procedure and confining pressure.

This paper presents a part of the pull-out testing program conducted in the Geosynthetic Engineering Research Laboratory at the Louisiana Transportation Research Center to evaluate the effect of related physical parameters on the pull-out resistance of geogrids. Tests are conducted on HDPE geogrids in two pull-out boxes. The large pull-out box has dimensions of 1.5 m (60 in.) length, 0.9 m (36 in.) width, and 0.76 m (30 in.) height. The small box is 1.22 m (48 in.) long, 0.6 m (24 in.) wide, and 0.45 m (18 in.) high. A compaction procedure is developed in order to control soil density and moisture content. An instrumentation array is implemented to monitor the pull-out load, pull-out rate, normal pressure, and the displacement distribution along the geogrid specimens.

The results of the pull-out tests in both boxes provide an evaluation of the effect of various parameters on the pull-out mechanism and suggest a standardized procedure for control of box boundary effects and other influencing parameters on the pull-out resistance of geogrids.

KEYWORDS: laboratory testing, pull-out, geosynthetics, geogrids, cohesive soils, granular soils.

¹Research Coordinator, Geosynthetics Engineering Research Laboratory, Louisiana Transportation Research Center, Baton Rouge, LA 70808.

²Administrator, Geophysical Systems, Louisiana Transportation Research Center (LTRC), Baton Rouge, LA 70808.

The considerable increase in utilizing the in-site cohesive soils in reinforced-soil structures raises the need for development of testing procedures to evaluate their interaction properties (i.e. pull-out resistance and shear stress-strain relationship). Clayey and silty clay soils have been successfully used with geosynthetics in the construction of walls and embankments [1,2,3]. However, limited research relevant to the evaluation of the interaction parameters of geosynthetics in cohesive soils has been done. Research on these parameters has been conducted using direct shear tests [4,5,6] and pull-out tests [7,8]. The various equipment and testing procedures makes it difficult to consistently compare the performance of the geosynthetics in different soils.

In determining the pull-out resistance of geosynthetics, several factors can affect the measured properties. These factors are generally related to testing equipment and the associated boundary effects, pull-out rate, reinforcement type and geometry, soil compaction procedure, soil properties (e.g. its grain size distribution, density and moisture content) and confining pressure.

In order to develop a methodology for testing soil-geosynthetics interface properties, it is necessary to evaluate the effect of these parameters on the interaction mechanism. This paper presents the results of pull-out tests on geogrids in two pull-out boxes of different dimensions to evaluate the effect of some of these parameters on the interaction mechanism.

EQUIPMENT DESCRIPTION

Two pull-out boxes were utilized in the evaluation of the pull-out resistance of geogrids. The large pull-out box has inside dimensions of 1.5 m (60 in.) length, 0.9 m (36 in.) width, and 0.76 m (30 in.) height. Figure 1 shows a view of the large box. The small box has dimensions of 1.22 m (48 in.) length, 0.6 m (24 in.) width, and 0.45 m (18 in.) height. The small box is movable to ease loading and unloading the soil and to facilitate compaction and moisture control of the cohesive soil. When testing, the small box is placed inside the large box to utilize the same hydraulic loading system for pull-out. Figure 2 shows a longitudinal cross section of the small pull-out box placed inside the large box.

Sleeve plates are placed on the top and bottom of the front wall slot to minimize the lateral load transfer to the rigid front wall during pull-out. In the large pull-out box, sleeve plates of 30 cm (12 in.) length are used with soil layers thicknesses of 30 cm above and 30 cm under the geogrid. In the small box, sleeve plates of 15 cm (6 in.) length are used with soil layers thicknesses of 22 cm (9 in.) above and 22 cm under the geogrid specimen. In both boxes, the geogrid specimens are bolted between two clamping plates that extend inside the soil to insure that the geogrid remains confined during the test.

The hydraulic loading system is mounted on the loading frame of the large box and it operates under displacement-rate controlled and load-controlled modes. Vertical pressure is applied through a confined air bag on the top of the soil.

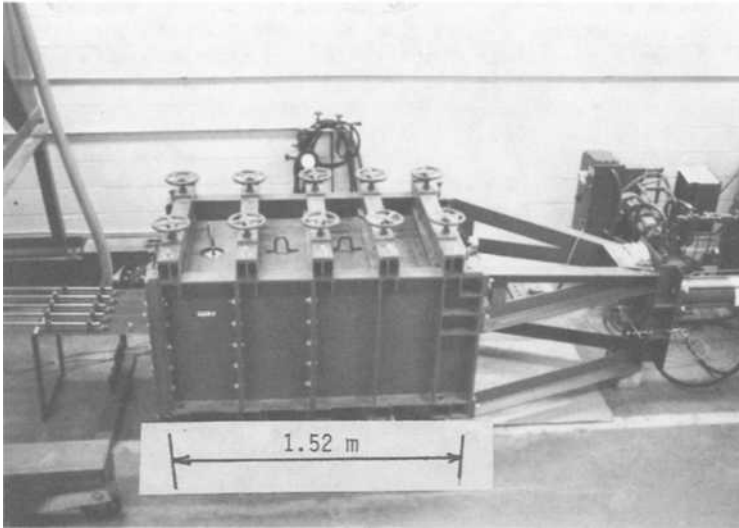


Figure 1-- View of the large pull-out box

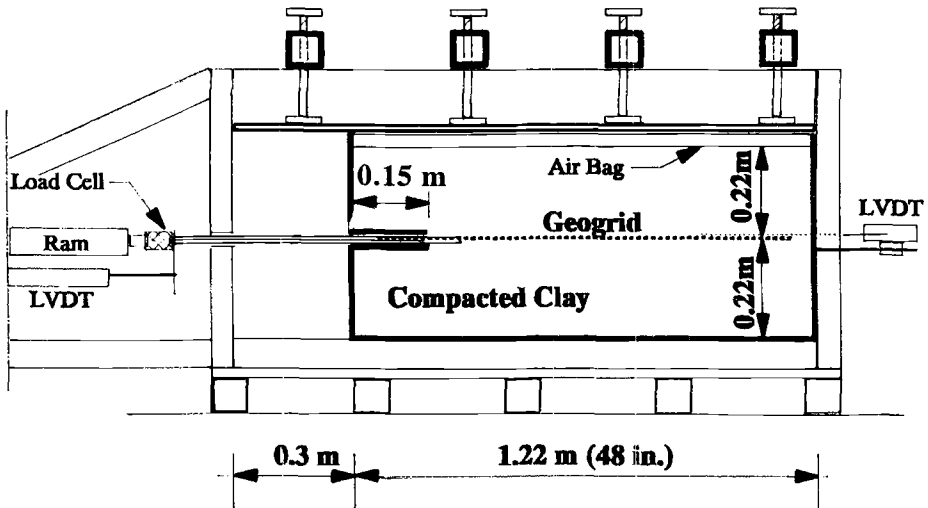


Figure 2-- Longitudinal cross section of the pull-out boxes

Instrumentation

A load cell and a Linear Variable Differential Transformer (LVDT) are mounted on the loading system to measure pull-out load and front displacement, respectively.

The displacements along the geogrid specimen are monitored using five LVDT's mounted at the rear table. Strain gauges are mounted on the geogrid longitudinal ribs to evaluate the local strains at the reinforcement. Earth pressure cells of 5 cm (2 in.) diameter are used to measure the normal pressure at different locations during pull-out. A data acquisition system is employed for the control of testing parameters and for monitoring the response parameters.

TESTING PROCEDURE

Pull-out tests were performed on HDPE geogrid specimens of 0.3 m (1 ft) width and 0.91 m (3 ft) length. Two different types of cohesive soils were utilized in the testing program. Table 1 displays the physical properties of both soils.

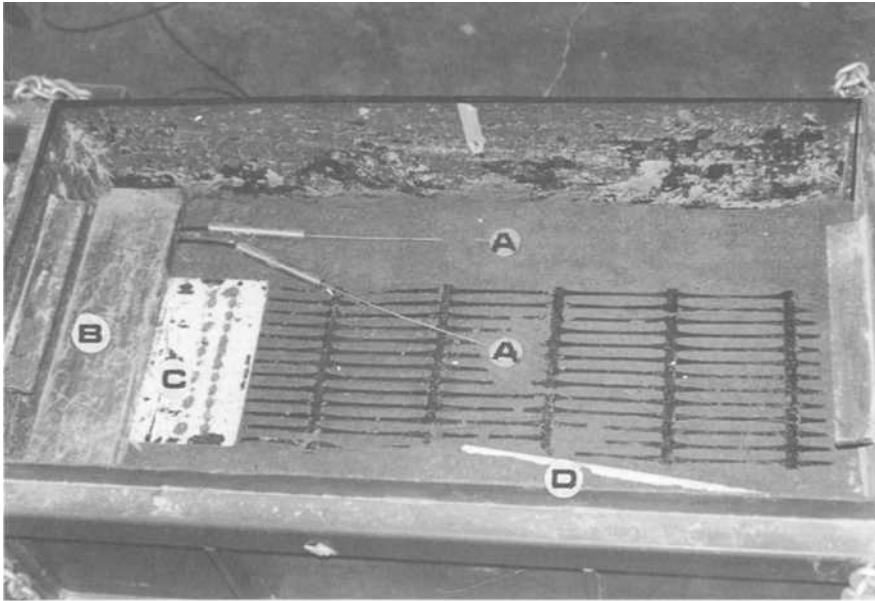
TABLE 1-- Properties of the cohesive soil.

type	L.L.(1)	P.I.(2)	%silt	%clay	w%(3)	γ_{max} t/m ³
A	27	6	72.0	19.0	15.5	1.72
B	46	24	42.0	49.0	21.0	1.52

- (1) Liquid limit
- (2) Plasticity index
- (3) optimum water content

The soil was prepared to the desired moisture content and was placed in 5 cm (2 in.) thick layers in the box. Compaction was carried out using a vibrating electric hammer. Each layer was compacted to the desired density using a predetermined compaction effort. After compaction, the density was measured for each two layers using a nuclear density gauge. Soil specimens were also taken to evaluate the moisture content (ASTM D 2216). The geogrid specimen was placed at mid-height of the soil and was connected to the LVDT's. Figure 3 shows the placement of the geogrid specimen in the small box.

Pull-out tests were performed in both soils under a confining pressure of 48.2 KN/m² (7 psi) and a constant displacement rate of 1.5 mm/min (0.06 in./min). Both soils were compacted to about 90% of their maximum dry density. Figure 4 depicts the results of six repetitive tests in soil-A under identical testing parameters; while Figure 5 depicts the results of three repetitive pull-out tests in soil-B.



(A) earth pressure cells
 (B) sleeve plate
 (C) clamping plates
 (D) plastic pipe to protect wires

Figure 3-- Displacement and pressure instrumentation of the geogrid in the small box

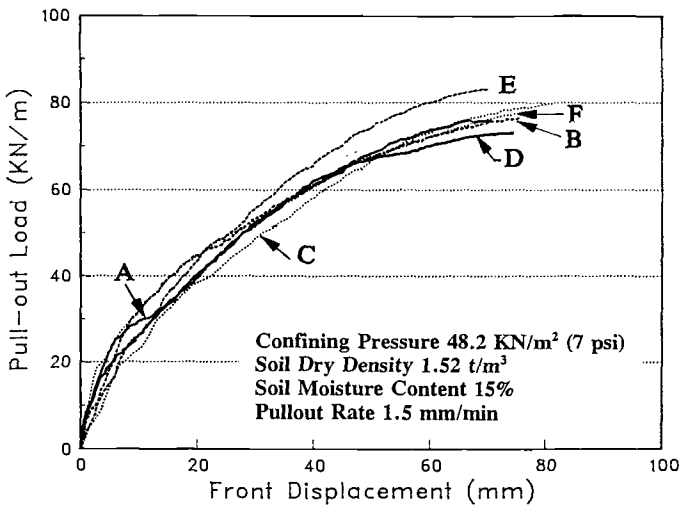


Figure 4-- Pull-out test results of geogrid in clay-A

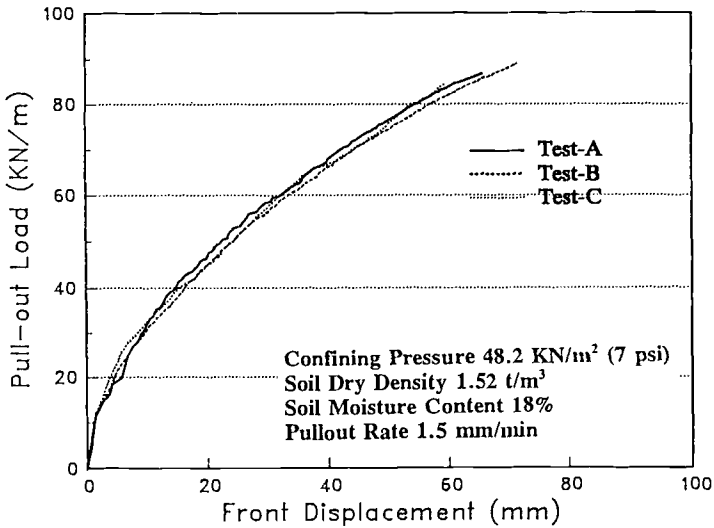


Figure 5-- Pull-out test results of geogrid in clay-B

Displacement measurements

The displacement along the geogrid specimen was monitored using five LVDT's at the rear table. The LVDT's were connected to the nodal points by inextensible wires. Strain gauges were also mounted on the longitudinal ribs in an attempt to correlate the strains calculated from the LVDT's measurements to those measured by the strain gauges. The locations of the strain gauges and the LVDT's nodal points along the geogrid specimen are shown in Figure 6.

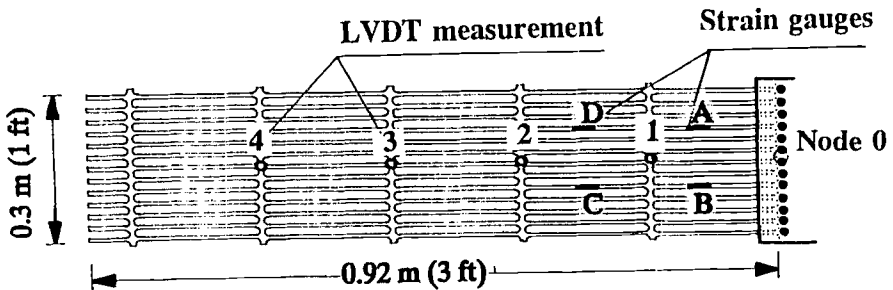


Figure 6-- Locations of displacement and strain measurements

The time-nodal displacement of three pull-out tests in soil-A are displayed in Figure 7. The results in the figure show that the slope of the time-displacement curve at the front node (node 0) is practically constant and equals the displacement-rate. At an early stage of pull-out, most of the load is carried out between node 0 and node 1 and high strains are mobilized at the front part of the geogrid. The interaction mechanism (demonstrated by both material elongation and shear resistance at the interface) progressively transfers to the rear nodes as the pull-out load increases to its peak.

The strain ϵ_i between two consecutive nodes is calculated from the LVDT's measurements by:

$$\epsilon_i = [\delta_i - \delta_{i-1}] / \Delta x$$

where δ_i and δ_{i-1} are the displacements at nodes i and $i-1$, respectively, and Δx is the length of the element. The calculated strains are plotted with those measured by the strain gauges in Figure 8. The figure demonstrates the difference between the local strains, measured by the strain gauges, and the strains developed between the transversal elements, particularly at higher strain levels.

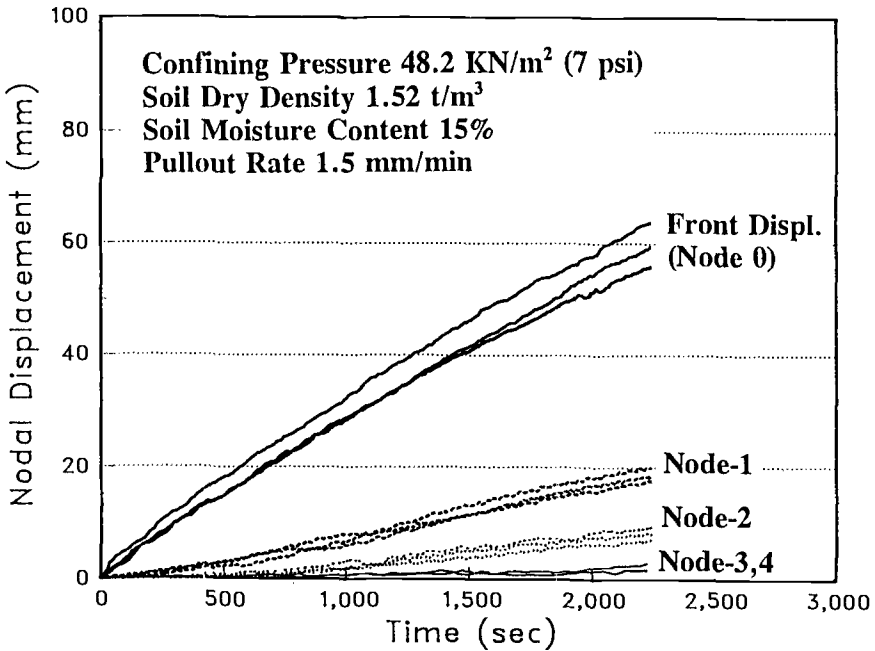


Figure 7-- Displacement of geogrid nodes during pull-out

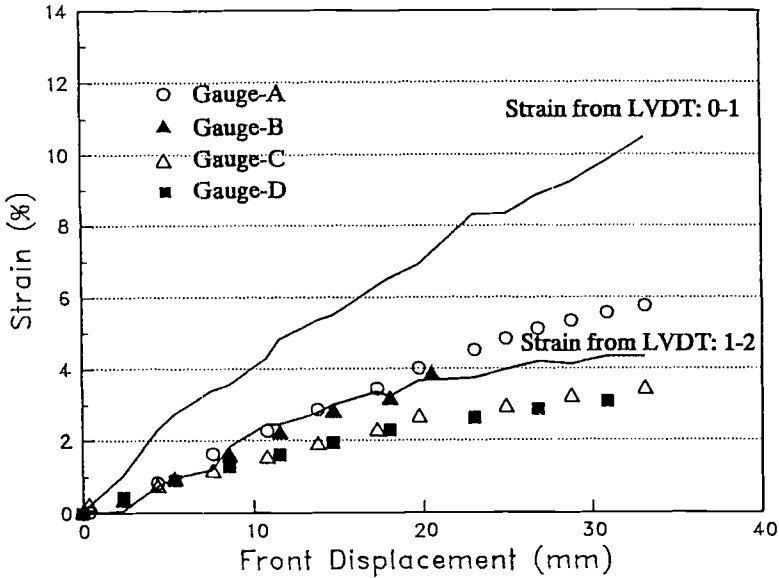


Figure 8-- Comparison of strain gauges and LVDT measurements

EFFECT OF BOX DIMENSIONS

The applied confining pressure can be partially carried by the friction along the side walls of the box [9]. This effect can be reduced by selecting sufficient distance between the geogrid and the side walls to keep the specimen under uniform normal pressure.

Pull-out tests to evaluate the effect of the specimen width/box width ratio were previously carried out in the large box. In these tests, a uniform blasting sand of dry density 1.7 t/m³ was used. HDPE geogrid specimens of widths from 0.3 m (1 ft) to 0.75 m (2.5 ft) were tested under confining pressure of 48 kN/m² and pull-out rate of 4 mm/min. The results of these tests are displayed in Figure 9. The results show that the pull-out loads/unit width of the geogrid are practically equal till a specimen width of 0.6 m is reached in the 0.9 m wide box. A reduction in the pull-out resistance is displayed when geogrid specimens of greater widths were tested. The results suggest a minimum distance of 15 cm (6 in.) between the grid and the box side walls.

The dimensions of the small box were selected to provide a distance of 15 cm between the grid and the box side walls and a total soil thickness of 45 cm (18 in.). A comparison between pull-out tests in both the large box and the small box is displayed in Figure 10. These tests were performed in soil-A. Testing parameters are kept identical in these tests and they are shown in the figure. The results show that pull-out resistances from both boxes are practically equal and suggest a minimum effect of the box boundaries in the small box.

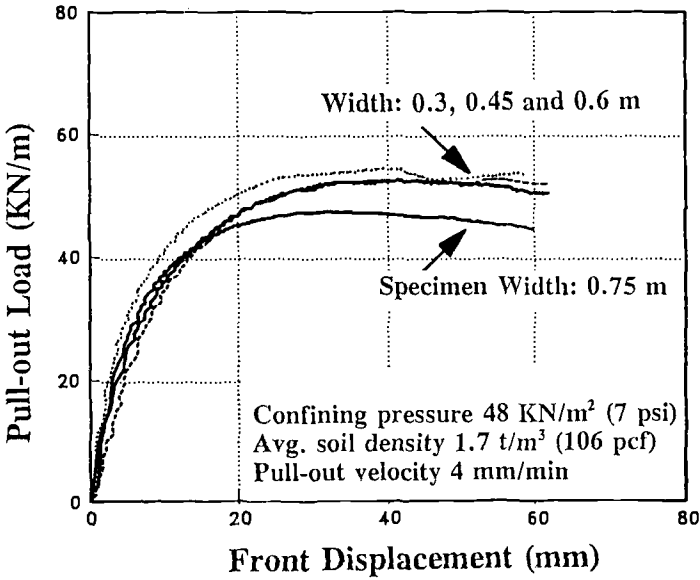


Figure 9-- Effect of specimen width on the pull-out resistance

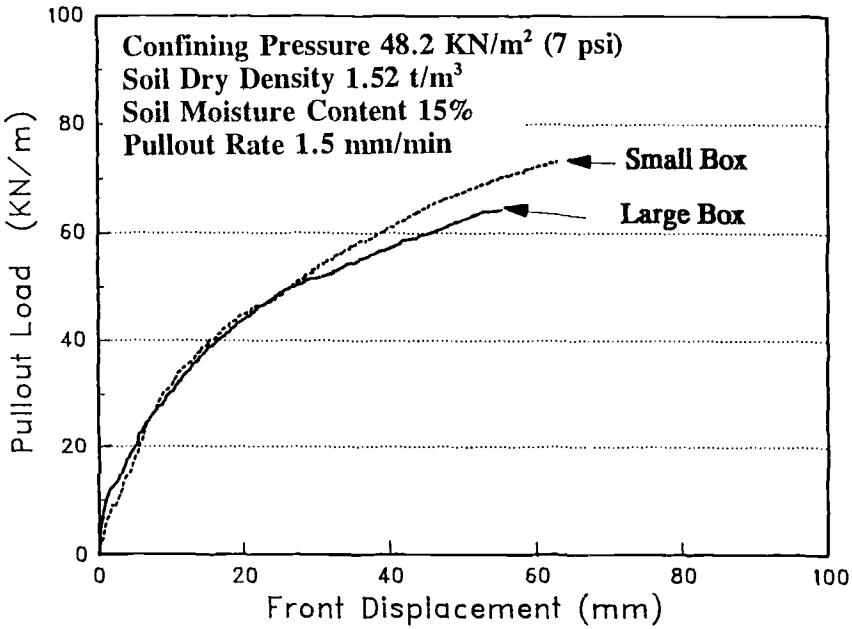


Figure 10-- Pull-out test results in the large and the small pull-out boxes

EFFECT OF MOISTURE CONTENT

The effect of an increase in the soil moisture content on the pull-out resistance of the geogrid is depicted in Figure 11. The figure displays average pull-out test results performed in soil-A with moisture contents of 15% and 20%. The soil was compacted to an average dry density of 1.51 t/m³ (94 pcf), and tested under confining pressure of 48.2 KN/m² and pull-out rate of 1.5 mm/min. The results show a decrease in the pull-out resistance as the water content increases from its optimum value to 20%.

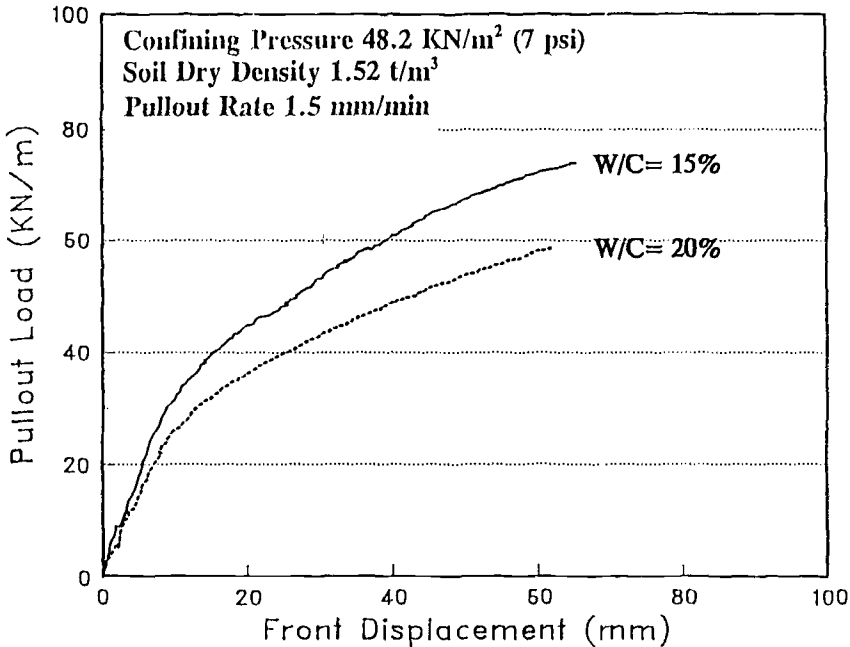


Figure 11-- Effect of soil moisture content on the pull-out

EFFECT OF SOIL CONFINEMENT

For geogrid reinforcement, the confined elongation during pull-out is restrained by the shear resistance at the soil-geogrid interface and by the passive soil resistance at the transversal elements. During pull-out, as the displacement of soil particles at the interface are restrained by the surrounding soil, an apparent increase in the normal stress results near the pull-out application point. In order to investigate the normal stress distribution on the geogrid specimen during pull-out, earth pressure cells were placed horizontally in different locations at the geogrid level in the pull-out boxes (see Figure 3).

The normal pressure measurements at different locations at the geogrid level during pull-out are shown in Figure 12. These tests were performed on soil-A compacted to a dry density of 1.51 t/m^3 (94 pcf), at a moisture content of 20%, and under a confining pressure of 48.2 KN/m^2 .

Before pull-out testing, the results in the figure display lower values of normal stress near the box side walls due to the friction between the rigid wall and the soil. During pull-out, the normal stresses in cells 3 and 4 (near the box walls) remain practically unchanged. Nevertheless, an increase in the vertical pressure at the vicinity of the pull-out application point is demonstrated in the pressure measurement of cell 1.

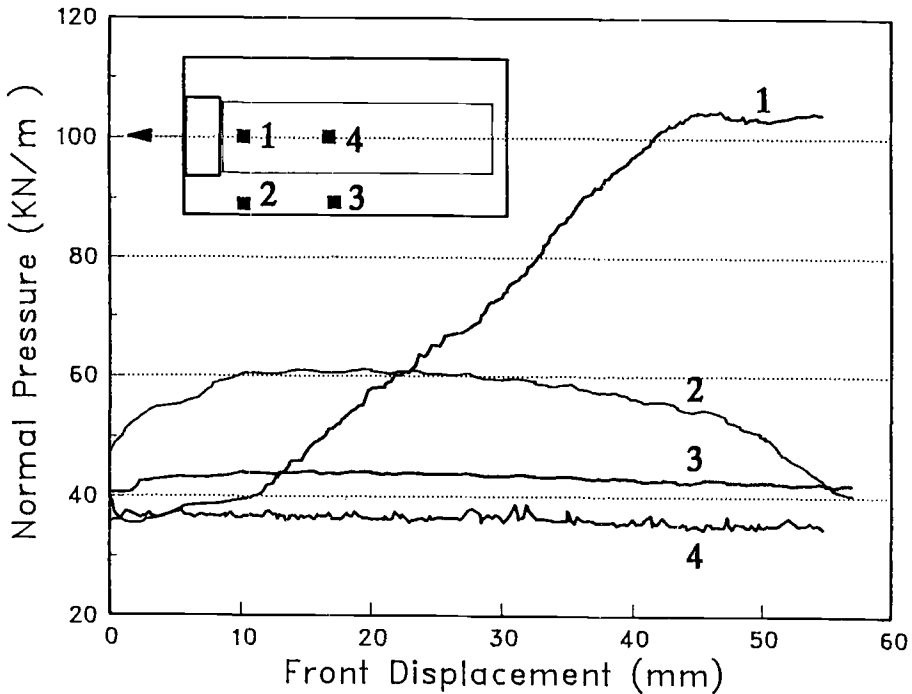


Figure 12-- Development of normal stress during pull-out

ANALYSIS OF TEST RESULTS

The major concern in the interpretation of the pull-out test results pertains to the effect of reinforcement extensibility on the pull-out resistance. Reinforcement extensibility result in a decreasing shear displacement distribution along its length. The interface shear stress is therefore not uniformly mobilized along the total reinforcement length and

the pull-out resistance becomes a function of the specimen length. The non-uniform displacement distribution along the reinforcement is displayed in Figure 13. In the figure, the nodal displacements at different pull-out loads are plotted along the length of the specimen.

The pull-out resistance of geogrid of a specific length in the field can be extrapolated from the measured displacement distributions in pull-out tests. The extrapolation approach is not in the scope of this paper. However, empirical approaches have been recommended to include the effect of extensibility in determining the pull-out resistance [10]. Several analytical approaches are also implemented in order to extrapolate the pull-out resistance of any reinforcement length [11,12,13].

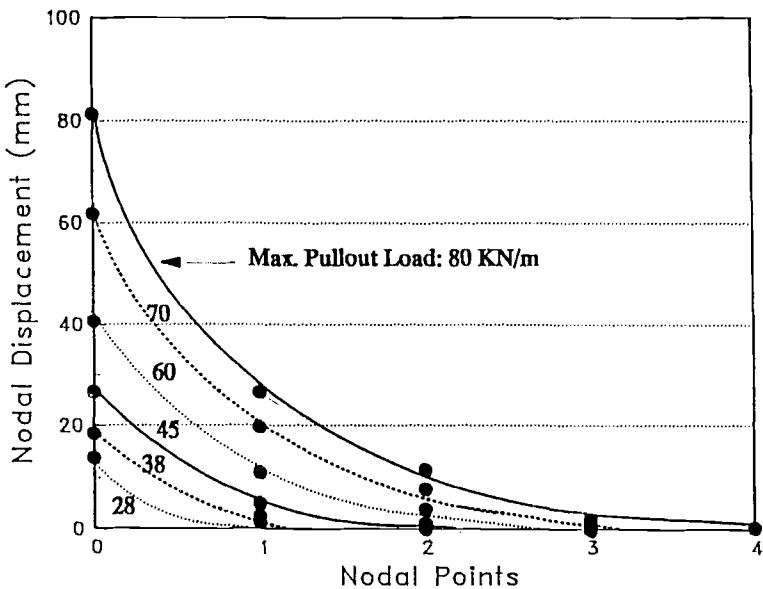


Figure 13-- Displacement distribution along the geogrid

CONCLUSIONS

Two pull-out boxes were utilized in the evaluation of the short term interface parameters of geogrids in cohesive soils. The instrumentation of the pull-out boxes permitted the measurement of the pull-out resistance and the displacement distribution along the confined geogrid.

The evaluation of earth pressure development during pull-out at different locations in the box demonstrates the importance of the effect of the specimen and the box dimensions on the pull-out interaction parameters. The friction between the soil and the box side walls can reduce the amount of normal pressure on the geogrid. The results suggest a minimum distance of 15 cm (6 in.) between the box and the specimen.

The results of the pull-out tests in both boxes also provide an evaluation of the effect of various parameters on the pull-out mechanism and suggest a standardized procedure for control of box boundary effects, soil density and moisture content. The long term pull-out behavior and the effect of the pull-out rate on the pull-out interaction mechanism in cohesive soils are yet to be evaluated in the testing program.

ACKNOWLEDGMENT

The results present a part of an ongoing research program on the evaluation of pull-out resistance of geosynthetics in cohesive soils. The research is supported by funds awarded by the Louisiana Transportation Research Center and the Federal Highway Administration.

REFERENCES

- [1] Hayden, R.F., Schmertmann, G.R., Qedan, B.Q., and McGuire, M.S., "High Clay Embankment Over Cannon Creek Constructed with Geogrid Reinforcement," Geosynthetics'91 Conference, Atlanta, 1991, pp. 799-822.
- [2] Bakeer, R.M., Hadj-Hamou, T., Duarte, F., and Saterlee, G.S., "Field Test of a Geotextile-Reinforced Levee," Transportation Research Record 1277, 1990, pp. 90-101.
- [3] Hannon, J.B., and Forsyth, R.A., "Performance of an Earthwork Reinforced System with Low Quality Backfill," Transportation Research Record 965, 1984, pp. 55-66.
- [4] Lafleur, J., Sall, M.S., and Ducharme, A., "Frictional Characteristics of Geotextiles with Compacted Lateritic Gravels and Clays," Geosynthetics'87 Conference, New Orleans, 1987, pp. 205-215
- [5] Richards, E.A., Scott, J.D., Bobey, L.W., and Diyaljee, V., "Shear Resistance Between Cohesive Soil and Geogrids," Geosynthetics'89, San Diego, pp. 489-500.
- [6] Ingold, T.S., "A Laboratory Simulation of Reinforced Clay Walls," Geotechnique, Vol 31, No. 3, 1981, pp. 339-412.
- [7] Fourie, A.B., and Fabian, K.J., "Laboratory Determination of Clay-Geotextile Interaction," Geotextiles and Geomembranes, Vol. 6, No. 4, 1987, p. 275-294.
- [8] Ingold, T.S., "A Laboratory Investigation of Grid Reinforcement in Clay," Geotechnical Testing Journal, Vol. 6, No. 3, 1983, pp. 112-119.
- [9] Palmeira, E.M., and Milligan, G.W., "Scale and Other Factors Affecting the results of Pull-out Tests of Grids Buried in Sand", Geotechnique, Vol. 39, No. 3, 1989, pp. 511-524.

- [10] Christopher, B.R., Gill, S.A., Giroud, J.P., Juran, I., Mitchell, J.K., Schlosser, F., and Dunncliff, J., "Reinforced Soil Structures, Design and Construction Guideline, FHWA Report No. RD-89-043, 1989.
- [11] Juran, I., Farrag, Kh., and Richmond, L., "Short and Long Term Performance of Polymeric Geogrids," Geosynthetics'91 Conference, Atlanta, Vol. 2, 1991, pp. 587-599.
- [12] Juran, I., and Chen, C.L., "Soil-Geotextile Pull-out Interaction Properties, Testing and Interpretation," Transportation Research Board, 67th Annual Meeting, 1988.
- [13] Yuan, Z., and Chua, K.M., "Analytical Model for Pullout of Soil Reinforcement," Transportation Research Record 1330, 1991, pp. 64-71.

Deron N. Austin¹, Kevin J. Wu², and David F. White³

THE INFLUENCE OF TEST PARAMETERS AND PROCEDURES ON THE TENSILE MODULUS OF STIFF GEOGRIDS

REFERENCE: Austin, D.N., Wu, K.J., and White, D.F., "The Influence of Test Parameters and Procedures on the Tensile Modulus of Stiff Geogrids", Geosynthetic Soil Reinforcement Testing Procedures, ASTM STP 1190, S.C. Jonathan Cheng, Ed., American Society for Testing and Materials, Philadelphia, PA, 1993.

ABSTRACT: Geogrid tensile strength at low strains is difficult to determine due to the non-linear, viscoelastic behavior of thermoplastic polymers. Their response to applied tensile loads is profoundly different from that of elastic materials including elastic structural metals. The stress-strain properties of plastics are not constant, varying greatly and nonlinearly with the test parameters. Therefore, if testing conditions are not controlled and accounted for, they can be inaccurate predictors of tensile performance. The measurement of tensile modulus is affected by such factors as temperature, sample length, gauge length, extension rate, and tension and strain measuring equipment.

It is not easy to define the effect of the numerous variables involved with the tensile testing of thermoplastic materials. However, the general effect of a few of the more important and controversial variables was investigated in order to provide some appreciation of the sources of variability. This paper presents the results and observations from an inter-laboratory study that determined tensile modulus of stiff polypropylene geogrids. Various test parameters and procedures affecting the measured results and their potential relevance to field performance were studied. Conclusions and guidelines are provided, and recommendations are made for modifications to current test methods when tensile modulus at low strains is of particular interest.

KEYWORDS: geogrid, polypropylene, tensile, extensometer, modulus, single rib, reinforcement, soil.

¹Products Engineer, Geosynthetics Division, TENAX Corporation, 8291 Patuxent Range Road, Jessup, MD 20794, USA.

²Geosynthetic Application Manager, Titan Geosynthetics Co., Ltd., Taipei, Taiwan.

³Program Manager, Geosynthetics Technology, TRI/Environmental, Inc., 9063 Bee Caves Road, Austin, TX 78733, USA.

BACKGROUND

History

The idea of reinforcing soft soils with stiff tensile elements in civil engineering projects dates back hundreds, even thousands, of years. In the colonial days, pioneers laid tree branches and logs over swampy areas to distribute traffic loads over a wider area. This technique served to reduce the stress induced on the foundation soils of roadways and haul roads.

With the development of high strength polymers in the 1960s, came innovative plastics applications in the civil engineering field. The early 1970s saw the development of a synthetic textile (i.e. "geotextile") that could be used within the aggregate base layer to confine soft subgrade soils and prevent base punching or localized shear failure. The 1980s brought about a completely new concept - the geogrid.

The geogrid features higher tensile modulus at lower strain levels than the geotextile and has an open geometry. The open geometry allows this tensile element to interlock with the material being reinforced, rather than lying above or below as a separate component. The geogrid assumes tensile strength when the surrounding soil strains due to applied stresses. Therefore, the geogrid does not rely on planar deflection to assume strength; the interlocking feature makes the geogrid an integral element of the foundation soil system. Traffic loads apply stress to the subsoil creating localized movements amongst soil particles, which interlocks with and strains the geogrid.

Production

Geogrids are typically manufactured from thermoplastic polymers, such as polypropylene or high density polyethylene. These products are either made from a unique extrusion or a punched sheet [1]. The former process extrudes molten polymer through a series of unique dies that creates a multi-planar extrusion which is then bi-dimensionally stretched. The stretching process orients the molecular chains into a post-yield state, thereby increasing the product's strength, resistance to creep and tensile modulus. The oriented geogrid strands (i.e. "ribs") are typically arranged in the field in the direction of the anticipated stress in the reinforced soil mass.

Geogrids manufactured from polypropylene are primarily stretched in two perpendicular directions; 1) along the roll length, and 2) across the roll width. Therefore, these products have an increased resistance to tensile stress throughout the entire horizontal plane of reinforcement. This type of stress environment is commonly encountered in the construction of roadways over soft soils.

Current Problems

Because of the rapid acceptance and usage of polypropylene geogrids in civil engineering applications, these products have gained attention at testing laboratories and standardization agencies. Specific testing procedures used by geogrid manufacturers and those followed by independent testing organizations are difficult to compare. Subsequently, the Geosynthetics Research Institute (GRI) of Drexel University and the American Society for Testing and Materials (ASTM) began drafting test methods. These standards began to take shape nearly five years ago and have been primarily based on one manufacturer's test methods.

Although specific steps in the test procedures are complete and accurate, the measurement of the tensile strength at low strains (tensile modulus) is difficult to accurately determine from these single rib test procedures. This is due to the viscoelastic or non-linear behavior of thermoplastic polymers, such as polypropylene. These plastics are complex aggregates of several elastic and fluid elements and, as a consequence, display properties between crystalline metals and viscous fluids [2]. Further complicating the matter is the fact that all extruded or sheet-punched geogrids are oriented, some at different and varying degrees. The mechanical stretching process is imperfect and may not produce adjacent geogrid ribs with exactly the same tensile strengths.

The ultimate tensile strength and elongation of single rib specimens can be measured from the test methods distributed by GRI or proposed by ASTM. The shape of the strength-strain curve is very sensitive. Several problems arise when attempting to measure the tensile properties of polypropylene geogrids. For starters, the strength-strain curves vary substantially with the rate of loading, temperature, gage length, and the type of instruments available [1]. They do not have well-defined yield points or true proportional limits. The deformation and breaking characteristics are greatly dependent upon time under load [2].

Unlike metals, plastic specification tests (data sheet properties) generally are not useful in predicting plastics performance. They are particularly inadequate in judging mechanical strength capabilities. In proper plastics design, the philosophy is to rely on prototypes and finite element modelling to select materials [2]. The properties of geogrids that have been made most available to specifiers and designers are the traditional metal design properties, derived from strength-strain tests, plus data from arbitrary ASTM index tests whose proper field of use is in material purchase specifications. Since data sheet properties have only a limited or general relationship to performance, the result has been the frequent misapplication of ASTM index test data for lack of proper and informed interpretation by the user.

Additional Considerations

Although inconsistencies do exist, the design engineer is still concerned with the strength-strain behavior of thermoplastic materials, namely polypropylene geogrids. The amount of required tensile strength and allowable elongation depends upon the application, some more critical than others. However, the importance of determining the tensile strength of geogrids at low strains for the purpose of design has never been proven. Theoretical methods have been proposed which takes into account three (3) main mechanisms through which a geogrid can improve the load carrying capacity of unpaved roads over soft soils. These theoretical influences are proposed as: (1) confinement of the subgrade soil, (2) improved load distribution, and (3) tensioned membrane effects [4]. Since the effects of the tensioned membrane theory is neglected in the method, it is unclear how the actual tensile properties of the reinforcement effects performance. Furthermore, current design literature from one geosynthetic manufacturer does not allow for the input of the tensile strength or modulus of the geogrid reinforcement for the design of haul roads over soft soils [5]. An extensive literature review by the Geosynthetics Research Institute also resulted with inconclusive findings regarding the tensile effects strength has on subgrade improvement [6].

We as civil engineers place a high degree of importance on the development of a full strength-strain plot for the determination of design and applicability. However, the current geogrid single rib test procedure drafted by the ASTM D35 Subcommittee on Mechanical Properties is only used to determine the ultimate strength and elongation of single rib geogrid specimens [7]. The test is written as an index test and is intended for

quality control purposes, not as a performance test. This ASTM proposed test method is based upon the standard procedures written in GRI Test Method GG1-87 [3]. However, the test could serve as a more useful tool if an attempt was made to model the stress mechanism in the laboratory of the actual application in the field. With these results, engineers and specifiers could utilize test methods that measured geogrid strength and elongation in the low strain range, data which are more pertinent to loading patterns and configurations found in the field.

Applications for the polyethylene geogrids are to lay the product horizontally within granular backfill in order to allow the construction of steeper slopes or less costly retaining walls. There are several tests currently used to assist the engineer with the determination of soil-geosynthetic interaction. Direct shear and pullout tests all yield pertinent information for performance test results. However, these tests are time-consuming and costly. To model this configuration in the laboratory with a quick, open air index tensile test, the tail of the geogrid is anchored (clamped) into the lower jaw (Figure 1). The single geogrid rib is strained at a constant rate of extension and strength resistance is measurement with a load cell to model the load application and resulting strain at the face of the structure. Data from the single rib test is calculated to provide a result in terms of strength per unit width. This field-laboratory relationship is excellent for specifiers on modular, reinforced retaining walls and reinforced steep slopes, but has little or no reliability on base reinforcement or soft soil stabilization projects.

When a polypropylene geogrid is laid directly above a soft subgrade to serve a load distribution function, the geogrid ribs strain locally from the movements of surrounding materials in a confined environment. Since there are no predefined anchor points for a geogrid used in base reinforcement, the extension measured in the laboratory at the ends of the sample has no bearing on the amount of localized tensile strength mobilized in the geogrid. The ability of the geogrid to absorb shear deformations of the surrounding soil is relative to the location of the applied traffic loadings and the localized strength of the subgrade soils. The strength response of the geogrid at low strain levels should be measured within the specimen's gauge length in order to properly measure localized strains (Figure 2). It is proposed that the index test to determine geogrid single rib tensile strength (particularly modulus) be application specific.

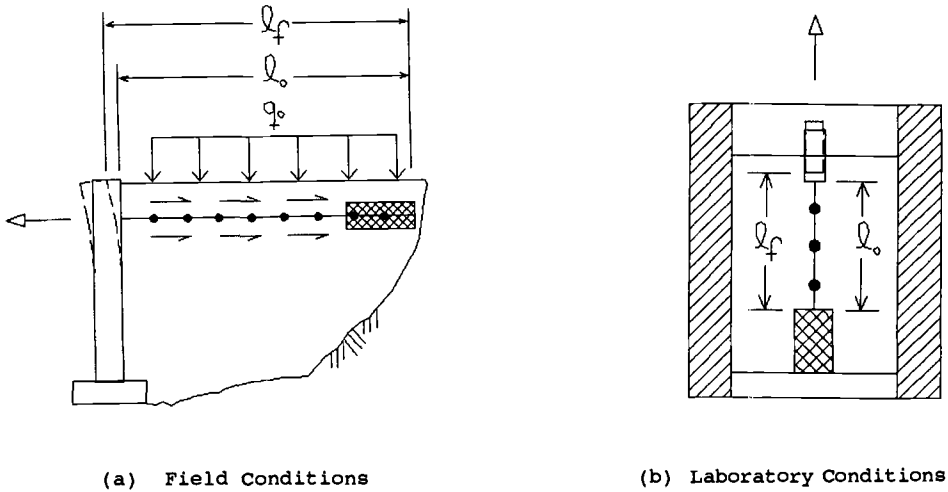


FIGURE 1 -- Uni-dimensional Strain Relationships
Steep Slope & Retaining Wall Reinforcement

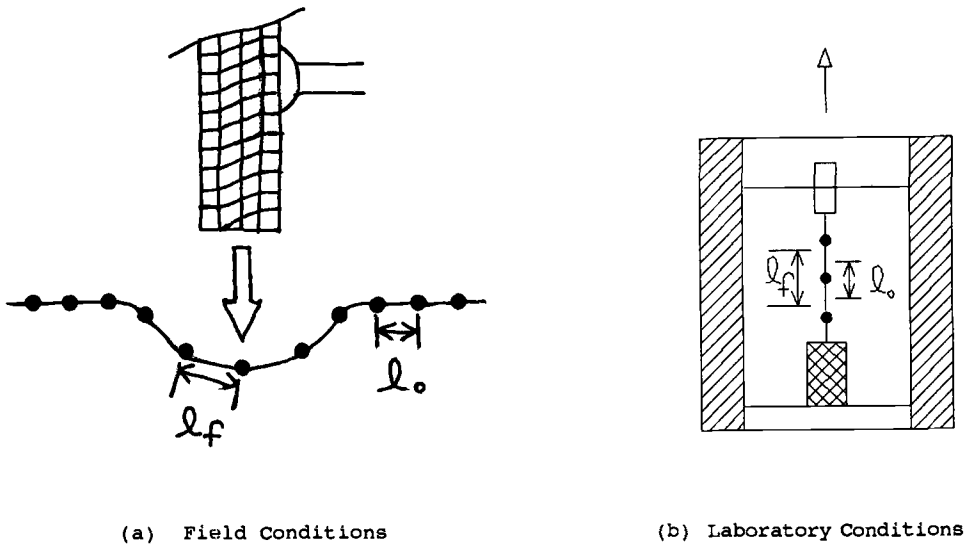


FIGURE 2 -- Multi-directional Strain Relationships
Base Reinforcement & Soft Soil Stabilization

LABORATORY INVESTIGATION

Geogrid Material

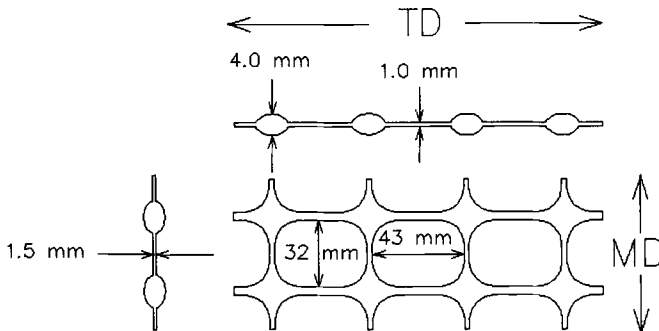
The supplied material was manufactured by RDB Plastotecnica (TENAX Group) of Vigano Brianza (Como), Italy. The geogrid evaluated was made from a unique polypropylene homopolymer extrusion that was biaxially-oriented with a stretching process. The published specifications for the geogrid material used in this study has the typical properties shown in Table 1 and a typical geometry as shown in Figure 3.

TABLE 1 -- Typical Properties of Geogrid Material

PROPERTIES	TEST METHOD	UNITS	TYPICAL VALUES	
			M.D.	T.D.
<u>Performance</u>				
Wide Width Tensile Strength	ASTM D4595	kN/m	14.3	17.2
Single Rib Tensile Strength	GRI-GG1	kN/m	14.5	17.5
Junction Strength	GRI-GG2	kN/m	13.0	15.8
<u>Composition</u>				
Polypropylene	ASTM D4101	%	98.5	
Carbon Black	ASTM D4218	%	1.5	
<u>Dimensions</u>				
Aperture Size	-	mm	32	40
Rib Thickness	-	mm	1.5	1.0
Junction Thickness	-	mm	4.0	
Open Area	-	%	75	
Roll Width	-	m	3.5	
Roll Length	-	m	100	
Gross Roll Weight	-	kg	85.5	

Notes: M.D. indicates machine (roll) direction; T.D. indicates transversal direction. All tensile properties reported as minimum average roll values, calculated from the 95 percent lower confidence limit.

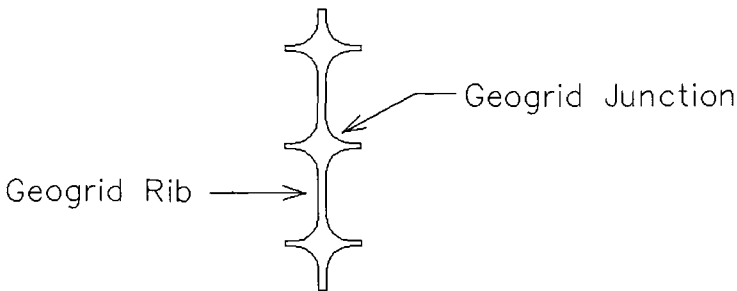
FIGURE 3 -- Typical Geogrid Geometry



Specimen Preparation

Individual single rib geogrid specimens were randomly sampled and cut from the supplied material according to sample preparation procedures outlined in GRI Test Method GG1-87 [3]. A large number of specimens were cut measuring three (3) junctions and two (2) ribs long. Approximately 20 specimens were cut measuring four (4) junctions and three (3) ribs long. All specimens were removed from the roll in the machine direction. A typical specimen for the single rib tensile test is shown in Figure 4.

FIGURE 4 -- Typical Geogrid Specimen
3 Junction, 2 Rib Configuration

Laboratory Equipment

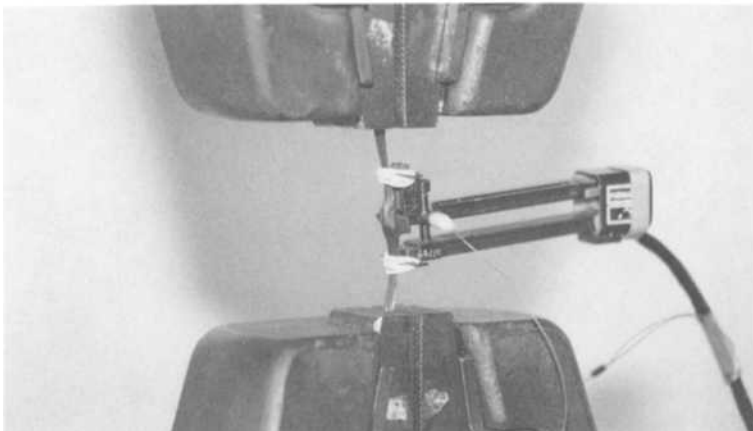
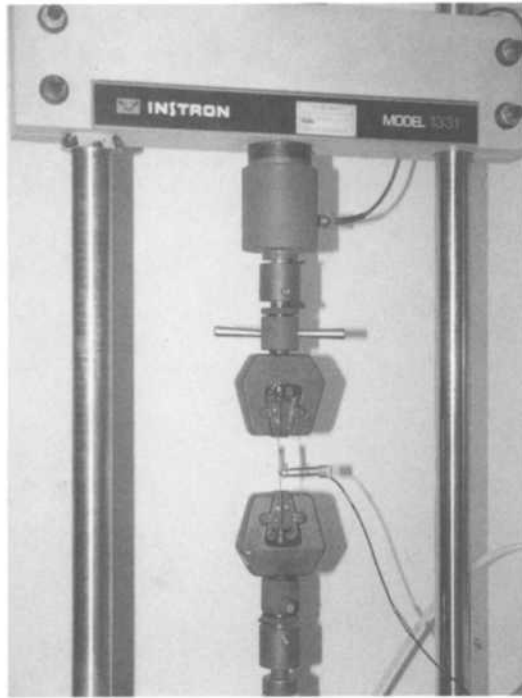
Two different tensile testing instruments were used for the single rib tensile tests. The majority of tests were performed using an Instron Model 1331 servo-hydraulic testing instrument. The servo-hydraulic testing machine differs from standard tensile equipment in that the source of motion applied to the material specimen is a hydraulic piston rather than a motor-driven screw driving a moving crosshead. The servo-hydraulic instrument is operated under the control of electronic components including a waveform generator (to apply cyclic waveforms such as ramp or sine wave loading patterns), a closed-loop servo control system (to provide a constant rate of load or strain increase driven by the transducer output), and signal conditioning (to convert transducer output to DC signals or digital formats). The servo-hydraulic instrument was selected since it makes accurate measurements of the piston's position possible via a linear variable displacement transducer (LVDT). Since the elongations of interest in this study were between 2 to 5 percent over a gage length of 71 cm, displacements were less than 1.5 mm. Therefore, these small measurements are made within the first few seconds of testing. Henceforth, errors due to uncertainty in the determination of crosshead position and rate of travel can be quite significant. The hydraulic piston with LVDT transducer does not have the slack and hysteresis associated with motor-driven screw drive machines which use chains or gears to move the crosshead.

The second testing instrument used was a United Model TM-10 screw driven testing instrument. Crosshead position and strains for this machine could only be determined by inferring the displacement applied to the sample from the crosshead speed and the elapsed time.

An external strain transducer (extensometer) was used in conjunction with the servo-hydraulic testing machine for some of the tests. The extensometer reduces uncertainty in the measurement of strain. However, the user is limited to fixed increments of gage length. The extensometer used has a range of ± 5.1 mm and is mounted to the tensile specimen with a pair of small knife blades and rubber bands. It is equipped with several adapters for gage lengths ranging from 12.7 mm to 50.1 mm. Because of these limitations on gage length, the extensometer must either be mounted across a junction, between a junction, or when fitted with the 50 mm adapter, across two junctions. Photograph 1 illustrates extensometer placement and attachment to single-rib geogrid specimens in the servo-hydraulic testing machine.

For all tests, self-tightening wedge grips were used with gripping at the junction.

PHOTOGRAPH 1 -- Test Arrangement
Servo-Hydraulic Tensiometer
and
Mounted Extensometer



Test Procedures

Single rib tensile tests were conducted on conditioned samples at the facilities of TRI/Environmental in Austin, Texas. Geosynthetic Research Institute Test Method GG1-87, "Geogrid Rib Tensile Strength" was followed to determine the single rib tensile response of each geogrid specimen [3]. During the test, data was recorded on a computerized data logger, and loads at the strain levels of interest (2, 3, and 5 percent) were determined by extrapolation from recorded the stress/strain data. From the results of the single rib test, the full width geogrid strength was determined.

The specific test parameter or procedure in question was altered for each individual test while others were held constant, so that the effect of each parameter could be discriminated. When the extensometer was not used, strain was determined by piston displacement as determined from LVDT output. Table 2 lists the parameters which were tested.

TABLE 2 -- Test Approach & Variables

TEST NUMBERS	VARIABLE UNDER STUDY
1,2,3	Temperature Effects
1,4,5,6,7	Strain Rate Effects
1,8	Length of Specimen
1,10,11,12	Gage Location & Extensometer Effects
1,9	Machine Type

PRESENTATION OF RESULTS

The average results for ten (10) samples for each test parameter and variable under study are summarized in Table 3. The parameters varied during the test included temperature, test speed, gauge length, gauge location, strain measuring equipment and the type of tensiometer used.

TABLE 3 -- Single Rib Tensile Test Results
Test Method GRI GG1-87

Test Number	Temperature Celsius (degrees)	Rate of Extension (mm/min)	Gage Length and Location	TENSILE MODULUS		
				2 Percent (kN/m)	3 Elongation (kN/m)	5 (kN/m)
1	23	50	3 Junctions	211.55	197.22	174.36
2	27	50	3 Junctions	199.86	179.35	168.82
3	32	50	3 Junctions	186.08	178.19	166.66
4	23	1.25	3 Junctions	159.61	147.11	130.50
5	23	12.5	3 Junctions	251.99	221.28	190.63
6	23	25	3 Junctions	214.62	193.42	174.35
7	23	125	3 Junctions	175.78	164.26	149.62
8	23	50	4 Junctions	189.58	170.18	151.26
9*	23	50	3 Junctions	163.52	134.22	126.73
10	23	50	25 mm** Between Junctions	170.67	170.54	169.04
11	23	50	25 mm** Across Junction	258.97	257.25	216.81
12	23	50	50 mm** Across Junction	205.42	202.66	191.93

* Indicates tensiometer used in these tests was the screw driven type.

** Indicates extensometer used in these tests in the determination of gage length and respective strain.

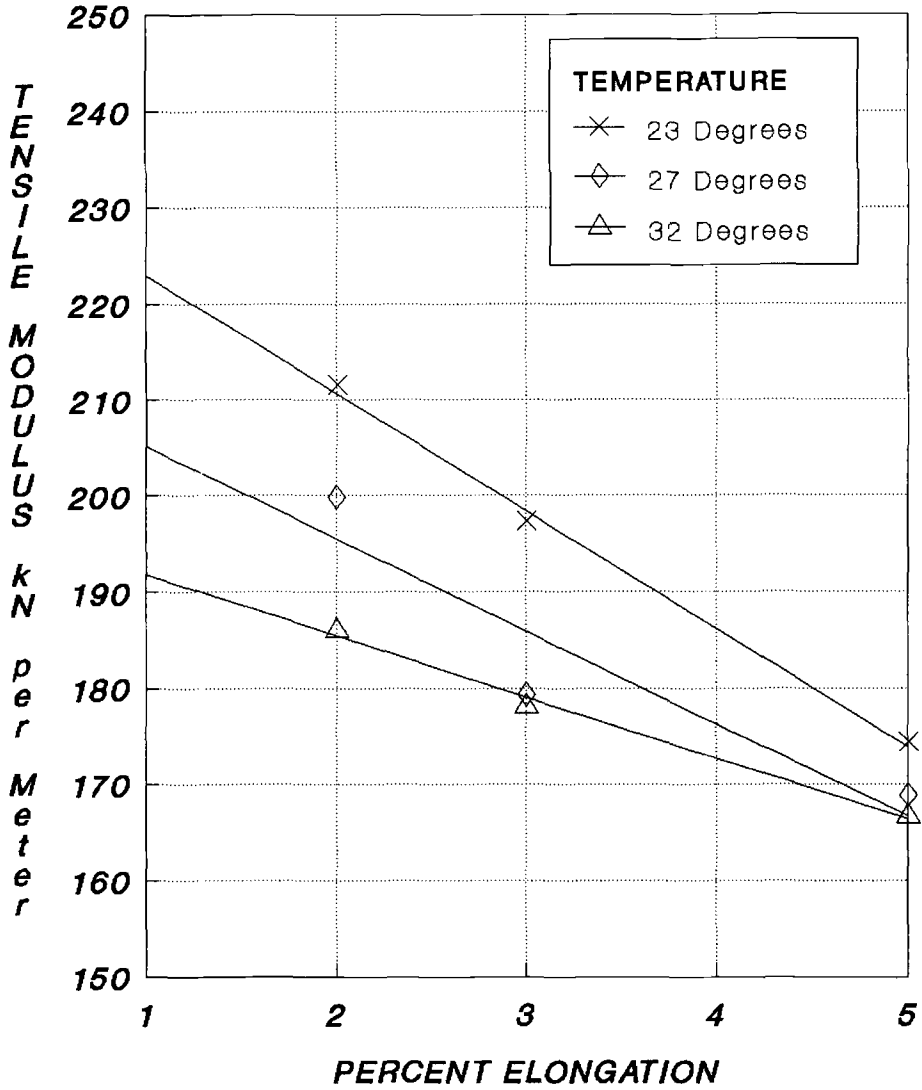
DISCUSSION AND ANALYSIS

Very good consistency and repeatable data was obtained from these single rib tensile tests. The effect of each variable was found to be consistent with expectations, except for the effect of strain rate. This variable led to unexpected results. A discussion of the effects observed as each parameter was investigated is provided below. Data plots are provided as Figures 5 through 9.

Temperature (Figure 5)

The three temperature levels plotted indicate a clear trend, consistent with expectations, where the tensile modulus decreases with an increase in temperature. The tensile modulus is shown to be more

FIGURE 5 -- Temperature Effects on Tensile Modulus



sensitive to temperature increases at lower strains, which is in agreement with the proposed arguments of this paper. As modulus is measured near 5 percent elongation, the differences in temperature increases become almost negligible. However, the variation in measured tensile modulus at strains below 4 percent is quite significant. At 2 percent elongation, slight changes in temperature result in marked changes in the measured tensile modulus. For example, these variation can be calculated and possibly classified as a percent error:

At 2 percent elongation, the temperature effects are as follows;

$$\frac{211.55 \text{ kN/m (at } 23^{\circ}\text{C)} - 199.86 \text{ kN/m (at } 27^{\circ}\text{C)}}{211.55 \text{ kN/m (at } 23^{\circ}\text{C)}} \times 100 = 5.52\% \text{ (1)}$$

and;

$$\frac{211.55 \text{ kN/m (at } 23^{\circ}\text{C)} - 186.08 \text{ kN/m (at } 32^{\circ}\text{C)}}{211.55 \text{ kN/m (at } 32^{\circ}\text{C)}} \times 100 = 12.1\% \text{ (2)}$$

A four (4) degree Celsius temperature variation is quite possible within a laboratory or production environment not controlled with a timed, central heating and air conditioning system. The importance of careful control over laboratory temperature is illustrated by this data. The proper conditioning of test specimens in accordance with GRI GGI-87 should also be considered important [3].

Gage Length (Figure 6)

The data suggest that shorter samples will yield higher tensile modulus, independent of the location along the strength-strain curve where the tensile modulus is obtained. At each strain increment, the same linear relationship governs the differences in modulus attributable to sample length. This trend is self-explanatory.

Strain Measuring Location & Equipment (Figure 7)

The relationships depict a linear trend where a gage length not measured with external extension recording equipment yields lower tensile modulus at lower strain levels. This may well be an underestimate of the tensile properties of the specimens. The tensile modulus is shown to be more sensitive to the method used to make elongation measurements at lower strains. As modulus is measured at 5 percent elongation, the differences become independent of the type of strain measuring equipment used to determine the tensile strength at the particular strain. However, the variation in measured tensile modulus at strains below 5 percent is significant. The variation can be calculated as a possible percent error:

At 2 percent elongation with and without an extensometer;

$$\frac{258.97 \text{ kN/m (with)} - 211.55 \text{ kN/m (without)}}{258.97 \text{ kN/m (with)}} \times 100 = 18.3\% \text{ (3)}$$

It is also clear that the mounting position of extensometer on the rib effects results. Apparently, elongation at low strains takes place preferentially between the junctions rather than across or just adjacent to the junctions. This would be expected, since the area between junctions presents a smaller cross sectional area resulting in higher localized stress and higher elongation.

FIGURE 6 -- Gage Length Effects on Tensile Modulus

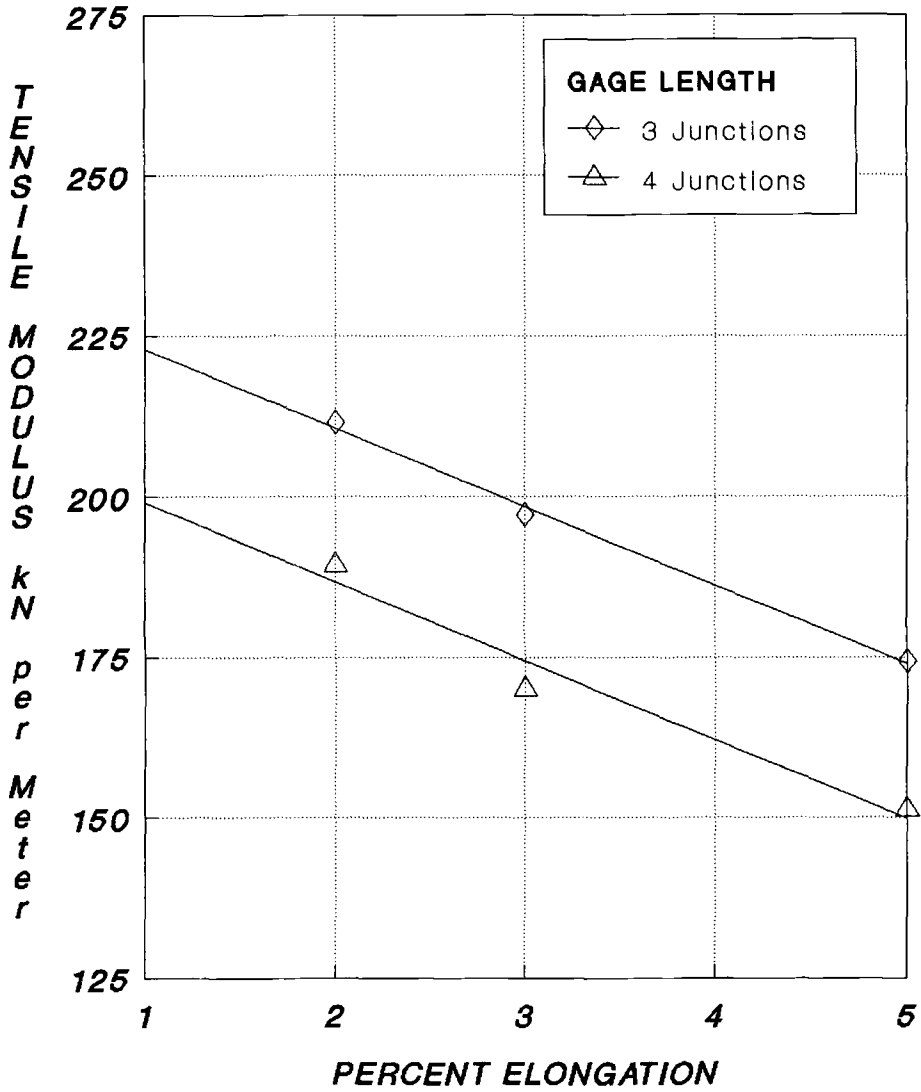
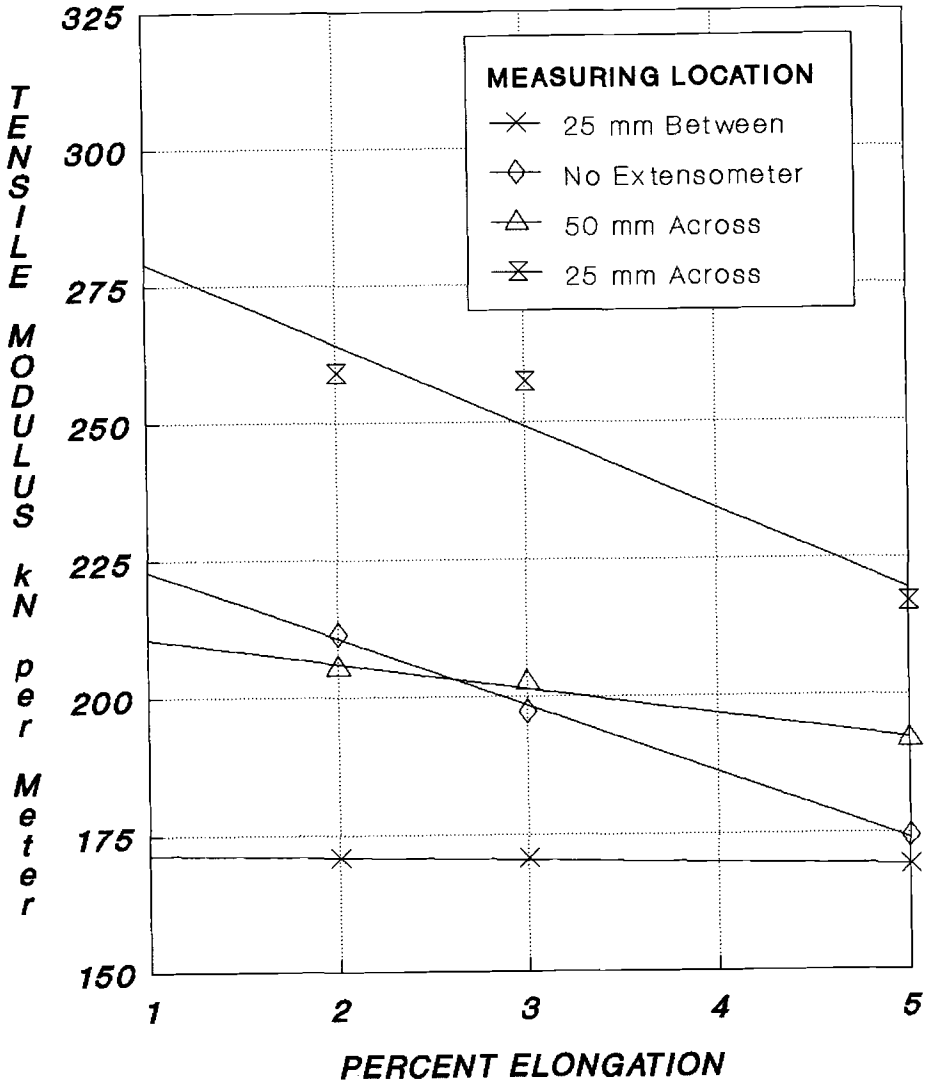


FIGURE 7 -- Strain Measuring Equipment & Gage Location Effects on Tensile Modulus



If the extensometer is not used, the evidence indicates that a lower and more conservative result may be expected. The argument could be made that, when an extensometer is not used, the behavior of several junctions is determined, better approximating the behavior of the sheet as a whole rather than measuring response of one localized area between or across one junction.

Machine Type (Figure 8)

Since there are two basic types of loading trains in typical tensiometers used in current laboratories, two identical tests were performed and the data was plotted. The differences due to slack that exists in the screw, or mechanical, driven tensile testing instrument is clearly shown on Figure 8. The consistently lower tensile moduli at elongations below 5 percent are an indication of the amount of internal and additional (apparent) elongation within the load train. A general relationship can be drawn from these observations and test results. For example, the variation can be calculated as a possible percent error:

At 2 percent elongation using a screw-driven drive train;

$$\frac{211.55 \text{ kN/m (servo)} - 163.52 \text{ kN/m (screw)}}{211.55 \text{ kN/m (servo)}} \times 100 = 22.7 \% \quad (4)$$

This difference is due to uncertainties associated with crosshead acceleration. For screw driven machines, a period of time is required for the crosshead to reach its full operating speed. This acceleration period is a function of slack in the load train, chain tension, and related mechanical considerations. This data shows that such factors are critical at testing speeds of 50 mm/min and higher, especially for modulus at very low strains (2 and 3 percent). Since the servo-hydraulic instrument has direct hydraulic drive, acceleration to full speed is almost immediate. A more accurate determination of crosshead position and rate can be made, since a direct indication of position is available through LVDT instrumentation.

A biased estimate of the actual tensile strengths at very low strains is obtained by use of a screw-driven tensile testing instrument. This source of error is significant. One could argue that, if screw driven machines are used, the downward bias could provide an unwarranted factor of safety in the test procedure and may result in overdesign or the rejection of acceptable products. It is clear, however, that inter-machine and inter-lab variability should be carefully considered in evaluating tensile results at low strains. (It should be pointed out that some screw machines have a means to determine crosshead position via a transducer which makes direct reading of position possible. This class of machine would be expected to provide better performance and more consistent results than the type used here, where displacement is inferred from elapsed time. However, slack in the load train and crosshead acceleration would still be expected to contribute some bias.)

Strain Rate (Figure 9)

The test results from the evaluation of the effect of testing speed (strain rate) were quite unexpected. Beginning with 12.5 mm/min, the plot depicts a linear variation that shows tensile modulus decreasing as the rate of strain is increased. The opposite would be expected. That is, modulus should increase as the testing speed is increased, since in the classical spring/dashpot model the elastic or "spring" component dominates at higher strain rates [2]. To further complicate the picture, tests at the slowest speed, 1.25 mm/min, resulted in a much lower modulus, reversing the trend.

FIGURE 8 -- Machine Type Effects on Tensile Modulus

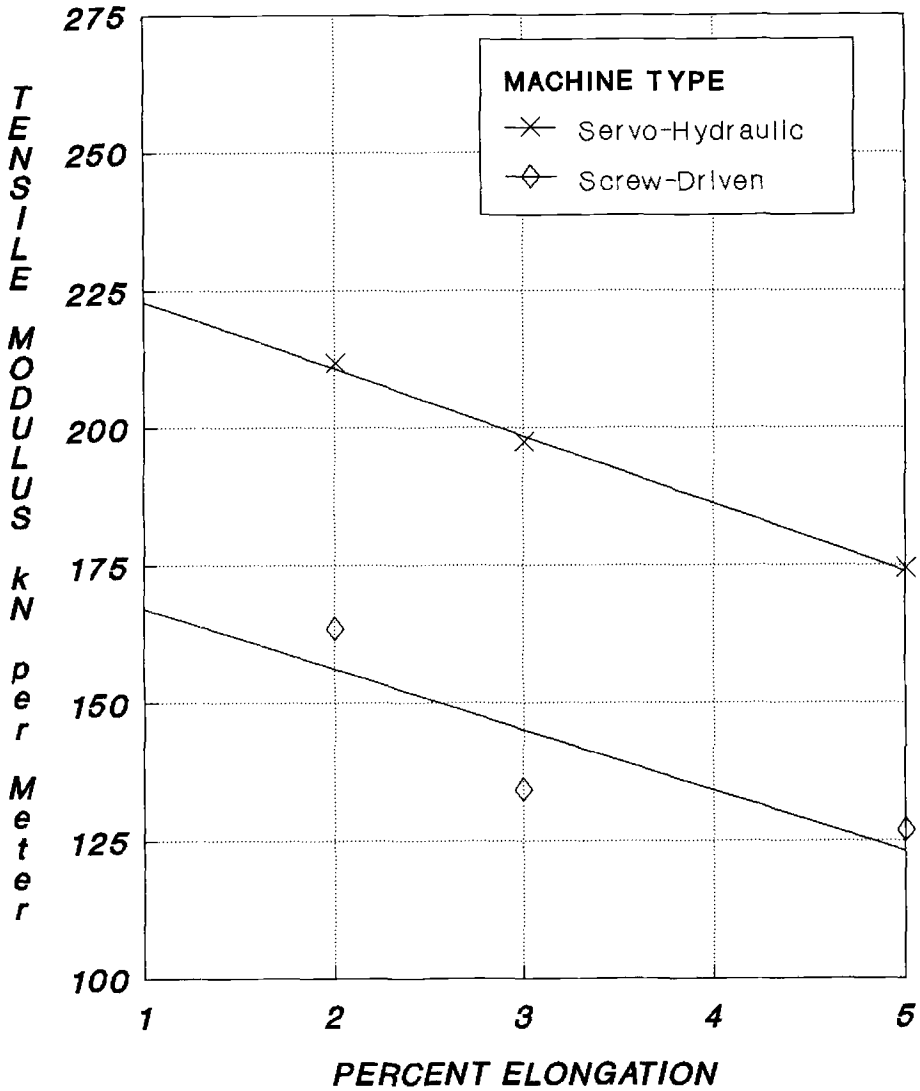
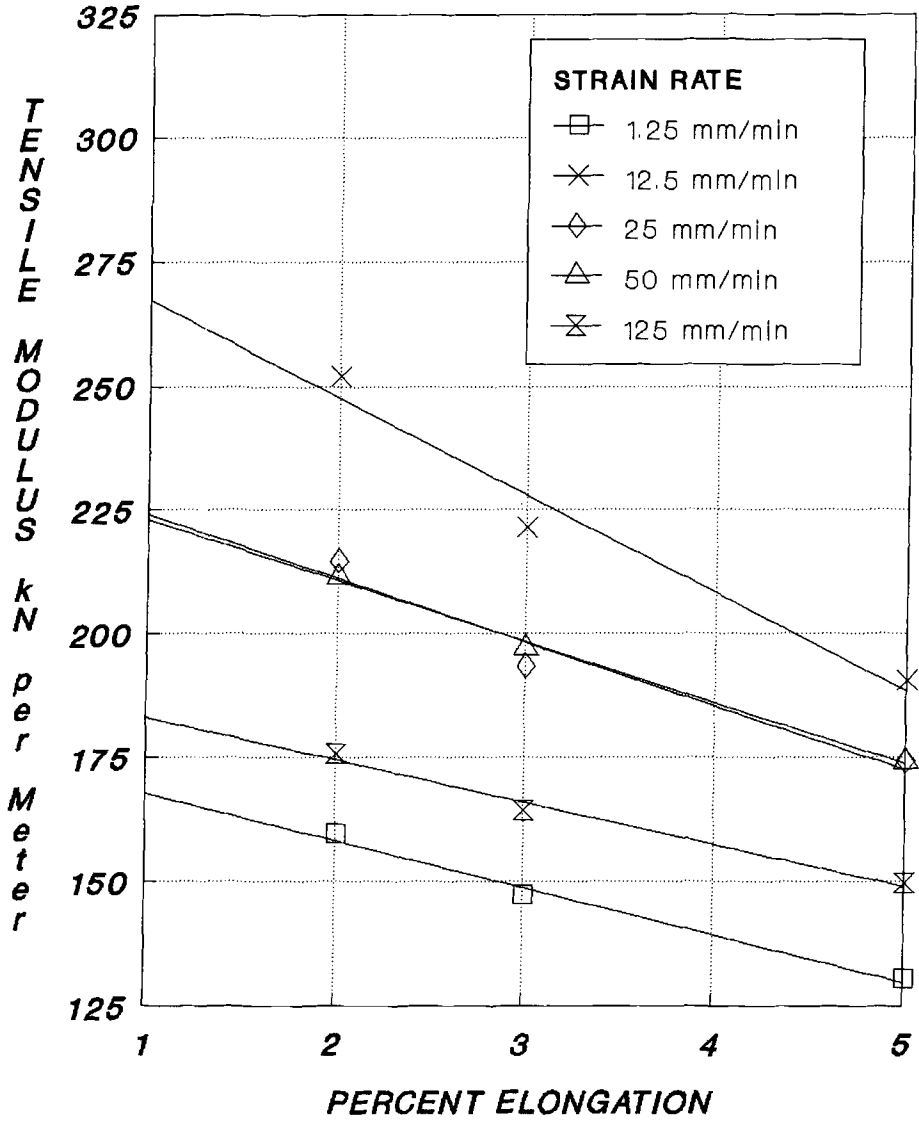


FIGURE 9 -- Strain Rate Effects on Tensile Modulus



It has been preliminarily proposed that this phenomenon may be due to the unique extrusion or stretching process used to manufacture the geogrids used in this investigation. It could be quite possible that by orienting the molecular chains within the rib, the common trend that higher testing speeds produce higher tensile modulus is not true with all oriented plastics. At higher strain rates, two factors may contribute to the observed decrease in tensile modulus:

- 1) As the strain rate increases, there is a gradual change in the location where most of the specimen elongation takes place. Because the product does not have a uniform cross-section, the single rib specimen behaves differently along its length. At 50 mm/min and higher speeds, most elongation takes place in the rib (Figure 7). At these high strain rates, the rib may not fully respond to the load application quickly enough. Therefore, it may be possible that a higher percentage of stress is induced on the non-oriented, but much thicker, junction.
- 2) It is also proposed that internal friction in the oriented geogrid rib may generate viscous heating. This heat may have the effect of reducing the tensile strength at low strains and high speeds very similarly to the way external temperature effects the tensile modulus (Figure 5).

The following observation was made with respect to samples tested at the slowest rate, 1.25 mm/min. The specimens did not fail after yield, but continued to elongate beyond the typical rupture strains that occurred at higher test speeds. Visual inspection of the samples showed clear evidence that plastic flow or creep was taking place. The junctions were stretched longitudinally indicating that non-recoverable, viscous flow under load had occurred. Apparently, at such slow speeds the specimen experiences a load regime more similar to static loading than a dynamic increase in load. Ultimate elongations were greater than 70 percent, where all specimens tested at higher speeds failed within the range 15 - 25 percent elongation. There is apparently a point of departure between 1.25 mm/min and 12.5 mm/min where creep begins to dominate over modes of stress/strain behavior and ultimate failure which are predominant at higher testing speeds.

CONCLUSIONS AND RECOMMENDATIONS

It was concluded that, for biaxially-oriented polypropylene geogrids, all of the test parameters investigated can have significant effects on the strength measurements at low strains. The effect of each must be understood and the variables controlled for proper measurement and interpretation. The following points are made:

1. Maintaining accurate temperature is very important in order to properly measure the tensile behavior of geogrids at low strains, and it must be carefully controlled in the laboratory setting.
2. The use of an extensometer provides an accurate and direct measurement of strain. If extensometers are used, however, the equipment should be capable of covering gauge length over at least two to three junctions so that the entire product's behavior may be sampled rather than a localized area at or adjacent to a single junction.
3. The influence of machine-dependent variables is important, especially with screw-driven equipment. With one screw-driven tensile testing machine, representative of those used in most geosynthetics labs, tensile modulus values measured at elongations below 5 percent were found to be 22 percent lower than those obtained with an LVDT-equipped servo-hydraulic instrument. The accuracy of the data obtained from the initial regions of the stress-strain curve with screw-driven equipment is questionable because of slack in the load train and crosshead acceleration.
4. Single rib tensile tests of geogrids are highly dependent on strain rate, and the rate should be agreed upon and understood as a key element of the test procedure by all parties involved.
5. Single geogrid ribs manufactured from a unique polypropylene extrusion tend to elongate primarily between junctions when tested in tension. However, the dominance of elongation at the junction versus rib elongation between junctions varies as a function of the strain rate.

It is recommended that future work to develop a single-rib tensile test consider the importance of modulus at low strains in the testing procedure. The determination of polypropylene geogrid tensile strengths at low strains is difficult to accurately determine and the respective strength-strain curves are not always constant. Once the data is obtained, the tensile strength is commonly published on a specification or material data sheet. The determination of the geogrid tensile strength of polypropylene geogrids does not currently model the product application of roadways constructed over soft soils. The actual design theories and procedures do not utilize these tensile values and this should be considered when selecting a polypropylene geogrid. Therefore, the use of extensometers or direct-reading instrumentation such as servo-hydraulic testing equipment should be required if these values are of particular interest.

REFERENCES

- [1] Hollaway, L.C., "Polymers And Polymer Composites in Construction," Thomas Telford Ltd., 1990, pp. 11-12, 19.
- [2] O'Toole, J.L., "Designing With Plastics," Modern Plastics Encyclopedia, revised and updated by Dr. James F. Carley, McGraw-Hill, 1989, pp. 404-406.
- [3] Geosynthetics Research Institute Test Method GGI-87, "Geogrid Rib Tensile Strength," modified January 1988, Philadelphia, PA.
- [4] Giroud, J.P., Ah-Line, C., and Bonaparte, R., "Design of Unpaved Roads and Trafficked Areas with Geogrids," Symposium on Polymer Grid Reinforcement in Civil Engineering, London, Paper No. 4.1.
- [5] Design Guidelines for Subgrade Improvement Under Dynamic Loading with Tensar Geogrids, Tensar Technical Note BR5, February 1987.
- [6] Koerner, R.M., and Wilson-Fahmy, R.F., "Polymeric Geogrid Utilization In Paved Roads," Draft Report #4 to Commonwealth of PA D.O.T. Office of Research and Special Studies, February 12, 1992.
- [7] ASTM Draft Designation D35.01.88.02, "Standard Test Method for Tensile Strength of Geogrid Ribs," Draft No.4, May 1990.

John N. Paulson, P.E.

HIGH STRENGTH POLYESTER GEOTEXTILE TESTING AND MATERIAL PROPERTY EVALUATION

REFERENCE: Paulson, J. N., "High Strength Polyester Geotextile Testing and Material Property Evaluation," *Geosynthetic Soil Reinforcement Testing Procedures, ASTM STP 1190*, S. C. Jonathan Cheng, Ed., American Society for Testing and Materials, Philadelphia, 1993.

ABSTRACT: High strength woven polyester geotextiles were tested for manufacturing quality control purposes, and for project approvals. This testing included both single end breaks, and full wide width strength testing. Wide strip tensile strengths were determined using ASTM D4595, "Tensile Properties of Geotextiles by the Wide Width Strip Method".

Results show consistency in single end breaks, with significant variability when full wide strip tensile specimens were tested. Results were variable both in ultimate strength determinations and at 5 and 10% strain. Several laboratories also tested this material, with their results presented. A summary of the results is discussed followed by recommendations for modification to ASTM D4595 to limit results variability.

KEYWORDS: Geotextile, Woven, Reinforcement, Polyester, Single End Break, Wide width, Tensile strength

Determination of tensile strength of geotextiles is a critical aspect of any soil reinforcement design. The strength imparted to the reinforced soil system is a key determinant included in vertical walls, slopes and embankment stability calculations. As a result, testing of materials to determine this tensile strength becomes critical.

Individual yarn (or single end) breaking strength is an indirect means of determining the woven geotextile tensile strength. Other industries, such as conveyor belt manufacturing, routinely certify material tensile strengths based on single end break results multiplied by the number of ends per unit width to determine the belt strength. Additionally, a small or ravel strip tensile strength test is used, where a 5cm (2 inch) wide specimen is tested to failure, with results reported as representative of the full belt width.

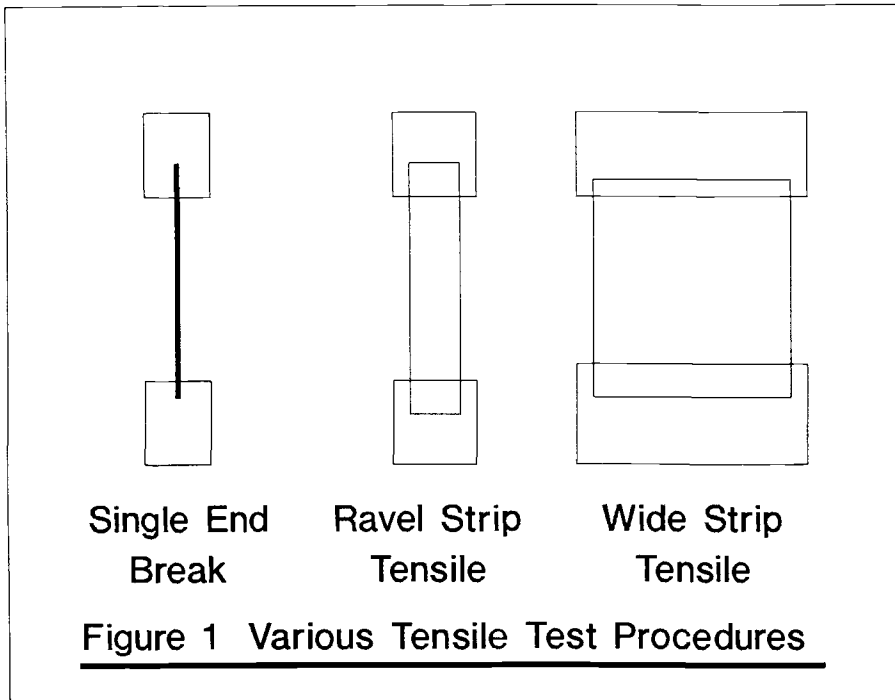
Specialty Products Marketing Manager, Exxon Chemical Geotextiles, Atlanta, GA 30339

The Geotextile community in North America has adopted wide strip testing as the accepted procedure for determining tensile strength. A precision and bias statement has not been included in the test procedure to date.

TEST PROCEDURES

Figure 1 compares three types of test procedures, single end break, 5 cm ravel strip, and 20cm wide strip. Each is briefly described below.

ASTM D2256 "Breaking Load (Strength) and Elongation of yarn by the Single Strand Method" is the test procedure for determination of single end breaking strength of individual yarns. ASTM D1682 "Breaking Load and Elongation of Textile fabrics" describes the ravel strip test method, where the breaking strength of a 5cm strip specimen is determined.



ASTM D4595 is used in geotextile testing to determine the load per 20 cm width (8 inches) and reporting the load, extension, and break or ultimate strength. It is currently the only geotextile test procedure where a "wide" strip is tested. This procedure provides a specimen wide enough to minimize 'necking' and other phenomenon which are prevalent with some types of geotextiles, mainly nonwoven fabrics.

Standard Industry practice is to test 20 cm wide samples, anywhere from 3 to 10 specimens per roll. Ultimate tensile strength, elongation, and load - strain characteristics are determined. If clamping or other problems are noticed by the operator during testing, common practice is to reduce the specimen width to 10 cm and retest. Narrower width specimen testing is allowed by the procedure (5.4.1) when clamping or other equipment limitations arise, or with woven geotextiles that exhibit strengths of 100kN/m. Unfortunately this is seldom done in practice, which may result in a significant understatement of a geotextiles actual strength.

YARN DESCRIPTION

Yarn utilized in the weaving of the geotextiles presented herein is a high molecular weight, high tenacity polyester yarn manufactured by the Hoechst Celanese corporation. This yarn, designated T800 is commonly used as tire cord yarn for the automotive industry. It has been extensively tested (ref 1) for strength and modulus.

Figure 2 summarizes yarn stress strain properties as determined using ASTM D2256. A typical yarn size is 1000 denier. A typical yarn of 1000 denier T800 material would possess a tensile strength of approximately .0872 kN. This is a common polyester yarn used in high strength geotextile weaving.

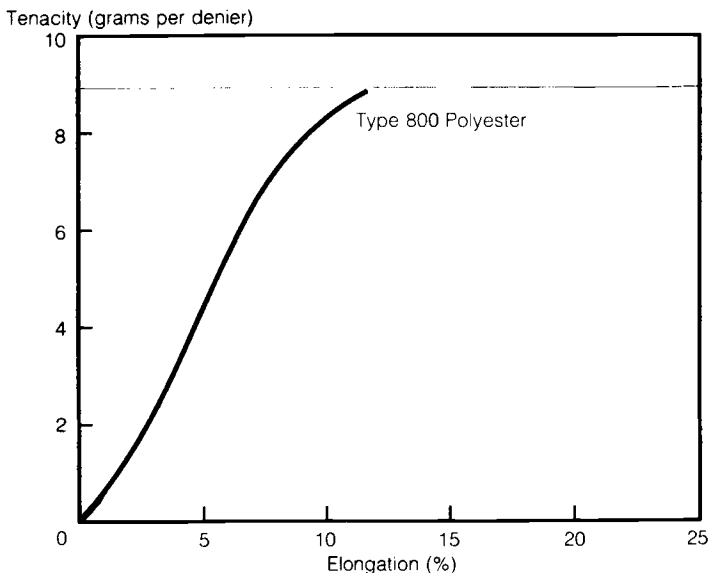


Figure 2 Typical load/strain properties of T800 yarn (Ref 1)

GEOTEXTILE FABRIC

Table 1 summarizes three woven geotextile material construction properties. These are all commercial products offered as soil reinforcement geotextiles. They are all woven using the T800 high tenacity polyester multifilament yarns.

ASTM1.wk1

TABLE 1
Polyester Yarn and Geotextile Information

Product	Construction		Yarn strength		Theoretical Strength		Actual Strength		Strength % Retained	
	Warp/Fill	Fill	Kn Warp	Kn Fill	Warp(Kn/m)	Fill(Kn/m)	Warp(Kn/m)	Fill(Kn/m)	Warp	Fill
GTF550T	39 (1000	19 x 2000)	0.076	0.151	116	113	99	96	86%	85%
GTF1000T	36 (2000	19 x 3000)	0.151	0.227	214	170	196	151	91%	89%
GTF1500T	36 (3000	19 x 3000)	0.227	0.227	322	170	290	157	90%	92%

NOTE: Yarn strength is after weaving. New yarn strength is .0872 Kn/1000 denier

Yarn construction is the 'recipe' for manufacturing a fabric, and includes the yarn size and the number of yarns per cm. Included in the table are the theoretical fabrics strength, computed by multiplying the number of yarns in each direction by the individual yarn strength. This yarn strength is determined after weaving, by separating the yarns from the wiven product, then testing them individually. This procedure is followed to eliminate any yarn strength losses that may come about from the weaving process.

The actual strength shown in the table is that obtained by testing 20 cm wide specimens, using ASTM D4595 test procedures. Note that the actual strength is only 85 to 90% of the theoretical. The differences come from variables introduced in sample preparation, clamping and laboratory procedure variability.

The yarn strength and construction allows the manufacturer to predict the finished product tensile strength. Wide width testing will only verify what the sum of the individual yarns predicts. It can never be greater than that theoretical maximum. However, if the specimen is not clamped uniformly, the wide width test results can be much less than that maximum, as discussed below.

LABORATORY TESTING RESULTS - GTF1000T

For a particular project the required geotextile tensile strength at a minimum elongation of 10% was specified as part of the project requirements. GTF1000T material was supplied. To verify material properties, samples were sent to several laboratories for testing of strength and modulus. Table 2 summarizes the results. All testing was performed with 20 cm wide specimens.

As seen, the ultimate strengths varied considerably, as did the strain at ultimate strength. Ultimate strength values ranged from a low of 162 kN/m to a high of 210kN/m.

Subsequently an extensive testing program consisting of 30 specimens tested in each direction, referred to as the RETEST, was performed at one of the four original laboratories to determine the intra-laboratory variability. These results are also shown in summary form on Table 2. Results reported still varied. While the tensile strength was more consistent, the strength at 10% strain was still variable. Standard deviations from the norm were above 10% in some cases (10%).

Laboratory		Date	Strength @ 5%		Strength @ 10%		Ultimate	Strength	Strain @ Failure	
			Warp	Fill	Warp	Fill	Warp	Fill	Warp	Fill
W	Dec 89		63	47			210	148	13.3	16
	May 90		65	59			202	160	11.8	15.1
	April 91				152	90	187	147	12.1	18.1
	May 91				150	92	190	147	11.8	15.8
G	April 91				146		179		11.4	
S	April 91				152	117	162	142	10.8	12.6
					149	107	173	143	12.6	11.2
Summary (Average)			64	53	150	101	186	148	12.0	14.8
Standard Deviation			1	6	2	11	15	6	0.7	2.3
Avg less 2 STD			63	41	145	79	156	136	10.5	10.2
RETEST PROGRAM										
August 91	Average		59	57	151	97	196	151	12.8	17.4
	Standard Deviation		7	4	14	8	7	5	1.0	1.4
	Avg less 2 STD		45	49	124	80	183	142	10.8	14.5

NOTE: All tensile strengths shown in Kn/m units

Variability in tensile strength with sample width is inevitable, due to the variables in the base polymer from which the yarn is produced. That variability in yarn breaking strength, and strain at failure indicates that if all the yarns were perfectly aligned load would not be shared equally. When test sample preparation, specimen clamping, and operator experience comes into play, further reductions in the "as tested" strength will arise.

Manufacturing quality control for this (and other polyester fabrics) dictates that yarns be tested after weaving, and the weave construction verified. This is common procedure in quality control programs for weaving operations.

Table 3 provides an example of typical QC test procedure results from 24 test specimens. Of particular interest on this summary table are the two columns labeled "construction" and "tensile". Construction refers to the count of the actual of number of yarns in each direction for the specimen. Tensile refers to the individual yarn tensile strength. Note the high level of uniformity in construction, and in single end strength.

Weave construction conformance results, when correlated with the yarn strength and yarn count testing provides sufficient data on what the maximum geotextile tensile strengths. Note again that with ASTM D4595 test procedures it is not possible to get "too high" a strength, that is, a material strength greater than physically possible. The fabric can only be shown to be as strong as the sum of the individual components.

INVOICE NO: 845616		WEIGHT	GAUGE	CONSTRUCTION	CRIMP	TENSILE	WIDTH
**** TEST METHOD ****		WTP-912	GAP-206	CNP-101	CRP-308	**(TNP-4202)**	WDP-144
DATE	ROLL NO.	OZ/SQ. YD.	(MILS)	WARP X FILL	WARP X FILL	WARP X FILL	INCHES
8/19/91	060340	17.46	0.039	35.8 X 18.9	4.5 X 1.6	35.4 X 56.2	149.70
8/23/91	060343	17.54	0.039	35.8 X 18.8	4.3 X 1.7	35.2 X 56.0	149.80
8/25/91	060376	17.38	0.040	35.8 X 18.9	4.4 X 1.4	34.8 X 56.2	149.80
8/27/91	060455	17.34	0.039	35.8 X 18.9	4.4 X 1.4	35.5 X 56.4	150.00
8/28/91	060557	17.46	0.039	35.7 X 18.8	4.2 X 1.5	35.3 X 56.8	149.70
8/28/91	060558	17.42	0.039	35.8 X 18.9	4.4 X 1.8	35.4 X 56.1	149.80
8/29/91	060577	17.34	0.040	35.7 X 18.7	4.3 X 1.4	35.6 X 56.3	150.10
9/01/91	060638	17.54	0.040	35.7 X 18.8	4.0 X 1.5	34.9 X 57.0	150.00
9/01/91	060640	17.49	0.039	35.8 X 18.8	4.1 X 1.8	35.2 X 56.2	149.80
9/01/91	060642	17.32	0.039	35.7 X 18.8	4.3 X 1.7	35.3 X 56.4	150.00
9/01/91	060652	17.42	0.040	35.8 X 18.9	4.5 X 1.2	35.3 X 56.3	150.00
9/02/91	060683	17.38	0.040	35.8 X 18.8	4.2 X 1.4	35.6 X 57.2	150.10
9/02/91	060811	17.49	0.040	35.7 X 18.9	4.1 X 1.5	36.1 X 57.0	150.20
9/04/91	060813	17.42	0.039	35.8 X 18.7	4.3 X 1.6	35.5 X 56.8	149.80
9/05/91	060819	17.25	0.039	35.7 X 18.9	4.5 X 1.7	35.4 X 56.5	149.80
9/10/91	060938	17.42	0.039	35.8 X 18.9	4.3 X 1.8	35.7 X 56.2	150.20
9/11/91	060952	17.38	0.040	35.7 X 19.0	4.5 X 1.4	35.2 X 56.7	150.10
9/14/91	060978	17.54	0.040	35.8 X 18.7	4.2 X 1.5	35.4 X 55.8	149.80
9/15/91	061085	17.49	0.040	35.7 X 19.0	4.6 X 1.7	35.8 X 56.1	149.80
9/17/91	061086	17.27	0.039	35.7 X 18.9	4.5 X 1.3	35.6 X 57.0	150.00
9/17/91	061121	17.25	0.039	35.8 X 18.8	4.0 X 1.6	35.4 X 56.6	150.10
9/17/91	061123	17.34	0.040	35.7 X 18.7	4.2 X 1.5	35.8 X 56.8	150.10
9/17/91	061124	17.38	0.039	35.8 X 18.8	4.0 X 1.4	36.8 X 56.5	149.80
9/19/91	061221	17.42	0.040	35.8 X 18.9	4.5 X 1.8	36.1 X 56.7	149.80
8/19/91	AVERAGE OF SHIPMENT	17.41	0.039	35.8 X 18.8	4.3 X 1.5	35.5 X 56.5	149.93
UPPER LIMIT:		18.09	N/S	37.0 X 20.0	5.0 X 2.0	NO UPPER LIMIT	**OPEN**
SPECIFICATION:		17.59	N/S	36.0 X 19.0	4.5 X 1.5	34.0 X 51.0	148.00
LOWER LIMIT:		17.09	N/S	35.0 X 18.0	4.0 X 1.0	34.0 X 51.0	147.00

Table 3 Typical QC weaving test results: Yarn & Fabric Construction

LABORATORY TEST RESULTS - GTF550T

A second example of laboratory testing performed on woven polyester geotextiles concerns GTF550T supplied for a landfill liner reinforcement project. The project required an ultimate wide width tensile strength value of 70kN/m, (ASTM D4595) well below the product capabilities as shown in Table 1. The product was tested by an independent laboratory and rejected because of low ultimate strength test results. This error caused the project to be delayed, opening the door for potential restitution from the manufacturer for failing to provide material meeting the specifications, when in effect it was a testing procedure error.

This laboratory was then contacted and their testing procedure discussed. It was learned that they had never tested any woven polyester geotextiles previous to this project. Their experience had been limited to nonwoven geotextiles, and some lightweight woven materials. They were following ASTM 4595 test procedures, using the wedge type clamps as illustrated in the standard. Strain was being measured with crosshead movement.

Table 4 Summary of Wide Width Tensile Strength Results

Specimen	MD1, MD2, MD3, MD4, MD5, MD6	TD1, TD2, TD3, TD4, TD5, TD6
W Width (kN/M)	61 65 66 72 65 61	62 73 72 69 67 75
Strain %	20 25 21 21 18 23	22 21 19 20 18 20

Results were approximately 60% of the product actual strength. Strains at failure were above 20%. This was from a fabric woven with a yarn with a breaking elongation of 10%. The high strains suggested that the specimen was not being uniformly loaded, but rather progressively loaded. Discussions with the lab revealed that the specimen was not breaking suddenly, but rather progressively, with no more than 1/4 the specimen failing at peak. They maintained that they were performing the test in accordance with the ASTM standard.

However, they agreed to test a narrower width sample, as allowed in the ASTM procedure. Results obtained with this narrower width (10 cm wide) sample became consistent with that obtained from more experienced laboratories (table 1 summary), and the product was allowed to be used on the project. The delay caused a week of lost time on the project, and additional testing money to be spent.

CONCLUSIONS

Woven high tenacity yarn polyester geotextiles at and above 100 kN/m tensile strength are sensitive to wide width strip tensile testing using ASTM D4595 procedures. The clamping mechanism, specimen width and operator skill in preparing the specimen in the clamps plays a significant role in the test outcome.

The use of single end break strength as a means of estimating material strength will result in overprediction of the wide specimen results.

This procedure cannot 'overpredict' the material strength, but can seriously underpredict the strength if samples are not not clamped and loaded uniformly.

The principle indication of this phenomenon is high strains at break or ultimate strength. This is an indication that the specimen was not loaded uniformly. Absence of a sharp and distinctive "pop" at failure is a second indicator.

Interlaboratory variability is observed with this procedure. The development of a precision and bias statement will aid in the understanding of this method limitations.

Laboratories must be sensitive to this behavior. When high strains at failyre are observed, or significantly low results are observed, laboratories can mitigate the effects of this by reducing the specimen width.

REFERENCE

- 1 Hoechst Celanese Corporation Technical Bulletin, TFB-2, "High Performance Geosynthetics from Trivera^R High Tenacity Polyester Yarns, Charlotte, NC 1988.

Daniele Cazzuffi¹, Luciano Picarelli,² Angelo Ricciuti,³ and Pietro Rimoldi⁴

LABORATORY INVESTIGATIONS ON THE SHEAR STRENGTH OF GEOGRID REINFORCED SOILS

REFERENCE: Cazzuffi, D., Picarelli, L., Ricciuti, A., and Rimoldi, P., "Laboratory Investigations on the Shear Strength of Geogrid Reinforced Soils," Geosynthetic Soil Reinforcement Testing Procedures, ASTM STP 1190, S. C. Jonathan Cheng, Ed., American Society for Testing and Materials, Philadelphia, 1993.

ABSTRACT: A new apparatus for direct shear and pull-out tests was conceived to study the soil-geosynthetic and the geosynthetic-geosynthetic interaction: it consists of a testing box, having a contact area of 0.1 m², with vertical and horizontal loads applied by an electronically controlled two-axis testing machine. Different types of geogrids (both uniaxially and biaxially oriented) were tested. Two different types of soil were used: silty sand and gravel. Particularly, direct shear tests were run using different testing rates (varying from 0.1 to 5.0 mm/min). The second part of the research concerned triaxial tests, using a very large cell (0.82 m height and 0.35 m diameter) and the same gravel soil. These tests were performed with and without the geogrid reinforcements. The direct shear tests have demonstrated that the rate of displacement does not influence significantly the soil-geosynthetic interaction. On the other hand, the triaxial tests have emphasized that the geosynthetic inclusion give a not negligible cohesion to the whole mass and determine peculiar modes of failure.

KEYWORDS: reinforcement, geogrid, silty sand, gravel, direct shear test, triaxial test, pull-out test.

The frictional characteristics have a primary importance in geosynthetics used for soil reinforcement: in fact, high frictional properties reduce the possibility of relative movements between the

¹Civil Engineer, ENEL SpA, CRIS, Milano, Italy.

²Professor, Second University of Naples, Italy.

³Consultant, Vaglio Basilicata, Potenza, Italy.

⁴Director, Tenax SpA, Viganò Brianza, Como, Italy.

reinforcing layers and the soil, and allow the transfer of stresses from the soil to the reinforcing elements.

The need for studies about frictional properties of geosynthetics originates from the observation that the value of the interface friction angle along a contact surface between soil and synthetic materials can be lower than the value of the internal friction angle of the same soil: in this case a weaker surface along the geosynthetic/soil contact may develop.

Geogrids, however, show very high frictional properties, which can be ascribed to the fact that, differently from geotextiles, which are in direct contact with the soil on all the surface, geogrids are not continuous along their plane but present regular holes which give a large open area, allowing a positive interlocking with the soil.

LABORATORY PROGRAM AND TESTED MATERIALS

The laboratory program has been aimed to obtain the strength characteristics of soil-geogrids interfaces and to analyse the overall behavior of a reinforced soil mass [1].

The first objective has been pursued by planning a specific program of direct shear and pull-out tests, which has allowed to analyse the efficiency of the geogrids and the influence of the displacement rate; the overall strength of reinforced soils has been measured by triaxial tests on large scale specimens, which have highlighted the role played by the reinforcing elements when placed normally to the maximum principal stress.

Tested Materials

Only cohesionless soils have been used: a silty sand (soil A) and a gravel (soil B), whose main characteristics are reported in Table 1, while the grain size curves are shown in Fig. 1. Both soils are from glacial deposits in Northern Italy. The gravels are constituted by particles with slightly rounded edges.

TABLE 1 - Characteristics of the soils used in the tests.

Soil	d ₁₀	d ₆₀	U _c	γ _d	w	S	n	Proctor density
	mm	mm	-	kN/m ³	%	-	-	kN/m ³
A:Sand	0.01	0.5	50	19.6	5.6	0.17	0.33	20.45
B:Gravel	2	3	1.5	18.2	12.8	0.73	0.32	18.75

Two different geogrids have been used, both produced in Italy by Tenax SpA: a HDPE mono-oriented geogrid, the Tenax TT 401 AMP, and a Polypropylene biaxially oriented geogrid, the Tenax LBO 301 AMP. The main mechanical parameters of the geogrids are reported in Table 2 and 3, while their stress-strain characteristics obtained in tensile tests are reported in Figs. 2 and 3.

Testing Program

The testing program has been carried out at the Tenax Geosynthetics Testing Laboratory and at the Geotechnical Laboratory of the University of Naples "Federico II".

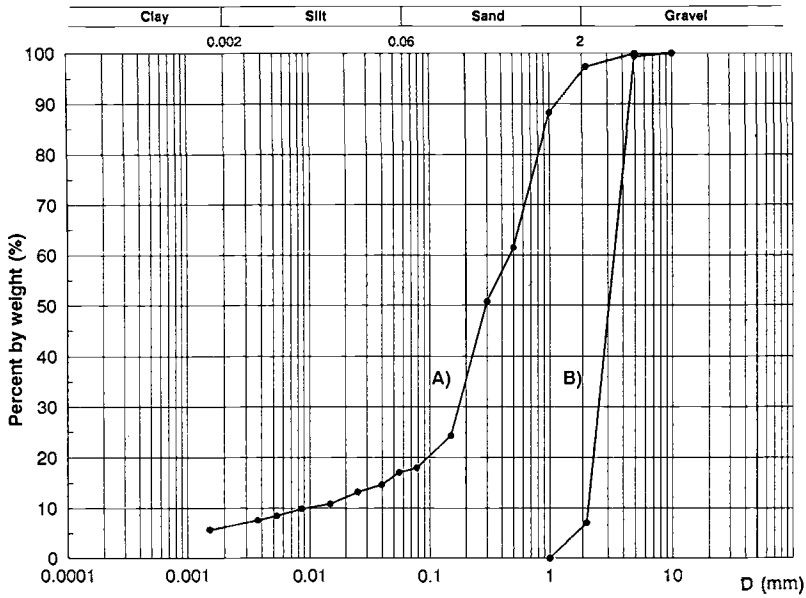


Fig. 1 - Grain size curves of the soils used in the tests.

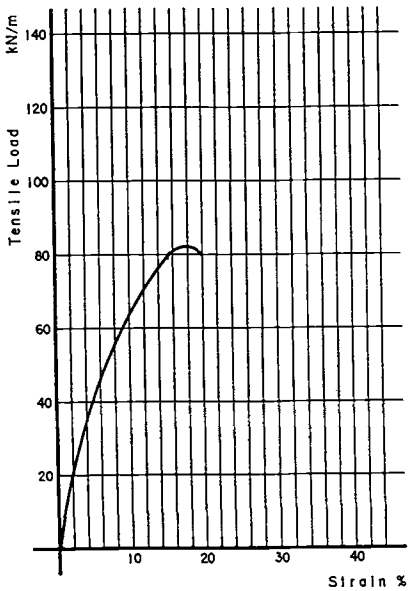


Fig. 2 - Stress-strain behavior in tensile tests of the mono-oriented geogrids

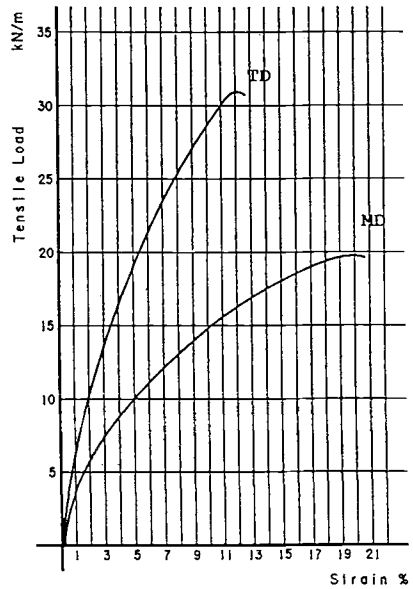


Fig. 3 - Stress-strain behavior in tensile tests of the biaxially oriented geogrids

TABLE 2 - Mechanical characteristics of Tenax TT 401 AMP mono-oriented integral geogrids.

Characteristics	Standard	Value	Unit
Wide width strip tensile strength	ASTM D4595	80.7	kN/m
Peak tensile strength (single rib)	GRI GG1	80.0	kN/m
Yield point strain (single rib)	GRI GG1	19	%
Secant modulus at 2 % strain	GRI GG1	1015	kN/m
Secant modulus at 5 % strain	GRI GG1	740	kN/m
Junction strength	GRI GG2	64.5	kN/m
Flexural rigidity	ASTM D1388	2025000	mg x cm

TABLE 3 - Mechanical characteristics of Tenax LBO 301 AMP biaxially oriented integral geogrids.

Characteristics	Dir.	Standard	Value	Unit
Wide width strip tensile strength	MD	ASTM D4595	19.5	KN/m
	TD		30.1	kN/m
Peak tensile strength (single rib)	MD	GRI GG1	19.5	kN/m
	TD		30.0	kN/m
Yield point strain (single rib)	MD	GRI GG1	20	%
	TD		11	%
Secant modulus at 2 % strain	MD	GRI GG1	285	kN/m
	TD		440	kN/m
Secant modulus at 5 % strain	MD	GRI GG1	180	kN/m
	TD		370	kN/m
Junction strength	MD	GRI GG2	18.0	kN/m
	TD		29.0	kN/m
Flexural rigidity	MD	ASTM D1388	850000	mg x cm
	TD		990000	mg x cm

Note: MD = Machine Direction (along roll length)

TD = Transversal Direction (across roll length)

At the Tenax laboratory direct shear tests on interfaces between soils and geogrids have been performed.

A newly designed apparatus (Fig. 4) was employed to perform both direct shear and pull-out tests. It can be considered as a development of the testing devices used by other Authors [2, 3, 4, 5].

The equipment is made up of two superimposed metal boxes. The upper box is supported on three wheels on two opposite faces, positioned on the raised and moulded edges of the lower box along its major dimension; the wheels allow the horizontal movement of the upper box relatively to the lower one.

The dimension of the two boxes are summarized in Table 4.

The soil was placed in the box and compacted by manual tamping in different layers, in order to obtain the values of density indicated in Table 1.

For soil-geosynthetic tests, a specimen of geogrid was fixed at the lower base of the upper box. The specimen had length and width large enough to cover completely the lower box.

Direct shear tests were run according to the procedure of a standard direct shear test performed with the traditional "Casagrande box".

The tests were carried out by means of a sophisticated electronically

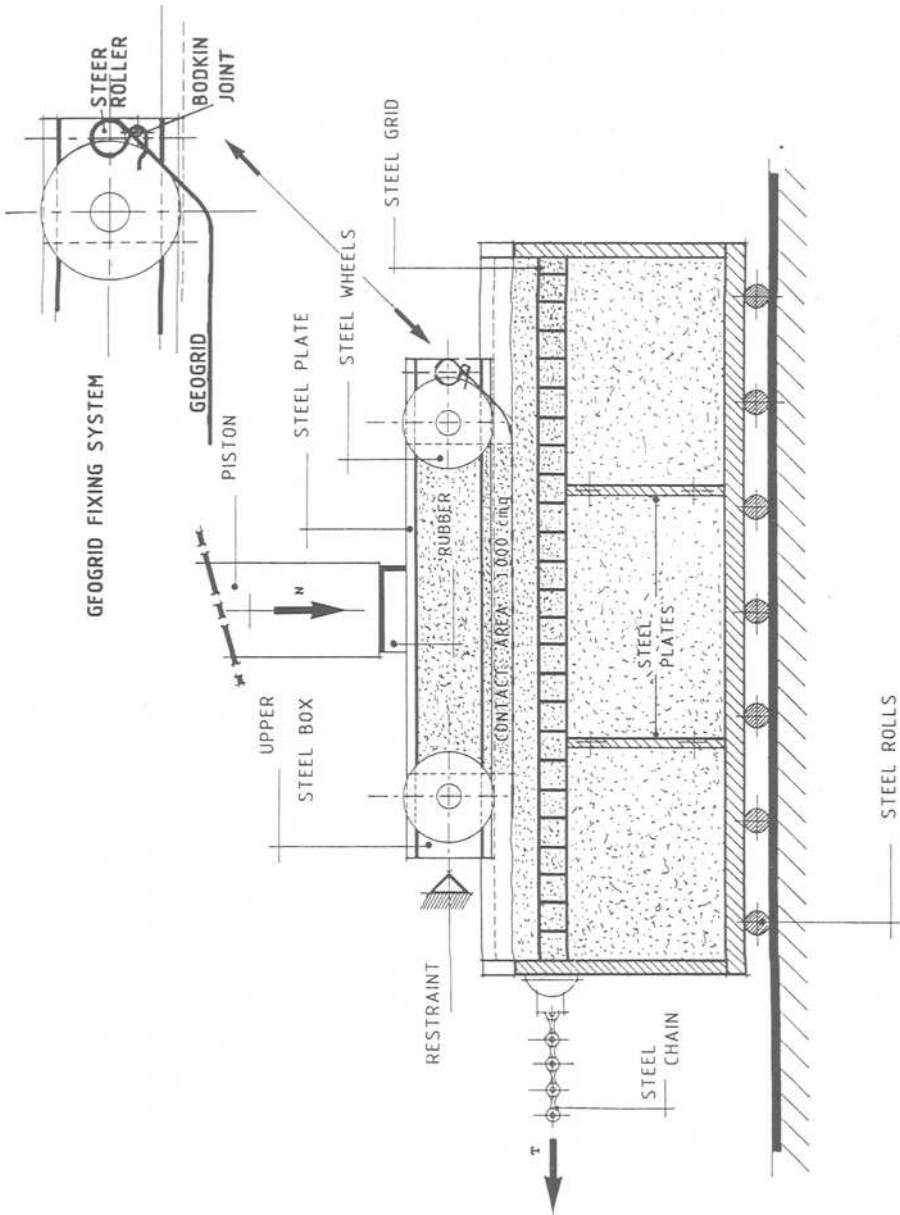


Fig.4 - Direct shear and pull-out apparatus prepared for direct shear tests.

TABLE 4 - Dimensions of the direct shear box used for tests.

	length [mm]	breadth [mm]	height [mm]	volume [litres]
Upper Box	316	316	100	100
Lower Box	670	470	225	708.5

controlled hydraulically activated testing machine, able to apply vertical and horizontal loads and to measure them with an accuracy of 0.01 kN out of 300 kN. Vertical and horizontal movements were measured with an accuracy of 0.1 mm out of 1000 mm. The vertical load, maintained constant for the whole duration of the test, was applied to a rubber plate positioned on the steel plate at the top of the upper box. The area of the rigid plate applying a uniform load to the soil in the upper box was 0.100 m². The horizontal load was applied directly to the lower box, running on rollers positioned at its base. The lower box was moved (in direction of its major dimension) at constant displacement rate relatively to the upper one, fixed to the structure of the testing machine.

The investigation has been performed on interfaces between Tenax TT 401 AMP geogrid and the soils A (silty sand) and B (gravel), applying a normal stress of 50, 100 and 200 kPa. In order to evaluate the efficiency of the contact, direct shear tests have also been performed on the soils alone (soil-soil interfaces).

In all the cases, the soils have been compacted directly inside the shear box, at a density of 19.6 kN/m³ for soil A and of 18.2 kN/m³ for soil B.

The possible influence of the testing rate $\dot{\delta}$ has also been considered by performing all the tests with three different displacement rates (0.1, 1 and 5 mm/min).

At the laboratory of the University of Naples "Federico II" a number of CID triaxial tests on large scale specimens have been carried out. These tests have been performed in a large apparatus having a diameter of 350 mm and a height of 820 mm.

In this case the soil B, reinforced with three layers of the Tenax LBO 301 AMP geogrids, installed horizontally respectively 205, 410 and 615 mm above the base, has been utilized. The picture in Fig. 5 shows the installation of a geogrid inside the soil specimen.

The results have been compared with those obtained on the unreinforced soil.

All the specimens have been compacted by means of a vibrating table directly inside the membrane in order to reach a density of 18.2 kN/m³. During the test the volumetric deformations have been obtained by measuring the volume changes of the water contained in the triaxial cell.

The cell pressures varied between 50 and 400 kPa and the rate of displacement was 0.3 mm/min.

RESULTS

Direct Shear Tests

A summary of the main results of the tests is reported in Fig. 6.

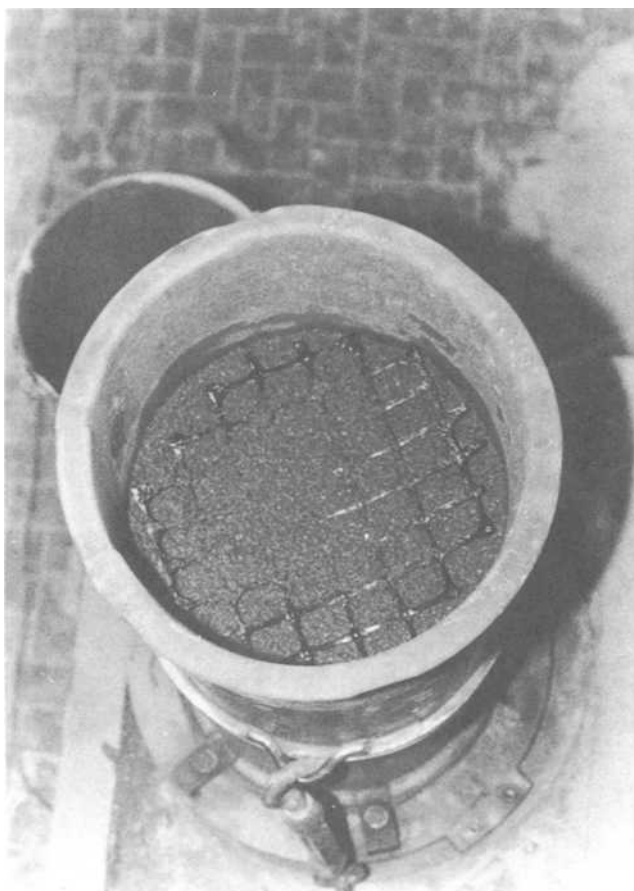


Fig.5 - Installation of a reinforcing element for a large scale triaxial test.

As it can be seen, the shear stress-displacement curves referring to the same materials and experimental procedures, but to different rates of displacement, always merge with similar initial module, displacements at the peak and strength.

It may thus be inferred that the rate of displacement $\dot{\delta}$ plays a minor role, being the results practically unaffected by this factor. Actually, the small differences observed appear substantially random, independently if the tests have been carried out on soils or interfaces, nor the normal stress seems to highlight a possible influence of δ . Therefore, these differences are likely due to small dishomogeneities of the tested specimens: it could be concluded that, at least for the considered soils, the tests procedures may be established neglecting the influence of the rate of displacement.

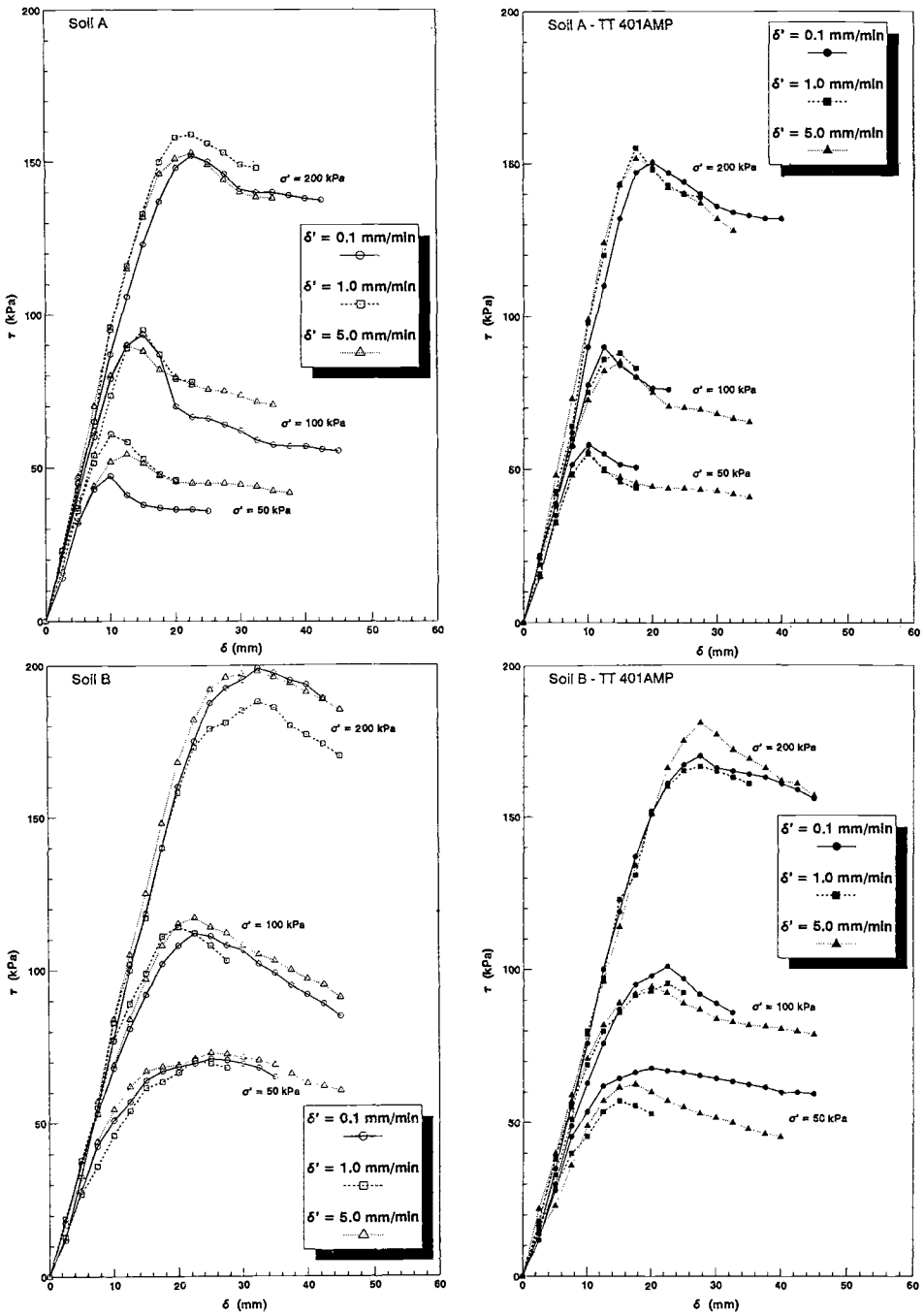


Fig. 6 - Diagram of the shear stress vs. displacement along interfaces in direct shear tests:

As to the influence of the geogrid, it appears that, mostly for the highest normal stresses, they determine a slight decrease of the shear displacement at the peak, which for soil A varies between 10 and 20 mm and for soil B between 15 and 30 mm.

Due to the negligible influence of δ on the shear strength, the failure envelopes have been obtained considering all the data, independently on the adopted rate of displacement (Fig. 7).

The value of the apparent friction angle can be assessed for every soil-geosynthetic interface and compared with the internal friction angle of the soil by modifying the Coulomb law with the introduction of the coefficient of interaction (or interface efficiency) f_{ds} , according to the equation:

$$\tau = f_{ds} \cdot \sigma' \cdot \tan \phi'_{ss} \tag{1}$$

where:

$$f_{ds} = \frac{\tan \phi'_{sg}}{\tan \phi'_{ss}} \tag{2}$$

ϕ'_{sg} = friction angle of the soil-geosynthetic interface

ϕ'_{ss} = friction angle of the soil.

Eq. 1 allows to get the shear stress along the soil-geosynthetic interface when the friction angle of the soil is known, as it usually happens in practice.

The results show the substantial agreement between the data obtained on soils alone and those typical of the interfaces: the cohesion obtained in both cases is probably due to the non linearity of the relationship between the shear strength and the normal effective stress.

Therefore the average friction angle has been calculated for each applied normal stress (Table 5). For sand-geogrid interfaces it ranges between 48.5° and 37.5°, while the overall figures, obtained from the envelopes in Fig. 7, show lower values of ϕ' , but with a substantial cohesion. Taking into account the results of the investigation (see Fig. 7 and Table 5), the efficiency of the contact sand-geogrid appears to be equal to 0.97. For gravel-geogrid interfaces the friction angle ranges between 51.5 and 41° and the efficiency resulted equal to 0.90.

TABLE 5 - Friction angle of soils and interfaces

Normal pressure (kPa)	Soil A		Interf.		Soil B		Interf.	
	ϕ'_{ss}	c' (kPa)	ϕ'_{sg}	c' (kPa)	ϕ'_{ss}	c' (kPa)	ϕ'_{sg}	c' (kPa)
50	47.5°		48.5°		55.0°		51.5°	
100	43.0°		41.5°		49.5°		44.0°	
200	38.0°		37.5°		44.0°		41.0°	
overall	33.3°	23	32.4°	23	36.2°	24	39.2°	31

All the obtained data substantially confirm other researches [6] about the shear strength at interfaces between cohesionless soils and geogrids. In fact, differently from other synthetic materials (woven and

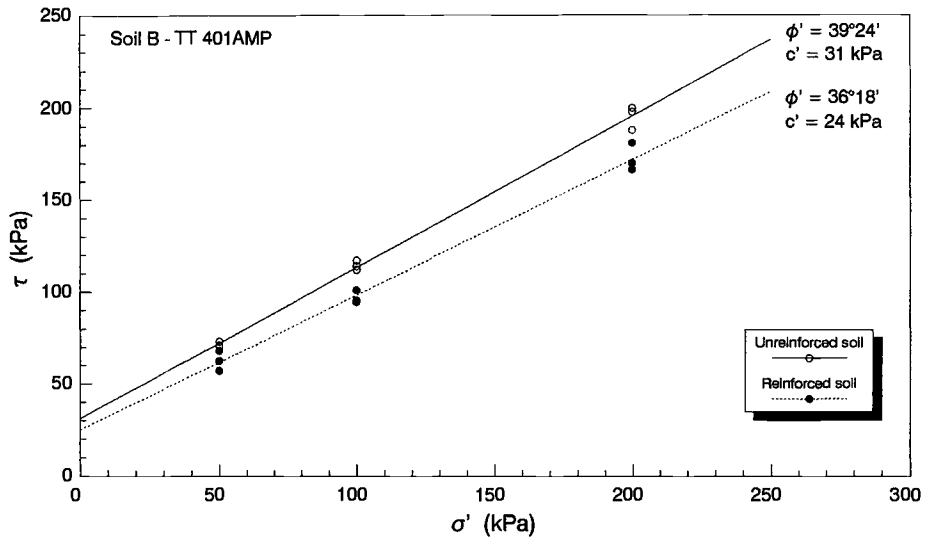
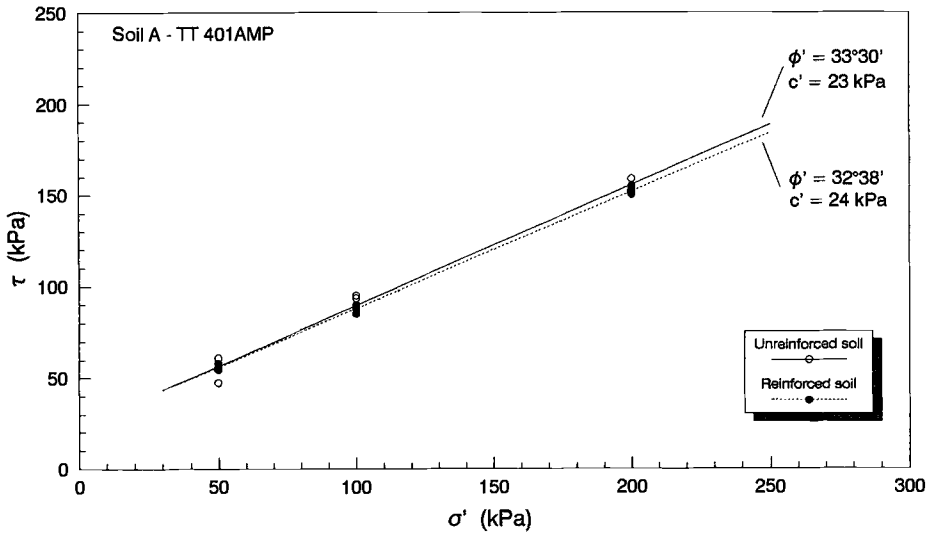


Fig.7 - Failure envelopes for the tested interfaces.

nonwoven geotextiles) the friction angle between soil and geogrid is similar to the internal friction angle of the soil alone; however, it is slightly lower for gravels, maybe due to an imperfect compaction of the soil inside the shear box. On the other hand, other experimental studies [7] showed higher values of f_{dS} for geogrid-gravel interfaces.

Pull-Out Tests

Pull-out tests were performed in order to obtain a better knowledge of the pull-out failure mechanism, which can occur in reinforcement applications, such as steep reinforced slopes and reinforced embankments.

The same equipment used for the direct shear test was used, but some modifications were introduced in respect to the direct shear test:
 - the steel rolls, set at the bottom of the lower box, were removed. The lower box was fixed to the upper box, which is restrained as well;
 - the horizontal load was applied directly to the geogrid, still positioned between the lower and the upper boxes. The geogrid was pulled out and moved relatively to the soil within the boxes;
 - vertical load was not constant during the test, but different levels of load were imposed in arithmetical progression (e.g. +20 kPa for every step), in order to obtain, quickly, values of pull-out resistance for every level of load, as shown in Fig. 8.
 The horizontal axis was moved at a constant testing speed of 1.0 mm/min. Pull-out resistance values can be compared with the internal friction angle of the considered soil, introducing a coefficient of interaction f_{po} into Coulomb's law:

$$\tau = 2 \cdot f_{po} \cdot \sigma' \cdot \tan \phi' \tag{3}$$

where:

$$f_{po} = \frac{F_h/E_v}{2 \cdot \tan \phi'_{ss}} \tag{4}$$

F_h = peak pull-out (horizontal) resistance measured in the test;
 F_v = vertical load applied during each step of the test.

Pull-out tests, performed at the Tenax Geosynthetics Testing Laboratory, allowed to determine f_{po} for the interfaces between the two geogrids and soils A and B. The results are summarized in Table 6.

TABLE 6 - Values of the coefficient f_{po} for different types of soil

Geogrid	Testing dir.	f_{po} Soil B		f_{po} Soil A	
		peak	resid.	peak	resid.
TENAX TT 401 AMP	Longit.	1.9	0.9	1.0	0.6
TENAX LBO 301 AMP	Transv.	2.0	1.2	1.2	0.8
TENAX LBO 301 AMP	Longit.	1.8	1.0	0.9	0.65

Two values of the coefficient of interaction f_{po} are given for every set of soil-geosynthetic interface. The former regards the first part of the test, with low values of vertical stress (less than 40 kPa) and slightly deformed tamped soil (having values of density equal to 100% of Standard

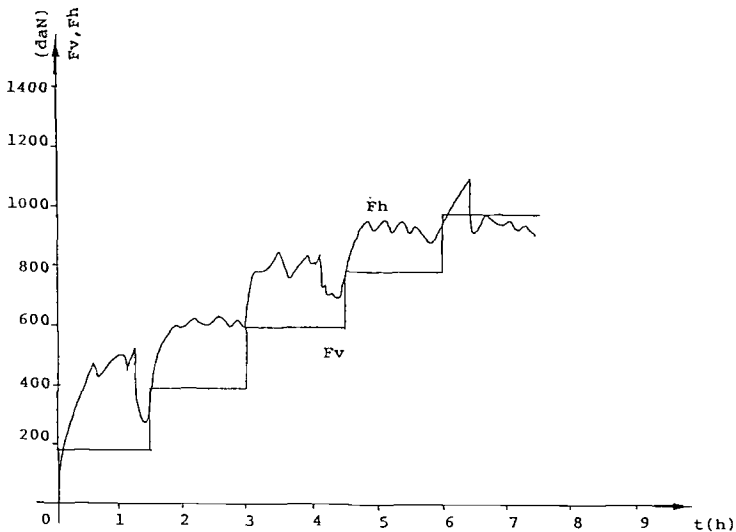


Fig.8 - Typical diagram of vertical and horizontal loads versus elapsed time for a pull-out test.

Proctor): it corresponds to the upper boundary of the pull-out resistance.

The latter value regards the second part of the test, with high values of vertical normal stress (between 40 and 120 kPa) and soil disturbed due to the large deformation: it corresponds to a residual, lower boundary value. It can be seen that the residual resistance is almost the half of the peak one: therefore a certain care shall be used in design to avoid that the peak pull-out resistance is reached, by assuming an adequate Factor of Safety.

CID Triaxial Tests

To the Authors' knowledge only few triaxial tests have been conducted until now on large scale specimens reinforced with geosynthetics.

Broms [8] carried out several tests on geotextiles-reinforced soils, adopting small specimens ($d=69$ mm) of uniform sands and a variable number of fabric elements: according to his research, the geotextiles determine an increase of the overall strength, which is directly related to the spacing of the fabrics; furthermore he observed an increase of the peak axial strain of the reinforced specimens.

Similar tests have been described by Chandrasekaran et al. [9], who have investigated the influence of: i) the spacing between horizontal reinforcing geotextiles layers; ii) the cell pressure; iii) the stiffness and the strength of the geotextiles. The tests involved a uniform sand reinforced with woven and nonwoven geotextiles equipped with strain gauges; the specimens had a diameter of 100 or 200 mm and the cell pressure varied between 25 and 80 kPa.

The results of such an investigation show that both the spacing of the fabric layers and their stiffness affects the mobilised interface friction, hence the overall strength of the specimens. From these

results, it may be inferred that the strength increase is due to an increase of the confining pressure in the soil between the fabrics. Similar results have been reported by some other researchers [10, 11, 12].

The experimental program described in this paper has been carried out with 0.1 m³ specimens of gravel reinforced with three layers of Tenax LBO 301 AMP biaxial geogrids.

The stress-strain curves obtained on both unreinforced and reinforced specimens are reported in Fig. 9.

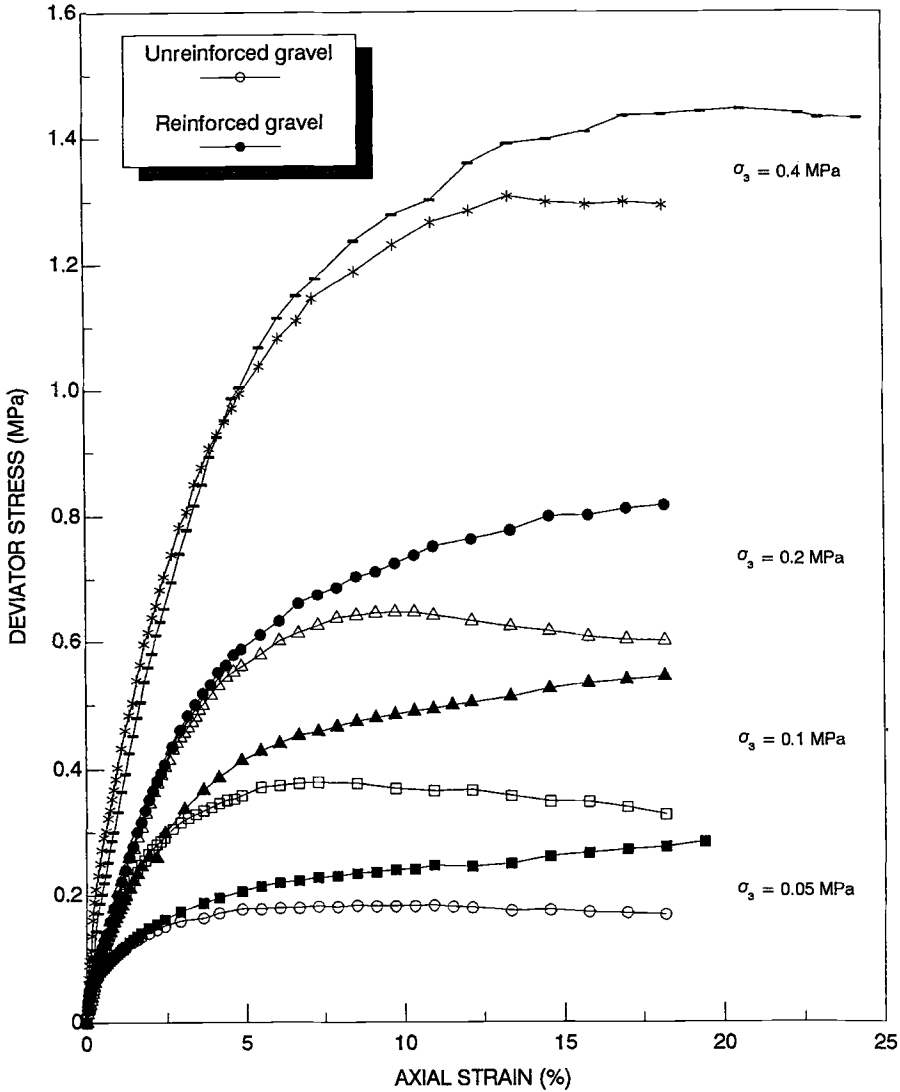


Fig.9 - Stress-strain curves obtained in large scale triaxial tests.

It shows quite clearly that the influence of the geogrids is practically unrecognizable up to an uniaxial strain ranging between 2.5% and 5%, depending on the confining pressure, while for higher strains it determine a valuable increase of the strength.

Furthermore, the shape of the stress-strain curves of reinforced specimen is typical of a strain-hardening material, with a progressive increase of the strength due to the increase of the shear stresses along the interface with the geogrids; on the other hand, the unreinforced specimens are characterized by a strain-softening behaviour.

In other words, it appears that the gravel placed between the geogrids is subject to a stress path different from that featured by the unreinforced specimens, being characterized by higher octahedral stresses, determining an increase of the strength and a more ductile behaviour.

With reference to the specimens subject to the extreme cell pressures, from Fig. 10 it seems that the geogrids determine a reduction of the volumetric strains, both for contractant and dilatant specimens.

Figure 11 shows the nominal stress paths, where the lines of equal strains are also indicated; the diagram shows once again that the effectiveness of the reinforcements increases with increasing strains. In terms of conventional shear strength parameters, the reinforced specimens are characterized by a considerable cohesion (31 kPa versus the 9 kPa measured for unreinforced specimens), while the friction angle (about 38°) is practically the same for both the cases (Fig. 12).

Two specimens after failure are shown in the pictures reported in Figs. 13 and 14: from Fig.13 the confining effect of the geogrids, which brings to a different failure mode if compared with that typical of homogeneous soils (Fig.14), is evident. Broms [8] already reported similar effects.

From these pictures the role played by the reinforcements (namely the deformations restraining and the confining effects) may be inferred.

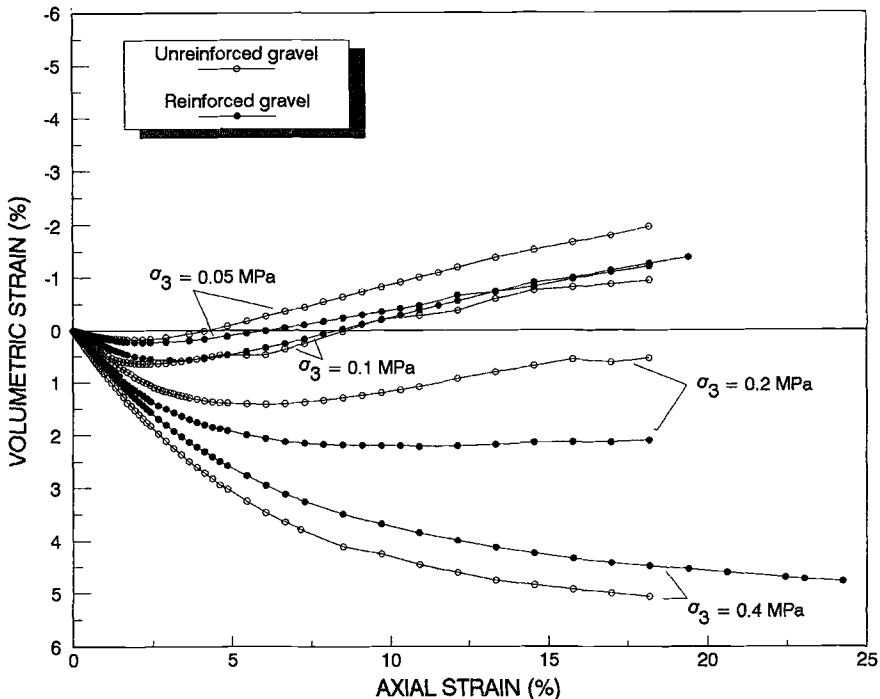


Fig.10 - Volumetric strain vs. axial strain (soil B) in large scale triaxial tests.

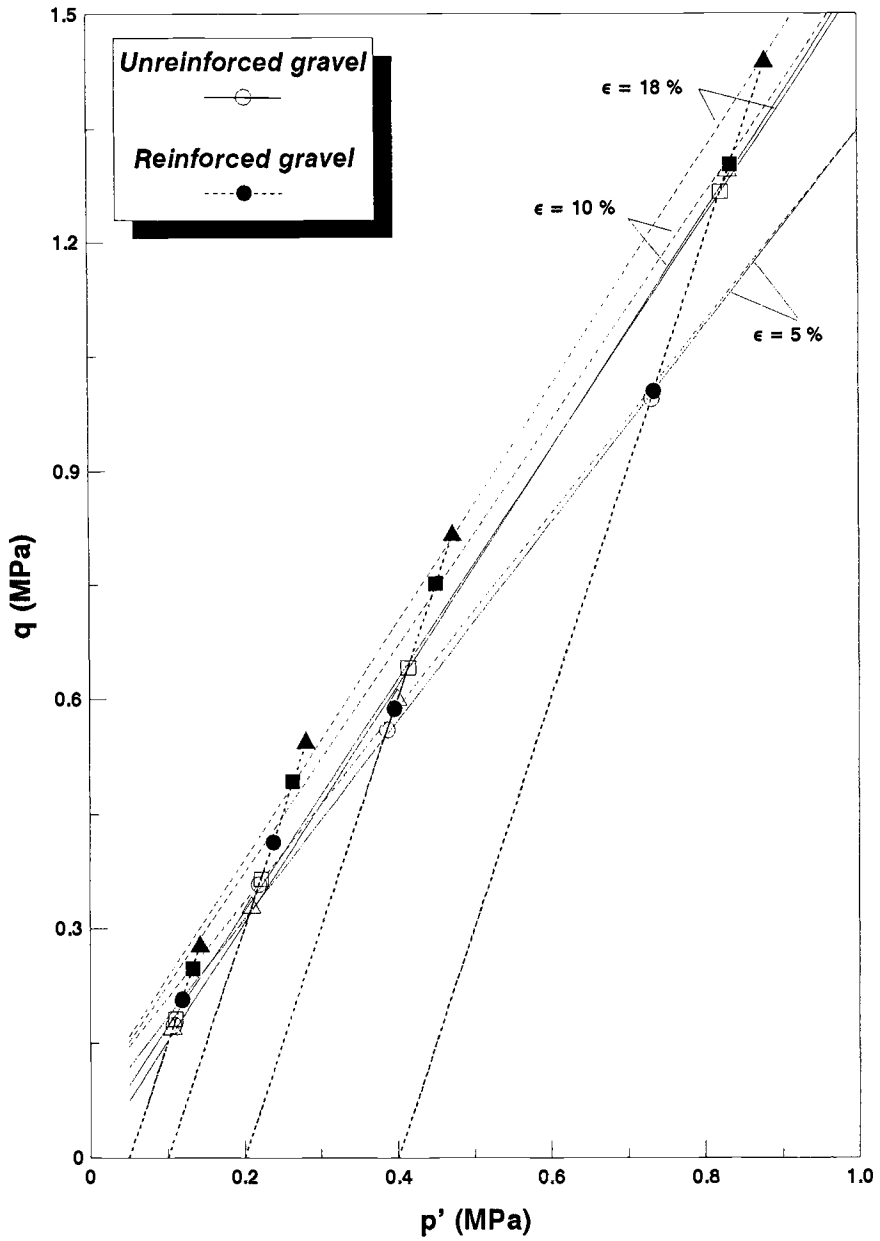


Fig.11 - Stress paths and curves of equal axial strain.

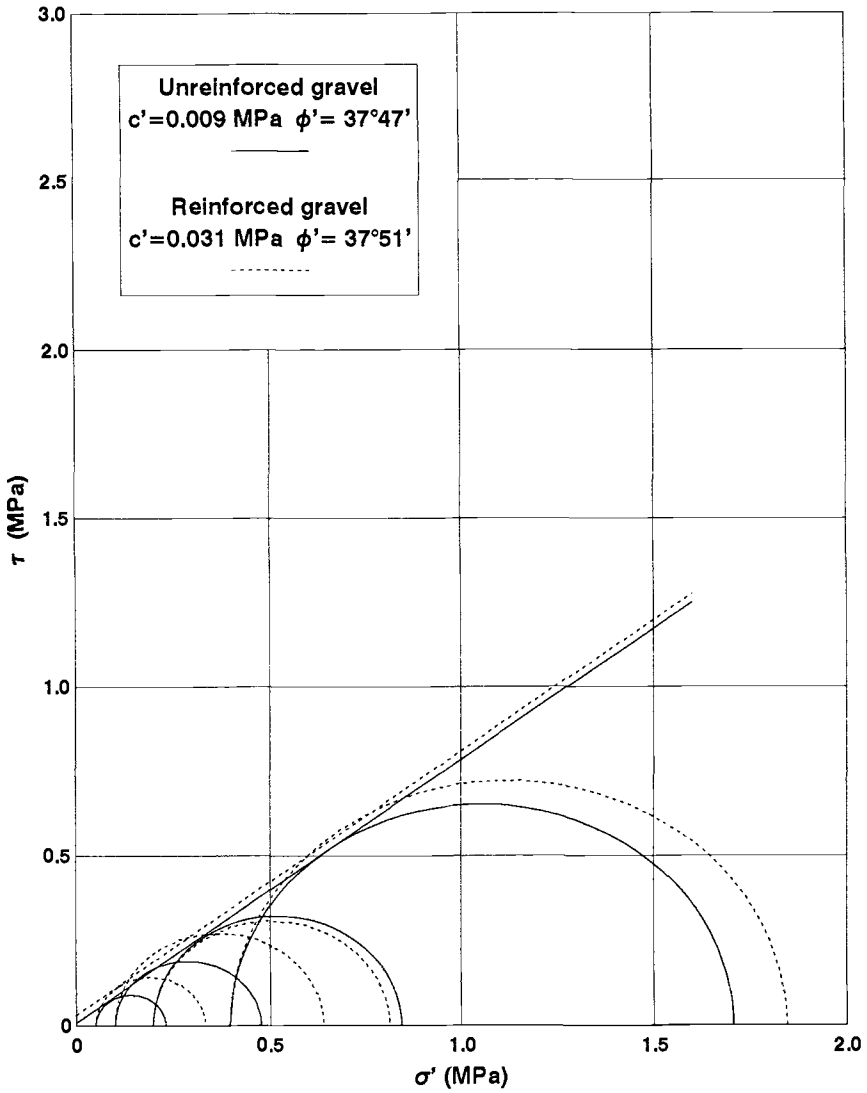


Fig.12 - Failure envelopes of reinforced and unreinforced specimens in large scale triaxial tests.

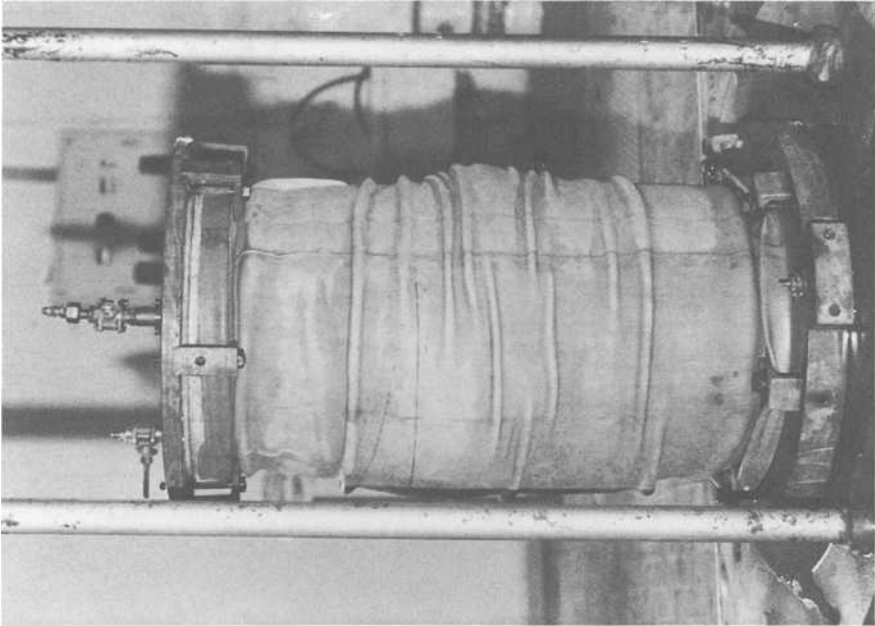


Fig.14 - An unreinforced specimen (soil B) after failure in large scale triaxial test.

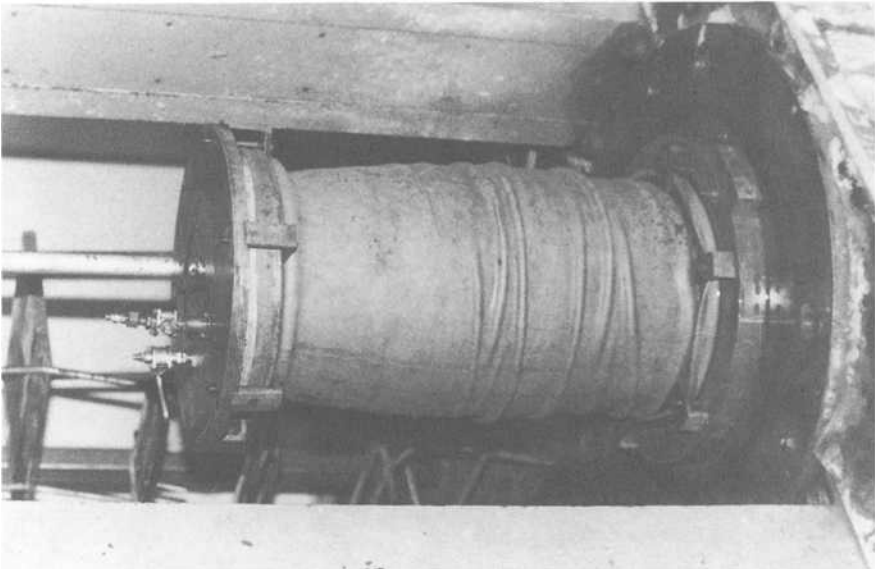


Fig.13 - A reinforced specimen (soil B) after failure in large scale triaxial test.

CONCLUSIONS

A laboratory investigation carried out on soils reinforced with geogrids allowed to obtain more information about the interaction between these different materials.

A series of direct shear tests carried out on interfaces between silty sands or gravels and geogrids demonstrated that, at least for the tested materials, the rate of displacement plays a negligible role (when limited between 0.1 and 5.0 mm/min).

Pull-out tests were performed with the same equipment used for the direct shear tests. Two values of the coefficient of interaction f_{po} were given for every set of soil-geosynthetic interface. The former with low values of normal stress (less than 40 kPa), the latter with high values of normal stress (between 40 and 120 kPa) and soil disturbed due to the large deformation. It can be seen that the residual resistance is almost the half of the peak one.

Some drained triaxial tests carried out on large specimens of gravel reinforced with three layers of a biaxially oriented geogrid have shown the modification of the mechanical behaviour up to failure due to the presence of the reinforcing elements and the increase of the overall shear strength of the reinforced materials, which get an apparent cohesion. However, the reinforcing effect of the geogrids is put into evidence only after rather high strains: this outlines the importance of the geosynthetic stiffness on the overall behaviour of the reinforced material.

ACKNOWLEDGEMENTS

The cooperation of Mr G. Cammarota in performing the triaxial tests and Mr I. DeFeo in performing the direct shear and the pull-out tests is gratefully acknowledged.

REFERENCES

- [1] Ricciuti, A., "Caratterizzazione meccanica di terreni rinforzati con geogriglie, (Mechanical properties of soils reinforced with geogrids)," Unpublished thesis, University of Naples, Italy, 1992.
- [2] Degoutte, G., Mathieu, G., "Experimental research of friction between soil and geomembranes or geotextiles using a 30 x 30 cm² shear box," Proc. III Int. Conf. on Geotextiles, Vienna, Austria, 1986.
- [3] Myles, B., "Assessment of soil fabric friction by means of shear evaluation," Proc. II Int. Conf. on Geotextiles, Las Vegas, Nevada, USA, 1982.
- [4] Miyamori, T., Iwai, S., Makiuchi, K., "Frictional characteristics of nonwoven fabrics," Proc. III Int. Conf. on Geotextiles, Vienna, Austria, 1986.
- [5] Williams, N.D., Houlihan, M., "Evaluation of friction coefficients between geomembranes, geotextiles and related products," Proc. III Int. Conf. on Geotextiles, Vienna, Austria, 1986.
- [6] Richards, E.A., Scott, J.D., "Soil geotextile friction properties",

Second Canadian Symp. on Geotextiles and Geomembranes, Edmonton, Alberta, Canada, 1985.

- [7] Rimoldi, P., Togni, S., "Soil-geosynthetic interaction through direct shear and pull-out tests," Proc. Sardinia'91 Int. Landfill Symposium, Cagliari, Italy, 1991.
- [8] Broms, B.B., "Triaxial tests with fabric-reinforced soil," Proc. Int. Conf. on the Use of Fabrics in Geotechnics, vol. 3, Ecole Nationale des Ponts et Chaussees, Paris, France, 1977.
- [9] Chandrasekaran, B., Broms B.B., Wong K.S., "Strength of fabric reinforced sand under axisymmetric loading," Geotextiles and Geomembranes, 8, 1989.
- [10] Long, N.T., Legeay, G., Madani, C., "Soil-reinforcement friction in a triaxial test," Proc. 8th Eur. Conf. on Soil Mech. and Found. Eng., Helsinki, Finland, 1979.
- [11] McGown, A., Andrawes, K.Z., Al-Hasani, M.M., "Effect of inclusion properties on the behaviour of sand," Geotechnique, 1978.
- [12] Yang, Z., "Strength and deformation characteristics of reinforced sand," PhD Thesis, University of California, USA, 1972.

Gunther E. Bauer¹, and Yijun Zhao²

EVALUATION OF SHEAR STRENGTH AND DILATANCY BEHAVIOR OF REINFORCED SOIL FROM DIRECT SHEAR TESTS

REFERENCE: Bauer, G. E. and Zhao, Y., "Evaluation of Shear Strength and Dilatancy Behavior of Reinforced Soil from Direct Shear Tests," Geosynthetic Soil Reinforcement Testing Procedures, ASTM STP 1190, S. C. Jonathan Cheng, Ed., American Society for Testing and Materials, Philadelphia, 1993.

ABSTRACT: In order to evaluate the shear strength and dilatancy behavior of coarse granular soils reinforced with geogrid a large direct shear apparatus (1000x1000x940 mm) was built. A series of shear tests were carried out to study the effect of geogrid orientation and soil volume changes on shear strength. A numerical model is proposed to calculate the shear strength increase. This is verified by the experimental results. Tensile strains in the geogrid can also be calculated using this model.

KEYWORDS: Direct shear test, reinforced soil, shear strength, soil dilatancy, geogrid, tensile strain.

The rapid development of geosynthetics for soil reinforcing is a historic milestone in soil improvement techniques. Initially, reinforced earth structures were built with metallic strips, granular backfill and facing panels. This application demonstrated an economic and technical advantage over traditional retaining structures. Problems of corrosion in steel, coupled with the development of polymer material led to a rapid increase in the utilization of geosynthetics in soil reinforcement.

The characteristics of polymers, such as high tensile strength, and low installation costs made their function quite attractive. Since geosynthetic materials do not possess much flexural stiffness any increase in shear resistance is attributed to the additional tensile strain mobilized in the reinforcement. Therefore, the efficiency of the reinforcement in providing an increase in shear resistance is highly dependent on the orientation of the geosynthetics with respect to the shear plane. The maximum efficiency should be expected when the orientation of the reinforcement coincides with the direction of the tensile strain of the soil.

The use of geogrids as reinforcement will also increase the bond between soil and reinforcement due to the bearing resistance of the

¹ Professor, Center for Geosynthetics Research Information and Development (C-GRID), Civil and Environmental Engineering Department, Carleton University, Ottawa, Canada, K1S 5B6.

² Ph. D. Student, Civil and Environmental Engineering Department, Carleton University, Ottawa, Canada, K1S 5B6

transverse members of the geogrid as well as interlock of the soil particles with the geogrid apertures. However, the interaction mechanism between geogrid and soil and the mobilization of tensile strain in the reinforced soil are not yet well understood and this phenomenon needs additional experimental exploration.

Direct shear tests are a suitable mean to study the interaction between soil and reinforcement because they can simulate the shear mechanism along a potential failure plane in a reinforced earth structure (Fig. 1).

The present study is aimed to investigate the load transfer mechanism between geogrids and soil by direct shear and to model this mechanism by relating the soil deformation to the shear strength increase. The objectives of this investigation were:

- 1) to evaluate the shear strength of unreinforced and reinforced granular soil using a large direct shear apparatus (1000x1000x940 mm)
- 2) to study the effect of orientation of the geogrid on the shear strength increase
- 3) to investigate the soil dilatancy behavior in unreinforced and reinforced soils, and
- 4) to model the interaction between soil and geogrid by relating the strength increase to the soil dilatancy behavior.

THEORETICAL MODELLING

To model the load transfer mechanism between soil and reinforcement during shear deformation is extremely complex. It is analytically difficult to account for all components of interaction between a granular soil and a geogrid. Sophisticated three-dimensional finite element

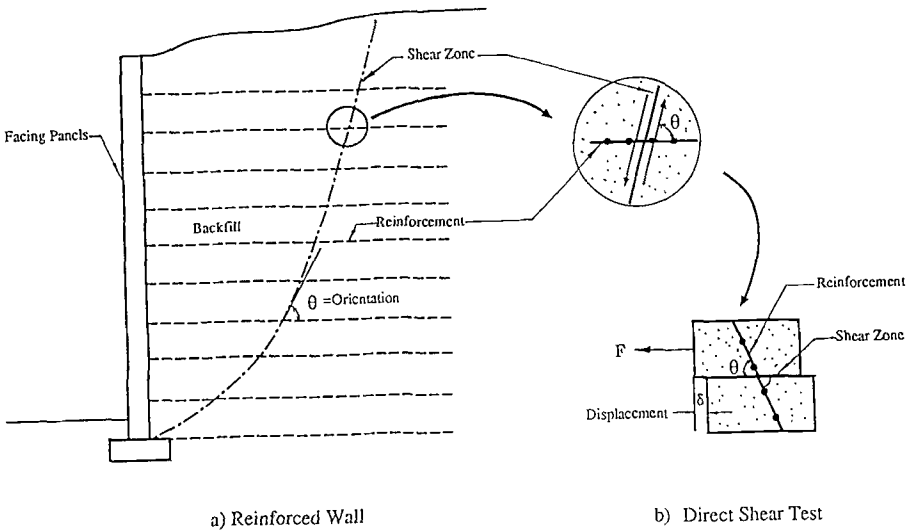


Fig. 1--Analogy between earth structure and direct shear test

analysis could be one of the methods but the mathematical formulation and algorithm can be very complicated. A more practical approach is to use a simple limit equilibrium model verified by experimental results. Four such models have been documented in the literature [1,2,3,4]. They are similar and are all based on the principle of limiting equilibrium. The model presented in this paper is a variation of models proposed by Palmeira [3] and Bauer [1].

The model presented in this paper is based on the following assumptions: 1) A definite shear zone is developed in the soil during direct shear. The thickness of this zone is 20 to 25 percent of the height of the sample in the shear box [1, 12]. 2) The soil, on either side of the horizontal shear zone, behaves like rigid blocks in which the reinforcement is firmly embedded. 3) The reinforcement is sufficiently long to prevent it from being pulled out. 4) The reinforcement is flexible (no bending stiffness). Any increase of shear strength of the composite is due to the mobilized tensile strain (or extension) of the reinforcement. 5) The dilatancy or contraction of the soil and the interaction between soil and reinforcement only happen in the shear zone. 6) Full bonding exists between soil and reinforcement.

Force Equilibrium

A simple static model of a reinforced composite in direct shear is shown in Fig. 2(a). The reinforcement is inclined at an initial angle of θ to the normal of the shear plane. This inclination angle will increase with the shear displacement Δx and the soil vertical displacement Δy (Fig. 2(b)) and is denoted by $\Delta\theta$.

The tensile force in the reinforcement, acting across the central plane, may be resolved into normal and tangential components.

We may define:

$$\sigma_{yy} = \frac{P+W}{A_s}, \quad \tau_{xy} = \frac{S}{A_s} \tag{1}$$

$$\sigma = \frac{N}{A_s}, \quad \tau = \frac{F}{A_s} \tag{2}$$

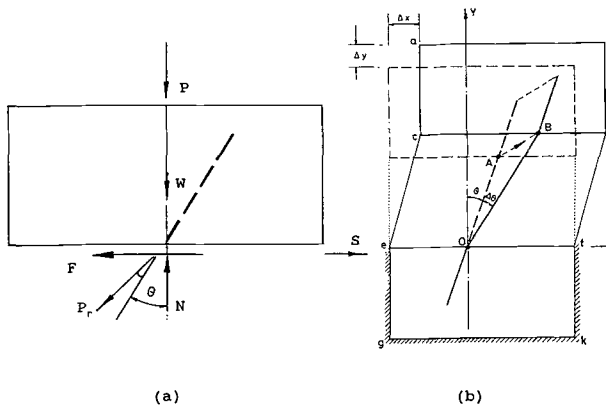


Fig. 2--Reinforced soil model in direct shear

where

P = applied surcharge,
 W = weight of soil above shear plane,
 S = applied shear force,
 A_s = cross sectional area of shear box,
 N = mobilized normal force on shear plane, and
 F = mobilized shear force on shear plane.

The force equilibrium can be written as

$$N = P + W + P_r \cos (\theta + \Delta\theta) \quad (3)$$

$$S = F + P_r \sin (\theta + \Delta\theta) \quad (4)$$

where

P_r = tensile force developed in the reinforcement.

From equations (1), (2), (3) and (4) the shear stress and normal stress on the shear plane can be expressed as

$$\tau = \tau_{xy} - \sigma_r \cos (\theta + \Delta\theta) \quad (5)$$

$$\sigma = \sigma_{yy} + \sigma_r \sin (\theta + \Delta\theta) \quad (6)$$

where

$\sigma_r = P_r/A_s$
 = tensile stress mobilized in the reinforcement.

According to Mohr- Coulomb theory

$$\tau = \sigma \tan \phi \quad (7)$$

where

ϕ = the angle of internal friction of the soil

Substituting equations (5) and (6) into (7) we obtain:

$$\begin{aligned} \tau &= \sigma_r [\sin(\theta + \Delta\theta) + \cos(\theta + \Delta\theta)\tan\phi] + \sigma_{yy} \tan\phi \\ &= C_r + \sigma_{yy} \tan\phi \end{aligned} \quad (8)$$

where

$C_r = \sigma_r [\sin(\theta + \Delta\theta) + \cos(\theta + \Delta\theta)\tan\phi]$
 = "apparent cohesion" of the reinforced soil.

Tensile strain in the Reinforcement

An idealized deformation mode of a reinforced soil specimen is shown in Fig. 2(b). The central zone of the specimen is the shear zone, whereas the upper solid block undergoes both horizontal and vertical displacements denoted, respectively, by Δx and Δy . Considering the segment OA of the reinforcement, the rotation of OA during shear can be expressed as [5]

$$\tan(\theta + \Delta\theta) = \frac{\tan\theta + \frac{\Delta x}{L\cos\theta}}{1 + \frac{\Delta y}{L\cos\theta}} = \frac{L\cos\theta + \Delta x}{L\sin\theta + \Delta y} \quad (9)$$

where L is the initial length of segment OA. The reinforcement is elongated by the amount of ΔL . From the geometry of Fig.2(b) the elongation of the reinforcement is

$$\Delta L = [(L \sin\theta + \Delta x)^2 + (L \cos\theta + \Delta y)^2]^{1/2} - L \quad (10)$$

$$\epsilon_x = \frac{\Delta L}{L} = \left[\left(\sin\theta + \frac{\Delta x}{L} \right)^2 + \left(\cos\theta + \frac{\Delta y}{L} \right)^2 \right]^{1/2} - 1 \tag{11}$$

The average tensile strain in the reinforcement, therefore, is

and $\tan\psi = \Delta x / \Delta y$ (12)

where ψ = the soil dilatancy angle [1].

Constitutive Relationship of Reinforcement

A tensile force versus tensile strain curve for the polyester geogrid is shown in Fig. 3 [6]. The constitutive relationship can be approximated by

$$\sigma_x = E_x \epsilon_x \tag{13}$$

where E_x = the modulus of elasticity of the geogrid.

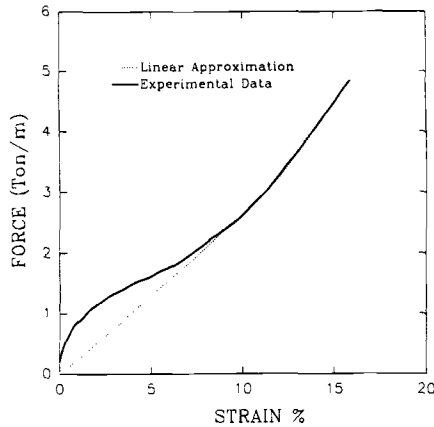


Fig. 3--Tension - strain relationship of polyester geogrid

EXPERIMENTAL PROGRAM

Direct Shear Test Apparatus

In order to achieve the objectives of this research a large direct shear box (1000x1000x940 mm) was built and automated. The test apparatus consisted of the following main components, (a) shear box, (b) shear force application, (c) surcharge load application and (d) a data acquisition and control system. The detailed description of the shear apparatus was given by Bauer et al. [7]. A schematic diagram of the test assembly is shown in Fig. 4.

Soil Properties.

Two granular soils were used as backfill material, a coarse sand and a crushed limestone aggregate. The coarse sand is commonly specified as backfill material for trenches and retaining walls and it is readily available. The grain size distribution of the sand was obtained from sieve

analysis and is shown in Fig. 5. The modified Proctor compaction test yielded a maximum dry density of 19.8 kN/m^3 with an optimum moisture content of 11 percent. The well-graded aggregate was crushed from a limestone rock meeting the specifications of the Ministry of Transportation of Ontario (MTO) for best granular fill (Granular "A"). It is generally specified as a load bearing base material in highway and embankment construction. Figure 5 also shows the grain size distribution for this material. The modified Proctor compaction test gave a maximum dry density of 22 kN/m^3 with an optimum moisture content of 6.8 percent. The dry densities corresponding to 90 percent of modified Proctor compaction was 19.8 kN/m^3 with a moisture content of 4 percent for aggregate and 18.1 kN/m^3 with a water content of 6 percent for the sand.

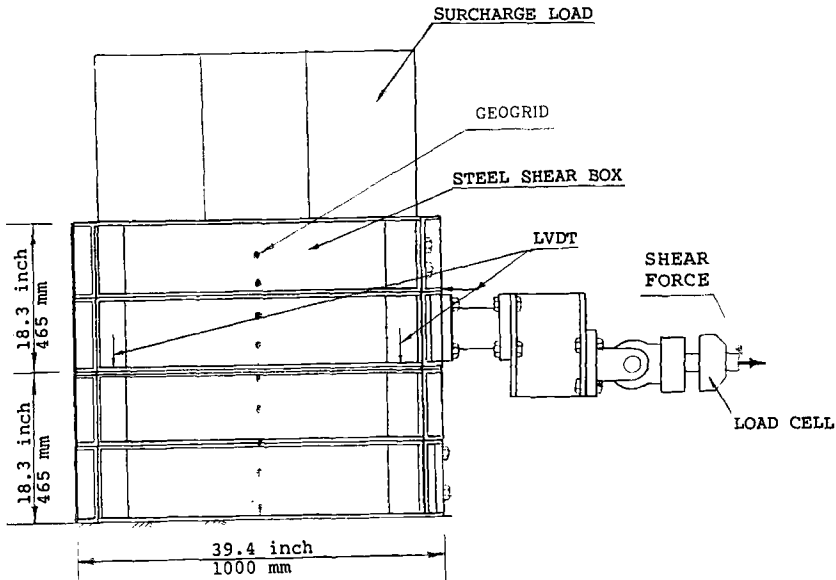


Fig. 4--Schematic diagram of direct shear apparatus

Properties of Geogrids.

Two different geogrids were tested as reinforcement, a woven polyester mesh with apertures of approximately 27 by 25 mm and an extruded uniaxial polyethylene grid with openings of 152 by 16 mm. The polyester grid was made from strands woven in two orthogonal directions with apertures. They were coated with polyolefin to resist chemical and moisture attacks. In all tests the embedded width of both grids were 975 mm while the length varied according to the orientation of the grid in the box. The uniaxial polymer grid was manufactured from sheets of polyethylene extruded and subsequently centered in one direction. This process aligns the polymer's long chain of molecules in the direction of draw and results in a grid with high one - directional tensile strength.

Test Preparation.

For a grid inclination of 90° with respect to the horizontal shear plane the geogrid was anchored to the bottom of the shear box and was also held in position by a clamping system before the soil was placed. For zero degree inclination, that is in a sliding test, the geogrid was kept

in place by clamping the geogrid to the stationary half of the shear box after the sand had been compacted to this level. For grid orientations of 45° and 60° two sets of frames were used to keep the geogrid positioned at the desired inclination.

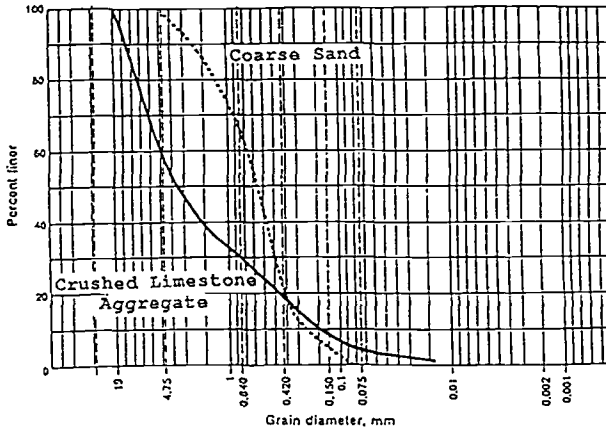


Fig. 5--Grain size distribution of test soils

The moist granular soil was weighed and deposited into the shear box in layers. Each lift was 150 mm high and was levelled manually. The compaction was done by an electric impact hammer having an attached flat plate. The density and moisture content were checked with a nuclear density meter at several locations for each lift. These quantities were verified by soil samples taken from the box.

The soil surface was carefully levelled as it reached the top of the box. The geogrid was then folded along the top surface in order to prevent pullout during a test. The last phase of the test preparation was to install and connect the LVDTs. An operational check of all instruments and the control system was performed.

Test Procedure.

All tests were run under a constant rate of displacement of 1 mm/min. as suggested by previous researchers [2,7,8]. A test was terminated automatically by the HP 9836 controller when the total horizontal displacement of the shear box reached 76 mm. This displacement was found sufficient in all tests to mobilize post peak strength behaviour of the unreinforced backfill.

EXPERIMENTAL RESULTS

Shear Strength Increase

Several series of shear tests were carried out to investigate the shear and deformation behaviour of two soils reinforced with geogrid. Figure 6 shows the test result of normalized shear stress against horizontal displacement of the 15 tests on natural and reinforced coarse sand. It can be observed that for small initial strains (displacement) the shear force (stress) increased linearly until a peak value was reached. The residual shear strength of sand was in the order of 20 to 30 percent lower than the peak strength. In contrast, the sand reinforced with geogrid yielded both high peak and residual shear strength values.

When the reinforcement was inclined at 45° and 60° no distinct peak values were observed. The shear stress kept increasing with the continuing shear displacement. Both geogrids exhibited similar test behavior and strength increases when embedded in the two soils. Due to space limitation, the results of the woven polyester grid is presented only in the following sections.

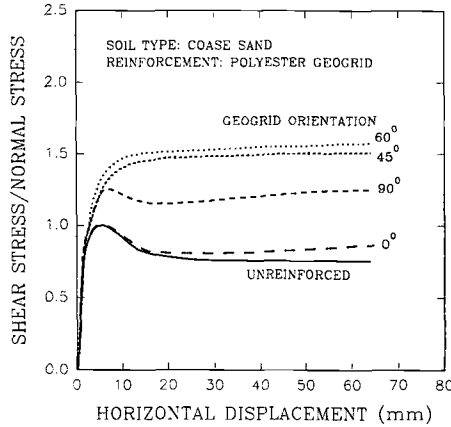


Fig. 6--Shear behaviour of natural and reinforced sand

The results of 15 shear tests on the unreinforced and reinforced crushed limestone aggregate is shown in Fig. 7. The shearing behavior of unreinforced aggregate is similar to that of unreinforced sand. A peak value was also observed. For all reinforced composites the residual strength increased substantially under continued shear displacement.

This strength increase of the reinforced soil can be presented in the form of shear stress vs. normal stress (Fig. 8). In all cases the reinforced soil exhibited an intercept with the shear stress axis when a straight line extrapolation was made. This intercept has been termed by some researchers as "apparent cohesion" or "additional confinement" [9,10,11].

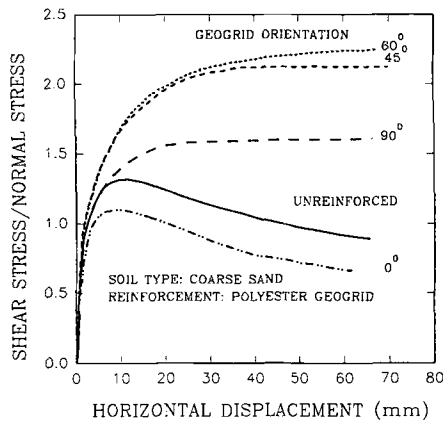


Fig. 7--Shear behaviour of natural and reinforced aggregate

Therefore, the shear strength of reinforced granular soils can be written as

$$s = c_r + \sigma' \tan \phi_r' \tag{14}$$

where

- c_r = apparent cohesion due to geogrid reinforcement,
- ϕ_r' = friction angle of the reinforced composite,
- σ' = effective normal stress.

Soil Dilatancy

Four LVDTs were used to monitor the vertical displacement of the soil in order to evaluate the soil dilatancy. The dilatancy behaviour of the coarse sand and reinforced sand is shown in Fig. 9 as an example. In all tests an increase in soil volume occurred on the shear plane. It was observed that the orientation of the reinforcement relative to the shear plane had significant influence on the soil dilatancy behavior. The magnitude of normal stress seemed to have little effect on soil dilatancy for the narrow range of normal stresses used in this investigation.

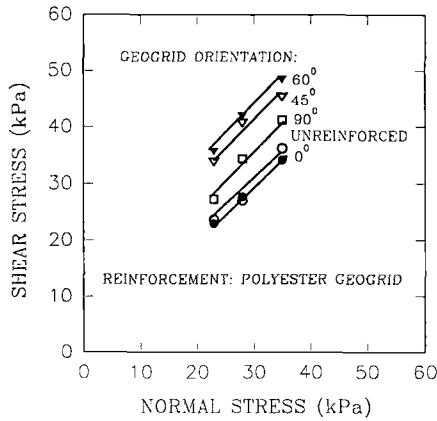


Fig. 8--Shear strength of natural and reinforced sand

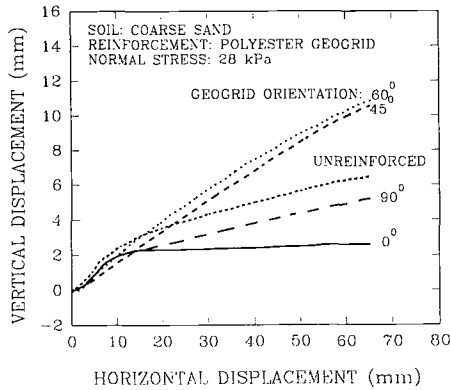


Fig. 9--Dilatancy behaviour of natural and reinforced sand

NUMERICAL SIMULATION

In order to verify the validity of the theoretical model of strength increase in direct shear a comparison with the experimental results were carried out. Figures 10 and 11 show the comparison of theoretical predictions and test results. These figures illustrate that the model can simulate the behavior of shear strength increase in direct shear due to the inclusion of a reinforcing element. The prediction by the model is in fair agreement with the test data considering the fact that a linear stress-strain relationship (Fig. 3) was used in the model. A more complete analysis is presently under way employing "bi-linear" and "best-fit" relations to better describe the actual stress-strain behavior in the lower strain range ($\epsilon < 10\%$).

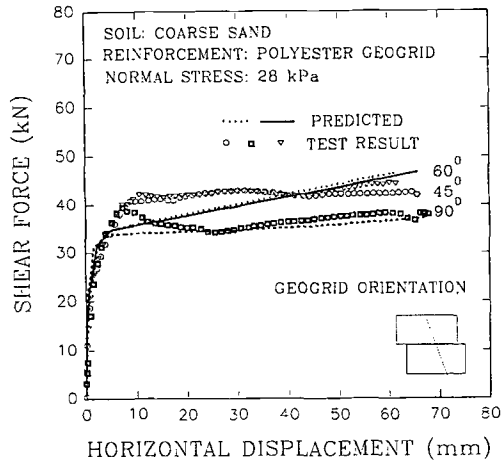


Fig. 10--Theoretical and experimental results for sand

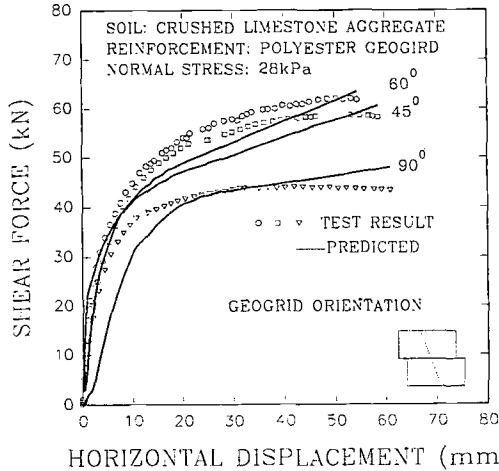


Fig. 11--Theoretical and experimental results for aggregate

NUMERICAL SIMULATION

In order to verify the validity of the theoretical model of strength increase in direct shear a comparison with the experimental results were carried out. Figures 10 and 11 show the comparison of theoretical predictions and test results. These figures illustrate that the model can simulate the behavior of shear strength increase in direct shear due to the inclusion of a reinforcing element. The prediction by the model is in fair agreement with the test data considering the fact that a linear stress-strain relationship (Fig. 3) was used in the model. A more complete analysis is presently under way employing "bi-linear" and "best-fit" relations to better describe the actual stress-strain behavior in the lower strain range ($\epsilon < 10\%$).

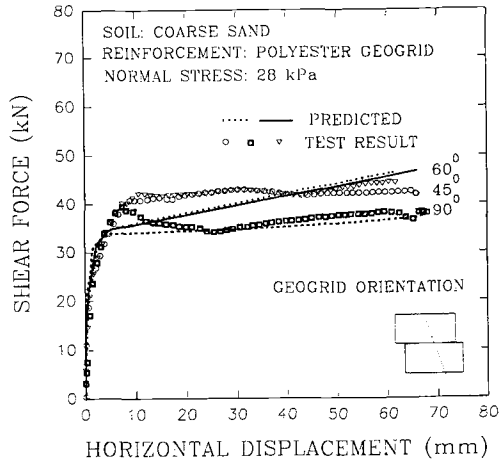


Fig. 10--Theoretical and experimental results for sand

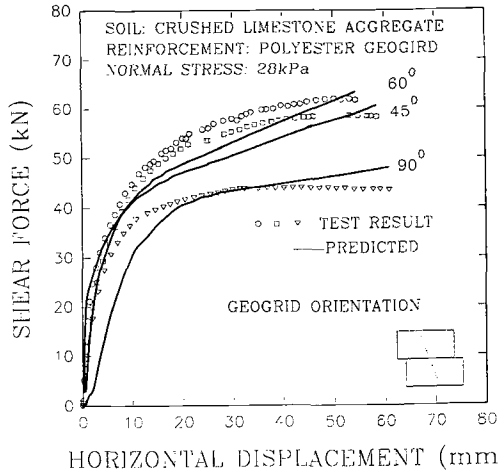


Fig. 11--Theoretical and experimental results for aggregate

SUMMARY AND DISCUSSIONS

Orientation Effect

The test results (Figs. 6, 7 and 8) show that the orientation of the geogrid with respect to shear plane has a significant effect on the increase of shear strength of the composite. The maximum increase occurs when the geogrid is orientated at 60° to the shear plane. A similar observation was made by Fatani et al. [8], Jewell and Wroth [2] and Gray and Ohashi [4]. At this orientation the combined effect of shear displacement and soil dilatancy will mobilize the most tension in the reinforcement. Fig. 12 shows a comparison of the developed tensile strain in the reinforcement embedded in sand at different inclinations. The figure indicates that at 60° inclination the maximum tensile strain is mobilized in the reinforcement compared to other inclinations.

In present design of reinforced earth structures the orientation effect is not taken into consideration. As indicated for the case of the reinforced wall in Fig. 2(a), the failure plane intersects most reinforcement elements at angles between 45 to 90° . This means that, according to the test results presented, a substantial increase in shear strength is realized.

Task Force 27 (Federal Highway Administration) recommends that the pullout resistance of geogrids be reduced by 40 to 50% depending on the percentage of the open area of the grid. This reduction, given as equivalent coefficient of direct sliding, C_{ds} , would reduce the anchorage capacity for the woven polyester grid by 50% ($C_{ds} = 0.5$) and that for the extruded mesh by 40% ($C_{ds} = 0.6$). It seems that additional tests are needed to clarify this aspect.

Most equilibrium analyses of reinforced earth structures consider the mobilized soil strength and the activated tension in the reinforcement as two separate entities assuming usually the same critical failure plane as that of an unreinforced soil structure. Future work is needed to clarify when the spacing of the reinforcement elements are sufficiently close to warrant the use of a global shear strength for the composite as given by Eq. 14.

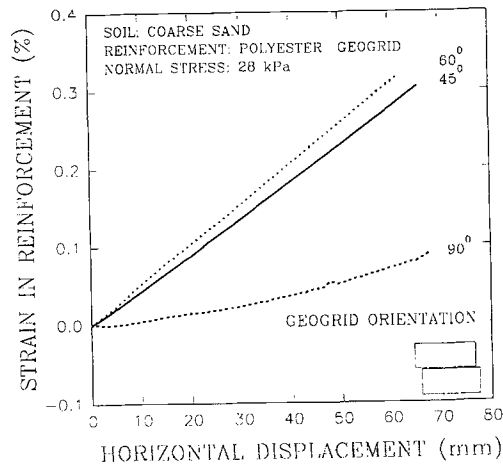


Fig. 12--Average tensile strain in the reinforcement

Soil dilatancy

Dense sands and gravels tend to dilate when sheared. Through load transfer from the soil to the reinforcement tensile strains are mobilized in the geogrid. This tensile strain contributes to additional shear strength of the composite. Thus the mobilization of tensile strain and corresponding tensile forces in a geogrid depends to a large extent on the amount of soil dilatancy.

This is clearly stated by Eq. 11 and Eq. 12. An increase of the tensile stresses in the reinforcement will, in turn, increase the "apparent cohesion" or the "confinement effect" of the composite as given by Eq. 8. The granular backfill in conjunction with the mobilized tension in the reinforcements acts similar to a composite having both granular and cohesive properties as expressed by Eq. 8.

CONCLUSIONS

In order to evaluate the shear strength and dilatancy behavior of reinforced granular soils a large direct shear apparatus (1000x1000x940 mm) was used. A series of direct shear tests were carried out and a large data base was developed. Based on the experimental results and previous research [1 and 3] a theoretical model was developed. Numerical simulation using the proposed model illustrates that the model is capable in predicting the shear strength increase in a direct shear test as well as calculating the tensile strain mobilized in a geogrid. The following conclusions can be drawn from the experimental study and theoretical analysis:

1. The large direct shear apparatus, although time consuming to run, was well suited to test compacted coarse granular soils and large specimens of reinforcements (geogrid).

The main advantages of this large test assembly is to determine the mechanical properties of representative specimens of geogrids embedded in soils placed under similar conditions as those in the field.

2. The shear strength of natural sand and crushed stone aggregate can be increased significantly when reinforced with geogrid.

3. Dense granular backfill dilates when sheared thereby mobilizing tensile strains in the geogrid through load transfer along the geosynthetic/soil interface. The magnitude of the tensile strain was directly related to the degree of soil dilatancy (Figs. 9 and 12).

4. The orientation of the geogrid with respect to shear plane has a marked effect on the mobilized shear resistance of the reinforced composite. At an orientation of 60° to the shear plane, the maximum shear strength increase was obtained by both experiment and by prediction.

5. The average tensile strain in the geogrid indicates that when the geogrid inclines to 60° the maximum tensile strain is mobilized. This inclination coincides with the direction of the minor principal strain in the soil [2,3]. Therefore, if practically possible, the alignment of the reinforcement elements should be as closely as feasible along the direction of minor principal strains mobilized in the soil.

REFERENCES

- [1] Bauer, G. E., Al-Joulani, N. M., and Fatani, M. N., "Load Transfer Mechanism of Reinforced Sand Subjected to Direct Shear," (Submitted for publication to the ASTM Geotechnical Testing Journal), 1992.

- [2] Jewell, R. A., and Wroth, C. P., "Direct Shear Tests on Reinforced Sand", Geotechnique, Vol. 37, No. 1, 1987, pp 53-68.
- [3] Palmeira, E. M., "The Study of Soil - Reinforcement Interaction by Means of Large Scale Laboratory Tests," Ph. D. Thesis University of Oxford, England, 1987.
- [4] Gray, D.H., and Ohashi, H., "Mechanics of Fibre Reinforcement in Sand," Journal of Geotechnical Engineering, ASCE, Vol. 109 (GT3), March, 1983, pp 335-353.
- [5] Juran, I., Ider, M. H., Chen, C. L., and Guermazi, A. "Numerical Analysis of the Response of Reinforced Soils to Direct Shearing," International Journal for Numerical and Analytical Methods in Geomechanics, Vol. 12, 1988, pp 157-171.
- [6] Razqapur, A. G., "Tensile Strength and Load - Deformation Characteristics of Conwed Stratagrids," Final Report Submitted to Conwed Plastics, 1990.
- [7] Bauer, G. E., Zhao, Y., and El-Shafei, M., "Direct Shear Box Tests on Geogrid," Final Report Submitted to Conwed Plastics, 1990.
- [8] Fatani, M.N., Bauer, G.E., and Al-Joulani, N., "Reinforcing Soil with Aligned and Randomly Oriented Metal Fibers," ASTM, Geotechnical Testing Journal, Vol. 14, No. 1, 1991, pp 78-87.
- [9] Broms, B. B., "Fabric reinforced retaining walls," Theory and Practice of Earth Reinforcement, A. A. Balkema Publishers Rotterdam, 1989, pp 3 - 31.
- [10] Jones, C. J. F. P. "Earth Reinforcement and Soil Structures," Butterworth and Co. (Publishers) Ltd, London, England, 1985.
- [11] McGown, A., Andrawes, K. Z. and Al Hasani, M. M., "Effect of Inclusion Properties on the Behaviour of Sand," Geotechnique, Vol. 28, No. 3, 1978, pp 327 - 346.
- [12] Koerner, R.M., Wayne, M.H. and Carroll, R.G., Jr., "Analytic behavior of Geogrid Anchorage," Proc. Geosynthetics '89, San Diego, CA, IFAl, pp. 525-536.

R. R. Berg,¹ and J. G. Collin²

MATERIAL PARAMETERS USED IN DESIGN OF GEOSYNTHETIC REINFORCED SOIL STRUCTURES

REFERENCE: Berg, R. R., and Collin, J. G.; "Material Testing for Design of Geosynthetic Reinforced Soil Structures," Geosynthetic Soil Reinforcement Testing Procedures, ASTM STP 1190, S. C. Jonathan Cheng, Ed., American Society for Testing and Materials, Philadelphia, 1993.

ABSTRACT: Limit equilibrium design of reinforced soil structures requires input of several material parameters. Properties required for design and status of standardized test methods and procedures by ASTM for definition of these properties are summarized. Results of a limited parametric study investigating effect of small variances (i.e., 10%) in material property values on design of reinforced soil structures are presented. Small variations in both soil friction angle and direct shear coefficient between soil and geosynthetic reinforcement have an economically significant impact on the design of reinforced walls and slopes, for the cases examined.

KEYWORDS: laboratory tests, reinforced soils, limit equilibrium analysis, soil shear strength

Analysis and design of reinforced soil structures requires definition of several properties of each material used in construction. Structures consist of soil and reinforcement materials, and in the case of near vertical structures a structural facing component. Parameters needed for limit equilibrium stability analyses, and available American Society for Testing and Materials (ASTM) procedures for testing and definition of applicable material properties, are summarized within. Limit equilibrium procedures are routinely used for design of geosynthetic reinforced soil structures.

Test methods for each of the properties required for definition of design parameters have not yet been standardized. Development status of test methods and standards of practice for definition of material properties are summarized. A limited parametric study of sensitivity of designs to accuracy of design parameter definition is performed and presented herein. The review of test methods needs and results of the parametric study form the basis for discussion on prioritization of test method development.

Results of the parametric analyses are also useful to designers of reinforced soil structures. The charts presented within illustrate the affect of inaccuracies in definition of material properties and design parameters. Deviations of $\pm 10\%$ in material properties are plotted in terms of affect on reinforcement quantities and volume of reinforced fill.

¹ P.E., Consultant, Woodbury, MN

² Ph.D., P.E., Vice President, Tensar Earth Technologies, Morrow, GA

DESIGN PRACTICEAnalysis Procedures

Common types of reinforced soil structures include retaining walls, steepened slopes, and embankments over soft soils. Structures are normally designed on the basis of limit equilibrium analyses. A tieback wedge model is normally used for retaining walls. Standard slope stability procedures (e.g., Bishops method) are used in the analysis of steepened slopes and embankments over soft soils. Computer programs and chart-form solutions are available for all three applications. Similar design input parameters, derived from definition of material properties, are used in limit equilibrium analyses of these three types of structures.

Input Parameters

Design parameters that may be used in limit equilibrium analyses of geosynthetic reinforced soil structures are summarized in Table 1. The parameters are differentiated by material type(s). One or several property tests may be required for definition of a particular material design parameter. Methods of testing for definition of these parameters are in various stages of development within ASTM.

TABLE 1 -- Summary of parameters required for design.

Material(s)	Design Parameter
soil	friction angle (degrees) cohesion (kN/m ²) unit weight (kN/m ³)
geosynthetic reinforcement	long-term allowable strength seam strength
soil-reinforcement interaction	pullout coefficient direct shear coefficient
reinforcement-facing material	allowable connection strength

TEST METHODS

Test methods and standards for defining limit equilibrium design parameters are summarized in Table 2. Stage of development, limitations of methods, and obstacles to development of procedures are discussed below, as applicable, by the four group of material(s).

Soil

Tests for quantifying shear strength parameters and density of soils are well established (Table 2). However, application of test results to analysis of reinforced soils is not as well defined. Specifically, the type of shear strength definition to use in analyses varies between European and American practice. Constant volume [1] or critical state [2] definition is used in European practice. Peak strength values are routinely used in American practice[3]. Peak shear

strength values are routinely computed with the ASTM test procedures listed in Table 2. The range of deviation between constant volume and peak friction angles for four soil types are presented in Table 3.

TABLE 2 -- Summary of test methods parameters.

Design Parameter	ASTM Test Method
soil	
- shear strength: friction angle (degrees) and cohesion (kN/m ²)	D 2166 Compressive Strength, Unconfined, of Cohesive Soils D 4767 Consolidated-Undrained Triaxial Compression Test on Cohesive Soils D 3080 Direct Shear Test of Soil Under Consolidated Drained Condition
- unit weight (kN/m ³)	D 698 Moisture-Density Relations of Soils and Soil-Aggregate Mixtures Using 5.5-lb Rammer and 12-in. Drop D 1557 Moisture-Density Relation of Soils and Soil-Aggregate Mixtures Using 10-lb Rammer and 18-in. Drop
geosynthetic reinforcement (long-term allowable strength)	
- creep	D5262 Evaluating the Unconfined Tension Creep Behavior of Geosynthetics
- installation damage	- in task group
- chemical dissolution	- not yet addressed
- chemical degradation	- balloting in subcommittee
- biological degradation	- not yet addressed
- seam strength	D4884 Strength of Sewn Geotextile
soil-reinforcement interaction	
- pullout coefficient	- balloting in subcommittee
- direct shear coefficient	D 5321 Determining the Coefficient of Soil and Geosynthetic or Geosynthetic and Geosynthetic Friction by the Direct Shear Method
reinforcement-facing material	
- connection strength	- in task group

Reinforcement

An ASTM standard of practice for defining long-term allowable strength of geosynthetic soil reinforcement elements does not exist. However, other standards [5,6,7], from the Geosynthetic Research Institute, have defined that long-term allowable strength is computed with several partial factors. These partial factors are to account for creep, chemical degradation, biological degradation, installation damage, and connection strength of the reinforcement. The formula for computing an allowable strength is typically presented in an equation similar to [8]:

$$T_a = \frac{T_{ult}}{FS_{CR} \times FS_{ID} \times FS_{CD} \times FS_{BD} \times FS_{JNT}}$$

where:

- T_a = long-term allowable geosynthetic tensile strength, (kN/m);
- T_{ult} = ultimate geosynthetic tensile strength, (kN/m);
- FS_{CR} = partial factor of creep deformation, ratio of T_{ult} to creep limiting strength, (dimensionless);
- FS_{ID} = partial factor of safety for installation damage, (dimensionless);
- FS_{CD} = partial factor of safety for chemical degradation, (dimensionless);
- FS_{BD} = partial factor of safety for biological degradation, (dimensionless); and
- FS_{JNT} = partial factor of safety for joints (seams and connections), (dimensionless).

Test procedures for defining these partial factors, or material properties, are therefore required. Development status of standard test procedures for these partial factors are summarized in Table 2. The creep, chemical degradation, and biological degradation factors are time dependent, and therefore present a greater challenge in developing test methods of reasonable duration that result in accurate definition for a long-term design life of 75 years or more. A creep test may be conducted in-isolation or in situ (i.e., within soil), with the latter environment adding complications to testing and method standardization. Another obstacle to standard development is possible synergy between degradation mechanisms, and modeling of such in laboratory tests. Synergy is addressed in the equation above by using the product of degradation factors, and not the sum, in the denominator.

TABLE 3 -- Constant volume versus peak soil friction angles (after [4]).

Soil Classification	Constant Volume Friction Angle (degrees)	Peak Friction Angle of Dense Soil (degrees)
silt (nonplastic)	26 to 30	30 to 34
uniform fine to medium sand	26 to 30	32 to 36
well-graded sand	30 to 34	38 to 46
sand and gravel	32 to 36	40 to 48

Soil-Reinforcement Interaction

A test method for defining pullout resistance of geosynthetics from soils is under development within ASTM, committee D35. This procedure is currently being balloted in the subcommittee stage. A direct shear interaction performance test, method D 5321, has recently been adopted.

Reinforcement-Structural Component Interaction

Test standards for defining this parameter are not yet established within ASTM. A new task group was recently (June, 1992) formed under ASTM Committee C15 to develop a standard for connection strength between geosynthetic reinforcement material and masonry retaining wall units.

ACCURACY OF DESIGN PARAMETERS

A limited study of the affect of accuracy in definition of design parameters (Table 1) on limit equilibrium design has been conducted. The purpose of the study was to provide a perspective on priorities of additional test method development within ASTM and provide guidance to designers of reinforced soil structures. Designers may gain insight as to the importance (i.e., economic impact) of definition of various material properties and design parameters.

This study was a limited parametric analysis. Reinforced slope and wall structures were examined. The amount of required reinforcement and volume of reinforced soil mass were computed with variations of a single design input parameter. The study did not examine design or safety of design with a probabilistic approach, such as used by Cheng and Christopher [9].

The allowable strength of the reinforcement, direct shear interaction coefficient, unit weight of the soil, and soil friction angle were varied by $\pm 10\%$. This percent value of variation does not address anticipated reliability of parameter definition. However, Cheng and Christopher [9] in a probabilistic review of reinforced slopes used variations of 5%, 12%, and 10% for soil unit weight, soil friction angle, and geosynthetic tensile strength, respectively. Interaction values were not addressed in their study. Variation of pullout interaction coefficient was also not within the scope of this paper. Assumptions, analytical method, and results for the two types of structures are as follows.

Economics of reinforced structure construction is affected both by the quantity of reinforcement required and the volume of reinforced mass. The volume of reinforced mass is more important in cut situations where costs for excavation and fill placement are incurred, versus fill situations where only placement costs are incurred.

Reinforced Slope Example

A single slope angle of 45° was used. Heights of 10, 20, and 30 m were analyzed. The base design values consisted of assumed values of: backfill soil friction angle equal to 32° , backfill soil cohesion equal to 0, backfill soil unit weight equal to 20 kN/m^3 , an allowable geosynthetic tensile strength equal to 30 kN/m , a direct shear coefficient equal to 0.9, and a stable foundation. A safety factor against instability of 1.5 was used for all cases.

The chart form solution presented by Schmertmann et al. [10] was used for computations. The computed value of reinforcement layers required were rounded up to the nearest whole number. The affect of direct shear interaction was computed by assuming that the driving force remained constant and that the resisting force had to increase to maintain a minimum factor of safety. The width of the reinforced mass was increased or decreased along its base to maintain a constant safety factor against sliding. The upper width of reinforced soil mass was held constant.

Results of the analyses are presented in Figures 1 and 2. Up to a 50% change in the amount of required reinforcement resulted from a 10% variation in soil friction angle. Variations of interaction coefficient, soil unit weight, and allowable geosynthetic tensile strength by $\pm 10\%$ had less of an impact on amount of tensile

reinforcement required, but were still significant as illustrated (Figure 1). The effects of varying these parameters on the volume of reinforced soil mass are presented in Figure 2. The volume does not vary with changes in soil unit weight and allowable geosynthetic strength, with the limit equilibrium charts used. A variation of $\pm 10\%$ of the soil-geosynthetic direct shear interaction coefficient results in a variation of $\pm 10\%$ in volume, respectively. A change in soil friction angle of $\pm 10\%$ results in approximately $\pm 20\%$ variation in volume, respectively.

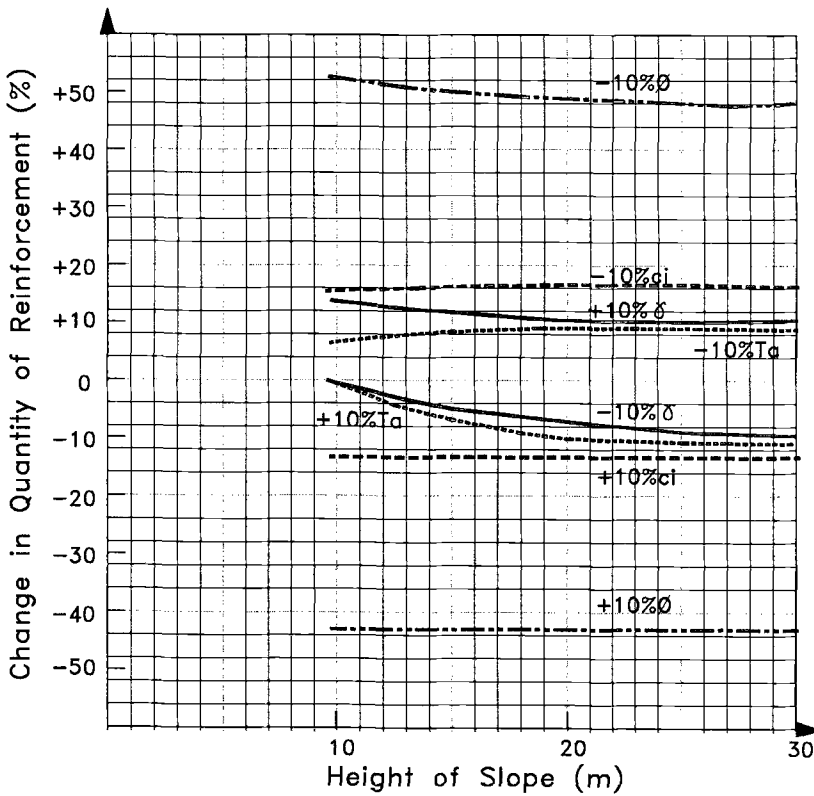


FIG. 1 -- Reinforced slope: change in quantity of reinforcement with $\pm 10\%$ variation in design parameters.

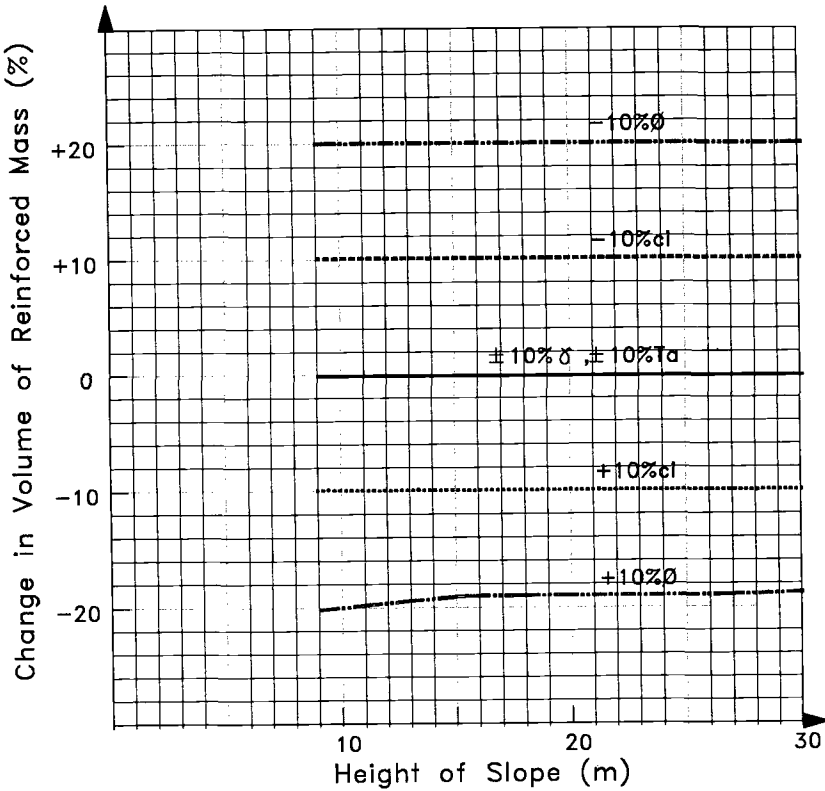


FIG. 2 -- Reinforced slope: change in reinforced soil volume with $\pm 10\%$ variation in design parameters.

Reinforced Wall Example

A vertical retaining wall with a flat fill on top and no surcharge was used in the analyses. A Rankine active lateral earth pressure theory was used to compute internal and external loadings. Heights of 3, 6, 9, and 12 m were analyzed. The base design values consisted of assumed values of: soil friction angle equal to 32° , soil cohesion equal to 0, soil unit weight equal to 20 kN/m^3 , an allowable geosynthetic tensile strength equal to 30 kN/m , and a direct shear coefficient equal to 0.9. The base soil parameters were used for the reinforced wall fill, retained backfill, and foundation soil zones. A safety factor against tensile failure of 1.5 was used for all cases. A factor of safety against sliding failure of 2.0 was used, and it was assumed that the critical sliding failure plane was at the soil-reinforcement interface. A minimum reinforcement length to wall height ratio was not used. A tieback-wedge analysis procedure was utilized.

The computed required layers of reinforcement were rounded up to the nearest whole number.

Results of the analyses are presented in Figures 3 and 4. Up to a 45% change in the amount of reinforcement required resulted from a 10% variation in soil friction angle. Variations of direct shear interaction coefficient, soil unit weight, and allowable geosynthetic tensile strength by $\pm 10\%$ had less of an impact, but were still significant as illustrated (Figure 3). The effects of varying these parameters on the volume of reinforced soil mass are presented in Figure 4. The volume does not vary with changes in soil unit weight and allowable geosynthetic strength. A variation of $\pm 10\%$ of the soil-geosynthetic direct shear interaction coefficient results in a variation of approximately $\pm 10\%$ in volume, respectively. A change in soil friction angle of $\pm 10\%$ results in approximately ± 20 to 25% variation in volume, respectively.

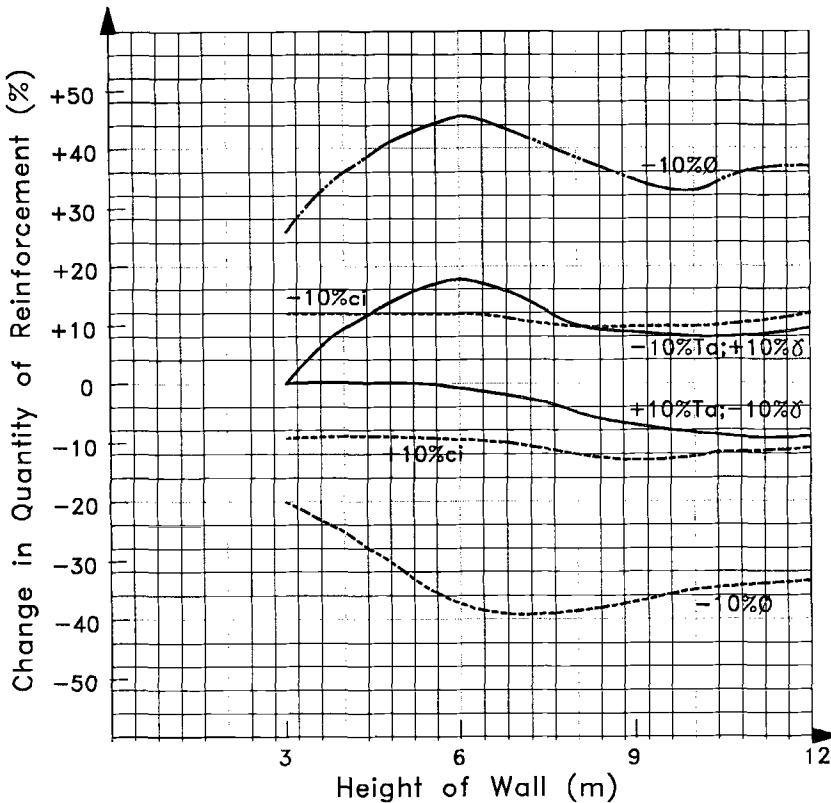


FIG. 3 -- Reinforced wall: change in quantity of reinforcement with $\pm 10\%$ variation in design parameters.

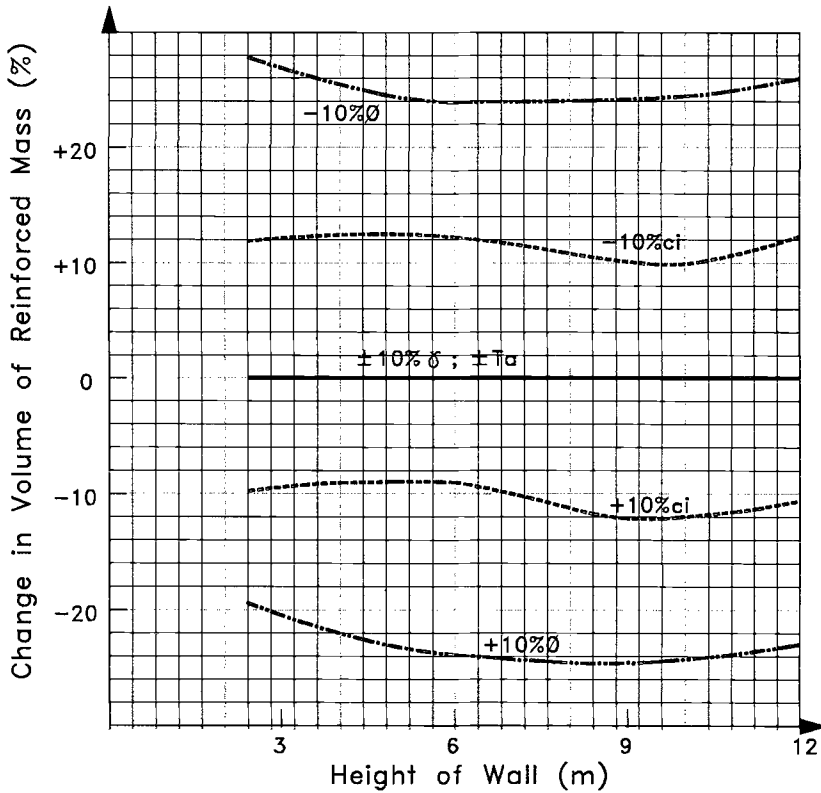


FIG. 4 -- Reinforced wall: change in reinforced soil volume with $\pm 10\%$ variation in design parameters.

DISCUSSION

Test Method Development

Design and construction of reinforced soil structures has become commonplace, though development of ASTM standards for defining material properties required for design is ongoing. The definition of long-term properties is a challenge in test procedures. Creep, chemical degradation, and biological degradation are long-term (i.e., design life of 75 to 100 years for some reinforced soil structures) concerns. Test procedures need to produce accurate results in a reasonable time frame (eg., 10,000 hours). Elevated temperatures may be used with polymers to accelerate testing, but how temperature may affect a particular chemical or biological environment is not well defined. In fact, the biological and chemical environments that geosynthetics may be exposed to are not well defined. Another challenge in long-term testing is the development

of procedures for testing and design application of confined (i.e., in soil) creep tests.

Soil-geosynthetic interaction parameters can have a significant impact on design (Figures 1 - 4). A method for determination of direct shear interaction coefficient has recently been adopted by the society. Development of a standard test method for pullout interaction is underway.

ASTM soil shear strength and unit weight tests are well established. Though what shear strength value, peak or constant volume, is an issue to be addressed by designers of reinforced soil structures.

Parametric Study

The parametric study was conducted with limit equilibrium analysis techniques. Results clearly indicate that a small (i.e., 10%) differential in soil friction angle results in a significant change in the amount of reinforcement material and volume of reinforced mass. The actual amount of variation is a function of the overall height of the structure, with increasing deviation with increasing structure height. The direct shear interaction coefficient also has a notable impact on reinforcement material and reinforced volume requirements.

Variations in the allowable tensile strength of the reinforcement and in the unit weight of the soil have less impact on structure quantities. Similar deviations of 10% result in less change in amount of reinforcement material required. Alterations of reinforcement tensile strength and soil unit weight, of any amount, do not affect the volume of reinforced soil mass, with the limit equilibrium analysis techniques used.

CONCLUSIONS

Material property test methods for defining reinforced soil structure design parameters have been partially established within ASTM. Particularly lacking, is property definition over the long-term design life of structures (eg., 75 to 100 years) for potential chemical degradation, potential biological degradation, and in situ creep. These parameters should be a priority for test method development within ASTM, in regards to design of reinforced soil structures.

Economics of reinforced soil structure designs are significantly more sensitive to small (i.e., 10%) variations in soil shear strength than to small variations in reinforcement tensile strength and soil unit weight, for standard limit equilibrium procedures utilized within. This fact highlights the importance of a comprehensive field and laboratory investigation program to satisfactorily define the friction angles of the construction fill soils. Economics are also sensitive to variations in direct shear interaction values, when the critical sliding plane of a structure occurs along such an interface. This fact highlights both the need to conduct direct shear interaction testing and, during analysis of reinforced soil structures, the need to check sliding of the reinforced mass along the geosynthetic-soil interface.

The practical conclusion from this study, is that designers should focus on comprehensive definition of design parameters which are most significant in the overall economics, and safety, of the reinforced soil structure. Conservative engineering estimation of design parameters which do not significantly impact project economics or safety may be appropriate for some projects.

REFERENCES

- [1] McGown, A., Paine, N., and DuBois, D., "Use of Geogrid Properties in Limit Equilibrium Analysis," *Polymer Grid Reinforcement*, Thomas Telford, London, 1985.

- [2] Jewell, R.A., "Strength and Deformation in Reinforced Soil Design," Keynote paper presented at the 4th International Conference on Geotextiles, Geomembranes and Related Products, The Hague, May 29, 1990.
- [3] Christopher, B.R., Gill, S.A., Giroud, J-P, Juran, I., Mitchell, J.K., Schlosser, and Dunnicliff, J., "Reinforced Soil Structures, Volume 1: Design and Construction Guidelines," FHWA-RD-89-043, National Technical Information Service, Springfield, VA, 1989.
- [4] Lambe, T. W. and Whitman, R.V., Soil Mechanics, John Wiley & Sons, New York, 1969, 553 p.
- [5] _____, "Design Guidelines for Use of Extensible Reinforcement (Geosynthetic) for Mechanically Stabilized Earth Walls," Task Force 27 Report, In Situ Soil Improvement Techniques, AASHTO, Washington, D.C., August, 1990.
- [6] _____, Standard of Practice GG4: Determination of the Long-Term Design Strength of (a) Stiff and (b) Flexible Geogrids, Geosynthetic Research Institute, Drexel University, Philadelphia, PA, (a) March 1990 and (b) January 1991.
- [7] _____, GRI Standard of Practice GT7: Determination of Long-Term Design Strength of Geotextiles, Geosynthetic Research Institute, Drexel University, Philadelphia, April, 1992.
- [8] Berg, R.R., "Guidelines for Design, Specification, & Contracting of Geosynthetic Mechanically Stabilized Earth Slopes on Firm Foundations," Industrial Fabrics Association International, prepared for U.S. Department of Transportation, Federal Highway Administration, October, 1992.
- [9] Cheng, S-C and Christopher, B.R., "A Probabilistic Review of Geotextile Reinforced Slope Design," Proceedings of Geosynthetics '91 Conference, Atlanta, February, 1991.
- [10] Schmertmann, G.R., Chouery-Curtis, V.E., Johnson, R.D., and Bonaparte, R., "Design Charts for Geogrid-Reinforced Soil Slopes," proceedings of Geosynthetics '87 Conference, New Orleans, February, 1987.

George R. Koerner,¹ Robert M. Koerner,¹ and Victor Elias²

GEOSYNTHETIC INSTALLATION DAMAGE UNDER TWO DIFFERENT BACKFILL CONDITIONS

REFERENCE: Koerner, G. R., Koerner, R. M. and Elias, V., "Geosynthetic Installation Damage Under Two Different Backfill Conditions," Geosynthetic Soil Reinforcement Testing Procedures, ASTM STP 1190, S. C. Jonathan Cheng, Ed., American Society for Testing and Materials, Philadelphia, 1993.

ABSTRACT: Six different geotextiles and one geogrid were placed on an angular, poorly graded gravel, backfilled with the same type of gravel, compacted in a standardized manner, and then exhumed within the same day. A visual damage assessment indicated that the exhumed geotextiles had 60 to 108 holes per square meter and the geogrids had approximately 4 damaged ribs per square meter. A large number of strength tests were performed on the exhumed samples and compared to the original (as-received) strengths to obtain an average percent retained strength. The results for the geotextiles were from 30% to 58% strength retained while the geogrid resulted in a 71% strength retained.

At a second site the entire study was repeated with new materials but now the soil was a poorly graded sand both beneath and above the geosynthetics. The same types of geotextiles and geogrids as with the first site were used in these tests. Here the results were very different, with no holes or damaged ribs, and average geotextile strengths retained from 72% to 96%. The geogrid had its full strength retained.

The data results in quantifiable values for installation damage partial factors-of-safety (the inverse of the strength retained), as well as guidance on the type of backfill soil to use with polymeric reinforcement. Clearly, angular gravel can be damaging to both geotextiles and geogrids and should only be used with considerable caution or with the addition of protection materials.

KEYWORDS: geotextiles, geogrids, polymeric reinforcement, reinforcement, installation damage, partial factors-of-safety, geosynthetic backfill, survivability.

¹Senior Research Specialist and Director of the Geosynthetic Research Institute at Drexel University, respectively, Philadelphia, PA 19104.

²President of V. Elias and Assoc., P.A., Bethesda, MD 20817.

INTRODUCTION

Geosynthetics are currently being used in a number of different soil reinforcement applications. Included in these applications are geosynthetic reinforced retaining walls, steep soil slope stabilization and improved bearing capacity of foundation soils. All of these applications require design procedures which are based on the strength of the geosynthetic material which is either a geogrid or a geotextile. Generally tensile strength, generated from wide width laboratory tests (ASTM D-4595), are used in the designs. For geogrids there is no formalized test method, however, the same general test protocol that is used for geotextiles can be reasonably adapted. The major modification for geogrids is in the size of the test specimen. For geotextiles the width is 200 mm and the length is 100 mm while in the case of geogrids the width and length depends on the repeat pattern of the individual product.

Such values of laboratory generated strength, however, are not the "allowable" values to be used in the final design. These as-received material test specimens usually do not include such items as installation damage, long term creep, chemical degradation, etc. Thus the initially measured laboratory test value of the considered material must be suitably reduced so as to reflect the anticipated in-situ behavior. One possible method to accomplish this modification is to include various in-situ mechanisms via partial factors-of-safety on the measured laboratory test value. This approach will take the general form as follows. Note that each of the specific items in the equation require a separate data base.

$$T_{\text{allow}} = T_{\text{ult}} \left[\frac{1}{FS_{\text{ID}} \times FS_{\text{CR}} \times FS_{\text{CD}} \times FS_{\text{X}}} \right] \quad (1)$$

where

- T_{allow} = allowable wide width tensile strength for use in design
- T_{ult} = ultimate wide width tensile strength on the as-received material (e.g., as measured in the ASTM D4595 test)
- FS_{ID} = partial factor-of-safety for installation damage
- FS_{CR} = partial factor-of-safety for creep
- FS_{CD} = partial factor-of-safety for chemical degradation
- FS_{X} = other partial factor(s)-of-safety depending on site specific and product specific conditions

This project was directed at providing a data base for geosynthetic installation damage for retaining wall and steep soil slope applications and similar reinforcement situations. In the study to be reported herein, two sites using very different backfill soils at the same wall location are evaluated. The first site had the geosynthetics placed between layers of angular, poorly graded, coarse stone. The second site was a repetition of the first, but now the geosynthetics were placed between poorly graded fine sand layers. Both sites included the placement of one geogrid and six different geotextiles. The strength behavior of the various geosynthetics before installation and

after exhuming was determined by evaluation of approximately 100 tests resulting in a percent strength retained for each product. Approximately 1500 individual tests were performed for this entire study. A number of different strength tests were performed to obtain an average value. Also included was a hole density study which was made immediately after exhuming the different geotextiles. From this task the number of holes per square meter and the percent hole area were also determined. For the geogrids the number of visually damaged ribs were evaluated.

INSTALLATION AND EXHUMING DETAILS

Both sites for the field study utilized full scale equipment for the placement of the various geosynthetics and were located at a permanent retaining wall construction site. The permanent wall was a conventional reinforced earth wall consisting of prefabricated concrete facing elements and wire mesh reinforcement. The lower two-thirds of the permanent wall was backfilled with crushed stone, and the upper one-third with sand. The gradation of these two backfill materials is given in Figure 1.

The availability of the above described construction site provided us the opportunity to install geosynthetic reinforcement materials in similar field conditions as was experienced by the permanent reinforcing steel wire mesh. Utilizing this opportunity allowed for a variety of geosynthetic materials to be assessed under the two very different soil backfilling materials.

The geosynthetics of Site #1 had stone beneath and above them, while Site #2 had sand beneath and above the geosynthetics. Backfill placement, lift height, spreading equipment, compaction equipment and methodology were done in a similar manner at each site and furthermore they were done similar to what was done with the permanent steel wire mesh. Placement of the backfill soil was by end dumping from 80 kN axle load trucks. Initial spreading and finish grading was by a Caterpillar D4H Dozer with 60 cm wide tracks. The ground contact pressure of this piece of equipment was approximately 40 kPa. Subsequent compaction was by an HRMM 133 kN vibratory steel wheel roller. The roller made 10 complete cycles, i.e., 20 single passes, over an approximately 250 mm thick compacted lift. The density of the final backfill was between 95% and 100% of modified Proctor compaction (ASTM D1557). The construction photographs of Figure 2 show the step-by-step installation process as well as the permanent wall facing elements in the background.

The geosynthetics that were placed within the described soil backfill layers are given in Table 1 along with their as-received (i.e., pre-construction) physical and mechanical properties. All tests were performed in the Geosynthetic Research Institute's (GRI) laboratory using standardized test equipment and procedures.

Each type of geotextile material that was placed in the field measured between 3.6 and 4.9 m long by 6.0 m wide. A continuous panel was made from the individual sections by sewing and/or stapling the roll

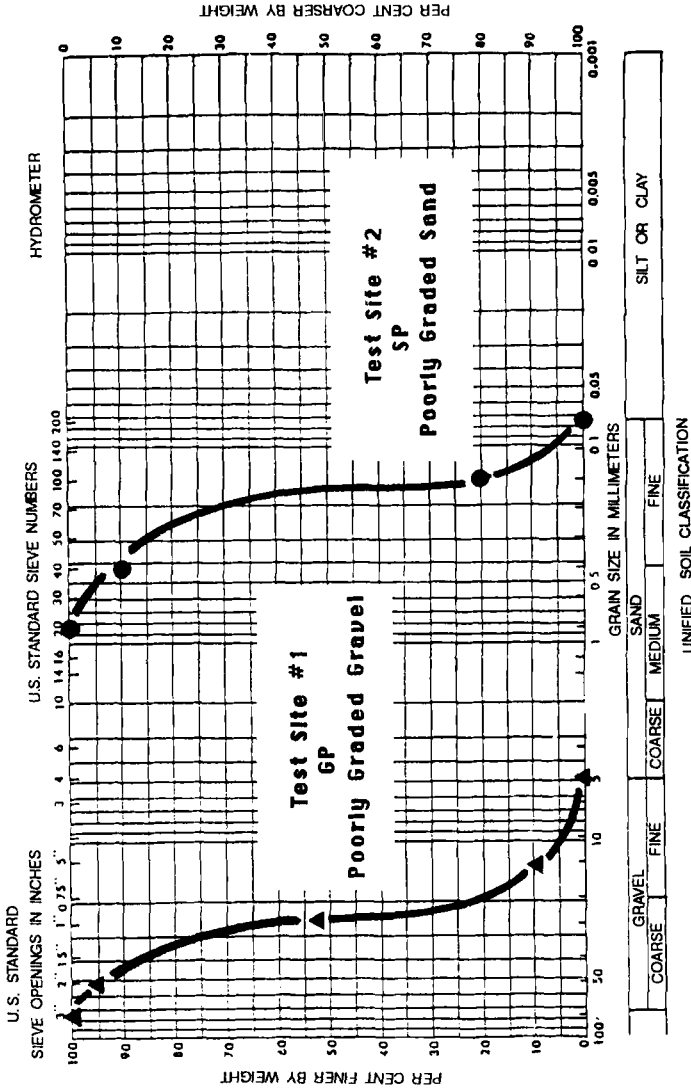


Fig. 1 - Particle Size Distribution Curves of Backfill Soils Used in the Two Test Sites



FIG. 2--Photographs of wall construction and geosynthetic layout.



FIG. 2--Continued.

TABLE 1--Details of the various geosynthetic materials placed at the installation sites.

SITE #1 - GEOSYNTHETICS PLACED WITHIN STONE BACKFILL

No. Type	Polymer	Weight (g/m ²)	Wide width- MD (1) (kN/m)	Wide width- XMD (1) (kN/m)	Grab (2) (kN)	Puncture (3) (kN)	Tear (4) (kN)	Burst (5) (kPa)
a	uniaxial geogrid	848	84.5	-	-	-	-	-
b	nonwoven needled	542	48.0	37.1	3.06	1.14	1.74	6240
c	nonwoven needled	203	17.7	11.6	1.02	0.45	0.71	2200
d	nonwoven needled	153	9.8	7.5	0.74	0.36	0.49	1800
e	nonwoven heat set	137	6.5	7.0	0.55	0.22	0.28	1220
f	woven slit film	203	33.6	34.0	1.33	0.47	0.71	4260
g	woven monofilament	220	48.5	33.6	1.93	0.75	0.32	3670

SITE #2 - GEOSYNTHETICS PLACED WITHIN SAND BACKFILL

No. Type	Polymer	Weight (g/m ²)	Wide width- MD (1) (kN/m)	Wide width- XMD (1) (kN/m)	Grab (2) (kN)	Puncture (3) (kN)	Tear (4) (kN)	Burst (5) (kPa)
a	uniaxial geogrid	848	84.5	-	-	-	-	-
b	nonwoven needled	542	48.0	37.1	3.06	1.14	1.74	6240
c	nonwoven needled	203	17.7	11.6	1.02	0.45	0.71	2200
d	nonwoven needled	153	9.8	7.5	0.74	0.36	0.49	1800
e	nonwoven heat set	115	6.8	7.7	0.47	0.23	0.21	1100
f	woven slit film	237	37.6	46.6	1.39	0.66	0.63	5070
g	woven monofilament	220	48.5	33.6	1.93	0.75	0.32	3670

notes: 1. ASTM D-4595 - "Tensile Properties of Geotextiles by the Wide-Width Strip Method"
 2. ASTM D-4632 - "Breaking Load and Elongation of Geotextiles (Grab Method)"
 3. ASTM D-3787 - "Puncture Strength of Geotextiles"
 4. ASTM D-4355 - "Trapezoidal Tearing Strength of Geotextiles"
 5. ASTM D-3786 - "Hydraulic Bursting Strength of Fabrics (Mullen Burst)"

edges together. In this manner the machine direction or warp direction was always perpendicular to the wall in the direction of the major principal stress. Five sections of 1.0 m wide geogrid were stapled together to form a panel 5.0 m wide by 6.0 m long. Thus a 6.0 m wide by 31.7 m long panel of different geosynthetics was placed and covered in the described backfilling manner. A schematic diagram of the actual placement layout is shown in Figure 3.

Exhuming of the geosynthetics at each site consisted of dozing off the upper 125 mm of the lift thickness and then carefully hand shoveling the remaining 125 mm of material. No damage due to retrieval of the geosynthetics was observed at any time. Due to the short time interval between placement and exhuming of the geosynthetic (which varied from 1 to 4 hours) there was no "bonding" of the geosynthetic materials to the soil beneath or above them. Thus, it was assumed that whatever damage may have occurred to the geosynthetics was done during the backfilling and compaction process, i.e., it is "installation damage" and not due to any other possible types of long-term degradation.

TEST PROCEDURE AND DETAILS

Upon exhuming the installed geosynthetics, a visual damage survey was made. For the geotextiles, this was done by vertically suspending the exhumed section of the fabric outdoors with sunlight behind it. From such a position the holes could be counted and their approximate size measured. Hole density and hole area values were then normalized by calculation of the full sample size to a square meter unit. Thus "holes per square meter" and "hole area as a percentage" is reported. For the geogrids, the number of "ribs broken (or severely damage) per square meter" is reported.

The exhumed geotextile samples were then cut into various sized wide width test specimens and tested. For each geotextile material, 10 specimens were tested in the machine direction and 10 specimens were tested in the cross-machine direction. The result of this testing was an average exhumed wide width strength value for each type of geosynthetic. These values were then compared to the average as-received (i.e., pre-construction) value from the same type of material. The result of such a comparison is the percent strength retained for each different material evaluated. Finally, the inverse of this value will be the factor of safety for installation damage. Note that the comparison tests on the non-installed geosynthetics were based on non-used sections of the same roll of material that was placed and exhumed. Thus there were no biases added to the resulting information by using different rolls or lots of materials.

The process was essentially the same for geogrids where 197 mm wide test specimens were used to accommodate an even number of ribs. The specimen lengths were 127 mm as measured from transverse rib to adjacent transverse rib. The rate of extension, type of grips, etc., were the same as with the geotextile wide width test method, ASTM D4595. Since the geogrids were of the uniaxial type, only the machine direction values were evaluated. For the exhumed geogrids the average wide width

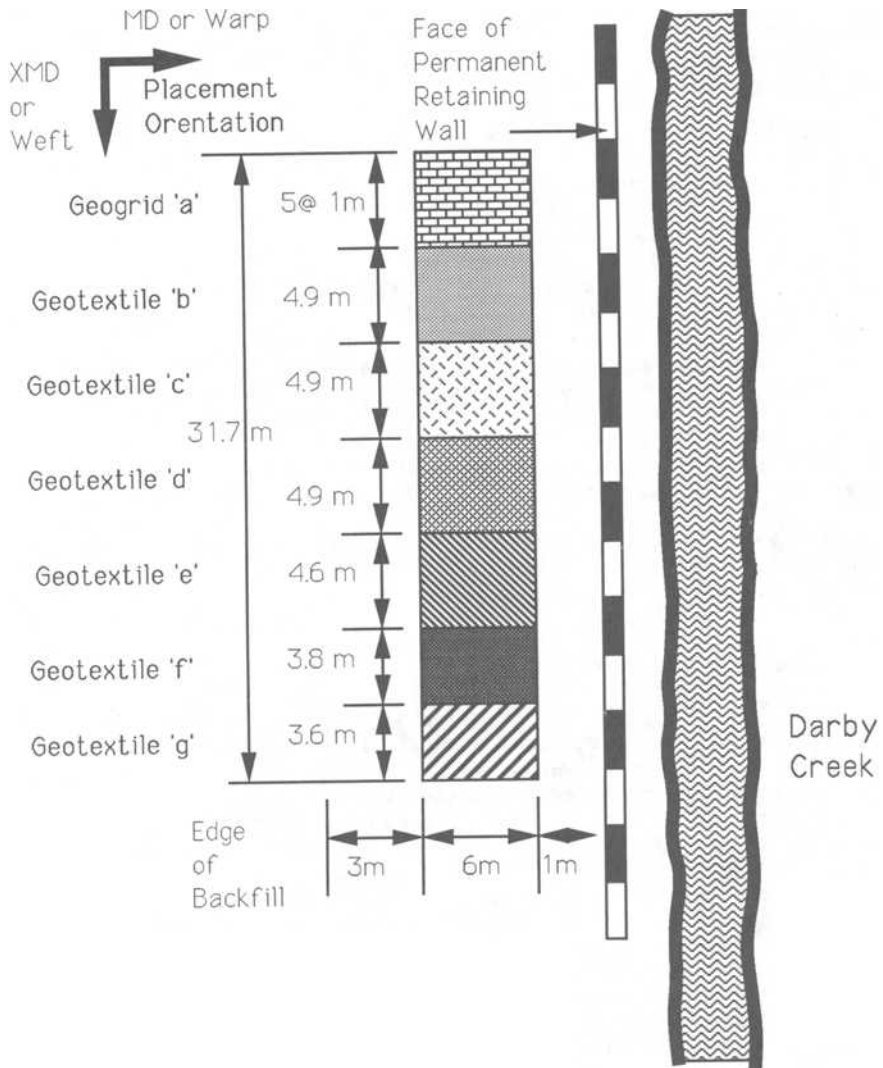


FIG. 3--Plan view of field layout of geosynthetic panel used in this study .

strength value was the average of forty-one (41) tests at Site #1 and twenty (20) tests at Site #2. This unbalanced number was required due to the variability of the damage, which was greater in the gravel of Site #1 than in the sand of Site #2.

For geotextiles, other index strength test values are invariably quoted in the technical literature. These are the following, along with their appropriate ASTM test procedures.

- Grab Tensile Strength, ASTM D4632
- Puncture Strength, ASTM D3787
- Trapezoidal Tear Strength, ASTM D4533
- Mullen Burst Strength, ASTM D3786

All of the geotextiles were evaluated for percent strength retained in each of the above tests. Note that tensile and trapezoidal tear tests were made in the machine direction only. Average values are used for the calculations. For the exhumed geotextiles, the average consisted of ten (10) specimens of each type. For the noninstalled comparison tests, the averages were also based on ten (10) tests of each type.

All tests were done at the GRI's Laboratory using the same test equipment for comparison testing. Furthermore, all testing was performed by the primary author.

TEST DATA AND RESULTS

Actual values from which the average results were obtained are given in the Appendix. The tables in the Appendix indicate the number of specimens tested, the average values and the standard deviation for both exhumed and as-received materials of the various groups of tests. The test data and results based on average values within each given type of test as described in the previous section are given in Table 2.

Apparent from the hole assessment values given in Table 2 is that the geosynthetics of Site #1 (using the gravel backfill) were severely damaged in comparison to those placed at Site #2 (using the sand backfill). The strength reduction values for all types of strength tests equally reflect the severity of the geosynthetic damage at Site #1 due to the gravel. The geogrid, however, was damaged less than any of the geotextiles. Within the geotextile group, the heaviest of the needle punched nonwoven geotextiles was the least damaged, although its strength reductions are still large, as well as are the large number of holes.

For Site #2, in the sand backfill, the geogrid experienced no visually damaged ribs nor measured strength reduction. The geotextiles had slight strength reductions, however, no holes were observed in any of the fabrics.

The strength reduction trends for both sites can be better seen when considering averages of the wide width values, the index strength test values and then the overall average values. Table 3 provides this

TABLE 2--Results from hole assessment and various strength tests performed.

SITE #1 (Gravel Backfill)		Percent Strength Retained									
Geosynthetic Type	Mass Per Unit Area (g/m ²)	Hole Assessment					Percent Strength Retained				
		Hole Area (%)	WW-M	WW-XM	Grab	Puncture	Tear	Burst			
Uniaxial Geogrid	848	-	71	-	-	-	-	-	-	-	-
Nonwoven needled GT	542	0.57	54	53	49	59	65	66	66	66	66
Nonwoven needled GT	203	0.99	20	38	43	40	40	38	38	38	38
Nonwoven needled GT	153	2.9	25	42	28	34	23	34	34	34	34
Nonwoven heat set GT	137	0.84	28	44	31	42	27	49	49	49	49
Woven slit film GT	203	0.81	20	26	24	45	31	33	33	33	33
Woven monofilament GT	220	0.79	34	33	44	36	79	42	42	42	42

SITE #2 (Sand Backfill)		Percent Strength Retained									
Geosynthetic Type	Mass Per Unit Area (g/m ²)	Hole Assessment					Percent Strength Retained				
		Hole Area (%)	WW-M	WW-XM	Grab	Puncture	Tear	Burst			
Uniaxial Geogrid	848	0	100	-	-	-	-	-	-	-	-
Nonwoven needled GT	542	0	85	92	77	100	97	95	95	95	95
Nonwoven needled GT	203	0	67	91	59	86	43	85	85	85	85
Nonwoven needled GT	153	0	82	87	65	74	50	71	71	71	71
Nonwoven heat set GT	115	0	84	95	75	76	70	85	85	85	85
Woven slit film GT	237	0	84	100	90	97	77	80	80	80	80
Woven monofilament GT	220	0	91	100	93	100	100	94	94	94	94

TABLE 3--Test results of previous table grouped into various categories.

SITE #1 (Gravel Backfill)

Geosynthetic Type	Mass Per	Hole Assessment	Percent Strength Retained		Factor of Safety for Installation Damage*
	Unit Area (g/m ²)	m ² Hole Area (%)	WW-ave.	All Tests.Ave.	
Uniaxial Geogrid	848	4	71	71	1.4
Nonwoven needled	542	46	0.57	60	1.7
Nonwoven needled	203	62	0.99	40	2.7
Nonwoven needled	153	74	2.9	30	3.2
Nonwoven heat set	137	46	0.84	38	2.7
Nonwoven slit film GT	203	54	0.8	33	3.3
Woven monofilament GT	220	50	0.79	50	2.2

SITE #2 (Sand Backfill)

Geosynthetic Type	Mass Per	Hole Assessment	Percent Strength Retained		Factor of Safety for Installation Damage*
	Unit Area (g/m ²)	m ² Hole Area (%)	WW-ave.	All Tests.Ave.	
Uniaxial Geogrid	848	0	0	100	1.0
Nonwoven needled	542	0	0	92	1.1
Nonwoven needled	203	0	0	68	1.4
Nonwoven needled	153	0	0	65	1.4
Nonwoven heat set	115	0	0	76	1.2
Nonwoven slit film GT	237	0	0	86	1.1
Woven monofilament GT	220	0	0	97	1.1

*Based on the average of all strength tests evaluated.

information where direct mathematical averages were made of the values reported in Table 2. Here it is seen that the wide width average values reasonably track the index test average values with a slight trend of index tests being higher at Site #1, and the reverse at Site #2. It is felt that the average values of all tests can be used to formulate our summary and conclusion.

SUMMARY AND CONCLUSIONS

The results of this study have shown that the soil type in which geosynthetics are placed, backfilled and compacted has an effect on their installation survivability. From the quantitative damage assessment values (i.e., the number of holes per square meter and the percent strength retained) shown in Tables 2 and 3 it is clear that geosynthetics placed within the angular crushed stone gravel backfill were damaged, while the same materials placed in a fine sand backfill showed little damage.

Since the goal of the study was to quantify a factor of safety for geosynthetic installation survivability, the inverse of the percent strength retained values shown in Table 3 is presented. We used the overall average all of the strength test results and separated out the geogrid from the geotextiles.

Quite clearly, the geogrids fared better than the geotextiles in the Site #1 gravel tests and responded very well in the Site #2 sand tests. It must be cautioned, however, that there are many types of geogrids on the market and this was only one type. Thus it is a product specific study in this regard. Conversely, a much broader range of geotextiles styles were evaluated including a variation of mass per unit area within one of these styles. Of the geotextiles, the heaviest weight needle punched nonwoven fabrics responded the most favorably.

The last column of Table 3 shows the factor of safety for installation damage from which we obtain the generalized recommended installation damage factors-of-safety of Table 4.

TABLE 4--Recommended factors-of-safety for installation damage of geosynthetics in reinforcement applications.

Type of Geosynthetic	Poorly Graded Gravel Backfill		Poorly Graded Sand Backfill	
	(Ave. Values)	(W.W. Values)	(Ave. Values)	(W.W. Values)
Geogrid ⁽¹⁾	--	1.4	--	1.0
Geotextile ⁽²⁾	2.6	4.3	1.2	1.3

(1) of the type used in this study.

(2) of any type provided it is greater than 150 g/m²; values can be reduced as per results of study if geotextiles have a mass per unit area greater than 300 g/m².

Note that the average of all test values (index and wide width) give somewhat lower factor-of-safety values than the wide width tests by themselves. These values of partial factors-of-safety for installation damage ("FS_{ID}") for the respective materials are recommended for design as per Equation 1 in the introduction to the paper.

In conclusion, it is felt that the type of backfill soil used for polymeric reinforcement (geotextiles and geogrids) must be fundamentally different than when using metallic reinforcement (steel strips or welded wire mesh). In the case of metallic reinforcement, corrosion has to be offset and the most positive way to do this is with coarse gravel backfill soils. Since corrosion is not a problem with polymeric reinforcement there is no need for such coarse gravel backfill materials. Even further, it is seen in this paper that such gravel backfill soils can be damaging to the geotextiles and geogrids that were evaluated in this study. For geosynthetics the backfill soil should only be coarse enough so as to have sufficient permeability to eliminate excess pore water pressures. Beyond such excess pore water pressure considerations, larger backfill particle sizes are not desirable, and should not be permitted unless careful consideration is given to installation damage and subsequent reduction in geosynthetic strength.

ACKNOWLEDGEMENT

This study was commissioned by Earth Engineering and Sciences, Inc. as part of a U.S. Federal Highway Administration Contract No. FHWA-RD-89-186, entitled "Durability/Corrosion of Soil Reinforced Structures". The entire report is available as of December 1990 where Appendix A contains all of the data from which this paper was developed. The opportunity of performing and presenting this information is appreciated.

APPENDIX

(Included in this Appendix are the test results of all tests conducted in the course of this study).

- Table A1 - Wide Width Tests (machine direction)
- Table A2 - Wide Width Tests (cross machine direction)
- Table A3 - Grab Tensile Tests (machine direction)
- Table A4 - Puncture Tests
- Table A5 - Tear Tests (machine direction)
- Table A6 - Mullen Burst Tests

TABLE A1--Wide width tensile tests (machine direction) ASTM D4595.
(values in units of kN/m)

SITE #1 (Gravel Backfill)

Geosynthetic Type	Mass Per Unit Area (g/m ²)	Number Tested		Ave. Value		Standard Deviation	
		As-Rec.	Ex.	As-Rec.	Ex.	As-Rec.	Ex.
Uniaxial Geogrid	848	10	41	84.5	60.0	24	40
Nonwoven needled GT	542	6	10	48.0	25.9	17	17
Nonwoven needled GT	203	5	10	17.7	3.7	5	6
Nonwoven needled GT	153	5	10	9.8	2.5	2	2
Nonwoven heat set GT	137	5	10	6.5	1.8	3	2
Woven slit film GT	203	5	10	33.6	6.8	6	12
Woven monofilament GT	220	5	10	48.5	16.5	5	30

SITE #2 (Sand Backfill)

Geosynthetic Type	Mass Per Unit Area (g/m ²)	Number Tested		Ave. Value		Standard Deviation	
		As-Rec.	Ex.	As-Rec.	Ex.	As-Rec.	Ex.
Uniaxial Geogrid	848	10	20	84.5	100.3	24	31
Nonwoven needled GT	542	6	10	48.0	41.0	17	13
Nonwoven needled GT	203	5	10	17.7	11.9	5	9
Nonwoven needled GT	153	5	10	9.8	8.1	2	6
Nonwoven heat set GT	115	10	10	6.8	5.8	2	5
Woven slit film GT	237	10	10	37.6	31.9	6	18
Woven monofilament GT	220	5	10	48.5	43.9	5	16

TABLE A2--Wide width tensile tests (cross machine direction) ASTM D4595.
(values in units of kN/m)

SITE #1 (Gravel Backfill)	Geosynthetic Type	Mass Per Unit Area (g/m ²)	Number Tested		Ave. Value		Standard Deviation	
			As-Rec.	Ex.	As-Rec.	Ex.	As-Rec.	Ex.
	Uniaxial Geogrid	848	-	-	-	-	-	-
	Nonwoven needled GT	542	6	10	37.1	19.8	3	13
	Nonwoven needled GT	203	5	10	11.6	4.4	4	6
	Nonwoven needled GT	153	5	10	7.5	3.2	6	5
	Nonwoven heat set GT	137	5	10	7.0	3.2	6	4
	Woven slit film GT	203	5	10	34.0	8.6	6	26
	Woven monofilament GT	220	5	10	33.6	11.0	1	19

SITE #2 (Sand Backfill)	Geosynthetic Type	Mass Per Unit Area (g/m ²)	Number Tested		Ave. Value		Standard Deviation	
			As-Rec.	Ex.	As-Rec.	Ex.	As-Rec.	Ex.
	Uniaxial Geogrid	848	-	-	-	-	-	-
	Nonwoven needled GT	542	6	10	37.1	34.1	3	9
	Nonwoven needled GT	203	5	10	11.6	10.5	4	9
	Nonwoven needled GT	153	5	10	7.5	6.5	6	3
	Nonwoven heat set GT	115	10	10	7.7	7.4	2	3
	Woven slit film GT	237	10	10	46.6	50.6	17	36
	Woven monofilament GT	220	5	10	33.6	34.7	1	9

TABLE A3--Grab tensile strength tests - ASTM D4632.
(values in units of kN)

SITE #1 (Gravel Backfill)	Geosynthetic Type	Mass Per Unit Area (g/m ²)	Number Tested		Ave. Value		Standard Deviation	
			As-Rec.	Ex.	As-Rec.	Ex.	As-Rec.	Ex.
	Uniaxial Geogrid	848	-	-	-	-	-	-
	Nonwoven needled GT	542	10	10	3.06	1.51	32	83
	Nonwoven needled GT	203	10	10	1.02	0.44	24	26
	Nonwoven needled GT	153	6	10	0.74	0.21	5	11
	Nonwoven heat set GT	137	6	10	0.55	0.17	5	14
	Woven slit film GT	203	6	10	1.33	0.32	17	29
	Woven monofilament GT	220	10	10	1.93	0.84	14	70

SITE #2 (Sand Backfill)	Geosynthetic Type	Mass Per Unit Area (g/m ²)	Number Tested		Ave. Value		Standard Deviation	
			As-Rec.	Ex.	As-Rec.	Ex.	As-Rec.	Ex.
	Uniaxial Geogrid	848	-	-	-	-	-	-
	Nonwoven needled GT	542	10	10	3.06	2.34	32	51
	Nonwoven needled GT	203	10	10	1.02	0.60	24	14
	Nonwoven needled GT	153	6	10	0.74	0.48	5	14
	Nonwoven heat set GT	115	10	10	0.47	0.35	13	14
	Woven slit film GT	237	10	10	1.39	1.25	10	11
	Woven monofilament GT	220	10	10	1.93	1.78	14	26

TABLE A4--Puncture resistance tests - ASTM D3787.
 (values in units of kN)

SITE #1 (Gravel Backfill)		Mass Per Unit Area (g/m ²)		Number Tested		Ave. Value		Standard Deviation	
Geosynthetic Type		As-Rec.	Ex.	As-Rec.	Ex.	As-Rec.	Ex.	As-Rec.	Ex.
Uniaxial Geogrid	848	-	-	-	-	-	-	-	-
Nonwoven needled GT	542	10	10	1.14	0.67	18	92	10	38
Nonwoven needled GT	203	10	10	0.45	0.18	10	22	9	22
Nonwoven needled GT	153	10	10	0.36	0.12	6	18	6	18
Nonwoven heat set GT	137	10	10	0.22	0.09	26	32	14	53
Woven slit film GT	203	10	10	0.47	0.21	14	53	14	53
Woven monofilament GT	220	10	10	0.75	0.27	14	53	14	53

SITE #2 (Sand Backfill)		Mass Per Unit Area (g/m ²)		Number Tested		Ave. Value		Standard Deviation	
Geosynthetic Type		As-Rec.	Ex.	As-Rec.	Ex.	As-Rec.	Ex.	As-Rec.	Ex.
Uniaxial Geogrid	848	-	-	-	-	-	-	-	-
Nonwoven needled GT	542	10	10	1.14	1.18	18	21	10	11
Nonwoven needled GT	203	10	10	0.45	0.39	10	11	9	8
Nonwoven needled GT	153	10	10	0.36	0.26	6	6	5	6
Nonwoven heat set GT	115	10	10	0.23	0.17	10	8	10	8
Woven slit film GT	237	10	10	0.66	0.64	14	16	14	16
Woven monofilament GT	220	10	10	0.75	0.75	14	16	14	16

TABLE A5--Trapezoidal tear tests -- ASTM D4533.
(values in units of KN)

SITE #1 (Gravel Backfill)

Geosynthetic Type	Mass Per Unit Area (g/m ²)	Number Tested		Ave. Value		Standard Deviation	
		As-Rec.	Ex.	As-Rec.	Ex.	As-Rec.	Ex.
Uniaxial Geogrid	848	-	-	-	-	-	-
Nonwoven needled GT	542	10	10	1.74	1.13	27	45
Nonwoven needled GT	203	10	10	0.71	0.28	12	29
Nonwoven needled GT	153	10	10	0.49	0.11	11	8
Nonwoven heat set GT	137	10	10	0.28	0.08	4	10
Woven slit film GT	203	10	10	0.71	0.22	18	27
Woven monofilament GT	220	10	10	0.32	0.26	8	28

SITE #2 (Sand Backfill)

Geosynthetic Type	Mass Per Unit Area (g/m ²)	Number Tested		Ave. Value		Standard Deviation	
		As-Rec.	Ex.	As-Rec.	Ex.	As-Rec.	Ex.
Uniaxial Geogrid	848	-	-	-	-	-	-
Nonwoven needled GT	542	10	10	1.74	1.69	27	65
Nonwoven needled GT	203	10	10	0.71	0.31	12	10
Nonwoven needled GT	153	10	10	0.49	0.24	11	19
Nonwoven heat set GT	115	10	10	0.21	0.15	6	8
Woven slit film GT	237	10	10	0.63	0.49	15	14
Woven monofilament GT	220	10	10	0.32	0.43	8	19

TABLE A6--Mullen burst tests - ASTM D3786.
(values in units of kPa)

SITE #1 (Gravel Backfill)		Mass Per Unit Area (g/m ²)		Number Tested		Ave. Value		Standard Deviation	
Geosynthetic Type		As-Rec.	Ex.	As-Rec.	Ex.	As-Rec.	Ex.	As-Rec.	Ex.
Uniaxial Geogrid	848	-	-	-	-	-	-	-	-
Nonwoven needled GT	542	10	20	6242	4148	30	145		
Nonwoven needled GT	203	10	20	2205	772	29	50		
Nonwoven needled GT	153	10	20	1798	599	40	42		
Nonwoven heat set GT	137	10	20	1220	599	13	37		
Woven slit film GT	203	10	20	4258	1426	20	127		
Woven monofilament GT	220	10	20	3672	1550	19	143		

SITE #2 (Sand Backfill)		Mass Per Unit Area (g/m ²)		Number Tested		Ave. Value		Standard Deviation	
Geosynthetic Type		As-Rec.	Ex.	As-Rec.	Ex.	As-Rec.	Ex.	As-Rec.	Ex.
Uniaxial Geogrid	848	-	-	-	-	-	-	-	-
Nonwoven needled GT	542	10	10	6242	5905	30	40		
Nonwoven needled GT	203	10	10	2205	1881	29	30		
Nonwoven needled GT	153	10	10	1798	1275	40	23		
Nonwoven heat set GT	115	10	10	1096	930	12	14		
Woven slit film GT	237	10	10	5071	4079	18	45		
Woven monofilament GT	220	10	10	3672	3459	19	46		

J. G. Collin,¹ and R. R. Berg²

COMPARISON OF SHORT-TERM AND LONG-TERM PULLOUT TESTING OF GEOGRID REINFORCEMENTS

REFERENCE: Collin, J. G. and Berg, R. R., "Comparison of Short-Term and Long-Term Pullout Testing of Geogrid Reinforcements," Geosynthetic Soil Reinforcement Testing Procedures, ASTM STP 1190, S. C. Jonathan Cheng, Ed., American Society for Testing and Materials, Philadelphia, 1993.

ABSTRACT: Long-term, 1000 hour sustained loading, and quick, strain rate of 1 mm per minute, soil-geogrid pullout was investigated with a laboratory test program. Results of the long-term and quick tests are compared and variations discussed. Geogrids of singular and of composite material manufacture were investigated. The test program was too limited in scope to extract any specific conclusions regarding the geogrids tested. However, differential between quick and sustained test results were significant enough to conclude that additional testing and investigation is warranted.

KEYWORDS: geogrids, silt, laboratory testing, pullout, creep

The design of steepened slopes and soil walls reinforced with geogrids must consider the long-term performance of the geogrid. Long-term criteria should be applied to both the tensile strength and to soil-interaction characteristics of a geogrid. Procedures [1,2,3] to compute long-term tensile strength values of geogrids have been established and are in routine use in North American practice. However, the current state-of-practice is to quantify soil-geogrid interaction coefficients with quick tests and assume adequacy of results for prediction of long-term performance.

This assumption may be valid for most cases, but may be unconservative for others, considering the variety of soils and geogrids currently used in construction. A limited test program was initiated to probe the validity of this assumption for determination of pullout interaction properties. The pullout performance of three geogrids in a single soil type was quantified with laboratory testing. Two geogrids of composite material manufacture and one of singular material manufacture were tested. Quick, strain rate controlled, and long-term sustained pullout tests were performed on each of the three geogrids.

¹ PhD, PE, Vice President, Tensar Earth Technologies, Morrow, GA 30260

² PE, Consultant, St. Paul, MN 55125

PULLOUT INTERACTION COEFFICIENT

Empirical equations for computation of pullout resistance and for computation of a pullout interaction coefficient for geogrids are summarized herein. These equations describe the mechanisms of soil-geogrid interaction, and form the basis for interpretation and discussion of the test data presented within.

The state-of-practice in design of reinforced soil structures is typically to use a coefficient of interaction, C_i , to compute pullout resistance of a geogrid. This interaction coefficient is usually derived from laboratory testing. An empirical formula and laboratory test results are used to determine C_i , in lieu of a theoretical determination of C_i . The interaction coefficient of a geogrid in a cohesionless soil, with a laboratory measured pullout capacity, is routinely computed with the following equation:

$$C_i = \frac{T}{2 \times A \times \sigma'_n \tan \phi} \quad \text{Equation 1}$$

where:

T	=	laboratory measured ultimate pullout capacity (kN/m)
A	=	plan area of geogrid embedded in passive soil zone (m ²)
C_i	=	pullout interaction coefficient (dimensionless)
ϕ	=	effective friction angle of the soil (degrees)
σ'_n	=	effective normal stress on geogrid (kN/m ²)

This interaction coefficient then may be applied to varying combinations of geogrid length, normal stress, and soil friction angles. The computed interaction factor, C_i , is dependent upon: (i) percent open area of the geogrid in plan view; (ii) frictional relationship between the geogrid material and soil; (iii) area of bearing surfaces perpendicular to tensile loading; (iv) bearing capacity of the surrounding soil; (v) strength of the junctions between perpendicular geogrid ribs; (vi) flexural stiffness of transverse ribs; (vii) soil grain size to grid aperture size relationship; and (viii) embedment length used in testing [4].

A test method standardizing procedures for measuring geosynthetic (including geogrids) pullout resistance in soil is currently in the process of development by Committee D35 of the American Society for Testing and Materials (ASTM). The current ASTM draft is similar to another test method, as described below. However, the calculation sections of the current draft ASTM procedure only define a pullout resistance (kN/m) and do not provide for computation of an interaction coefficient. Thus application of results is limited to only the specific combination(s) of geogrid, soil, embedment length, and normal pressure used in the laboratory.

A test method standardizing laboratory pullout testing of geogrids was published by the Geosynthetic Research Institute (GRI) in 1991 [5]. Determination of an interaction coefficient is defined as either short-term or long-term by this standard, and is dependent on the method of pullout force application. Short-term testing with controlled strain rate, controlled stress rate, or incremental stress methods of pullout force application provide short-term interaction coefficients. A constant stress (creep) method of pullout force application yields a long-term pullout coefficient. An interaction coefficient, independent of load application method, is calculated (when using cohesionless soils) as follows:

$$C_i = \frac{P}{2 \times L \times W \times \sigma'_n \tan \phi'} \quad \text{Equation 2}$$

where:

- P = force from jacking system (kN)
 W = width of the test specimen (m)
 C_i = pullout interaction coefficient (short-term or long-term, dimensionless)
 L = length of the tested specimen (m)
 ϕ' = soil friction angle effective of the soil degrees
 σ'_n = effective normal stress on geogrid (kN/m²)

Typical design practice is to define an interaction coefficient with a controlled strain (deformation) method of testing, per the GRI test method, and apply the coefficient to long-term designs.

TEST PROGRAM

Purpose

A test program was developed to examine long-term performance of both singular and composite manufacture type of geogrids. The results of approximately 1000 hour sustained load pullout tests were compared with quick pullout test (strain rate of 1 mm/min) to determine an efficiency of the geogrid with respect to pullout. Efficiency was computed as the ratio of long-term coefficient of interaction to the short-term coefficient of interaction, within this paper. Use of quick tests to define long-term pullout capacity for use in design, inherently assumes that an efficiency of 100% or greater exists between long-term and short-term pullout capacity.

Material

Soil-The soil used in this test program was from Washington County, Mississippi and has a classification as determined with the Unified Soil Classification System, of SP (poorly-graded sand). The particle shapes are subrounded to rounded.

A maximum effective friction angle of 28 degrees and zero cohesion were determined from direct shear tests. Direct shear testing was conducted both immediately after normal load application and after holding the normal load for 1000 hours. The maximum effective friction angle was the same for both cases. A 0.5 by 0.5 m shear box was used. The shear tests were conducted at a strain rate of 1mm/mip. The sand was compacted to a dry density of approximately 16.3 kN/m³ for all pullout tests, and for the direct shear test.

Geogrids-The properties and geometric dimensions of the three geogrids used in this test program are listed in Table 1. Geogrids "A" and "C" are of composite construction of woven polyester fibers covered with a coating. Geogrid "A" coating is a plasticized polyvinyl chloride and geogrid "C" coating is a plasticized acrylic. Geogrid "B" is of singular manufacture of an extruded, punched and drawn sheet of high density polyethylene.

TABLE 1 - PROPERTIES OF GEOGRIDS TESTED^a

Property	Geogrid "A"	Geogrid "B"	Geogrid "C"
Manufacture	composite	singular	composite
Polymer Composition	polyester	polyethylene	polyester
Junction Method	woven & coated	planar	knitted & coated
Mass/Unit Area, g/m ²	590	1120	190
Aperture Size, mm			
longitudinal	81	137	22.5
transverse	13	15	21.5
Thickness, mm			
at rib	1.4 ^b	1.8	2.2
at junction	2.3 ^b	5.8	2.3
Wide Width Strip Tensile (ASTM D4595), kN/m			
2% strain	23	38	17.5
5% strain	36	69	27
ultimate	86	117	93.5

^a Values from [6] and [7].

^b Values measured in laboratory, published data not available.

Equipment-The pullout box used is 0.9 m wide by 2.1 m long, and is 0.5 m deep. The pullout specimen was centered within the box depth. The normal force was applied with a pressurized air bladder system. The system was regulated to maintain the desired pressure within ± 1 kPa.

Friction at the face of the box was minimized by the use of two tapered steel plates, 13 mm thick. The two plates extend back into the soil 125 mm and form a sleeve in which the test material travels between. The plates are tapered at the leading edge to a thickness of 3 mm.

Procedure

Both the quick and sustained (long-term) pullout tests were performed in general accordance with GRI Test Method GG5 - "Geogrid Pullout" [5] and the draft ASTM standard. Interaction coefficient computations with these two standards were previously discussed.

The actual test procedure used was as follows: (i) test specimens approximately 1.25 m long were cut from bulk samples; (ii) test specimens were prepared for testing by casting one end of each specimen in a low temperature curing epoxy and allowing the specimen to cure for 24 hours (the epoxy was used to form the clamp for pullout testing); (iii) the lower portion of the pullout box was prepared by compacting the sand to the desired density; (iv) pullout specimen was placed in the pullout box above the compacted lower sand; (v) upper door and sleeve of the pullout box were installed above the pullout specimen; (vi) upper portion of the pullout box prepared by compacting the sand above the pullout specimen to the desired density; (vii) air bladder system installed above the upper sand; (viii) pullout specimen attached to the

pullout load harness; (ix) a confining pressure of 48.3 kPa (± 1 kPa) was applied to the test specimen and maintained; (x) various electronic instrumentation used for measuring load and displacements attached and computer data acquisition system initiated; (xi) quick test initiated at a constant displacement rate of 1 mm per minute; (xii) test continued until a constant load was recorded or failure occurred within the test specimen; (xiii) repeat steps (i) through (x) using virgin geogrid samples; (xiv) sustained test initiated at a constant displacement rate of 1 mm per minute until desired long-term load is reached; (xv) maintain desired long-term load for approximately 1000 hours; (xvi) after 1000 hours continue testing at a constant displacement rate of 1 mm per minute until failure.

The constant tensile load values for the three geogrids were set equal to an estimated or published creep limit strength of the specific material. The creep limited strength is defined as the limit state tension in Task Force 27 [2] guidelines, and also defined as the ultimate strength divided by a partial factor of safety for creep in the GRI Standard Procedure GG4 [3]. This creep limited tensile strength value would be divided by additional partial factors to account for material unknowns and variations, construction variations, degradation potential of geogrid, installation damage, and seam strength efficiency (if applicable). The product of these additional partial safety factors is approximately equal to 1.5. Thus the design tensile strength value, that dictates pullout design load, is approximately equal to the creep limited strength divided by 1.5. The factor of safety against pullout failure is normally taken as a value of 1.5. Thus the pullout value used to compute a design embedment length is roughly equal to the creep limited strength.

Use of constant tensile loads defined as noted above result in loads of varying percentages of ultimate pullout load determined with quick tests. The sustained loads applied to geogrids "A", "B", and "C" were 78, 71, and 86 percent of the quick ultimate pullout load, respectively.

TEST RESULTS

Computed Interaction Values

The results of both the quick and sustained tests for geogrids A, B, and C are shown in Figures 1, 2, and 3, respectively. The short-term and long-term coefficients of interaction C_{is} and C_{il} and the efficiency factor (E_p) are listed in Table 2. The efficiency factor, (E_p) is defined, within the context of this paper, as:

$$E_p = \frac{C_{iL}}{C_{iS}} \times 100 \quad \text{Equation 3}$$

Total displacement of the geogrid specimens was measured at four points along the embedment depth, for the sustained load tests. Locations of the four points are illustrated in Figure 4. Displacement at all four points of geogrid "A" continued to increase over time (Figure 5). The average displacement between points 1 and 4 was 15 mm and displacement at point 1 was 38 mm. An average movement of 8 mm and displacement of point 1 of 21 mm were recorded for geogrid "B" (Figure 6). Displacements in geogrid "C" were significantly larger (Figure 7). An average movement of 38 mm and point 1 movement of 93 mm were noted for geogrid "C".

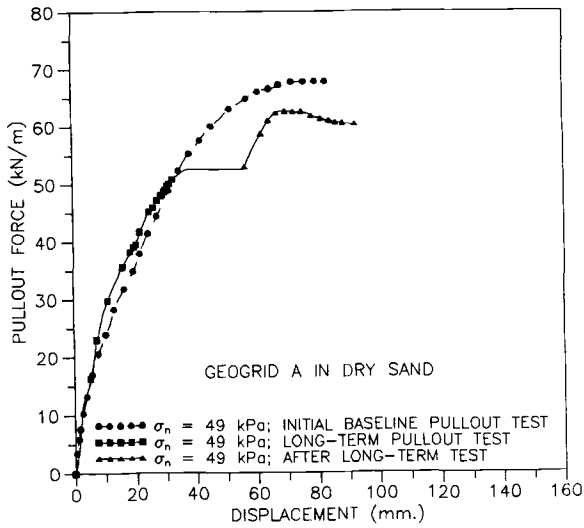


FIGURE 1 - Pullout Resistance - Geogrid A

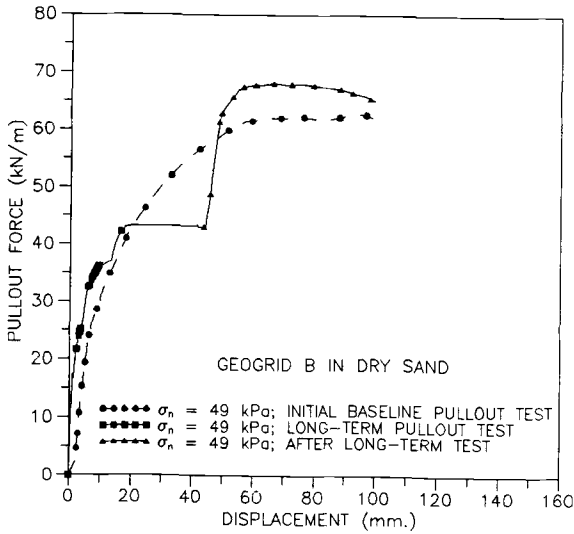


FIGURE 2 - Pullout Resistance - Geogrid B

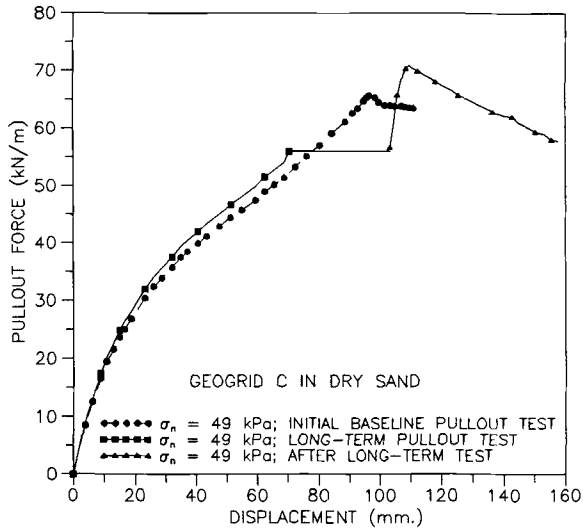


FIGURE 3 - Pullout Resistance - Geogrid C

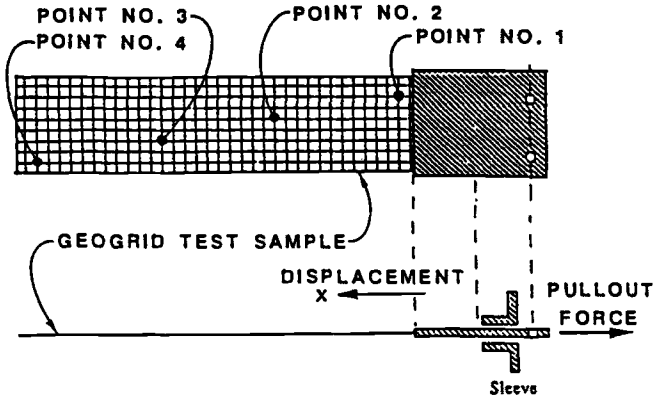


FIGURE 4 - Location of Displacement Monitoring Points Along Length of Geogrid

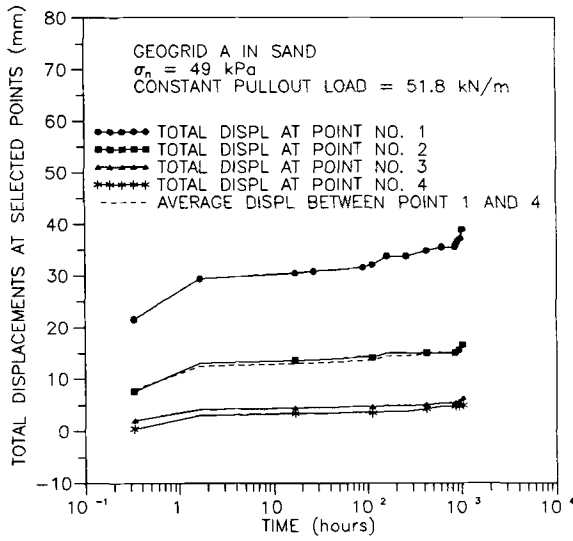


FIGURE 5 - Long-Term Pullout - Geogrid A

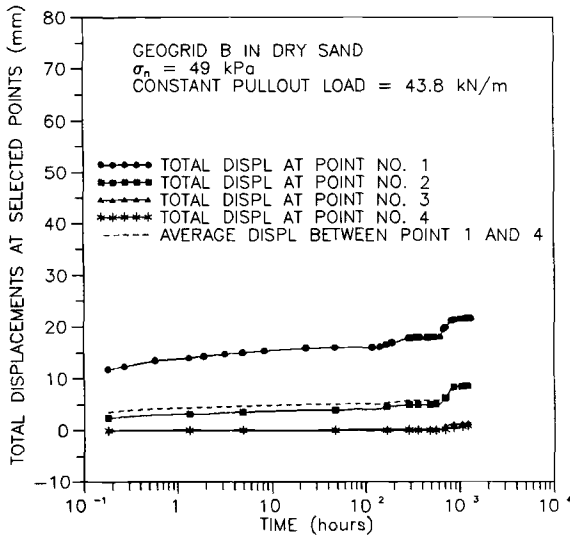


FIGURE 6 - Long-Term Pullout - Geogrid B

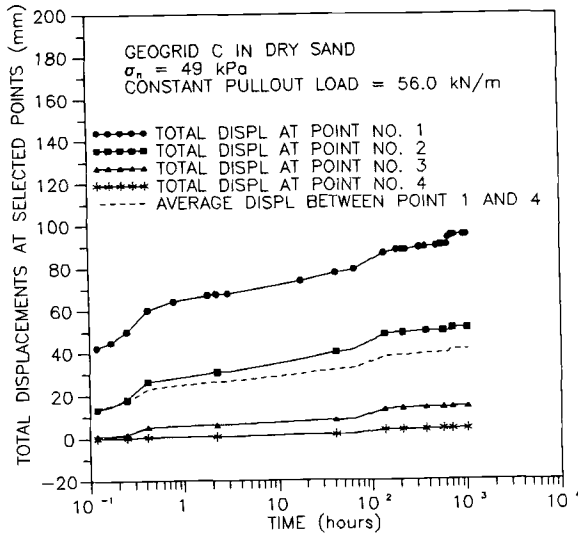


FIGURE 7 - Long-Term Pullout - Geogrid C

TABLE 2-Pullout test results.

	Geogrid		
	A	B	C
Manufacture:	composite	singular	composite
C_{iL}	0.99	1.09	1.12
C_{iS}	1.06	1.00	1.03
E_p	93%	109%	108%

Limitations of Test Program

This was a limited test program, which restricts use and interpretation of results. The testing was limited by: i) only one soil type; ii) only one long-term load level per geogrid; iii) long-term loading of only approximately 1000 hour duration; and iv) not modelling for any chemical or biological degradation effects. Tests have not been repeated (due to time constraints) and, therefore, duplication of test results has not yet been examined.

DISCUSSION

The efficiency factors for the three geogrids, "A", "B", and "C", were 93%, 109% and 108%, respectively. These values may be interpreted as an indication that the long-term pullout performance of geogrids may not be accurately predicted from quick tests. The results may also be interpreted as indicating approximately equal, within limitations of experimental error, long-term and short-term performance.

These initial test results indicate that the interaction coefficient C_i , as computed with the empirical formula, equation 2, may vary over time. The empirically computed interaction value consists of a conglomeration of several factors. It is assumed that geometric and normal pressure factors remain constant during the sustained load test and are equal (for each geogrid type) in the sustained and quick tests. With this assumption, the differences in pullout capacity between quick and sustained tests are attributable to deviations in soil, soil-geogrid frictional characteristics, bearing load on the geogrid or creep within the geogrid structure.

Identification of specific mechanism(s) resulting in C_i varying between quick and sustained testing was not warranted with this limited test program. However, a change in soil-geogrid friction or in bearing load would have had to occur, if it assumed that the laboratory techniques prevented variations of as placed soil properties.

CONCLUSIONS

The pullout test results presented here do not demonstrate that it can be assumed that the long-term performance of geogrids can necessarily be determined through quick tests. Short-term coefficient of interaction C_{is} may not be equal to the long-term coefficient of interaction C_{il} . Computed interaction values varied between quick and long-term pullout testing for the three cases examined, though testing was limited as previously discussed. The difference in performance might be attributed to either a change in the geogrid-soil frictional strength and/or bearing load of the geogrid over the 1,000 hour test time. Specific mechanisms defining a change over time were not identified for the tests conducted.

The test program was too limited in scope to extract any specific conclusions regarding the geogrids tested. However, differential between quick and sustained test results were significant enough to conclude that additional testing and investigation is warranted. Additional test programs should use different soil types, confining pressures, constant pullout tensile loads, and geogrids, and repeat tests to further investigate and define long-term pullout performance.

REFERENCES

- [1] Bonaparte, R. and Berg, R.R., "Long-Term Allowable Tension for Geosynthetic Reinforcement," Proceedings of Geosynthetics '87 Conference, New Orleans, LA, Industrial Fabrics Association International, 1987, pp 181-192.
- [2] _____, "Design Guidelines for Use of Extensible Reinforcements (Geosynthetic) for Mechanically Stabilized Earth Walls in Permanent Applications," Task Force 27 Report, In Situ Soil Improvement Techniques, AASHTO, Washington, D.C., August 1990.

- [3] _____, Standard of Practice GG4: Determination of the Long-Term Design Strength of (a) Stiff and (b) Flexible Geogrids, Geosynthetic Research Institute, Drexel University, Philadelphia, PA, (a) March 1990 and (b) January 1991.
- [4] Bonczkiewics, C., Christopher, B.R., and Atmatzidis, D.K., "Evaluation of Soil Reinforcement Interaction by Large Pullout Tests," presented at Transportation Research Board Annual Meeting, Washington, D.C., January 1988.
- [5] _____, Test Method GG5: Geogrid Pullout, Geosynthetic Research Institute, Drexel University, Philadelphia, PA, January 1991.
- [6] _____, "1991 Specifier's Guide," Geotechnical Fabrics Report, Industrial Fabrics Association International, Vol.8, No.7, St. Paul, MN, December 1990.
- [7] _____, "1992 Specifier's Guide," Geotechnical Fabrics Report, Industrial Fabrics Association International, Vol.9, No.9, St. Paul, MN, December 1991.

A. Ghani Razaqpur¹, Gunther E. Bauer², Abdel O. A. Halim³ and Yijun Zhao⁴

PULLOUT RESISTANCE AND LOAD-SLIP RESPONSE OF MECHANICALLY DAMAGED GEOGRIDS

REFERENCE: Razaqpur, A. G., Bauer, G. E. Halim, A. O. A. and Zhao, Y., "Pullout Resistance and Load-Slip Response of Mechanically Damaged Geogrids," Geosynthetic Soil Reinforcement Testing Procedures, ASTM STP 1190, S. C. Jonathan Cheng, Ed., American Society for Testing and Materials, Philadelphia, 1993.

ABSTRACT: Pullout tests were conducted on 30 pre-damaged specimens of a uniaxial and a biaxial polyester geogrid to determine the effect of damage on their pullout resistance and end displacement. The specimens were embedded in crushed aggregates and subjected to surcharge loads of 14 kPa and 20 kPa. The results showed that substantial damage in the tested specimens could reduce their maximum pullout force by up to 33% and their pullout stiffness by 50%, where pullout stiffness is defined by the ratio of the maximum pullout force to the corresponding slip (kN/mm). For moderate amounts of damage, the reduction was in the order of 10% to 14%. These results suggest that the present safety factors for installation damage (1.1 to 3.0) may be applicable to pullout resistance, but they may need to be modified for controlling displacements in geogrids.

KEYWORDS: damage, displacement, force, geogrid, polyester, pullout, factor of safety

Construction of soil structures reinforced with geosynthetics generally requires the use of heavy machinery and if sufficient care is not exercised, the reinforcement will be damaged in the process. It is practically impossible to predict the actual manner and extent of damage that a given reinforcement may suffer under all construction conditions. The extent, severity and type of damage will depend on the degree of care exercised during the construction, the type of machinery employed, the type of fill material, and the mechanical and geometric properties of the reinforcement. This variability is confirmed by test results reported by Koerner and Koerner [1]. They reported test results on geotextiles exhumed from a number of actual construction sites from which they concluded that installation, or site, damage can cause strength reductions of 0% to 30%. Bush and Swan [2] tested exhumed specimens of polypropylene geogrids from one construction site and

^{1, 2, 3} Professor, Center for Geosynthetics Research Information and Development (C-GRID), Civil and Environmental Engineering Department, Carleton University, Ottawa, Canada, K1S 5B6.

⁴ Ph. D. Student, Civil and Environmental Engineering Department, Carleton University, Ottawa, Canada, K1S 5B6.

reported little loss of strength. A number of laboratory [3,4] investigations and field tests [5,6] have confirmed the damage caused to geosynthetics by installation and construction processes. The majority of those studies have been concerned with geotextiles, and damage has been defined by reduction in tensile and burst strength, grab, puncture and tear resistance, and the number of holes per square meter. Based on the results of those studies, current practice recommends [1] a partial factor of safety (FS) against installation damage ranging from 1.1 to 3.0.

The reduction in many of the properties mentioned earlier is not relevant to geogrids. Geogrids are characterized by large apertures and their most significant mechanical properties are tensile strength, pullout resistance, and sliding shear resistance. To the writers' knowledge, none of the above studies have considered the effect of site damage on the pullout resistance of a geogrid. The damage process is stochastic; consequently, its laboratory simulation is inevitably idealized. Considering the variability involved, a method was devised in the present investigation which can be used to rationally determine the effect of installation damage upon the pullout resistance of a given geogrid. The proposed method does not address the susceptibility of a geogrid to damage, but rather it focuses on the effect of a certain amount of damage on the pullout resistance. It will be seen in the sequel that even a relatively large amount of damage did not substantially affect the pullout resistance of one of the geogrids tested in this investigation.

EXPERIMENTAL PROGRAM

Test Specimens and Soil Properties

Two types of high tenacity polyester geogrids, known by the trademark names of STRATAGRID⁵ 3022 and 9027, were tested. For simplicity, henceforth the two grids will be referred to as grids DX and DT, respectively. They both have a knitted structure with knitted junctions, and are manufactured with a polyolefin coat for additional protection. Based on the manufacturer's specifications, grid DX is designated as biaxial with an average tensile strength of 30.1 kN/m in the machine direction (MD) and 28.4 kN/m in the transverse direction (TD). Grid DT is uniaxial with average tensile strengths of 88.6 kN/m and 27.5 kN/m in the MD and TD directions, respectively. The aperture size and dimensions of the grids are shown in Fig. 1. The figure also shows five test specimens of grid DX (specimens DX1 to DX5) and twelve specimens of grid DT (specimens DT1 to DT12). The DX specimens were 207 mm wide, the DT specimens were 214 mm wide, while all the specimens were 890 mm long.

The grids were embedded in crushed limestone with a mean grain size of 8.0 mm. The aggregates were well-graded and representative of those used for granular load bearing base material in practice.

Site Damage Simulation

As stated earlier, the amount and type of damage inflicted on a grid in actual construction will be random in nature. Pullout resistance, as expected, is affected by loss of rib and/or junction strength. To simulate the combined loss of rib and junction strength, specimens DX1 to DX5, and DT1 to DT4, were pre-damaged by cutting and removing certain sections of the geogrid as illustrated in Fig. 1.

⁵ STRATAGRID[®] is a registered trademark of CONWED Plastics Co. of Minneapolis, MN, USA.

Different damage configurations were introduced. It may be noticed that in some cases over 40% of the longitudinal ribs were severed in the

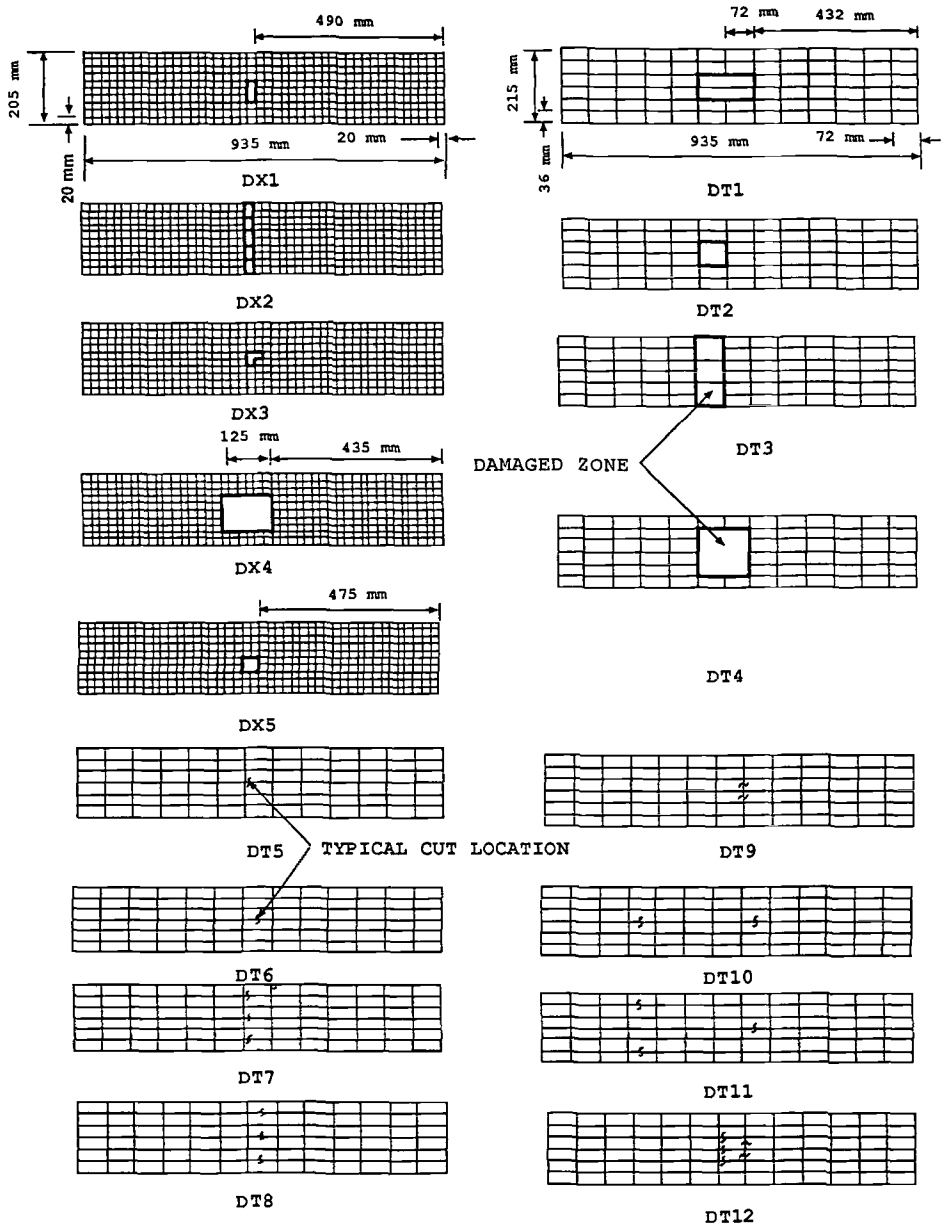


Fig. 1--Geogrid Test Specimens

middle zone of the specimens.

To simulate rib damage only, specimens DT5 to DT12 were pre-damaged by severing the longitudinal and/or transverse ribs at different locations but keeping the junctions intact, Fig.1. It is to be noted that the induced damage in the first group of specimens reduced the net surface area and stiffness of the specimens. In the second group, only the stiffness was affected. The position of the cuts from the junction was varied as may be seen by comparing specimens DT5 and DT6 (Fig. 1). For reference purposes, for both geogrids one intact specimen of the same dimensions as those in Fig.1 was also tested.

Test Procedure

A pullout apparatus was used to determine the pullout force versus displacement response of the geogrids. As schematically illustrated in Fig. 2, the rig consisted of a steel box, a pulling mechanism, and a data acquisition system, attached to an X-Y plotter. The steel box was 1.04 m long, 0.23 m wide and 0.38 m deep. The inside of the box was lined with polished stainless steel to minimize side friction effects.

A 10 mm wide slot was cut in the narrow end of the box at mid-height of the wall to pull the grid through. The aggregates were placed in the box and were tamped by hand to the required density. In every test, the aggregates were placed corresponding to 100 percent of Standard Proctor density, similar to the pullout tests carried out by others [7,8]. The grids were placed horizontally at the elevation of the slit and were subsequently clamped to the pulling mechanism. Figure 3 shows one of the specimens being placed in its position. Placing of the aggregates was continued until the tank was full. The aggregates were then partially excavated to slope towards the slot, Fig. 2, in order to prevent the soil particles from wedging into the slot. Using lead shots a surcharge was placed at the soil level surface, and the load cell and displacement transducer were connected to the X-Y plotter. A surcharge of either 14 kPa or 20 kPa was applied. After each test, the box was completely emptied and the preceding operation was repeated

The grid was pulled horizontally at a rate of 1.0 mm/min. and the tests were terminated when the end displacement reached approximately 30 mm. A load cell monitored the pullout force, and the pulled end displacement of the mesh was monitored by a linear variable displacement transformer (LVDT). The load-displacement response of the specimens was continuously recorded by the X-Y plotter.

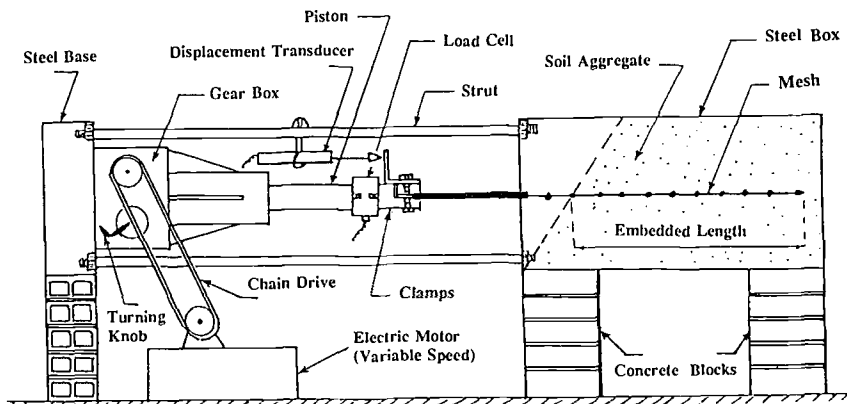


Fig. 2--Pullout Test Apparatus

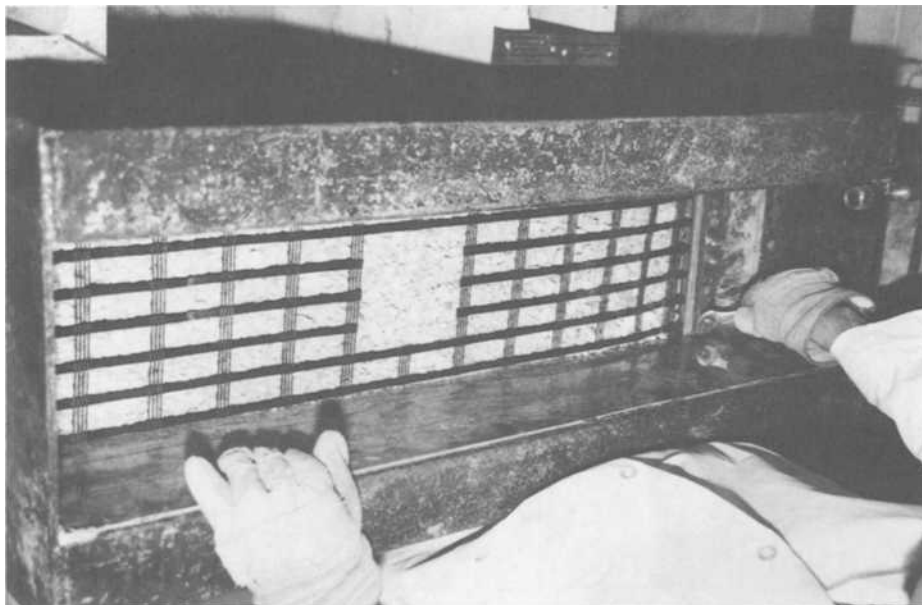


Fig. 3--Typical Specimen Placement in the Pullout Box

RESULTS AND DISCUSSION

Specimens with Sections Cut and Removed

The pullout load versus mesh end displacement for all the specimens is shown in Figures 4 to 9. Figures 10 and 11 show the pre-damaged zones of specimens DX4 and DT4 before and after testing. We notice in the latter figure that DT4 is essentially the same before and after testing while in DX4 some of the junctions were severed by the pullout process. This behaviour was typical for practically all the specimens of the two geogrids.

Figures 4 and 5 show the results for specimens DX1 to DX5 under surcharge loads of 14 kPa and 20 kPa, respectively. It may be observed that most of the specimens reach their peak pullout force at essentially the same displacement. The peak force herein refers to the maximum force in the force-displacement graphs shown. The maximum pullout force for each specimen is shown in Table 1, which also shows the ratio of the maximum force in the pre-damaged specimens to that in the undamaged specimen tested under the same conditions. The undamaged specimens are designated as DXU and DTU in Table 1. It should be mentioned that pullout tests carried out in a large box (1.5 m x 1.0 m x 1.2 m) on similar undamaged specimens have shown essentially the same response as reported here. The results presented are believed to be unaffected by the size of the box to any significant degree.

TABLE 1--Maximum Pullout Force in the Test Specimens

Specimens	Surcharge 14 kPa		Surcharge 20 kPa	
	Max. Pullout Force, F (kN)	$\frac{F_{DAMAGED}}{F_{UNDAMAGED}}$	Max. Pullout Force, F (kN)	$\frac{F_{DAMAGED}}{F_{UNDAMAGED}}$
DXU	2.43	1.00	2.54	1.00
DX1	2.14	0.88	2.26	0.89
DX2	2.00	0.82	2.14	0.84
DX3	2.29	0.94	2.60	1.02
DX4	1.71	0.70	1.71	0.67
DX5	2.34	0.97	2.47	0.97
DTU	2.64	1.00	3.30	1.00
DT1	2.83	1.07	3.51	1.06
DT2	2.69	1.02	3.20	0.97
DT3	2.26	0.86	3.10	0.94
DT4	2.37	0.90	3.29	1.00
DT5			3.23	0.98
DT6			3.47	1.05
DT7			3.00	0.91
DT8			3.14	0.95
DT9			3.43	1.04
DT10			3.37	1.02
DT11			3.23	0.98
DT12			3.14	0.95

From the results in the table, we can see that damage to the biaxial geogrids has reduced their pullout resistance from 0% to 33%. By comparing Figs. 4 and 5, we can observe that increasing the surcharge from 14 kPa to 20 kPa had a minor effect on the maximum pullout force. This would suggest that interlock was the major pullout resistance mechanism in these specimens.

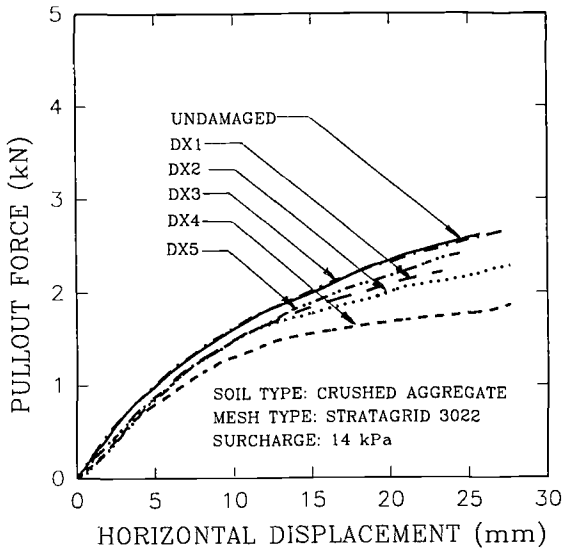


Fig. 4--Pullout Response of DX Specimens under 14 kPa

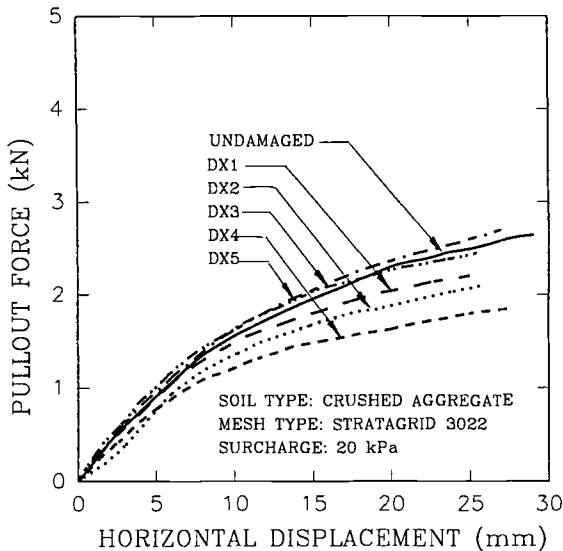


Fig. 5--Pullout Response of DX Specimens under 20 kPa

Figures 6 and 7 show the results for specimens DT1 to DT4 under surcharges of 14 kPa and 20 kPa, respectively. Here one can observe that the magnitude of the displacement corresponding to the maximum force increases with increased damage. Specimens DT3 and DT4 in Fig. 6 reach their peak resistance at almost twice the corresponding displacement of the undamaged specimen. This suggests that the uniaxial specimens become more extensible (undergo higher displacement under the same applied pullout force) with increased damage, but they still achieve relatively high peak forces. In Table 1, it can be seen that the maximum reduction in the pullout force is only 14%, which occurred in specimen DT3 under a surcharge of 14 kPa. Under the higher surcharge of 20 kPa, the largest reduction again occurred in specimen DT3 and was only 6%. Hence, like the biaxial geogrid (DX), the higher surcharge has some effect on the pullout load of the uniaxial geogrid (DT). This would suggest that the frictional mechanism plays a more significant role in the pullout resistance of the uniaxial compared to that of the biaxial geogrid.

Specimens with Ribs Cut Only

Figures 8 and 9 show the pullout force versus displacement curves for specimens DT5 to DT12 under a surcharge load of 20 kPa. The magnitude of the maximum pullout force for each specimen, together with its ratio to that of the undamaged specimen, are shown in Table 1. We observe in the latter figures that damage to a large portion of a specimen cross section makes the mesh more extensible in pullout. For example, specimen DT12 reaches its maximum force at a displacement of approximately 30 mm compared to a displacement of about 15 mm for the undamaged specimen. Table 1, on the other hand, indicates that the largest reduction in the maximum force is only 9%, which occurs in

specimen DT7. Comparing the response of specimens DT5 and DT6, or DT7 and DT8, one can observe that cutting the ribs near the junctions tends

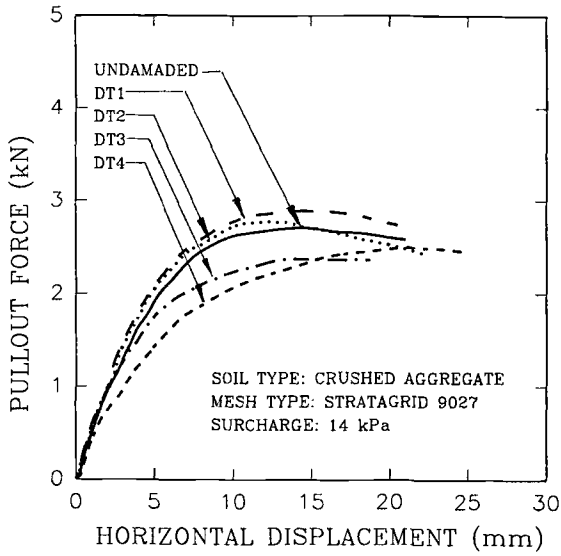


Fig. 6--Pullout Response of DT Specimens under 14 kPa

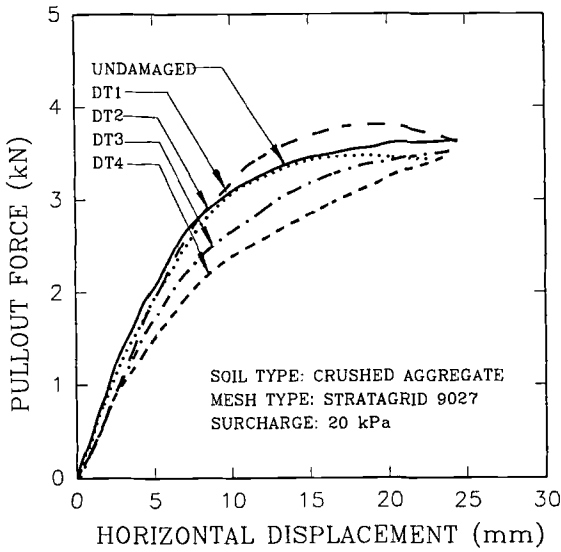


Fig. 7--Pullout Response of DT Specimens under 20 kPa

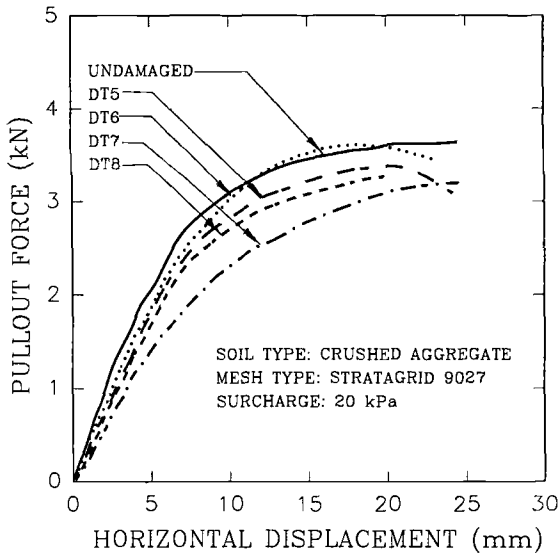


Fig. 8--Pullout Response of DT5-DT8 Specimens under 20 kPa

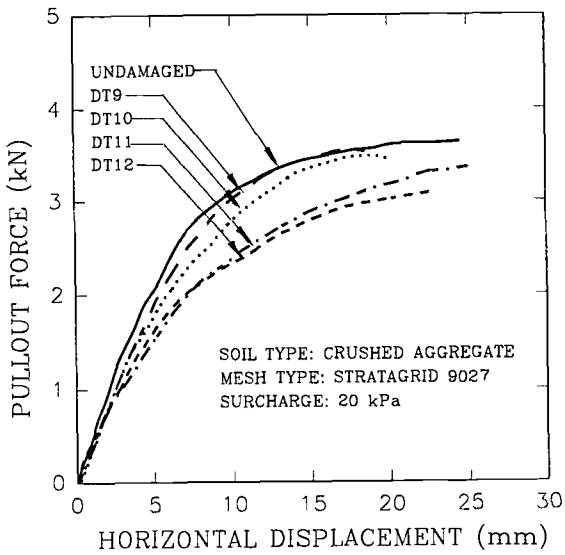


Fig. 9--Pullout Response of DT9-DT12 Specimens under 20 kPa

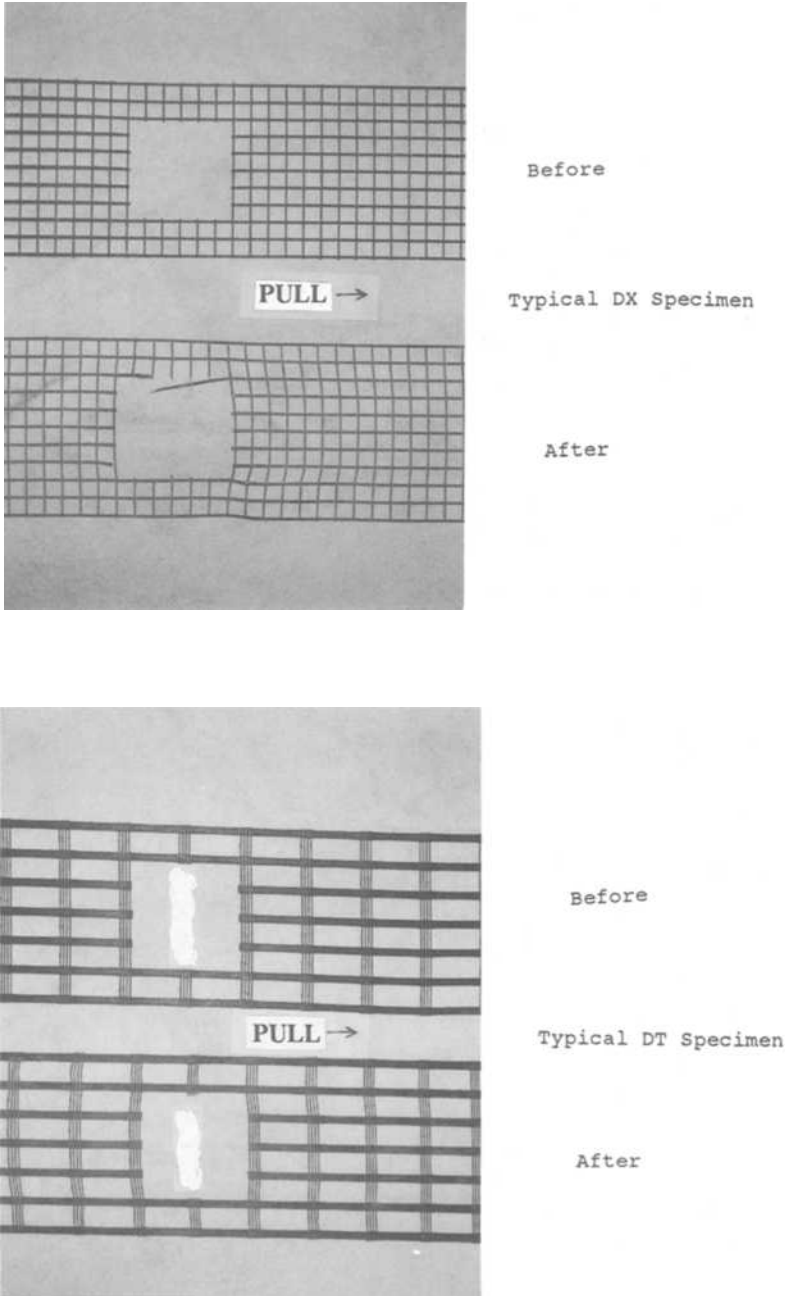


Fig. 11--Pre-damaged Zone of DT Specimen before and after Test

to make the mesh more extensible. In comparing the response of the specimens DT5 to DT12 with those of DT1 to DT4, it becomes evident that in the present tests, and for the geogrid concerned, severing the ribs has essentially the same effect as severing and removing the section of the geogrid.

CONCLUSIONS

The effect of damage on the pullout resistance of the two geogrids in the present investigation varied from 0% to 33%. For the weaker biaxial grid, the simulated damage caused significant reduction in the pullout resistance, regardless of the applied surcharge. For the stronger mesh, the maximum reduction in the peak pullout force was only 14%. On the other hand, the increase in the extensibility of the stronger mesh, caused by the damage, was as high as 100% in some cases. It should be noted that the pullout resistance of some of the specimens apparently increased by as much as 7%. While such an increase is theoretically possible, the apparent increase may also be a consequence of the inherent variability in the test procedure. A larger sample base, particularly undamaged samples, would be required to statistically assess whether the increase actually occurs.

The reductions in the pullout force observed herein are in the same range as the reductions in the tensile strength of exhumed geosynthetics from actual sites as reported in [1]. The results suggest that the partial factor of safety for controlling geogrid deformations due to pullout need not be the same as that controlling the peak pullout force. It would appear from the present results that current partial factors of safety against site, or installation, damage, which are derived from tensile tests on exhumed geogrids, may also be applicable to pullout force. The required partial factor of safety for controlling pullout displacements may be higher than those for pullout force.

The preceding observations and conclusions are based on a limited set of tests and should be considered tentative. To arrive at more definitive conclusions, a more comprehensive study, with a larger sample population, would be needed.

REFERENCES

- [1] Koerner, R.M. and Koerner, G., "A Quantification and Assessment of Installation Damage to Geotextiles", GRI Report #2, Geosynthetics Research Institute, Drexel University, Philadelphia, 1988.
- [2] Bush, D.I. and Swan D.B.G., "An Assessment of the Resistance of Tensor SR2 to Physical Damage During Construction and Testing of a Reinforced Soil Wall", Proceedings of the Conference on applications of Polymeric Reinforcement in Soil Retaining Structures, Royal Military College, Kingston, Ontario, 1988.
- [3] Watts, G.R.A. and Brady, K.C., "Site Damage Trials on Geotextiles," Proceedings, Geotextiles, Geomembranes and Related Products, Den Hoedt (ed.), Balkema, Rotterdam, 1990.
- [4] Troost, G.H. and Ploeg, N.A., "Influence of Weaving Structure and Coating on the Degree of Mechanical Damage of Reinforcing Mats and Woven Geogrids, Caused by Different Fills, during Installation," Proceedings Geotextiles, Geomembranes and Related Products, Den Hoedt (ed.), Balkema, Rotterdam, 1990.
- [5] Lindh, E., "Abrasion Damage to Geotextiles Used in Gravel Road Pavements on Frost-Damaged Roads in Sweden," Proceedings,

Geotextiles, Geomembranes and Related Products, Den Hoedt (ed.), Balkema, Rotterdam, 1990.

- [6] Druell, A.G. and Perrier, H., "Damage on Geotextiles during Rockfills Placing," Proceedings, Geotextiles, Geomembranes and Related Products, Den Hoedt (ed.), Balkema, Rotterdam, 1990.
- [7] Shang, Q. "Pullout Resistance of Geogrids Determined in a Large Test Facility", M. Eng. Thesis, Department of Civil Engineering, Carleton University, Ottawa, Canada, 1986.
- [8] Mowafy, Y. M. "Analysis of Grid Reinforced Earth Structure", Ph. D. Thesis, Department of Civil Eng. Carleton University, Ottawa, Canada, 1980.

A. N. Netravali,¹ R. Krstic,¹ J. L. Crouse,² L. E. Richmond,³

CHEMICAL STABILITY OF POLYESTER FIBERS AND GEOTEXTILES WITHOUT AND UNDER STRESS

REFERENCE: Netravali, A. N., Krstic, R., Crouse, J. L., and Richmond, L. E., "Chemical Stability of Polyester Fibers and Geotextiles Without and Under Stress," Geosynthetic soil Reinforcement Testing Procedures, ASTM STP 1190, S. C. Jonathan Cheng, Ed., American Society for Testing and Materials, Philadelphia, 1993.

ABSTRACT: High tenacity industrial grade polyester fibers were aged up to three months, in various chemicals at different stress levels. The accelerated aging was done at temperatures up to 70°C, which is thought to be the maximum underground temperature for applications such as surface veneers for waste landfills. The chemicals used in the study include trichloroethylene, deionized water, sea water, and 2% solutions of sulfuric acid and sodium hydroxide. The stress values used were 0 MPa, 100 MPa, and 260 MPa. The fibers were tested for their mechanical and thermal properties as a function of aging.

The results suggest that there are no changes in the fiber strength and glass transition temperature (T_g) after aging in trichloroethylene, sea water, and deionized water under any stress level and test temperatures. However, there is a small increase in the melting temperature indicating the possibility of crystal growth, especially at 70°C, due to the annealing effect.

Significant degradation in fiber strength is seen after a week of aging in sulfuric acid solution (~1.1 pH) at room temperature and 40°C. Under the severe acidic conditions, at 70°C and higher stress levels, the fibers completely disintegrated after one week.

In the strong alkaline condition (~13.7 pH), strength decreases of 33% and more than 50% are seen under 0 and 100 MPa stress levels within the first week of aging in NaOH, at RT. All fibers, regardless of stress, did not survive one month in the highly alkaline environment.

These results suggest that 1) severe hydrolysis occurs in strong alkaline and acidic media 2) no hydrolysis occurs under more normal soil conditions (~pH 7-8) at temperatures up to 70°C and 3) higher stress levels do not significantly affect the degradation process.

KEYWORDS: polyester, chemical aging, hydrolysis, thermal properties, mechanical properties

¹Assistant Professor and research assistant, respectively, Fiber Science Program, Department of Textiles and Apparel, Cornell University, Ithaca, NY 14853.

²Senior Development Chemist, Firestone Fibers and Textile Company, P. O. Box 450, Hopewell, VA 23860.

³Manager, Product Development, Conwed Plastics, 770 - 29th Avenue, S.E., Minneapolis, MN 55414.

INTRODUCTION

New technologies, through the use of geosynthetics, have emerged recently in the geotechnical and civil engineering applications. Geosynthetics include all thin, impervious, flexible membranes (geomembranes), woven, knitted and nonwoven fabrics (geotextiles), geogrids, and geocomposites used in geotechnical and civil engineering applications [1]. Geosynthetics are most commonly made from polymeric materials such as polyester (PET), high and medium density polyethylene (HDPE, MDPE), polyamides (nylon), polypropylene (PP), chlorinated polyethylene (CPE) and polyvinyl chloride (PVC).

For geosynthetics to function in aggressive underground environments, they should be resistant to various forms of environmental degradation. Depending on the function for which they are used, these materials need to perform from a relatively few years, as in the case of some storage units, to up to 100 years or more, as in the case of hazardous waste landfills. The medium and long term performance of geosynthetics depends on the aging (degradation) characteristics of the constituting polymers in the underground chemical and microbial environment, the stresses generated during the application and use and their manufacturing processes.

Polymer degradation is mainly caused by breakage of chemical bonds (in the backbone) of the macromolecules of which the polymer is made. The degradation can occur due to various modes of initiation. These include thermal, mechanical, chemical, photochemical, biological, and ionizing radiation modes. In general, most polymers are susceptible, to some degree, to degradation when exposed to water, oxygen and ultraviolet (UV) light. Polymers can be used successfully within a given temperature range, depending on the type of polymer used. A higher temperature may lead to decrease in stiffness and strength, reduction in chemical resistance and increase in degradation rate. All these factors decrease the life of geosynthetics and affect their long term performance.

The resistance of nonpolar, semi-crystalline HDPE, MDPE and PP to attack by natural and man-made chemicals is fairly well known. The polar nature of polyesters and nylons leads to slightly lower chemical resistance. However, their higher strength and abrasion resistance makes them suitable for many applications. The high strength, in the case of polyester fibers, results from their crystalline nature as much as the inherent chain stiffness due to the presence of aromatic group.

The effects of water, temperature, alkalies and acids on various geotextiles have been studied by several researchers [2-7]. The effects of high levels of alkalinity on the strength of PET and PP geotextiles have been investigated by Halse et al. [2,3]. In their experimental study, each geotextile was exposed to tap water, NaOH and $\text{Ca}(\text{OH})_2$ solutions of pH 10 and pH 12 for up to 120 days at room temperature. Although no strength loss was observed for tap water and pH 10 exposures, PET geotextiles exposed to pH 12 solution recorded a strength loss of between 30-50% after 120 days. The decrease in strength was attributed to hydrolysis that resulted in etching of the fiber surface.

Horz [4] has compiled detailed information on the chemical resistance of several polymers, obtained from a number of geotextile manufacturers. In general, the results for polyester geotextiles showed good resistance to organic and dilute inorganic acids even at low pH values. Degradation was seen to occur rapidly as the acid concentration increased. Polyesters were particularly sensitive to ammonia and NaOH solutions. At concentrations above 15 percent, polyester yarns were completely destroyed by these chemicals [4].

The influence of ammonia and other chemicals on polypropylene and polyester geotextiles was studied by Montalvo [5] at room temperature for a period of 56 days. While polypropylene geotextiles were unaffected, polyester geotextiles recorded significant strength loss in ammonia solution. Risseeuw and Schmidt [6] reviewed the hydrolysis of polyester yarns in water and other chemical conditions. Polyester (PET) is synthesized from terephthalic acid and ethylene glycol. Under strong acidic and alkaline conditions, PET undergoes hydrolysis, wherein a long chain linear molecule is split by a water molecule resulting in a scission of an ester linkage [6]. Risseeuw and Schmidt concluded that polyester fibers with low molecular weights between 15,000 and 20,000 g/mole and carboxyl end-group contents of 50 meq/kg were not seriously affected by hydrolysis. They further concluded that fibers with molecular weight of 30,000 g/mole and a carboxyl end-group content of less than 25 meq/kg can be expected to have over 100 years of service life in saturated soil with a pH between 2 and 10.

Results obtained by Mathur et al. [7] involving polyester and polypropylene geotextiles have indicated that under alkaline conditions (buffer solution of pH 10) PET fibers lose all their strength after six weeks of immersion at 95°C. However, the loss of strength at room temperature (20°C) and at temperatures up to 70°C, under the same alkaline conditions, is insignificant. This suggests that the degradation reaction occurs at a significantly higher rate at 95°C, which is much higher than the glass transition temperature of approximately 73°C for PET. Koerner et al. [8] have suggested using an Arrhenius model to predict the geosynthetics degradation behavior. They have presented a list of mechanical and physical properties that could be used for Arrhenius modeling [8]. Mathur et al. [7] used the Arrhenius model to fit the breaking strength and strain data. The value obtained for activation energy for alkaline and acidic hydrolysis for PET geotextiles was approximately 25 kcal per mole. Their results on PP geotextiles suggested that for pH 3, pH 10 solutions and for sea water, PP geotextiles do not undergo any degradation even at high temperatures of up to 95°C.

The degradation reactions, involving exposure to liquids, are diffusion controlled and diffusion occurs more readily in the amorphous regions than the crystalline region. As a result, the polymer molecule degradation (bond scission) initially occurs in the amorphous region. In the case of PET, the hydrolysis reaction may occur at any ester site. This is the reverse of a polymerization reaction (depolymerization) and is favored in an alkaline medium [6]. Each molecular scission reduces the molecular weight and the magnitude of the resulting molecular weight change depends on where the polymer chain scission occurs. Mathur et al. [7] noted that the degraded molecules then slowly leach out reducing the amorphous content, thus increasing the "apparent" fiber crystallinity. Their results also showed an increase in crystal size with aging, as indicated by an increase in melting temperature. However, this probably was a result of annealing above the glass transition temperature. Once the amorphous region was decreased, the crystallites were slowly attacked. The result was a significant decrease in molecular weight contributing to the fiber strength loss. The decrease in molecular weight was confirmed by a decrease in intrinsic viscosity [7].

In all the studies mentioned above, the specimens were exposed to the chemicals, under no stress. In an actual field situation, however, the geosynthetics, and thus the fibers, are invariably under some stress. The actual value of the stress will depend on the particular

application and the local conditions. Molecular degradation of PET fibers, under stress, in chemical environments has not been reported before. The fibers, under stress, may exhibit smaller diffusion coefficient due to the enhanced molecular orientation in the amorphous region, resulting in a slower rate of degradation. At the same time, the bonds under stress may be more susceptible to hydrolysis. Further, the results discussed above applied to only the particular PET fiber studied. The results could be different for different fibers depending on the molecular weight, carboxyl end-group content, crystal size, crystallinity, and amorphous orientation. In this paper we present the results of the chemical aging study done on high tenacity industrial grade polyester fibers under zero and two different stress levels.

EXPERIMENTAL

Exposure Conditions

High tenacity industrial grade (HTIG) polyester yarns obtained from Firestone Fibers and Textile Company were aged in deionized water, sea water, trichloroethylene, sulfuric acid (2% solution), and sodium hydroxide (2% solution) under zero and two stress levels. The sea water environment was simulated using "Instant Ocean" brand sea salt mixture which is commonly used for sea water fish aquariums [7]. The stress values used were 0 MPa, 100 MPa and 260 MPa which initially produced 0%, 1%, and 4% fiber strains respectively. It may be noted here that at higher temperatures, the actual specimen strains may be much higher. To age the specimens, they were placed in a glass tank containing the solution and loaded by a dead weight hanging outside the tank. The schematic of the setup is shown in Figure 1 below. To age the specimens under no stress, yarns were hung on glass rods in the form of loose bundle, in glass jars containing the solutions.

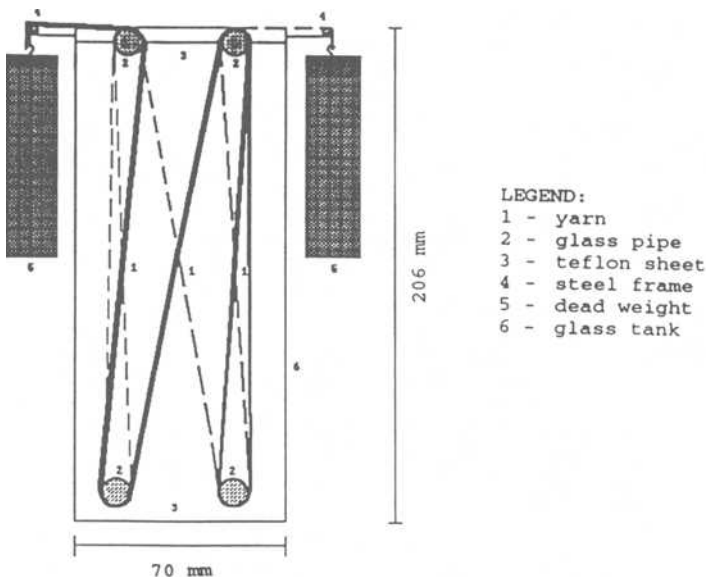


FIG. 1--Schematic of the yarn aging setup showing two yarns.

The specimens were aged at room temperature (21°C), 40°C, and 70°C for periods of one week, one month, and in some instances, three months. Four air circulating ovens, each containing 2 aging setups, were used for elevated temperature aging and the temperatures were maintained within $\pm 2^\circ\text{C}$. For trichloroethylene, aging was carried at room temperature only. At the end of each exposure, the specimens were removed from the ovens, washed thoroughly in reverse osmosis water and dried for at least 24 hours prior to testing.

Tensile Testing

The tensile tests were performed at ASTM standard laboratory atmospheric conditions of 21°C and 65% RH, on an Instron Universal Testing Machine (model #1122), interfaced with an IBM AT computer. Twenty five fibers, 200 mm long, were extracted from the yarn. Upon extraction, each fiber was divided in half. Using one half, the cross-sectional area of the fiber was determined by the vibroscope technique described by ASTM 1577 and the mass density of the fibers of 1.4 g/cm³. The mass density was obtained from linear density gradient column measurements using a mixture of heptane and carbon tetrachloride. The other half of the fiber was mounted on a paper tab following a modified procedure of ASTM D3379. A drop of DuroTM Master Mend quick setting epoxy was used to bond the fiber ends to the tab at a gauge length of 30 mm. All the tests were carried out at a strain rate of 0.17 min⁻¹. The failure stress of each fiber was calculated using the force at break and the cross-sectional area measurement made on that particular fiber's adjacent half. More details of the tensile testing procedure can be found elsewhere [9].

Thermal Analysis

The glass transition temperature (T_g), melting point (T_m), and heat (enthalpy) of fusion (ΔH) were determined using a Perkin-Elmer DSC-4 with a System-4 microprocessor controller and a model 3700 data station. Specimens weighing between 5 and 10 mg were scanned from 50°C to 300°C at a rate of 10°C/min in a nitrogen atmosphere. During the first run, values for the melting characteristics, T_m and ΔH were obtained. However, it was difficult to detect the T_g due to the plasticization effect of the diffused water. Another significant factor contributing to the difficulty in T_g detection, is the high crystallinity of the PET yarns which reduces the amorphous amount to levels below the DSC sensitivity. After the first run, specimens were quenched at 320°C/min and reheated at 10°C/min. The volatiles were eliminated in the first heating run while at the same time the amorphous content increased due to quenching. As a result, the T_g values could be easily obtained from the second run. In addition, the first run erased the different thermal history of the specimens due to the aging carried out under different temperatures. As a result, all the specimens had equal thermal history for comparing their T_g values. The T_g , T_m , and ΔH values for the specimens treated under exposed conditions were compared to the values obtained for the untreated specimens. Three specimens were tested for each condition.

RESULTS AND DISCUSSION

Fiber strength is related to the fiber morphology, molecular weight and chemistry of the inherent polymer. Fiber breaking stress results before and after aging in deionized water, sea water, and trichloroethylene, for one week, one month, and three months are presented in Table 1a. It can be seen that there is no change in the fiber breaking stress, under any treatment conditions, indicating that no significant hydrolysis has occurred up to 70°C even under stress level of 260 MPa. These results agree with those obtained by Montalvo [5] showing no loss of strength for geotextiles treated in sea water, at room temperature up to 60 days. Halse et al. [3], who studied effects of tap water for up to 120 days, showed that the treatment has no effect on the strength of PET geotextiles. Observations by Thomas and Verschoor [10] and Sprague [11] also suggest no overall deterioration of properties after 120 days exposure to distilled and deionized water at 50°C. Our results suggest that stress levels of up to 260 MPa do not affect the hydrolysis process for up to three months of exposure in deionized and sea water at temperatures up to 70°C.

Table 1a -- Fiber Break Stress Results

	Deionized Water			Sea Water			Trichloroethylene
	Stress* (GPa)			Stress* (GPa)			Stress* (GPa)
	RT	40°C	70°C	RT	40°C	70°C	RT
CF	1.14	1.14	1.14	1.14	1.14	1.14	1.14
W0	1.18	1.21	1.16	1.17	1.15	1.20	1.06
M0	1.12	1.02	1.12	1.16	1.12	1.09	1.10
W1	1.10	1.19	1.15	1.14	1.12	1.09	1.14
M1	1.08	1.11	1.13	1.12	1.15	1.08	1.23
3M1	1.13	1.14	1.08	1.17	1.10	1.03	----
W4	1.15	1.16	1.17	1.23	1.17	1.12	1.16
M4	1.14	1.04	1.16	1.12	1.16	1.14	1.11
3M4	1.18	1.17	1.03	1.07	1.16	1.05	----

* Each value is an average of 25 tests

- RT - room temperature
- CF - control fiber
- W0 - 1 week; 0 stress
- M0 - 1 month; 0 stress
- W1 - 1 week; 100 MPa
- M1 - 1 month; 100 MPa
- 3M1 - 3 months; 100 MPa
- W4 - 1 week; 260 MPa
- M4 - 1 month; 260 MPa
- 3M4 - 3 months; 260 MPa

Table 1b gives the T_m , ΔH , and T_g values for the untreated fibers and for those treated under different conditions. As mentioned earlier, the T_g of the fibers could not be detected in the first DSC run. The reported values are for the second DSC run after quenching the specimen at 320°C/min. The T_g values vary within a small range of 78°C and 80°C indicating no molecular weight degradation. The results also show a slight increase in the ΔH values as well as the T_m values for all treatment conditions, indicating increased crystallinity as well as crystal size respectively. The increased crystallinity is possibly due to the annealing effect rather than the aging treatment. These results are similar to those obtained by Mathur et al. [7] and Jailloux, Ballara and Verdu [12,13] for PET geotextiles aged under no stress. These results confirm that deionized and sea water do not affect PET fibers at stress levels of 260 MPa and 70°C temperature, for up to three months.

Table 1b -- DSC Results

	Control	Deionized Water		Sea Water		Trichloroethylene	
Temperature	RT	70°C		70°C		RT	
Time/stress		W4	M4	W4	M4	W4	M4
T_m (°C)*	259	263	263	262	261	264	263
ΔH (cal/gm)*	10.5	10.5	11.2	12.5	11.2	12.6	12.2
T_g (°C)**	78.7	79.0	78.8	79.0	79.2	79.8	79.2

* Each value is an average of three readings

** T_g values are obtained from the 2nd run

Mathur et al. [7] termed the increase in the ΔH values, during the initial few weeks, as increase in the "apparent" crystallinity. They attributed it to the hydrolysis of the readily accessible amorphous regions in the initial period, while the crystalline regions that are not being attacked, remain unaffected. The diffused water or the chemical reduces the T_g drastically, which increases the segmental motion of the molecules and the free volume in the material. It is possible that the enhanced molecular mobility in the amorphous region enables molecules to get incorporated into the existing crystals. This process, involving an increase in crystallinity and hence the density, is called chemicrystallization [12]. The increased crystal size is reflected in slightly higher value for T_m .

Fiber breaking stress results before and after treating the fibers in 2% solutions of sulfuric acid and sodium hydroxide are presented in Table 2a. It can be seen that for fibers treated in sulfuric acid at room temperature and 40°C, there is no loss in strength after one month of aging at any stress level. These data agree with the results presented by Horz [4] and Davis [14] which show no strength loss for PET

fibers treated for 12 months with up to 15% concentration of sulfuric acid (pH 0.1) at room temperature. However, at 70°C, the fibers at higher stress levels show severe degradation. During the aging, these yarns broke, and as a result the data for one month is not available. Under the severe conditions of three degradation agencies; mechanical stress, higher temperature and the sulfuric acid, the hydrolysis of the PET occurs synergistically. It is quite possible that the hydrolysis rate is not changed but the effects are detected earlier due to the constant stress. Mathur et al. [7] have shown that in acidic buffer solution of pH 3, the degradation within the first week is not significant at 70°C, when the geotextiles are under no stress.

Table 2a -- Fiber Break Results

	Sulfuric Acid (pH 1.1)			Sodium Hydroxide (pH 13.7)		
	Stress* (GPa)			Stress* (GPa)		
	RT	40°C	70°C	RT	40°C	70°C
CF	1.14	1.14	1.14	1.14	1.14	1.14
W0	1.20	1.12	1.13	0.68	0.78	0.24
M0	1.14	1.19	1.07	0.62	0.00	0.00
W1	1.18	1.15	NA	0.37	0.00	0.00
M1	1.17	1.15	NA	0.00	0.00	0.00
3M1	1.17	1.09	NA			
W4	1.08	1.23	NA	0.42	0.00	0.00
M4	1.13	1.16	NA	0.00	0.00	0.00
3M4	1.12	NA	NA			

* - Each value is an average of 25 tests
 NA - Specimen broke during exposure

The effect of 2% NaOH solution (13.7 pH) on the fiber strength is more severe than sulfuric acid. The fibers lose over 45% of their strength within the first week, under no stress and over 60% under a stress of 100 MPa. Under higher stress levels or at temperatures above room temperature, the fibers did not survive one month. These results are severe compared to those obtained at 70°C, under no stress by Mathur et al. [7]. They observed that when exposed to pH 10, the PET fibers retained more than 80% of the strength after 6 weeks at 70°C and showed very little change thereafter up to six months. However, it must be noted that the present experiments conducted in pH 13.7 under stress, are severe compared to the treatment by Mathur et al. [7], of pH 10 with no stress.

Results obtained by Thomas and Verschoor [10], after treating various geotextiles for 98 days at 50°C, showed that some continuous filament geotextiles were unaffected by NaOH solution (pH 12) while

other staple geotextile fabrics were susceptible to NaOH solution. It was believed that some of the staple fibers were of a lower grade i. e. lower molecular weight and therefore were less resistant to hydrolysis. Halse et al. [2,3] observed that the strength of PET geotextiles in the pH 12 solution decreased by 30-50% after 120 days of exposure. Jailloux et al. [15] observed that accelerated aging at high temperatures (95°C) gives useful information about their degradation behavior. Their results on high-tenacity PET yarns showed strength reduction of over 40% in Ca(OH)₂ (pH 13) at 95°C, within the first two days and strength loss of over 80% for NaOH (pH 13) in 28 days. PET hydrolysis in alkaline solution was also confirmed by Solbrig and Obendorf [16]. Solbrig and Obendorf observed etching marks on the fiber surfaces that contained delustrant TiO₂ particles. In the present research there is some indication that stress promotes the PET hydrolysis especially in alkaline medium. We are further investigating the interaction between stress and degradation in several chemical environments.

Table 2b -- DSC Results

Temperature	CF	Sulfuric Acid (pH 1.1)			Sodium Hydroxide (pH 13.7)				
		RT	40°C		70°C		RT		
Time/stress		W1	W4	M4	W0	M0	W0	M0	W1
T _m (°C)*	259	262	263	263	264	262	264	262	265
ΔH(cal/gm)*	10.5	11.8	10.6	11.5	11.6	10.6	12.3	10.5	14.0
T _g (°C)**	78.7	79.7	79.5	79.9	78.7	79.0	79.9	79.0	80.0

* Each value is an average of three readings

** T_g values are obtained from the 2nd run

Table 2 shows the T_m, ΔH, and T_g values obtained for the fibers treated with sulfuric acid and sodium hydroxide. These results indicate somewhat higher ΔH values for one week aging period and lower values for longer aging period of one month. The melting temperatures are higher for both aging periods. This again indicates higher crystallinity as well as larger crystal size. As in the case of deionized water and sea water, the T_g values do not show any change. Fibers that were highly degraded could not be analyzed in the DSC to observe changes in the T_g to assess the molecular weight changes.

CONCLUSIONS

The results show that high tenacity industrial grade PET (HTIG/PET) fibers are not affected after three months of exposure to deionized water and sea water and temperatures up to 70°C and trichloroethylene at room temperature for one month under stress. Under

these exposure conditions, the stress does not seem to have any significant effect on the hydrolysis process. The PET fibers, however, undergo severe hydrolytic degradation in 2% solutions of sulfuric acid (pH 1.1) and sodium hydroxide (pH 13.7) under stress. Under such conditions, stress appears to be an additional factor in the degradation process. These conditions, pH 1.1 and pH 13.7, however, may be too severe to be encountered in regular geotechnical engineering application. The DSC results suggest some crystal growth as well as increased crystallinity, possibly due to the annealing effect.

FUTURE WORK

The results presented here are a part of a wider study of the chemical resistance of HTIG/PET fibers, under stress, currently being conducted at Cornell. We are continuing the extended term aging in the chemicals discussed here and plan to extend the study to several other chemicals. We also plan to do the intrinsic viscosity measurements of the specimens to observe the molecular weight changes.

ACKNOWLEDGEMENTS

The authors would like to thank Ashish Mathur for his valuable contribution in this study.

REFERENCES

- [1] Giroud, J. P., "Geotextiles and Geomembranes," Geotextiles and Geomembranes, vol. 1, 1984, pp. 5-40.
- [2] Halse, Y., Koerner, R. M. and Lord, A. E., "Effect of High Levels of Alkalinity on Geotextiles. Part 1. Ca(OH)₂ Solutions," Geotextiles and Geomembranes, vol. 5, 1987, pp. 261-282.
- [3] Halse, Y., Koerner, R. M. and Lord, A. E., "Effect of High Levels of Alkalinity on Geotextiles. Part 2. NaOH Solutions," Geotextiles and Geomembranes, vol. 6, 1987, pp. 295-301.
- [4] Horz, R. C., "Geotextiles for Drainage, Gas Venting and Erosion Control at Hazardous Waste Sites". EPA Report No. 600/2-86/085 Sept. 1986, pp. 2/26-2/44.
- [5] Montalvo, J. R., "Evaluation of the Degradation of Geosynthetics", Geosynthetics 1989 Conference Proceedings, IFAI, St. Paul, 1989, pp. 501-512.
- [6] Risseeuw, P., and Schmidt, H. M, "Hydrolysis of HT polyester Yarns in Water at Moderate Temperatures," Proceedings of the Fourth International Conference on Geotextiles, Geomembranes and Related Products, Den Hoedt (Ed.), Balkema, Rotterdam, 1990, pp. 691-696.
- [7] Mathur, A., Netravali, A. N. and O'Rourke, T. D., "Effect of Chemical Aging on Geotextiles I: Physio-Mechanical Properties of Polyester and Polypropylene Geotextiles" to be submitted, Geotextiles and Geomembranes, 1992.

- [8] Koerner, R. M., Lord, A. E., and Hsuan, Y. H., "Arrhenius Modeling to Predict Geosynthetic Degradation," Geotextiles and Geomembranes, vol. 11, 1992, pp. 151-183.
- [9] Netravali, A. N., Henstenburg, R. H., Phoenix, S. L., and Schwartz, P., "Interfacial Shear Strength Studies Using the Single-Filament-Composite Test. I Experiments on Graphite Fibers in Epoxy," Polymer Composites, vol. 10, 1989, pp. 226-241.
- [10] Thomas, R. W. and Verschoor, K., "Geosynthetics: Microstructure and Performance," ASTM STP 1076, I. D. Peggs (Ed.), American Society for Testing and Materials, Philadelphia, PA, 1990, pp. 4-16.
- [11] Sprague, C. J., "Leachate Compatibility of Polyester Needle-punched Nonwoven Geotextiles," ASTM STP 1081, R. M. Koerner (Ed.) American Society for Testing and Materials, Philadelphia, PA, 1990, pp. 212-221.
- [12] Jailloux, J. M. and Verdu, J., "Kinetic Models for the Life Prediction in PET Hygrothermal Aging: A Critical Survey," Proceedings of the Fourth International Conference on Geotextiles, Geomembranes and Related Products, Den Hoedt (Ed.), Balkema, Rotterdam, 1990, p.727.
- [13] Ballara, A. and Verdu, J., "Physical Aspects of the Hydrolysis of Polyethylene Terephthalate," Polymer Degradation and Stability, vol. 26, 1989, pp. 361-374.
- [14] Davis, G. W., "Aging and Durability of Polyester Geotextiles," 2nd GRI Seminar on Durability and Aging of Geosynthetics, GRI, Philadelphia, 1986, pp. 65-81.
- [15] Jailloux, J-M., Anderson, P. L., and Thomas, R. W., "Chemical-Compatibility Studies of Polyester Filaments and Yarns to be used in Geocomposites. Phase 1: Tests at 95°C," Geotextiles and Geomembranes, vol. 11, 1992, pp. 277-290.
- [16] Solbrig, C. M. and Obendorf, S. K., "Alkaline Hydrolysis of Titanium Dioxide Delustered Poly(ethylene Terephthalate) Yarns," Textile Research Journal, vol. 61, 1991, pp. 177-181.

Donald G. Bright¹

TESTING FOR BIOLOGICAL DETERIORATION OF GEOSYNTHETICS IN SOIL REINFORCEMENT AND STABILIZATION

REFERENCE: Bright, D. G., "Testing for Biological Deterioration of Geosynthetics in Soil Reinforcement and Stabilization," Geosynthetic Soil Reinforcement Testing Procedures, ASTM STP 1190, S. C. Jonathan Cheng, Ed., American Society for Testing and Materials, Philadelphia, 1993.

ABSTRACT: Over the past decade, critical earthen structures have been designed to incorporate geosynthetics. To facilitate proper design and assure long-term stability, it is necessary to know the susceptibility of these geosynthetics to biological deterioration. The perception is that the polymers and their additives used in geosynthetics are not susceptible to biological degradation. However, the literature clearly shows that some polymers and common additives are susceptible. Through mutation, microorganisms can develop specificity towards a host material. Biocides exhibit specificity and limited effectiveness. Unfortunately, current test methods are quite inadequate, for many reasons, in assessing the biological stability of the geosynthetics on the market today. A alternative test protocol circumvents these shortcomings and accounts for synergistic effects, heretofore ignored. A means of predicting long-term stability through superposition principles is suggested.

KEYWORDS: biological degradation, geosynthetics, microorganisms, biocides, synergisms, test standards

INTRODUCTION

Critical earthen structures are commonly designed for lifetimes as long as 100 years and are expected to remain stable over this duration. In the past ten years, these structures have been designed to incorporate geosynthetics fabricated of polymer(s) To facilitate

¹Manager, The Tensar Corporation, 1210 Citizens Parkway, Morrow, Georgia 30260.

proper design in the beginning and assure long-term stability, it is necessary to know the mode, mechanism, and profile with time of biological deterioration of these geosynthetics.

It has long been the perception within the geotechnical industry that the primary polymers used in geosynthetics are not susceptible to microbial attack. However, recent information shows that susceptibility of these polymers depends upon the chemistry of their monomeric repeat units [1,2,3]. Geosynthetics composed of polymers with certain additives exhibit a susceptibility [4,5,6,7] and synergistic behavior. Biological degradation of these additives can initiate and propagate the deterioration of the primary polymer(s). This can result in the eventual deterioration of the whole geosynthetic product [6,7] thus affecting its long-term durability.

The microorganisms causing the biodeterioration are found all over the world existing in a wide range of environmental conditions [8], from the tropics to the polar regions [9]. These microorganisms require a source of carbon for growth and obtain it from enzymatic induced reactions degrading organic based materials [10,11], such as some polymers and some additives used in geosynthetics. Factors affecting biodeterioration of the host geosynthetic are its polymeric chemistry [1,2,3] and molecular weight, specific additives [4,5,6,7], surface characteristics, and physical state [8,12,13]. Environmental factors controlling biodeterioration are temperature, humidity, pH, osmotic pressure, redox potential of the host geosynthetic [8,12,13], and its surroundings.

Unfortunately, there are currently no uniform or formalized test methods accounting for the effect of the aforementioned parameters in evaluating the biodegradability of polymers, their composites, and their additives [2,4,14]. Existing test standards specify microbes that are not necessarily representative of actual field environments and do not provide a protocol for testing alternative microbes. The presence of microorganisms growing on a geosynthetic is, in itself, not necessary sufficient proof of biological deterioration [15]. Rigorous proof requires that an unmistakable change occurs in an essential property pertinent to the long-term durability of the geosynthetic in which the suspected microorganism(s) is the sole deteriorative agent [15].

MICROORGANISMS

Identification and Concentration

Microorganisms of importance in biodeterioration are bacteria, fungi, actinomycetes, algae [4,8,13] and yeast [16]. Their concentration in the soil varies by class: bacteria (1000 pounds/acre, or about 1 billion/gram of dry soil, or about a trillion/cubic inch of soil), fungi (10-20 million/gram of dry soil), and actinomycetes (0.1-36.0 million/gram of soil) [3,4,17,18].

Conditions for Growth

Ambient and higher temperatures, high humidity, and the absence of UV light favor the growth of fungi while bacteria frequently need the presence of moisture for reproduction [10,11]. Fungi are more adaptive to growing under adverse conditions [19]. The most favorable thermal conditions for fungi are 30 °C, but they can survive below 0 °C and above 65 °C. A relative humidity (RH) of 95-100% are the most conducive to growth, but fungi can still thrive at a 70% RH. [11,20] Microorganisms require a source of carbon for growth and obtain it from enzymatic induced degradation of organic materials [10,11] such as polymers and their additives.

Mechanism of Activity

To grow, microorganisms excrete enzymes into the surrounding medium. These enzymes degrade the host material by breaking down its large molecular units into much smaller units to serve as food for the microorganisms. [11,12,21] The net effect is a reduction in molecular weight, a deterioration of physical properties, and eventual disintegration of the host material [10]. One microorganism may have an initial advantage with the immediately available food, but it may be replaced or joined by other microorganism(s) leading to a succession of microorganism(s) [8]. Thus, a particular microorganism(s) initiating degradation is not necessarily the same microorganism(s) that perpetuates degradation. Given the inherent nature of rapid mutation, microorganisms can product enzymes specifically suited to the host material [1]. The level of enzymatic activity varies according to the microorganism, culture medium, food, and the presence of inhibitors (i.e., biocides) [22]. Microbial enzymes can promote several other degradative reactions: oxidation-reduction, decarboxylation, and hydrolysis [1,3,11,12,19,23,24].

SUSCEPTIBILITY OF POLYMERS AND ADDITIVES

Polymers and their additives contain carbon, and microorganisms require a source of carbon to survive and perpetuate themselves [4,8,25]. Thus, the susceptibility to microbial attack of polymers and additives used in geosynthetics for soil stabilization and reinforcement of critical earthen structures for the long-term should be a concern.

Microbes produce enzymes that attack many polymers [1] and additives, but the resulting degree of degradation is controlled by conditions in surrounding environment (i.e., RH, pH, temperature) and the following chemical, molecular, and physical properties of the geosynthetic:

1. Monomeric chemistry [1,2,3],
2. Molecular weight level [1,4],
3. Availability and accessibility of molecular chain end groups [1,4],
4. Hydrophobicity [1], and
5. Surface area to volume ratio [1].

Enzymology can explain this biodegradation. First, enzymes require accessibility to the sites where the polymer is susceptible to

attack [1,2]. Low surface area to volume ratio, crystallinity, and hydrophobicity can control accessibility. Second, there must be present specific chemical groups that are susceptible to enzymatic attack [1,2] for the generation of food. Polymer chemistry and molecular weight level are controlling factors here. Microorganisms tend to attack the end groups of the lower molecular weight chains [1,2]. With the number of end groups being inversely proportional to the molecular chain length, average molecular weight is controlling. Any branching along the molecular chains usually terminates microbial attack [15].

The susceptibility is dependent on the chemistry of the polymer's monomeric repeat unit. Polymers with mixed linkages, such as -COO- , -CO- , and -CN- (e.g., polyesters, polyamides, polyurethanes), show a much greater susceptibility to biodegradation via hydrolytic attack than polymers with simple aliphatic linkages, such as -C-C- (e.g., polyethylene, polypropylene). [1,2,3,26]

Testing the susceptibility of composite products is complicated by the diversity of product structure, e.g., laminations or blends. Thus, evaluating deterioration is not straight forward. Each component should be assessed on its own merit. [27] Since there exists the potential of a synergistic behavior between components whereby the degradation of one through its physical loss and/or by-product(s) can affect the susceptibility of the other(s), the product should be tested as a composite structure as well.

Biocides are added to impede the growth of or to destroy the microorganisms [13,14]. They impede or destroy by interfering with the metabolism of the microorganisms and preventing amitosis. Biocides differ widely in the extent of their effectiveness, and different biocides block different enzymatic mechanisms. [14,28] A fungicide prevents specific fungal growth but remains ineffective against bacterial attack, and the same functionality is true for a bactericide [6]. Thus, a biocide exhibits specificity.

CURRENT TEST METHODS AND PROBLEMS

There are no uniform or formalized test methods for determining biodegradability of polymers [2,4,14], but there are two elements to such testing [2,14]. The first is incubation in environments conducive to microbial attack of the polymers. Second is the measurement of the degree of degradation through change in both chemical and physical properties.

Historically, the testing is divided into two categories: laboratory testing and field studies. Laboratory testing permits greater experimental control, but this is at the expense of not being able to duplicate actual exposure conditions. Field studies involve soil burial lasting up to several years. However, burial tests have problems with reproducibility due to the difficulty in controlling environmental conditions and microbial population. [2,14] Also, the conditions under which microorganisms grow in a controlled laboratory are radically different from those prevailing in the field test [14]. A polymeric product may exhibit marked resistance to fungi or bacteria in laboratory tests, but undergo deterioration when exposed to soil

suggesting that the soil contains constituents which are absent in the laboratory tests. [27]

American Society for Testing and Materials (ASTM)

ASTM Test Method for Determining Resistance of Synthetic Polymeric Materials to Fungi (G 21-85) and ASTM Test Method for Determining Resistance of Plastics to Bacteria (G-22-85) evaluate the resistance of polymeric materials to fungal and bacterial attack, respectively. Both tests assume that the polymeric portion of the product is resistant to attack, but the literature suggests otherwise [1,2,3,26]. Other components or additives (i.e., plasticizers, lubricants, stabilizers, and colorants) are the principal component susceptible to microbial attack. Any loss of these additives results in increased modulus (stiffness), changes in weight, dimensions, and other physical properties. Pronounced changes in physical properties are usually observed on polymeric films or coatings where the surface to volume ratio is high, and where additives can diffuse to the surface and then be consumed by microorganisms.

Both tests list specific microbial culture(s) for evaluating resistance. It is erroneous to assume that these microorganisms will biodegrade a geosynthetic polymer, and there are no provisions on mixing organisms that are more likely to attack a particular polymer [2]. Substitutions are permissible, but there is no stipulation or protocol as to possible changes necessary in test procedures when using other microorganisms.

The time frame for the ASTM G-21 and G-22 tests is 3 weeks. If either test is prolonged beyond 4 weeks, results become questionable due to dehydration and breakdown of the agar, and depletion of its mineral nutrients [29]. This time frame is not necessarily sufficient time to recognize or detect sufficient changes in those properties impacting performance as a result of microbial activity, especially with high molecular weight polymers. For life expectancies out to 100 years, 3 weeks is also quite insufficient a time basis for any meaningful extrapolation.

ASTM G-21 and G-22 fail in determining the resistance of polymeric materials that may be aging with time due to temperature, weathering or leaching of additives (potential food and/or nutrients). Once the natural surface film is removed, particularly with vinyl systems, the ability to control surface contaminants is reduced. How important is each component in the total product in the overall deteriorative process? Attempting to correlate laboratory and field testing is a difficult problem. There is insufficient knowledge to predict from these laboratory tests the performance of vinyl systems in the field. Thus, these testing procedures are not truly adequate, and new procedures should be developed. [30]

American Association of Textile Chemists and Colorists (AATCC)

AATCC also has tests for the evaluation of microbial attack on fabrics: AATCC Test Methods for Fungicides, Evaluation on Textiles: Mildew and Rot Resistance of Textiles (AATCC 30-1986), Antibacterial Activity of Fabrics, Detection of Agar Plate Method (AATCC 90-1982), and Antibacterial Finishes on Fabrics, Evaluation of (AATCC 100-1986).

AATCC 90 and 100 specify microbes for agar test which are potentially pyrogenic to humans, but may not be cultures common to geotechnical soils. AATCC 30 soil burial tests are conducted in organically rich soils which are not typical of geotechnical soils either. Test duration is 2 to 28 days for agar tests and 6 weeks maximum for soil burial tests. These tests are not representative of geotechnical environments nor of sufficient duration for prediction of long-term performance.

AN ALTERNATIVE TEST PROTOCOL

Geosynthetic Product

Identify each product component, such as polymer(s) and principal additive(s) (i.e., plasticizers, stabilizers, lubricants, etc.) present in sufficient quantity that any loss would cause a change in product performance. The additive carbon black used as a stabilizer against ultra-violet light degradation is not considered susceptible to microbial attack [31]. For any polymer(s), identify its monomeric chemistry and molecular weight level to establish potential susceptibility.

Microbial Selection

Biological resistance testing should be with microbes common to soils used in the geotechnical structure. Microbial(s) identification, selection, and associated soil chemistries will be the subject of a future paper(s).

Component and Product Testing

Testing for biological susceptibility should be in three stages: preliminary screening, environmental simulation, and laboratory and field trails.

Preliminary screening--Preliminary testing provides a quick assessment of the growth/no growth capability of a particular microbe on an additive (e.g., plasticizers, lubricants, stabilizers), and the efficacy of a biocide [26]. Some additives are resistant when present as the sole carbon source, but the presence of other additives as potential nutrients in the same composite can stimulate the utilization of that additive by microbe [12,26]. Since the converse could be true, testing of individual additives would establish which additive(s) alone are susceptible. Then the preliminary screening of the additives collectively, as in the composite product, would account for synergistic effects. Susceptibility could shift from one additive(s) to other additive(s) which may or may not be essential to long-term product performance.

If the geosynthetic product is comprised of two or more polymeric products (e.g., lamination or geotextile on a polymeric substrate), then the polymeric products should be assessed separately and collectively (i.e., the geosynthetic product) to account for synergistic effects.

If a biocide is used, it should be tested against the various microbes to establish a baseline of its effectiveness with which to compare when incorporated into the product.

Environmental simulation--This test is designed to account for the end use of the geosynthetic while maintaining a reasonable amount of control on the environmental conditions of soil and humidity [26] and temperature. The material may then undergo artificial aging to simulate the effects of daily temperature cycles, atmospheric conditions, and weathering [26].

Laboratory trials--Specimens are buried in trays of soil (called soil burial beds) for predefined periods of time, usually about 4 weeks [26] to 12 weeks which may not be sufficient to recognize changes in mechanical properties [32]. Fortunately, these beds can be kept active for several years permitting much longer test periods. Soil burial is recognized as an aggressive environment for assessment of the biological stability of materials in contact with soils during their service life. [26] The soil can be typical of a particular geotechnical application, or the soil could be organic thus simulating an accelerating test. The problem with organic soils is correlating results with actual field performance. The soil bed is then inoculated with the appropriate microbe(s). A sufficient number of specimens are buried. Performance parameters (e.g., tensile, elongation, etc.) and product composition (e.g., plasticizer and/or biocide content via weight loss) are monitored with time. Effectiveness of a biocide can be evaluated through its inhibition of microbial attack on additive(s) identified in preliminary screening as being susceptible.

Field trials--Field trials are usually long-term tests being much greater than one year. They should encompass climates ranging from humid tropical conditions to freeze/thaw situations. Thus, the design of a field trial is of paramount importance: choosing exposure sites, the best means to present the material to the environment, the number of samples, the frequency of sample examination and procedure, and evaluation tests and protocol. [26]

Environmental simulation testing and field trials could be circumvented if there exists field performance data of long-term duration on a product(s). Such data should include field performance from above- and/or in-ground installations with exposure to multiple atmospheres and soil chemistries, respectively, and microbes. The duration should be at least a decade, preferably multiple decades so as to establish clear profile of product behavior/response to biological attack.

Temperature Level and Time Duration

Microbes survive below 0 °C and to above 60 °C [11,20]; their growth rate is at a maximum in the 25 - 30 °C range [26]. Since soil burial trays used in laboratory tests can be kept active for years [26], environmental simulation could be for 10,000 hours at multiple temperature levels (e.g., 20, 30, and 40 °C) so as to establish a basis for possible extrapolation of product resistance/susceptibility via principles of time-temperature superposition. This length of testing, hopefully, would render some assessment of the effects of product aging on susceptibility, and allow sufficient time for mutation of enzymes exhibiting specificity towards their host material(s) [1].

FACTS

1. Microorganisms exist over a wide range of environmental conditions.
2. Through mutation, microorganisms can develop specificity towards available nutrient sources.

CONCLUSIONS

1. Current test methods are inadequate in assessing the biological stability of the geosynthetic products on the market today.
2. An alternative test protocol addresses the short comings of current methods and accounting for potential synergistic effects.
3. The simpler the chemistry of the polymer(s), the fewer the number of additives, and the lower their the quantity in a geosynthetic product, the simpler is the testing for assessment of biological deterioration.

REFERENCES

- [1] Huang, J-C., et al., "Biodegradable Plastics: A Review", Advances in Polymer Technology, 1990, 10 (1), 23-30.
- [2] Aminabhavi, T. M., et al., "A Review on Biodegradable Plastics", Polymer-Plastics Technology Engineering, 1990, 29 (3), 235-62.
- [3] Rodriguez, F., "The Prospects for biodegradable plastics", Chem Tech, 1971, 409-15.
- [4] Koerner, R. M., Designing with Geosynthetics, Prentice Hall: Englewood Cliffs, N. J. (1990) pp. 106,303,393-5.
- [5] Mills, J. and H. O. W. Eggins, "The Biodeterioration of Certain Plasticisers by Thermophilic Fungi", International Biodeterioration Bulletin, 1974, 10 (2), 39-44.
- [6] Stahl, W. H. and H Pessen, "The Microbiological Degradation of Plasticizers", Applied Microbiology, 1953, 1, 30-5.
- [7] Williams, G. R. and R. Dale. "Shorter Communications The Biodeterioration of the Plasticiser Dioctyl Phthalate", International Biodeterioration Bulletin, 1983, 19 (1), 37-8.
- [8] Seal, K. J. and H. O. W. Eggins, "The Biodeterioration of Materials", Essays in Applied Microbiology, J. R. Norris and M. H. Richmond editors, John Willey & Sons: London (1981) pp. 2-8,15-19.
- [9] Butler, N. J. and H. O. W. Eggins, "Microbiological Deterioration and the Tropical Environment", Microbiological Deterioration in the Tropics, Society Chemical Industry: London (1966) pp. 3-12.

226 GEOSYNTHETIC SOIL REINFORCEMENT TESTING PROCEDURES

- [10] Heap, W. M. and S. H. Morrell, "Microbiological Deterioration of Rubbers and Plastics", Journal Applied Chemistry, 1968, 18, 189-94.
- [11] Tirpak, G., "Microbial Degradation of Plasticized PVC", SPE Journal, 1970, 26 (7), 26-30.
- [12] Seal, K. J., "Biodeterioration of Materials Used in Civil Engineering", Microbiology in Civil Engineering, P. Howsam editor, Chapman and Hall: London (September 3-5, 1990) pp. 39-52.
- [13] Shapiro, O. and L. Magier, "Biocide Application Plays Many Roles in Adhesives", Adhesives Age, 1991, 34 (2), 22-4.
- [14] Bessems, E., "Some Microbiological Problems of Fabrics Coated with Plasticized PVC", Journal Coated Fabrics, 1979, 9, 26-37.
- [15] Hueck, H. J., "Criteria for the Assessment of the Biodegradability of Polymers", International Biodeterioration Bulletin, 1974, 10 (3), 87-90.
- [16] Osman, J. L., et al., "The Ability of Selected Yeast Cultures to Degrade Plasticized Polyvinyl Systems", Developments in Industrial Microbiology, 1972, 11, 447-51.
- [17] Connolly, R. A., "Soil Burial Tests: Soil Burial of Materials and Structures", The Bell System Technical Journal, 1972, 51 (1), 1-21.
- [18] Rankilor, P. R., Membranes in Ground Engineering, John Wiley: New York (1981) pp. 65-83.
- [19] Cadmus, E. L., "The Biological Stability of Polymers", Journal Coated Fabrics, 1977, 7, 33-42.
- [20] Campbell, R., "Microbiology of Soils", International Conference on the Implications of Ground Chemistry and Microbiology for Construction, A. Brian Hawkins editor, University of Bristol: Bristol, England (29 June - 1 July, 1992).
- [21] MacLachlan, J., et al., "Attack of Bacterial and Fungi on Rubbers and Plastics in the Tropics", Microbiological Deterioration in the Tropics, Monograph # 23, Society Chemical Industry: London (1966) pp. 185-99.
- [22] Lazar, V., "The Study of Microbiological Corrosion of Plastics in Romania", International Biodeterioration Bulletin, 1975, 11 (1), 16-23.
- [23] Fields, R. D. and F. Rodriguez, "Microbial Degradation of Aliphatic Polyesters", Proceedings of the Third International Biodegradation Symposium, J. M. Sharpley and A. R. Kaplan editors, Applied Science Publishers: Kingston, Rhode Island (August 17-23, 1975) pp. 775-84.

- [24] Frobisher, M., Fundamentals of Microbiology, W. B. Saunders Co.: Philadelphia (1968) pp. 66-68.
- [25] Pankhurst, E. S., et al., "The Ability of Polymers or Materials Containing Polymers to Provide a Source of Carbon for Selected Microorganisms", Proceedings of the Second International Biodeterioration Symposium, A. H. Walters and E. H. Hueck-Van der Plas editors, Halsted Press: Lunteren, The Netherlands (1971) pp. 76-90.
- [26] Allsopp, D. and K. J. Seal, Introduction to Biodeterioration, Edward Arnold: London (1986) pp. 39-49.
- [27] Burgess, R. and A. E. Darby, "Microbiological Testing of Plastics", British Plastics, 1965, 38 (3), 165-9.
- [28] Jakubowski, J. A., et al., "Microbiology of Modern Coatings Systems", Journal Coatings Technology, 1983, 55 (705), 49-53.
- [29] Potts, J. E., "Biodegradation", Aspects of degradation and Stabilization of Polymers, H. H. G. Jellinek editor, Elsevier: Amsterdam (1978) p. 620.
- [30] Yeager, C. C., "Laboratory and Service Tests for PVC", Biodeterioration of Materials, A. Harry Walters and J. J. Elphick editors, Elsevier: Amsterdam (9 -14 September, 1968) pp. 151-61.
- [31] Tsuchii, A. et al., "The Effect of Compounding Ingredients on Microbial Degradation of Vulcanized Natural Rubber", Journal Applied Polymer Science, 1990, 41 (5&6), 1181-1187.
- [32] Seal, K. J., et al., "Microbiological testing of plastics", Kunststoffe German Plastics, 1986, 76 (1), 22, 61-62.

Yick G. Hsuan,¹ Robert M. Koerner,¹ and Arthur E. Lord, Jr.,¹

A REVIEW OF THE DEGRADATION OF GEOSYNTHETIC REINFORCING MATERIALS AND VARIOUS POLYMER STABILIZATION METHODS

REFERENCE: Hsuan, Y. G., Koerner, R. M., and Lord, A. E., Jr., "A Review of the Degradation of Geosynthetic Reinforcing Materials and Various Polymer Stabilization Methods," Geosynthetic Soil Reinforcement Testing Procedures, ASTM STP 1190, S. C. Jonathan Cheng, Ed., American Society for Testing and Materials, Philadelphia, 1993.

ABSTRACT: The paper describes the two major degradation mechanisms of geosynthetics: oxidation of polyolefins (polyethylene and polypropylene), and hydrolysis of polyester (polyethylene terephthalate). These are the polymers which comprise the vast majority of geotextiles and geogrids used for soil reinforcement. Details of the degradation mechanisms of each material and their consequences are described based on the presently available literature. The influence of material structure, in particular the orientation, and ambient environmental conditions on the degradation are also discussed. The mechanisms and methods of stabilization which are currently used to minimize degradation are also presented. Finally, the paper concentrates on various possible test methods which can be used for monitoring the degradation of geosynthetic materials.

KEYWORDS: degradation, oxidation, hydrolysis, polyolefins, polyethylene, polypropylene, polyester, polyethylene terephthalate, free radical, geosynthetics.

Durability is necessarily a major issue for all polymeric geosynthetics, including reinforcing materials such as geotextiles and geogrids, when long design lifetimes are required. Such is the case with reinforcement of walls and slopes which have design lifetimes of 75-100 years. Frequently asked questions with regard to degradation focus on the following considerations:

- fundamental degradation mechanism(s) involved with the specific polymer;

¹Drs. Hsuan, Koerner, and Lord are Assistant Professor, Director and Professor respectively, at the Geosynthetic Research Institute, Drexel University, Philadelphia, PA 19104

- type of tests to properly model the degradation phenomenon;
- the rate of degradation over time;
- the properties that are affected most significantly; and
- alternative additives that a manufacturer may utilize in order to limit or minimize the degradation phenomena.

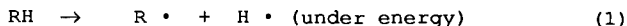
This paper attempts to address these issues as far as oxidation of polyolefins and hydrolysis of polyester are concerned.

Both of the above mentioned degradation processes involve altering the chemical structure of the materials; this generally involves side chain breaking, chain scission, or cross-linking in the polymer chains. The specific mechanisms and extent of the degradation are dependent on the type of polymer, its formulation and additives, and various external environmental factors which include exposure to moisture, oxygen, sunlight, heat, radiation, bacteria, as well as the type and magnitude of the mechanical stress. In most cases, the degradation is caused by a combination of these factors. For a large majority of soil covered geosynthetics, the degradation phenomena commonly encountered during the service lifetime are oxidation of polyolefins and hydrolysis of polyester. Certainly, there are many other possible degradation causes, such as ultraviolet light [1], nuclear radiation effects [2] and biodegradation [3], but they are the special situations and are beyond the scope of this paper.

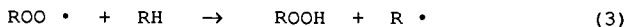
OXIDATION IN POLYOLEFINS

At ambient temperatures and in the absence of sunlight the rate of oxidation of polyolefins is very slow. When oxidation does eventually occur, the first step is the formation of free radicals which subsequently react with oxygen and start a series of chain reactions, as sequentially described in Equations (1) to (6) [1]. The process leads to an auto-acceleration reaction. The rate of reaction in a pure polymer is slow at the beginning and then it gradually accelerates, as shown in Figure 1, curve "b". In the induction period, the hydroperoxides (ROOH) are forming but do not decompose. The onset of oxidation probably depends on both the concentration and decomposition of hydroperoxides (ROOH) [4].

Initiation :



Propagation:



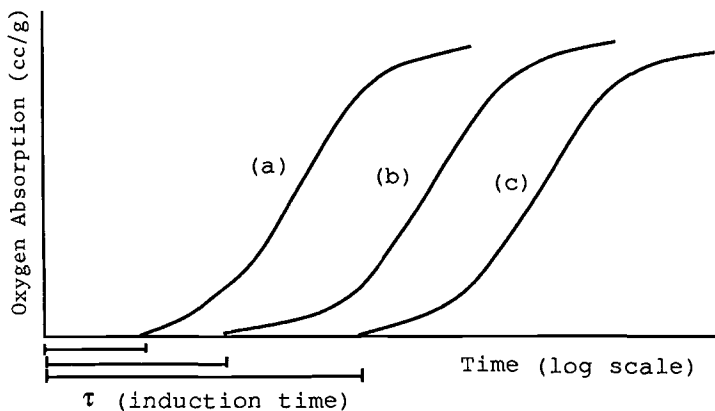
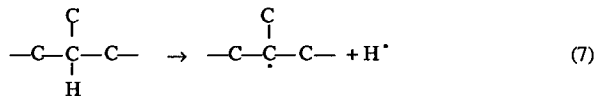


Fig. 1 -- Idealized oxygen absorption curves for oxidizing polymers under various conditions: (a) Transition element effects, (b) Pure polymer, (c) Oriented polymer

Material Effects on the Oxidation Reaction

The chemical and physical structure of the polyolefin can certainly affect the rate of oxidation, since these features control the formation of free radicals and the diffusion of oxygen into the polymer. Four major factors will be discussed.

(a) Tertiary carbon atom -- Pure polypropylene (PP) is much more susceptible to oxidation than pure linear polyethylene (PE), particularly high density polyethylene (HDPE). This is because a greater number of tertiary carbon atoms are present in PP than HDPE. A tertiary carbon atom is the carbon atom which bonds with three other carbon atoms and one hydrogen atom. The C-H bond can rapidly dissociate to form a tertiary carbon free radical, as shown in Equation (7) [5,6].

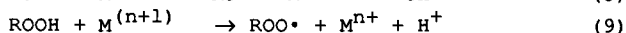
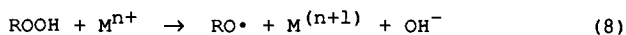


In PP, every second carbon atom in the backbone of the polymer chain is a tertiary carbon. This increases the probability of free radical formation compared to HDPE in which only the branch junctions contain the tertiary carbon atoms.

(b) Crystallinity -- In polyolefins, oxidation takes place almost entirely in the amorphous phase of the polymer. This is because oxygen can diffuse easier in the amorphous phase than in the crystalline phase [7]. Rapoport et al. [8] demonstrated that the molecular mobility within the amorphous phase plays a vital part in oxygen diffusion, i.e., the higher the temperature, the greater the rate of oxygen diffusion through the amorphous phase.

(c) Molecular weight -- Since the oxidation reaction induces chain scission in the polymer chains, a high molecular weight polymer would probably perform better than a low molecular weight polymer. In particular, the distribution of the molecular weight is the most important factor to the rate of oxidation. The distribution curve gradually shifts towards the low molecular weight region as the oxidation reaction progresses [9].

(d) Transition metals -- An oxidation reaction of polyolefins can be catalyzed in the presence of transition elements, e.g. Co, Mn, Cu and Fe [10,11,12]. The sources of these elements can come from the residual catalysts used to polymerize the polymer or trace metals added into the process. One of the main functions of a metallic catalyst during oxidation is believed to be to promote the breakdown of hydroperoxides via "Redox" reactions, as shown in Equations (8) and (9). The induction period of the oxidation reaction is consequently shortened, as illustrated in Figure 1, curve "a". The order of catalyst activity of the transfer metals varies from polymer to polymer.



(e) Orientation (Stretching) -- Many geosynthetic products, including geogrids and geotextiles, which are used in reinforcement applications are highly oriented materials. Their microstructure is substantially different from non-orientated materials. The Peterlin Model [13] describes the polymer orientation mechanism under tensile stress. This elongation results in a much denser amorphous phase and higher crystallinity than that in the comparable isotropic material. This dense structure retards the diffusive mobility of oxygen thus delaying the onset of oxidation, see Figure 1, curve "c".

External Effects on the Oxidation Reaction

The oxidation reaction in polyolefins is rather sensitive to the surrounding environment. Any environment which can accelerate the decomposition of the hydroperoxide would logically increase the rate of oxidation. Four considerations are described.

(a) Energy effects -- Heat and sunlight are the two common types of the energy that geosynthetics could be exposed to. In reinforcement applications, however, the material is most likely covered by soil, eliminating the sunlight effect. Hence, the supplied energy to initiate the free radical and accelerate the decomposition of hydroperoxide comes from heat, i.e. thermal energy (recall Equations (1) and (4)).

(b) Soil chemistry - Soil contained transition elements may be a concern regarding the rate of oxidation reaction of the geosynthetics. As described in the "transition metals" section, certain transfer metals have a catalysing effect on the oxidation. Wisse [14] has demonstrated the negative influence of iron oxide on PP geotextiles. A polypropylene geotextile was contaminated by rusting steel wires which were lying upon

the fabric. However, the effects of soil containing trace amounts of transition metals have not been evaluated to any extent.

(c) External stress -- The interaction between the polymer and oxygen under a constant tensile stress is referred to as the stress crack behavior of the material [4, 15]. Figure 2 shows a steady state creep curve which is divided into two regions. The causes of failure vary in the different regions, and they are described below:

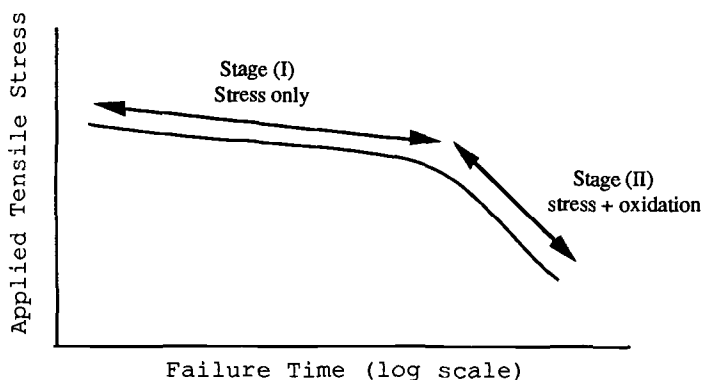


Fig. 2 -- Typical steady state creep response curve.

The Stage (I) region covers the high applied stresses and a broad, but short, failure time range. The failure is solely caused by the external applied stress, and the failure mode is dominated by ductile behavior. The Stage (II) region represents low applied stresses and relatively long failure times. Failure could be caused by stress alone or a combination of stress and oxidation, depending upon the length of time to failure. The contribution of oxidation to the failure mechanism increases with time. The failure mode is dominated by slow crack growth, which is a brittle failure process.

For an oriented material, the failure time in Stage (II) would be longer than in non-oriented material, if the direction of applied stress is the same as the oriented direction. Otherwise shorter failure times would be obtained [16].

(d) Annealing -- Annealing is treatment of the finished product by heating. Rapoport et al. [17] observed that annealing can counteract the oxidation retardation generated by stretching. This phenomenon is illustrated in Figure 3. The explanation offered is that polymer chains in the amorphous phase of an oriented material are in a non-equilibrium elongated configuration. Annealing brings the chains back to equilibrium, increasing chain mobility and reducing packing density. Thus oxygen can diffuse into the amorphous phase easier, causing quicker oxidation than in the non-annealed oriented material. However, for such changes to occur, the annealing temperature needs to be higher than the temperature at which the stretching was conducted.

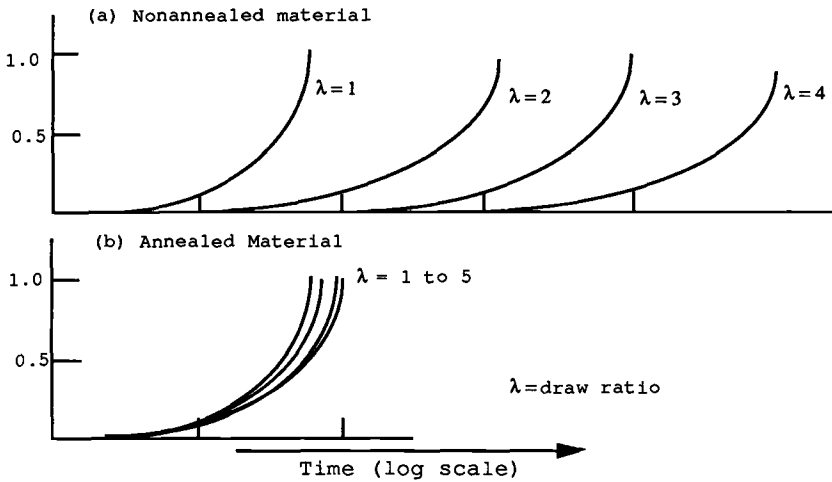


Fig. 3 -- Effect of annealing on the induction period of oxidation (after reference [17])

Methods to Minimize Oxidation

Since the prevention of oxygen meeting the surface of geosynthetic material is practically impossible, manufacturers have developed other methods to minimize oxidation degradation. For example, antioxidants and carbon black are routinely used in the polymer blend. Metal deactivators may also be added. Each is briefly explained.

(a) Antioxidants -- Antioxidants are used as additives to counteract the oxidation reaction. The activity is focused in two stages: initiation (Equations 1 and 2) and propagation (Equations 3 to 6). At the initiation stage, the function of an antioxidant is to scavenge (i.e., chemically combine with) the free radicals, converting them into stable molecules. At the propagation stage, the oxidative product, ROOH, is the sole target. The function of the antioxidants is to convert this highly reactive hydroperoxide (ROOH) into a more stable form, such as ROH. A recently developed antioxidant family is Hindered Amine Light Stabilizers (HALS) which are used in many geosynthetic materials.

(b) Carbon black -- The most widely used light stabilizer in geosynthetic materials is carbon black. The primary function of carbon black is a light screen (reducing penetration of ultraviolet radiation into the polymer matrix). Waler and Juzkow [18] show that 3% carbon black enhances the performance of certain antioxidants to a great extent, as shown in Figure 4. However, Roots [19] indicated that carbon black usually reduces the heat stability of the polymer.

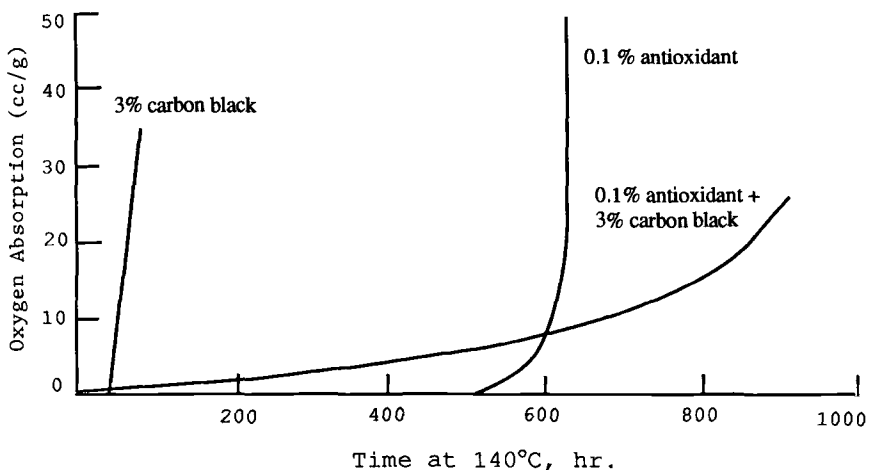


Fig. 4 -- Synergistic effect of an antioxidant and carbon black on thermal oxidation of polyethylene. (After reference 17)

(c) Metal deactivators -- If transition metal ions in the soil become a concern, metal deactivators can be added to chelate (i.e., to capture and surround) the metal ions and reduce their catalytic effect on the decomposition of ROOH [20]. The possible metal deactivators are various oxamide derivatives $(RNHC=O)_2$.

Suggested Methods for Evaluating Oxidation

Most or probably all geosynthetic products made from polyolefins contain some type of antioxidant. Hence it is important to recognize that test methods aimed at evaluating the thermoxidative stability of polyolefins would most likely challenge the lifetime of the antioxidants in the polymer rather than the stability of the polymer itself. In other words, the service life of the material is probably dictated by the efficiency of the antioxidants.

If one wants to use accelerated laboratory incubation methods to evaluate performance and lifetime, an oven aging procedure is recommended. Test samples are placed in a forced air oven at desired temperatures dependent on the type of polyolefin. Gray [21] used 150°C for polypropylene and 120°C for polyethylene. A minimum of three different test temperatures should be used to evaluate a given material. After a specific time interval, the incubated samples are removed and tested so that the lifetime of the material can be predicted using an extrapolation method, such as Arrhenius Modeling [22]. It is important to note that, for evaluating an oriented product, the test temperature must be below the temperature at which the material was stretched or oriented. This will preserve the dense packed structure of the material, so that the test results will be more realistic. However, if samples are being retrieved from the field in order to assess the degree

of oxidation, they should be utilized directly and need not be incubated.

In either case (laboratory or field), the following test methods are recommended to evaluate the initial stages of degradation. (Note that a wide range of more conventional physical/mechanical tests can be used to evaluate advanced stages of degradation).

(a) Oxidative induction time (conventional) -- Oxidative induction time (OIT) of a polymer is measured using conventional differential scanning calorimeter (DSC). The OIT is the length of time required to decompose the polymer at 200°C under oxygen atmosphere. The closest related standard is ASTM D3895. The method is often used as a QA/QC test for confirmation purposes or possibly a test to monitor polymer aging. However, the test should not be used for comparing products with different antioxidant formulations, since OIT varies with different types of antioxidants. Some antioxidants yield a high OIT value at 200°C, but may not necessarily provide a long duration at the ambient temperature, and visa versa [21]. The problem with this test is the high test temperature at which the test specimen is in molten stage. At that temperature, some antioxidants may perform very poorly but they can function very well at the ambient temperature. Since the material is always used at lower temperatures when it is solid, the interpretation of the results are very difficult.

(b) Oxidative induction time (high pressure) -- In order to overcome the high test temperature of the conventional test as described above, the test can also be performed under high pressure in a high pressure DSC cell at a temperature below 200°C. Cadwallader [23] has used 5.5 MPa (800 psi) oxygen at temperatures of 180°C and 130°C for testing HDPE geomembranes. His results show a better distinction between different formulations at 130°C, but the test takes a much longer time than at 180°C. In addition, the method is criticized because of the high oxygen pressure used during the test, since such a condition would not be encountered in any real life situation. The high pressure may even change the mechanism of the degradation process.

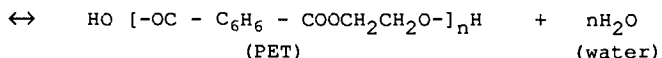
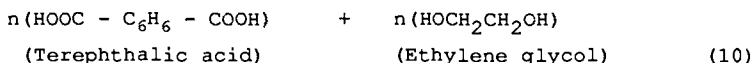
(c) Fourier transform infrared spectroscopy (FTIR) -- Once the antioxidants have been completely consumed, oxidation starts to propagate in the polymer. The result of the oxidation of polyolefins is the formation of carbonyl group (C=O) in the polymer chains. Such groups can be detected using FTIR. The characteristic absorption band of this group is in the vicinity of 1735 cm^{-1} [24]. Since oxidation first takes part at the surface and then gradually infiltrates into the material, the test is performed using a reflectance mode. It allows the IR beam to be reflected from the sample surface, subsequently analyzing the surface material [25].

(d) Gel permeation chromatography (GPC) -- It was stated previously that oxidation induces chain scission lowering the molecular weight and subsequently changes the molecular weight distribution curve of the polymer. GPC is a unique technique used to analyze molecular weight distribution of polymeric materials [26]. However, for polyolefin geosynthetic materials, high temperature GPC is required. In addition,

significant amounts of filtration are needed to separate the carbon black particles from the polymer.

HYDROLYSIS OF POLYESTER

One of the major concerns of geosynthetic reinforcement materials made from polyester is the potential long-term hydrolytic reaction. The particular polyester used to make geotextiles and geogrids is polyethylene terephthalate (PET). This compound is formed by a reaction between terephthalic acid and ethylene glycol, as seen in Equation 10 [27].



This is an equilibrium reaction in that water must be continuously removed to achieve high efficiency and a high molecular weight polymer. It should be recognized that the reaction can be reversed, i.e., PET polymer can react with water and revert to compounds with acid or hydroxide end groups. This reverse reaction is the hydrolytic reaction of PET, reducing the molecular weight via chain scission [28].

Material Effects on the Hydrolytic Reaction

The hydrolytic properties of PET are strongly dependent on the chemical and physical structure of the specific product. From a chemical aspect, carboxyl end groups (CEG) and ester groups in the polymer are the most important factors. From a physical aspect, the molecular weight, crystallinity, orientation, and diameter of fibers are the major factors. Each of these factors will be discussed below:

(a) Carboxyl end group (CEG) concentration -- Carboxyl end groups are defined as the $-\text{COOH}$ groups situated at the end of the molecular chains. Not every polymer chain contains a carboxyl end group. This is dependent on the polymerization process. The concentration of CEG could vary from 10 to 40 meq/kg. In neutral water (pH = 7), Ravens and Ward [29] found that carboxyl groups catalyze the hydrolysis of PET. They proposed that the rate of hydrolysis is proportional to the square root of the CEG concentration.

(b) Molecular weight -- Molecular weight can directly affect the CEG concentration under the same polymerization conditions. A polymer with a higher molecular weight would contain less CEG than a lower molecular weight polymer. Sprague [30] observed that a PET geotextile with a lower molecular weight degrades faster than one with a higher molecular weight in a calcium hydroxide solution at 50°C.

(c) Crystallinity -- The rate of hydrolytic reaction is based on the diffusion of water into the polymer [31]. In a PET material, diffusion is governed by the amount of amorphous phase material.

(d) Orientation -- Orientation of the product has a significant effect on the diffusion rate as described in the polyolefins section. Orientation reduces the diffusion rate of the penetrant. McMahon et al. [32] found that the rate of hydrolysis of PET fibers is decidedly slower than that of films or sheets due to the highly uniaxial orientation of the fiber.

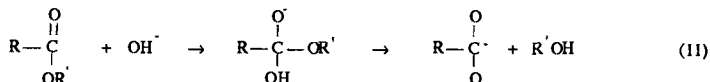
(e) Diameter of the fiber -- In an alkalie environment the hydrolytic reaction is a topochemical reaction (i.e., reaction takes place on the surface of the fibers) [33, 34]. If the overall properties are the same, fibers with a larger diameter would degrade more slowly than those with a smaller diameter.

External Effects on the Hydrolytic Reaction

The surrounding environment has a significant impact on the hydrolytic mechanisms of PET geosynthetics. Two different phenomena can occur in PET dependent on the exposure conditions. In neutral water (i.e. pH = 7) and acidic conditions (pH < 7), the hydrolytic reaction is an "internal" hydrolysis. The reaction is mainly governed by the diffusion of water and H⁺ ions into the amorphous phase. In contrast, "external" hydrolysis occurs under alkaline conditions (pH > 7) with the presence of calcium ions. Here the rate of reaction is strongly dependent on the surface area of the material. The following discussion describes factors which have significant influence on hydrolysis:

(a) Temperature -- The rate of hydrolytic reaction increases with temperature. This is why most laboratory studies utilize high temperatures to accelerate the reaction. However, caution must be applied. Since at pH ≤ 7, the reaction is diffusion controlled, the rate of diffusion would likely vary above and below the glass transition temperature (which is around 70°C). However, McMahon et al. [32] did not observe any erratic changes in the reaction rate within the 60°C to 100°C temperature range using unoriented sheet samples.

(b) pH level -- The hydrolytic reaction is accelerated substantially by alkaline environments [35, 5]. The hydrolytic process involves ester groups (R-COO-R') in the PET chain being attacked by the hydroxide group (OH⁻), as expressed by Equation 11. This reaction is essentially irreversible, since the stable carboxylate anion (RCOO⁻) is unlikely to react with an alcohol to reform ester.



(c) Cation effects in alkaline media -- An alkaline solution, say pH = 12, can be obtained using various hydroxide compounds with different cations, such as NaOH, KOH, Ca(OH)₂, or Mg(OH)₂. Their effects on hydrolysis vary. Halse et al. [33, 36] and Sprague [30] found that Ca²⁺ ions have a greater effect on the rate of the hydrolytic reaction than Na⁺ ions at the same pH level and temperatures. However, the reason for such variation is not clear.

Factors for Improving Hydrolysis Resistance in PET

Unlike polyolefins, there are no specific additives to retard hydrolysis in PET materials. The resistances to hydrolysis must come from the polymer itself. As described previously, there are five material factors which relate to the hydrolytic performance of PET: carboxyl end groups, molecular weight, crystallinity, orientation, and fiber diameter. Proper manipulation and control of these factors improves the hydrolysis resistance of the polymer.

Suggested Methods of Evaluating Hydrolysis

The hydrolysis reaction of PET polymers is most sensitive to high pH solutions and high temperatures. Thus for accelerated laboratory testing, samples placed in constant temperature baths containing various solutions should be utilized. The European Standard CEN/WG5/N37 [37] has established two different procedures for evaluating both "internal" and "external" hydrolysis. The "internal" hydrolysis test is performed at 135°C saturated steam conditions, and the "external" hydrolysis test is performed at 65°C and pH = 11 containing calcium ions. In addition, the long term performance evaluation using a minimum of three different test temperatures should be carried out so that properties can be predicted through data extrapolated methods, such as Arrhenius Modeling [22]. The incubated samples are taken out for testing at prescribed incubation intervals. However, if samples are retrieved from the field in order to assess the degree of hydrolysis of a PET geosynthetic, such test samples should be used directly.

In either case (laboratory or field), the following test methods are recommended to be performed for evaluating the initial stages of degradation. (Note that a wide range of more conventional physical/mechanical tests can be used to evaluate advanced stages of degradation).

(a) Solution viscosity -- This is a technique used to measure the viscosity molecular weight of the material which is one particular value on the molecular weight distribution curve. This value decreases as chain scission increases. The test procedure to be followed is ASTM D 4603 [38]. Certainly, one can use GPC to analyze the entire molecular weight distribution curve, but GPC is more difficult to perform and more costly. The only requirement of the test sample is that it must be soluble in a solvent at a moderate temperature (not higher than 30°C).

Table 3 -- Summary of internal and external factors affecting polymer degradation and recommended analytic test methods*

Polymer (reaction)	Material factors	External factors	Test methods (properties)
polyolefins (oxidation)	tertiary carbons (branch density in PE) crystallinity orientation molecular weight (MW)	temperature transition metals applied stress annealing	OIT (conventional and high pressure) FTIR (carbonyl group) GPC (MW)
polyester (hydrolysis)	CEG concentration molecular weight (MW) crystallinity orientation fiber diameter	temperature alkaline level cation effect	solution viscosity (MW) titration (CEG concentration) microscopy (morphology & fiber diameter)

* Note, as degradation proceeds a number of physical and mechanical test methods will eventually indicate the polymer's change in properties, e.g., strength, elongation, modulus, creep, stress relaxation, impact resistance, etc.

(b) Titration -- This method is used to measure the concentration of the carboxyl end groups which are acidic and can be neutralized by an alkaline solution. The detail of the test will not be presented here due to space limitation, but is described in Reference [32]. The amount of CEG increases with increasing chain scission.

(c) Quantitative microscopy -- The "external" hydrolysis on the PET fibrous material is a topochemical reaction. The surface morphology can be used to evaluate this phenomena. In addition, for PET geotextiles or geogrids, the reduction in fiber diameter can be measured as the reaction process progresses.

SUMMARY

This paper presents an overview of the mechanisms of oxidation and hydrolysis for polyolefins and polyester, respectively. These two polymer types are widely used in the manufacture of geotextiles and geogrids for reinforcing applications. The polymer also indicates how such mechanisms are affected by the material (internal) properties and external environments. These internal and external factors are summarized in Table 3 together with suggested methods for evaluating the effects of these different long term degradation phenomena.

ACKNOWLEDGEMENTS

The funding for this study was provided by the Geosynthetic Research Institute's Consortium of Member Organizations. Our sincere appreciation is extended.

REFERENCES

- [1] Grassie, N. and Scott, G., Polymer Degradation and Stabilization, Published by Cambridge University Press, 1985.
- [2] Phillips, D.C., "Effects of Radiation on Polymers," Materials Science and Technology, Vol.4, 1988, PP 85-91.
- [3] Albertsson, A.C. and Banhidi, Z.G., "Microbial and Oxidative Effects in Degradation of Polyethene," Journal of Applied Polymer Science, Vol.25, 1980, PP. 1655-1671.
- [4] Rapoport, N.Ya. and Zaikov, G.E., "Kinetics and Mechanism of the Oxidation of Stressed Polymer," Developments in Polymer Degradation - 6, 1986, pp 207-258.
- [5] Morrison, R.T. and Boyd, R.N., Organic Chemistry, 3rd Ed., Published by Allyn and Bacon, Inc, Boston, 1974.
- [6] Hansen, R.H., Russell, C.A., D.E. Benedictis, T., Martin, W.M., and Pascale, J.V., "Inhibition of the Copper-Catalyzed Oxidation of Polypropylene," Journal of Polymer Science: Part A, Vol.2, 1964, PP 587-609.

- [7] Michaels, A.S., and Bixler, H.J., "Solubility of Gases in Polyethylene," *Journal of Polymer Science*, 50, 1961, PP. 393-412.
- [8] Rapoport N.Ya., Berulava, S.I., Kovarskii, A.L., Musayelyan, I.N., Yershov, Yu.A., and Miller, V.B., "The Kinetics of Thermo-oxidative Degradation of Oriented Polypropylene in Relation to the Structure and Molecular Mobility of the Polymer," *Vysokomol. Soyed*, A17:11, 1975, PP 2521-2527. (Translated in *Polymer Sci. U.S.S.R.*, 17:11, 1975, PP 2901-2909).
- [9] Holmström, A., "The Course of Thermo-oxidative Degradation of LD- and HD-Polyethylene Under Accelerated Testing Conditions," Durability of Macromolecular Materials, Edited by Eby, R.K., ACS Symposium Series 95, ASC Washington, D.C., 1979, pp.45-62.
- [10] Chan, M.G. and Allara, D.L., "Infrared Reflection Study of the Mechanism of Oxidation at a Copper-Polyethylene Interface," *Journal of Colloid and Interface Science*, Vol.47, No.3, June 1974, pp 697-704.
- [11] Osawa, Z., and Ishizuka, T., "Catalytic Action of Metal Salts in Autoxidation and Polymerization. X. The Effect of Various Methal Stearates on the Thermal Oxidation of 2,6,10, 14-Tetramethylpentadecane," *J of Applied Polymer Science*, Vol. 17, 1973, pp 2897-2907.
- [12] Reich, L., Jadrnicek, B.R., and Stivala, S.S., "Effect of Oxidation-Reduction Potential on the Metal Salt-catalyzed Autoxidation of Atactic Polypropylene," *J. Polymer Sci.*, A-1, 9, 1971, pp 231-233.
- [13] Peterlin, A., "Molecular Mechanism of Plastic Deformation of Polyethylene," The Meaning of Crystallinity in Polymers, Ed by Price, F.P., *J. of Polymer Science*, Part C, *Polymer Symposia*, No.8, 1966, pp 123-132.
- [14] Wisse, J.D.M., "The Role of Thermo-oxidative Ageing in the Long-Term Behaviour of Geotextiles," Durability of Geotextiles, Rilem, 1988, pp.207-216.
- [15] Halse, Y.H., Lord, A.E. Jr., and Koerner, R.M., "Ductile-to-Brittle Transition Time in Polyethylene Geomembrane Sheet," Geosynthetic Testing for Waste Containment Applications, ASTM STP 1081, R.M. Koerner, ed., ASTM, Philadelphia, 1990, pp 95-109.
- [16] Shanahan, M.E.R., "The Role of the Liquid in Environmental Stress Cracking of Polyethylene," *Journal of Materials Science Letters*, 2, 1983, pp 28-32.
- [17] Rapoport, N.Ya., Livanova, N.M., and Miller, V.B., "On the Influence of Internal Stress on the Kinetics of Oxidation of Oriented Polypropylene," *Vysokomol. soyed*. A18 : 9, 1976, PP 2045-2049. (Translated in *Poly. Sci. U.S.S.R.*, 18, 1977, PP. 2336-2341.)

242 GEOSYNTHETIC SOIL REINFORCEMENT TESTING PROCEDURES

- [18] Walker, D.M., and Juzkow, M.W., "PE/Carbon-black Survives 20 Years of Weathering in Canada," Modern Plastics, May 1983, pp 68-72.
- [19] Root, S., "Stabilization of Polypropylene Fiber for Textiles and Geotextiles," Ciba-Geigy Corp. Internal Report, 1987.
- [20] Hawkins, W.L., "Recent Advances in Mechanisms for the Stabilization of Polyolefins," J. Polymer Sci., Symp. No. 57, 1976, PP 319-328.
- [21] Gray, R.L., "Accelerated Testing Methods for Evaluating Polyolefin Stability," Geosynthetic testing for Waste Containment Applications, ASTM STP 1081, R.M. Koerner, ed., ASTM, Philadelphia, 1990, pp 57-74.
- [22] Koerner, R.M., Lord, A.E., Jr., and Hsuan, Y., "Arrhenius Modeling to Predict Geosynthetic Degradation," J. Geotextiles and Geomembranes, 11, 1992, pp 151-183.
- [23] Cadwalladar, M.W., "The Relation of High Pressure OIT to Oven Aging for HDPE Liner", 4th Int. Conf. on Geotextiles, Geomembranes and Related Products, Netherlands, May 1990, p 593.
- [24] Conley, R.T., Infrared Spectroscopy, Published by Allyn and Bacon, Inc., Boston, 1966.
- [25] Thomas, R.W., "An Introduction to IR Spectroscopy for Geosynthetic Applications," Geotechnical Fabrics Report, September 1991, pp 22-24.
- [26] Halse, Y., Mertz, J., and Rigo, J.M., "Chemical Identification Methods used to Characterize Geomembranes," Rilem Report 4, Geomembranes : Identification and Performance Testing, Ed. by Rollin A.L. and Rigo, J.M., Published by Chapman and Hall, London, 1991, pp 316-336.
- [27] Odian, G., Principles of Polymerization, Second Edition, Published by Wiley-Interscience, New York, 1981.
- [28] Zimmermann, H., "Degradation and Stabilization of Polyesters," Developments in Polymer Degradation - 6, Edited by N. Grassie, 1986, pp 79-119.
- [29] Ravens, D.A.S., and Ward, I.M., Trans. Faraday Soc., 57, 1961, pg. 150.
- [30] Sprague, C.J., "Leachate Compatibility of Polyester Needle-punched Nonwoven Geotextiles," Geosynthetic Testing for Waste Containment Applications, ASTM STP 1081, R.M. Koerner, ed., ASTM, Philadelphia, 1990, pp 212-224.

- [31] Golike, R.C. and Lasoski, S.W. Jr., "Kinetics of Hydrolysis of Polyethylene Terephthalate Films," *J. of Phys. Chem.*, 64, 1960, pp 895-898.
- [32] McMahon, W., Birdsall, H.A., Johnson, R.G. and Camilli, C.T., "Degradation Studies of Polyethylene Terephthalate," *J. of Chemical and Engineering Data*, 1959, pp 57-79.
- [33] Halse, Y., Koerner, R.M. and Lord, A.E., Jr., "Effect of High Levels of Alkalinity on Geotextiles. Part 1 : Ca(OH)₂ Solutions," *J. of Geotextiles and Geomembranes*, 5, No. 4, 1987, pp 261-282.
- [34] Namboori, C.G.G. and Malcolm, H.S., "Steric Effects in the Basic Hydrolysis of Poly(ethylene Terephthalate)," *J. of Applied Polymer Sci.*, Vol.12, 1968, pp 1999-2005.
- [35] Risseeuw, P. and Schmidt, H.M., "Hydrolysis of HT Polyester Yarns in Water at Moderate Temperatures," 4th Int. Conf. on Geotextiles, Geomembranes and Related Products, Netherlands, May 1990, pp 691-696.
- [36] Halse, Y., Koerner, R.M., and Lord, A.E., Jr., "Effect of High Levels of Alkalinity on Geotextiles. Part 1 : Na(OH) Solutions," *J. of Geotextiles and Geomembranes*, 6, No. 4, 1987, pp 295-306.
- [37] Proposed European Standard CEN/W5/N37 "Hydrolysis of Polyester".
- [38] ASTM D 4603 "Viscosity of Poly(Ethylene Terephthalate (PET), Inherent, Determining".
- [39] Haslam, J., Willis, H.A. and Squirrell, D.C.M., Identification and Analysis of Plastics, Second Edition, Published by Butterworth & Co., Ltd., London, 1972.

Author Index

- A**
- Abramanto, M., 1
Austin, D. N., 90
- B**
- Ballegeer, J. P., 16
Bathurst, R. J., 32
Bauer, G. E., 138, 195
Berg, R. R., 152, 184
Bright, D. G., 218
- C**
- Cancelli, A., 64
Cazzuffi, D., 119
Collin, J. G., 152, 184
Crouse, J. L., 207
- E**
- Elias, V., 163
- F**
- Farrag, K. A., 76
Fleck, J. A., 49
- G**
- Germaine, J. T., 1
Griffin, P., 76
- H**
- Halim, A. O. A., 195
Hsuan, Y. G., 228
- K**
- Koerner, G. R., 163
Koerner, R. M., 49, 163, 228
Krstic, R., 207
- L**
- Larson, D. G., 1
Lord, A. E., Jr., 228
- M**
- Montanelli, F., 64
- N**
- Netravali, A. N., 207
- P**
- Paulson, J. N., 111
Picarelli, L., 119
- R**
- Razaqpur, A. G., 195
Ricciuti, A., 119
Richmond, L. E., 207
Rimoldi, P., 64, 119
Simac, M. R., 32
- W**
- White, D. F., 90
Whittle, A. J., 1
Wilson-Fahmy, R. F., 49
Wu, J. T. H., 16
Wu, K. J., 90
- Z**
- Zhao, Y., 138, 195

Subject Index

A

Aggregates, 195
 ASTM standards, 152
 D 61: 16
 D 1682: 16
 D 4595: 32, 111
 Automated plane strain
 reinforcement cell, 1

B

Backfill, 163
 Bearing capacity, 64
 Biocides, 218

C

Chemical stability, 207
 Clay liners, 49
 Cohesive soils, 76
 Compaction procedure, 76
 Composite material, geogrid, 184
 Concrete block units, 32
 Confinement, 16, 49
 soil, lateral spreading, 64
 Creep, 284

D

Degradation, fiber, 207, 218, 228
 Dilatancy, soil, 138
 Direct shear test, 119, 138, 152
 Displacement, 195

E

Extensometer, 90

F

Factors-of-safety, 195
 partial, 163

G

Geocells, 64
 Geogrids
 damaged, 195
 degradation of, 228
 installation damage, 163
 modular block, 32
 pull-out testing, 76, 119,
 184, 195
 tensile modulus, 90
 Geonets, 49
 Glass transition temperature,
 207
 Grain size distribution, 76
 Granular soils, 76, 138
 Gravel, 119, 163

H

Hydraulic testing, 64
 Hydrolysis, 207, 228

I

Installation damage, 163, 195

L

Limit equilibrium, 152
 Liners, clay, 49
 Loading, 32, 184
 deformation properties, 16
 extension modulus, 49
 pull-out, 76
 transfer evaluation, 1

M

Microorganisms, effect on
 geosynthetics, 218
 Moisture content, soil, 76

248 GEOSYNTHETIC SOIL REINFORCEMENT TESTING PROCEDURES

N

Needle-punched geotextiles, 49
Nonwoven geotextiles, 16
 needle-punched geotextiles,
 49

O

Oxidation, 228

P

Planar reinforcement, 1
Plane strain test, 1
Polyester, 111, 195, 207, 228
Polyethylene terephthalate, 228
Polymeric degradation, 207, 218,
 228
Polymeric reinforcement, 163
Polyolefins, 228
Polypropylene, 90, 228
Pull-out tests, 76, 119, 184, 195

R

Ribs, geosynthetic
 installation damage, 163
 single, 90
Rubber membrane, 16

S

Sand-steel data, 1
Shear failure, 64
Shear lag analysis, 1
Shear strength, 119, 138, 152
Shear stress strain, 76
Silt, 184
Silty sand, 119

Single end break, 111
Single rib, 90
Slippage, 16
Soil friction angle, 152
Stability, fiber, 228
 biological, 218
 chemical, 207
Standards (See also ASTM
 standards)
 degradation, 218
 geocells, 64
Steel sheet inclusion, 1
Stiffness, 16
Strain rate, 184
Stress degradation, 207
Stress strain
 curves, 16
 shear, 76

T

Tensile properties
 D 61: 16
 D 1682: 16
 D 4595: 32, 111
 modulus, 90
 strain, 138
 strength, 49
 stress, 64
 measurement, 1
Triaxial test, 119

W

Wide width strip method
 D 4595: 32, 111
Wide width tension test, 49
Woven geotextiles, 16, 49
 polyester, 111

ISBN 0-8031-1885-6